Intelligent Infrastructures for Charging Reservation and Trip Planning of Connected Autonomous Electric Vehicles

By

Palwasha Waheed Shaikh

A thesis submitted to the Faculty of Engineering
in conformity with the requirements for the M.A.Sc. degree
in Electrical and Computer Engineering

School of Electrical Engineering and Computer Science
University of Ottawa
Ottawa, ON, CA

Abstract

For an environmentally sustainable future, electric vehicle (EV) adoption rates have been growing exponentially around the world. There is a pressing need for constructing smart charging infrastructures that can successfully integrate the large influx of connected and autonomous EVs (CAEVs) into the smart grids. To fulfill the aspiration of massive deployment of autonomous mobility on demand (AMoD) services, the proposed fast and secure framework will need to address the long charging times and long waiting times of static charging. It will also need to consider dynamic wireless charging as a viable solution for the CAEVs on the move. In this thesis, a novel three-layer charging system design of static and dynamic wireless charging that can operate with the existing wired charging infrastructure and standards for Intelligent Transportation System (ITS) is presented. This internet of things (IoT) application is accompanied by a proposed handshake protocol with light-weight request message frames. It employs vehicle to infrastructure (V2I) and vehicle to grid (V2G) communications for fulfilling charging requests of CAEVs with the shortest possible route to the destination. The charging requests of the CAEV users are fulfilled by dynamically distributing the request over the three different types of charging equipment. Further, the requests are serviced and billed privately and securely using two different proposed payment schemes with the encrypted virtual currency. The hardware independent system can detect misalignment of the CAEVs on the wireless charging pads and the speed issue errors in dynamic wireless charging systems as well as avoid free-riders. Additionally, the proposed dynamic wireless charging network (DWCN) design specification tool is analyzed. The suggestions made by the tool for building a DWCN can enable implementers to achieve the desired charging delivery performance at the lowest cost possible. Finally, the presented system is simulated, and this verified and validated simulator is revealed to make reservations and plan trips with minimum waiting times, travel costs, and battery consumption per vehicle trip. The system results proved 90.25% charge delivery efficiency. This system is then compared with alternative system designs to help showcase its ability to aid implementers and analysts in making design choices with the simulation.

Acknowledgement

Firstly, praises and thanks to Almighty Allah for bestowing me with the understanding and strength needed to complete this thesis successfully.

I would like to express my deepest gratitude to my thesis supervisor, Dr. Hussein T. Mouftah, who gave me the opportunity to do research. The completion of this thesis would not have been possible without his persistent support and guidance. I thank him for his timely advice and confidence in me and my abilities. His words have always convincingly conveyed a spirit of adventure and fostered inspiration and excitement regarding research work. His overwhelming attitude to help his students has been deeply inspiring and motivational. It only strengthened my desire to contribute to the field and pursue a doctorate. It was a great privilege and honor to work and study under his guidance. I look forward to the same in the future with the utmost excitement and armed with my unwavering dedication and passion to learn and contribute.

I would like to sincerely express my appreciation towards the entire University of Ottawa's School of Electrical Engineering and Computer Science for cultivating an environment where researchers and life-long learners like myself can freely explore, learn and grow. I am deeply indebted to all the professors who have taught me during my graduate studies and have passed on their invaluable teachings that helped develop my skills and personality.

I revere the strength, moral support, and endless prayers and blessings extended with love by my supportive and loving parents, Eng. Abdul Waheed Shaikh and Dr. Farah Waheed, my sweet brother, Eng. Shahroz Waheed Shaikh and my kind grandma/nanoo, Sitara Latif. Their unwavering support has guided me through the most challenging of situations, and their cheers have always been the loudest for even my smallest of achievements. Their reassuring smiles and their silent prayers have always been the loudest to motivate me and renew my confidence. Their unfaltering belief in me and my skills is overwhelming, and without them, I would not have been able to reach this far. They have always let me spread my wings and their unconditional love has always helped me fearlessly soar higher into the unknown. A mere thank you may not be able to express deep gratitude, yet I try: Thank you!

Palwasha W. Shaikh

Table of Contents

List of Figures

List of Tables

List of Acronyms

AEVs	Autonomous Electric Vehicles
AMoD	Autonomous Mobility on-Demand
AVs	Autonomous Vehicles
CAD	Canadian Dollars
CAEVs	Connected and Autonomous Electric Vehicles
CAN	Caltech Adaptive Charging Network
CC	Cabled Charging
CC/CV	Current/Constant Voltage
CCN	Cabled Charging Network
CI	Confidence Interval
CNH	Charging Network Head
CNs	Charging Networks
CPs	Credit Points
CRNs	Common Random Numbers
CVs	Connected Vehicles
CWPT	Capacitive Wireless Power Transfer
DoT	UK Department of Transport
DSRC	Dedicated Short Range Communication
DWC	Dynamic Wireless Charging
DWCN	Dynamic Wireless Charging Network
EC-WPT	Electric Coupled Wireless Power Transfer
EDC	Energy Distribution Center
EPA	Environmental Protection Agency
ESP	Energy Service Provider
EVDB	Electric Vehicle Data Base
EVs	Electric Vehicles
EVSE	Electrical Vehicle Supply Equipment
FEL	Future Event List
GA	Ground Assembly
GHG	Greenhouse Gas
GIDAS	German In-Depth Accident Study
GM	General Motors
ICS	Improved Chrono-SPT
IEC	International Electrotechnical Commission
IoT	Internet of Things
ISO	International Organization for Standardization
ITS	Intelligent Transportation System
IWM	In-Wheel Motor
JPL	Jet Propulsion Laboratory
KAIST	Korea Advanced Institute of Science and Technology
KDC	Key Distribution Center
KU	Khalifa University
Li-Fi	Light Fidelity
LiC	Lithium-ion Capacitor
MaaS	Mobility as a Service
MC-WPT	Magnetic Coupled Wireless Power Transfer
MED	Mobile Energy Disseminator
MINLP	Mixed Integer Non-Linear Programming
MIP	Mixed Integer Programming
ML	Machine Learning
MoD	Mobility-on-Demand
MR-WPT	Microwave Radiation Wireless Power Transfer
MWCVs	Mobile Wireless Charging Vehicles
NEDC	New European Driving Cycle
NHTSA	National Highway Traffic Safety Administration
OBU	On Board Unit
OLEV	On-line Electric Vehicle
ORNL	Oak Ridge National Laboratory
OWPT	Optical Wireless Power Transfer
OWPT	Optical Wireless Power Transfer
PATH	Partners of Advanced Transit and Highways
PHEV	Plug-in Hybrid Electric Vehicle
PI	Prediction Interval
PMPT	Permanent Magnetic Coupling Power Transfer
PMs	Permanent Magnets
QoE	Quality of Experience
QoS	Quality of Service
QWC	Quasi-Dynamic Wireless Charging
RDW	Dutch Vehicle Authority
RIPT	Resonant Inductive Power Transfer
RSU	Road Side Units
SAE	Society of Automotive Engineers
SAEVs	Shared Autonomous Electric Vehicles
SAVs	Shared Autonomous Vehicles
SMIRF	Shaped Magnetic Field Resonance

SoC	State of Charge
SWC	Static Wireless Charging
SWCN	Static Wireless Charging Network
SWPT	Stretchable Wireless Power Transfer System
TMR	Tunneling Magnetoresistive
TOU	Time of Use
UPS	United Postal Services
UTET	Ultrasonic Transcutaneous Energy Transmission
V2G	Vehicle to Grid
V2I	Vehicle to Infrastructure

V2V	Vehicle to Vehicle
VA	Vehicle Assembly
VDIS	Vehicle Detection and Information System
W-IWM1	First Generation Wireless In-Wheel Motor
WCPs	Wireless Charging Pads
WEVCSs	Wireless Electric Vehicle Charging Systems
WLTP	Worldwide Harmonized Light-Duty Vehicles Test Procedure
WPT	Wireless Power Transfer
WSNs	Wireless Sensor Networks

List of Symbols

α	Significance level
A_x	Map area x that has two sub-regions each and is connected to another area let's say y, A_y, by a highway lane
β	Proportion of time server is idle
B	Total server busy time
B_{cons}	SoC of a CAEV's Battery that is consumed (kWh)
B_{curr}	Current SoC of a CAEV's Battery (kWh)
B_{effic}	CAEV's Battery efficiency (kWh/m)
B_{max}	Maximum power of a CAEV's Battery (kWh)
C_{CAD}	Cost of energy delivered to the CAEV's Battery (CAD)
C_{CP}	Cost of energy delivered to the CAEV's Battery (CP)
C_{route}	Cost of the shortest route calculated by the Dijkstra's algorithm (m)
C_{track}	Amount of energy delivered by the track for charging (kWh)
Cl_{Ax}	All CN location nodes that fall in A_x
Cl_{Axy}	All CN location nodes that fall in A_x and in sub-region y
Cl_{AxAy}	All CN location nodes that fall in both A_x and A_y
CN_ID	ID of the CN that is reserved for the CAEV to obtain the requested charging
$confirm\_ID$	Reservation confirmation ID of the CAEV for the confirmed charging reservation
$curr\_balance$	Current balance of the CAEV's user account in CPs
$curr\_SoC$	Current SoC of the CAEV (%)
$curr\_speed$	Current speed of the CAEV (km/h)
$dest\_ID$	Final destination ID of the CAEV
dur	Estimated charging duration of the CAEV at a CN (min)
E_{deliv}	Energy delivered by the EVSE to the CAEV's Battery
$\mathrm{E}(\hat{\theta})$	Expected value of the estimator
$EVSE_{reserv}$	EVSE that has been reserved for a charging session at a CN
$EVSE\_ID$	ID of the EVSE of a CN that is reserved for the CAEV to obtain the requested charging
$\hat{e}(t)$	The difference between the capacity of the battery and the energy stored in it at time t
end_time	Reservation end time for CAEV to receive charging from a reserved EVSE at a CN

F_{req}	Charging Reservation Request Frame
$F_{confirm}$	Charging Reservation Confirmation Frame
g_{WCP}	Gap between two WCPs installed in series (m)
H	Half-length of the confidence interval
λ	Throughput of a system
$\hat{\lambda}$	Long-run average arrival rate or throughput
L	Average number of CAEVs in a system at any given time unit
$\hat{L}$	Long-run average number of CAEVs in a system at any given time unit
L_{Axy}	All map location nodes that fall in A_x and in sub-region y
$L(t)$	Number of CAEVs in the system at time t
l_{EVSE}	Length of EVSE (m)
l_{track}	Length of the charging track (m)
l_{WCP}	Length of a WCP (m)
loc_ID	Location ID of the EVSE of a CN that is reserved to deliver charging to the requesting CAEV
N	Number of arrivals
$\mathrm{N_A}$	Number of CAEV arrivals
N_D	Number of CAEV departures
N_{days}	Number of days for simulation
N_{EVSE}	Total number of EVSEs
N_{ts}	Number of time slots needed for a charging session
N_{ts}^{EVSE}	Number of time slots per EVSE of a CN
N_{WCP}	Total number of WCPs
N_{WCP}^{EVSE}	Total number of WCPs per EVSE
n	Number of observations
n_{Axy}	All map nodes that fall in A_x and in sub-region y
ϕ	Mean measures of performance for continuous-time data
$\hat{\phi}$	Sample mean based on sample size n for continuous-time data
P_a	Probability of an accident to occur on a DWCN highway lane
P_s	Probability of a CAEV to skip the charging session
pos_x	CAEV's current x position reading (m)
pos_y	CAEV's current y position reading (m)
Q	The total wait time spent in a queue of a CN
$Q_{EVSE_{reserv}}$	The queue of an EVSE at a CN
ρ	Proportion of time server is utilized
R	Number of replications
$\bar{r}$	Maximum charging rate of the on-board charger

$r(t)$	Pilot signal passed to the battery
$\hat{r}(t)$	Charging rate to charge a battery at time t
r_{acc}	The rate of acceleration and deacceleration of a CAEV
r_{charge}	Charging rate of an EVSE of a CN
r_{CP}	Rate of purchasing 1 CP virtual currency (CAD)
r_{energy}	Rate of delivering 1kWh energy (CAD)
r_{steer}	The rate of steering to the right and left of a CAEV
req_ID	Randomly generated unique reservation request ID for the CAEV
req_SoC	Requested SoC by the CAEV (%)
S	Standard deviation
S^2	Variance
S_{CN}	Set constant speed for the CAEV to receiving charging from the CN (m/s)
S_{tol}	Set speed tolerance for the CAEV to receive charging from the CN
SoC	State-of-charge of the battery
SoC_{CC}^{left}	Battery SoC request unfulfilled by the CCN
SoC_{DWC}^{left}	Battery SoC request unfulfilled by the DWCN
SoC_{req}	Battery SoC requested by the CAEV for charging reservation
SoC_{SWC}^{left}	Battery SoC request unfulfilled by the SWCN
$source\_ID$	Current location ID of the CAEV
$start\_time$	Reservation start time for CAEV to receive charging from a reserved EVSE at a CN
θ	Mean measures of performance for discrete-time data
$\hat{\theta}$	Sample mean based on sample size n for discrete-time data
T	Total simulation time
T_{CC}^{dur}	Charging duration of a charging session at CCN (min)
T_{CN}^{dur}	Charging duration of a charging session at a CN (min)
$T_{dur}^{ts_{extrac}}$	Charging duration of the time slots extracted (min)
T_{DWC}^{dur}	Charging duration of a charging session at DWCN (min)
T_E^{CN}	End time of the charging session at a CN (min)
T_i	Total time from [0,T] which contained i CAEVs
T_Q	Average waiting time per CAEV spent in a queue of CN
Ts	Average service time per CAEV for a system or CN
T_S^{CN}	Start time of the charging session at a CN (min)

T_{SWC}^{dur}	Charging duration of a charging session at SWCN (min)
T_{tarr}	True arrival time of the CAEV at a CN
T_{tdept}	True departure time of a CAEV from the system (min)
T_{track}	Time to cover the length of the charging track (s)
$t_{\frac{\alpha}{2},R-1}$	Quantile of t-distribution with R-1 degrees of freedom at cuts off the area of each side of the t-distribution's tail by $\frac{\alpha}{2}$
th	Transition from the bulk stage to the absorption stage of the charging process
th_{CC}	Threshold of charging CC can provide to a CAEV battery (%)
th_{DWC}	Threshold of charging DWC can provide to a CAEV battery (%)
th_{SWC}	Threshold of charging SWC can provide to a CAEV battery (%)
$time\_arr$	Arrival time of the CAEV into the system (min)
$time\_dept$	Departure time of the CAEV from the system (min)
ts_{avail}	List of time slots available for reservation of an EVSE
ts_{dur}^{CN}	One time slot duration set for a CN (min)
ts_{extrac}	List of time slots extracted from the available time slots of an EVSE
ts_{left}	List of time slots that are left over
ts_{reserv}	List of time slots reserved for a CAEV at an EVSE of a CN
$type\_CN$	Type of CN to fulfill the charging request of the CAEV
v_{curr}	Current velocity of CAEV
v_{recomm}	The recommended speed to travel over the charging track (m/s)
W_{tol}^{x}	Tolerance for alignment on the x-axis (m)
W_{tol}^{y}	Tolerance for alignment on the y-axis (m)
W_x^S	Embedded WCP's starting position on the x-axis relative to the road or ground (m)
W_x^E	Embedded WCP's ending position on the x-axis relative to the road or ground (m)
W_y^S	Embedded WCP's starting position on the y-axis relative to the road or ground (m)
W_y^E	Embedded WCP's ending position on the y-axis relative to the road or ground (m)
w	Average system waiting time for a CAEV
$\hat{w}$	Long-run average wait time
$\bar{Y}$	Point estimator
$Y(t)$	Simulation's continuous-time data
Y_i	Discrete-time simulation data's ith observation

Chapter 1 Introduction

1.1 Short Background

The existing privately owned transportation model is comprised mostly of vehicles with internal combustion engines. The fossil fuel powered vehicles contribute to noise and air pollution, lead to parking issues in densely populated cities, and have low utilization rates [1]. Traffic demand in urban transportation systems is increasing quickly due to rapid urbanization, thus resulting in traffic congestion coupled with air pollution. For instance, [2] listed Montreal, QC, Canada as the 19th most traffic congested city across the globe with an average person spending 63 hours per year stuck in traffic during on-peak periods. Further, the reported greenhouse gas (GHG) emissions produced by the transportation sector totaled 186 megatons of CO_2 for the same year [3]. Since the world urban population is predicted to increase by 2.5 billion at the end of 2050, the current transportation model is deemed environmentally unsustainable for the future [4], [5]. The best solution to this problem would be the convergence of three emerging key technologies: electric vehicles (EVs), autonomous vehicles (AVs), and mobility-on-demand (MoD).

First, EVs are an efficient alternative to internal combustion engine vehicles in terms of costs and quality of driving [6]. EVs have the potential to dramatically reduce CO_2 emissions and dependence on oil, and promote the generation of renewable energy for a positive environmental impact [7]–[10]. However, EVs are still not as widely adopted due to shorter driving range and longer charging times [11], [12]. To address the challenge, many companies like Charge Point, Siemens, BP and Shell [13], EV manufacturers like Tesla [14], and Renault [15], and countries like US [16], [17], Canada [18], [19] and UK [20] have started initiatives to build a large number of charging stations with fast chargers. Investing in the construction of large charging stations is only profitable if a large number of EVs exist [21]. However, consumers are more likely to buy EVs only if the charging stations are available in the first place.

Second, autonomous EVs (AEVs) are predicted to provide a safer and higher quality of transportation [22]. AEVs also enable mobility for people unable or unwilling to drive [22], [23]. More importantly, vehicle automation would significantly save labor costs, as no human drivers will be needed. Shared AEVs (SAEVs) can further reduce traffic jams, GHG emissions and transportation costs by increasing vehicle utilization and opening up parking spaces [24]. Ride-hailing services are a clear initial market for SAEVs. The prior will lead to a transformational technology known as autonomous mobility on-demand (AMoD) whereby

SAEVs provide personal on-demand transportation for individuals, or small groups of commuters [25]. Other advantages include the fact that car ownership is reduced, and less up-front charges which means low-income people may be better served [26], [27].

Wireless power transfer (WPT) is of interest, as it can alleviate concerns of wired EV and AEV charging by reducing battery cost, recharge time and weight [28]. Three types of wireless charging exists: 1) Static wireless charging (SWC) enables charging an EV while parked, 2) Quasi-dynamic charging systems are installed in dynamic environments like bus stations, traffic lights and taxi stops to provide charging while parked, and 3) Dynamic wireless charging (DWC) systems are installed on long tracks of roads to charge EVs in motion [29]. The most promising WPT technique with high power transmission over longer charging distances is magnetic resonance coupling due to its efficiency of 96 % at resonant frequency [30]. It is an active area of research, and ways to deploy this technology in a cost-effective manner on a wider scale are being explored.

In 2019 the overall number of EVs on road was 7.2 million, and it is estimated to be 245 million by 2023 with a projected electricity demand of 550 TWh [31]. These EVs seeking charging randomly from public charging stations are susceptible to long waiting times and risk running out of battery. As the number of EV increases, a smart charging infrastructure is required to avoid power allocation failures and to optimize the electricity flow across the city's smart grid. The existing literature [32]–[35] focuses on determining the timing of wired charge scheduling of EVs charging demand management. The few papers that exist for wireless charging like [36], [37] are strictly for SWC. Even fewer papers like [38], [39] exists for only charging management of DWC of electric buses in controlled lab like environments. So, the powerful combination of EVs, AEVs and MoD enabled by WPT and Internet of Things (IoT) is considered in this thesis.

IoT is made up of various objects called smart devices that are interconnected via the internet for collecting, refining, processing, and communicating important information over a network [40]. Connected and autonomous EVs (CAEVs) are part of the IoT [40] and the future smart city by being able to access the internet and communicate with surrounding vehicles and infrastructures using Vehicle to Vehicle (V2V), Vehicle to Infrastructure (V2I) and Vehicle to Grid (V2G) communications [41]. CAEVs [37] are the key to successfully build an intelligent charging network infrastructure for intelligent transportation system (ITS).

1.2 Motivation

The existing transportation system is mainly comprised of fossil fuel powered vehicles contributing to GHG emissions, which are involved in traffic congestions and are unsustainable for the future. A trend towards EVs is noticed. However, EV adoption has both psychological and technical barriers like range-anxiety that is the fear of running out of charging, heavy and expensive batteries, long waiting times at charging stations, and long charging times. WPT is seen as the solution to overcome these barriers and boost adoption rates of CAEVs. The WPT systems in comparison to existing wired systems are relatively easy to use with park and charge actions and are much safer with elimination of wires. In particular, the DWC systems can facilitate reduction in battery costs and weight as the CAEV receives charging on the move. These CAEVs may still be vulnerable to traffic congestion, as they roam around randomly seeking for charging with range-anxiety. Even if the CAEV makes it to the charging station they may have to suffer long waiting times. There is a need for a smart charging infrastructure with charging reservation and trip planning system to help enable CAEVs to receive charging as it travels to its destination on the shortest route possible. Further, the smart charging infrastructure needs to be interoperable with not only existing wired charging systems but also future wireless charging systems to be future proof. Such an IoT powered system can unlock the potential of CAEVs and completely shift the paradigm of current and future transportation systems.

1.3 Objectives

This thesis aims to present a novel intelligent charging network infrastructure that can facilitate static and dynamic wireless charging systems. The system should be able to operate with the existing wired charging infrastructure and standards for ITS in a smart city. It also will enable IoT applications like charging reservation and trip planning systems. A charging reservation and trip planning system application would then be designed to fulfill large charging requests dynamically over different types of wired and wireless charging networks falling along the shortest route of a CAEV user's requested trip. To exchange a CAEV user's request and reservation confirmation information securely, light-weight message frames would be designed. The system application would aim to reduce the charging station waiting time, payments, travel cost, traffic congestion and energy consumption for each CAEV's trip with one or more charging reservations over several charging networks of different types. To ensure vehicle owner's anonymity and privacy, the IoT system application will securely service and bill the CAEV users in real-time with suitably designed billing methods and payment schemes.

Additionally, wireless charging system issues like misalignment errors, speed issue errors, charge stealing or free-riders, unfair billing and road accidents on DWC systems would be addressed by the accompanying handshake protocol to ensure safe and proper delivery of charging. Lastly, to address the lack of DWC systems and their standards, a DWC design specification tool would be created. The design specification tool would automatically build a DWC system from given input parameters for realistic testing and simulation. It is an essential part of the objectives to develop a simulation tool to carry out all these sophisticated functions.

1.4 Thesis Contributions

The following are the main thesis contributions:

1. The development of a novel three-layer scalable system architecture and charging network hierarchy with accompanying handshake protocol and light-weight message frames enabling dynamic fulfillment of charging requests over one or multiple charging networks of static wired, static wireless or dynamic wireless charging type.
2. The provision of the built in interoperability of the architecture that makes the system compatible with existing wired charging infrastructure and its standards, and contributes to the developing wireless charging standardization efforts led by the International Organization for Standardization (ISO), the International Electrotechnical Commission (IEC) and the Society of Automotive Engineers (SAE) [42]–[44]. This system can then be used as a framework for actual implementation by government and private agencies to build future-proof and sustainable CAEV charging networks.
3. The design and implementation of a discrete event simulator of a charging reservation and trip planning system, which can work both independently and in combination with other simulators like Caltech's ACN-Sim [45].
4. The development of a handshake protocol that inadvertently helps avoid free-riders on the DWC lane with authentication and synchronization schemes, allows the CAEV to leave the highway lane and resume charging on the same lane, and also fairly deals with accidents and breakdowns on the DWC lanes.
5. The development of the detection and reporting of misalignment error and speed issue error to the CAEV that feeds as input to the automated driving feedback system, is presented for wireless charging systems to ensure safe and efficient delivery of charging.
6. The provision of the architecture and protocol that can accommodate two kinds of fair real-time metered billing schemes which use encrypted virtual currency for secure

charging session payments over different types of charging networks. The billing schemes maintain anonymity and location privacy of the CAEV user, but with traceability of the charging reservations.

7. The development of the DWC network design specification tool that can help implementers build DWC lanes with their desired parameters and design goals, thus saving cost and time of deployment.

1.5 Thesis Outline

Chapter 2 conducts a literature survey on existing WPT technologies that guides the development of the presented charging system architecture and handshake protocol in Chapter 3. Chapter 4 details the design of the discrete event simulator that helps realize the system architecture in Chapter 3 as a charging reservation and trip planning system. Next, the simulated results are collected, verified and validated against other alternative systems for analysis, comparison and discussion in Chapter 5. Chapter 6 concludes this thesis along with discussions of possible future direction of the work presented.

1.6 List of Publications

The following are the list of publications produced from this thesis work:

1. P. W. Shaikh and H. T. Mouftah, “Connected and Autonomous Electric Vehicles Charging Reservation and Trip Planning System”, *Proceedings IEEE IWCMC’2021 Vehicular Communications Conference,* Harbin, China, June-July 2021, pp. WM-4.6.1-WM-4.6.6
2. P. W. Shaikh and H. T. Mouftah, “Intelligent Charging Infrastructure Design for Connected and Autonomous Electric Vehicles in Smart Cities”, *Proceedings IEEE IM 4th International workshop on Intelligent Transportation and Autonomous Vehicles Technologies (ITAVT2021)*, Bordeaux, France, May 2021, pp. 992-997.
3. P. W. Shaikh and H. T. Mouftah, “Handshake Protocol and Design of Connected Autonomous Electric Vehicles Charging Reservation and Trip Planning System”, submitted to IEEE Transaction on Intelligent Vehicles.
4. P. W. Shaikh and H. T. Mouftah, “Survey on Wireless Electric Vehicle Charging Systems in Smart Cities”, submitted to IEEE Communications Surveys and Tutorials.

The following are the list of other publications:

1. P. W. Shaikh and I. W. Damaj, "Analysis of Pipelined KATAN Ciphers under Handle-C for FPGAs," *2018 International Conference on Innovations in Information*

Technology (IIT), 2018, Al-Ain, UAE, Nov. 2018, pp. 163-168, doi: 10.1109/INNOVATIONS.2018.8606012.

2. P. W. Shaikh, M. El-Abd, M. Khanafer and K. Gao, "A Review on Swarm Intelligence and Evolutionary Algorithms for Solving the Traffic Signal Control Problem," in *IEEE Transactions on Intelligent Transportation Systems*, doi: 10.1109/TITS.2020.3014296.

Chapter 2 State of the Art – Wireless Electric Vehicle Charging Systems

2.1 Introduction

Internal combustion engine vehicles are identified as a major source of GHG emissions. The convergence of electrification, automation and WPT technologies presents a perfect solution for the sustainability of both the environment and the transportation system. In ITS, a typical application of IoT is the IoV where the smart devices are restricted to vehicles. IoV helped boost the emerging technology of connected vehicles (CVs), which can interconnect with other CVs and surrounding infrastructures using V2I and V2V communication technologies, respectively [46]–[50]. These CVs are typically equipped with an on-board unit (OBU) possessing data storage, processing and communication capabilities, global positioning system, and sensors. ITS and CAEVs together with IoV have the potential of creating a more efficient and sustainable transportation system. To increase the adoption rate of the CAEVs, three broad types of charging options have been researched: 1) Battery Swapping, 2) Cabled Charging (CC) and 3) WPT.

Battery swapping method extensively explored in [51]–[59] involves having a reserve of batteries that are fully charged, and whenever an EV needs charging it will swap its depleted battery with one of the batteries that is fully charged within a short span of time. It was conceptualized to address the long charging times and long waiting times at CNs. However, this method has not been successful in reality due to lack of standardizations for type, size, power and method of charging batteries. Further, it is difficult to carry fully charged batteries for all types of EVs in the market, and this method proved expensive for not only the consumers but also for the companies that provided such services. For instance, the Israeli company Better Place lost $812 million and went bankrupt [60]. Though, a Chinese battery swapping company, Nio, in 2020 claimed that in its three years of operation it has completed 500,000 battery swaps with 143 swapping stations in over 58 cities, and is very optimistic about its expansion [61]. But, scaling the operation to other countries like Canada with severe temperature changes coupled with the absence of standards makes battery swapping still an unrealistic and expensive business model.

CC or wired charging approach is the one most widely used and researched today as evident in [62]–[72]. This reliable option has universally accepted and available standardization specifications. In contrast to the fossil fuel alternatives, CC systems are also cheap and environmentally viable in the long-term to fulfill low emissions goal. However, its

users might be prone to electric shocks if its aging components are not properly maintained. It is also highly unpredictable in harsh environments like dust and underwater, thus putting the user's safety at risk. The convenience of use is also compromised due to long charging times and scheduling charging during off-peak times. Further, it is unsuitable for automatic operation applications.

The main focus of this chapter is on WPT. Compared to CC, WPT offers considerably higher safety. It saves its users from electric shock by eliminating the electric contact between the vehicle and the charging unit thanks to the wireless nature of charging. It is more suitable for automatic applications with built-in user friendliness where the EV user just needs to drive the vehicle onto the charging area while keeping proper alignment in mind to efficiently receive charge. Wireless charging for EVs can be done using stationary or static wireless charging (SWC), quasi-dynamic wireless charging (QWC), and dynamic wireless charging (DWC) systems. These WPT charging systems for EVs are more convenient, as battery cost, recharge time, and weight can be reduced [28].

The purpose of this chapter is to give a general overview of all the different types of WPT technologies that exist in literature. This chapter also highlights the different aspects of wireless electric vehicle charging systems (WEVCSs). It surveys the available and developing SWC and DWC systems' design and architecture, optimal charging schedules, billing and reservation schemes and future trends. The WEVCSs are also advocated to increase the proliferation of CAEVs in smart cities for a safer, economical and sustainable transportation system.

This chapter's section 2 outlines and compares the existing and recent WPT technologies. Section 3 surveys WEVCSs focusing on SWC and DWC systems and their additional features, wireless charging infrastructure allocation problem, charging reservation systems, and optimization of CAEV routes with charging scheduling. Future trends and novel concepts for WEVCS are explored in Section 4. Section 5 addresses the hurdles to the adoption of CAEVs. Finally, Section 6 concludes this chapter.

2.2 Wireless Power Transfer Technologies

WPT technologies can be categorized based on distance and can be further divided based on the medium for WPT. In near-field WPT, we have magnetic coupled WPT (MC-WPT) and electric coupled WPT (EC-WPT). In far-field WPT, we have optical WPT (OWPT), ultrasonic transcutaneous energy transmission (UTET) and microwave radiation WPT (MR-WPT). Figure 2.1 provides an overview of all the existing types of WPT technologies.

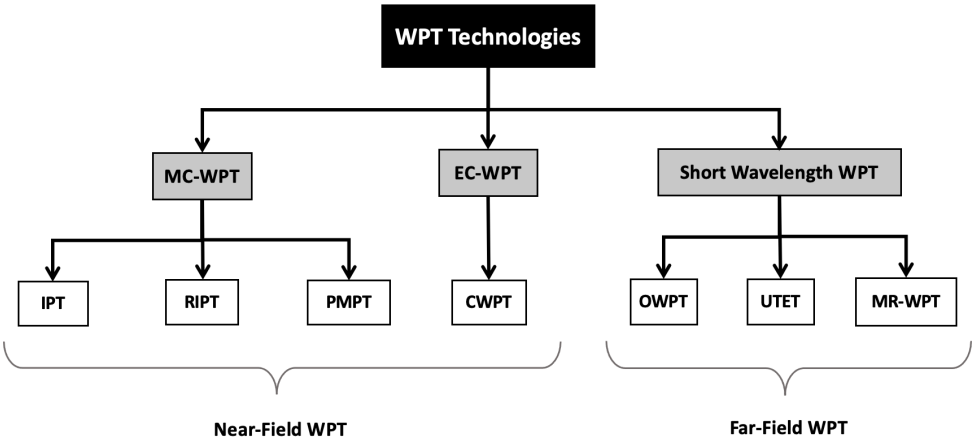

Figure 2.1: Overview of existing and recent WPT technologies.

2.2.1 Near-Field Wireless Power Transfer

A. Magnetic Coupled Wireless Power Transfer (MC-WPT)

i) Inductive Power Transfer (IPT)

Nikola Tesla in 1914 was able to demonstrate WPT by successfully illuminating phosphorescent lamps with Tesla coils using IPT [73]. This technology uses the law of electromagnetic induction, and has been tested and used in low to high power applications. With an air gap of 0.5 mm for WPT, IPT is highly efficient with 99.5% efficiency at 6.6 kW power level [74]. General Motors (GM) introduced the Chevrolet S10 EV in 1996, which was charged by the Magne-Charge IPT (J1773) system to provide Level 2 (6.6 kW) slow and Level 3 (50 kW) fast charging [75]. Soon after, the Magne-Charge became a popular IPT application. University of Georgia's research work [76] demonstrated their Level 2 (6.6 kW) IPT EV charger that used a 10 kW coaxial winding transformer to charge battery voltages from 200-400 V at 77 kHz operating frequency [76].

ii) Resonant Inductive Power Transfer (RIPT)

RIPT is the most well-known and advanced version of the traditional IPT, in terms of design, power electronics and wireless transformer coils. RIPT is able to achieve a better balance between air gap distance and power transfer efficiency compared to IPT by using double-tuning to achieve air gap distances of up to 50 cm. The power supplied from the grid to the RIPT system is converted several times within the system with primary DC-AC conversion holding the most importance. The most commonly used DC-AC module for EV charging is the full bridge inverters due to their ability to produce high-power capacity while obeying wireless charging standards for frequency operation (81.38 kHz–90 kHz) [77]. The commercially available DRIVE 11 RIPT system of WiTricity [78] for EV charging achieves a proven 94.0% efficiency at 11 kW power level with air gap distance ranging from 10 to 15 cm.

iii) Permanent Magnetic Coupling Power Transfer (PMPT)

It is distinguishable with its use of magnetic interaction between synchronously rotating permanent magnets (PMs) for magnetic coupling [79], [80]. The pros of PMPT technology is in its ability to operate at low frequencies to effectively eliminate problems of electromagnetic field exposure and foreign object heating [81], [82]. But, it is still vulnerable to noise, vibration, and harshness issues [81], [82]. Compared to other options of WPT, it has relatively low efficiency due to low power level and low frequency level operations at larger air gap distances. The choice of PM's material and selection of the rotation speeds is also critical. In [80], the lab prototype of 1.6 kW is demonstrated to transfer power with an air gap of 15 cm at 81% efficiency. However, at 159 Hz the PMs begin losing synchronization speed and their transmission power is significantly impacted. So, the speed of the PMs require constant adjustment with the help of feedback systems from the secondary side to the primary side to prevent upper power limit form exceeding. Hence, PMPT is advocated for static WPT rather than dynamic WPT applications in [83]. Elix Wireless Charging Systems Inc. in collaboration with the University of British Columbia announced its 10 kW WPT solution for static charging using PMPT technology in 2013 [79], [80], [84].

B. Electric Coupled Wireless Power Transfer (EC-WPT)

i) Capacitive Wireless Power Transfer (CWPT)

This technology uses coupling capacitors to enable low-cost and low-power but small air gap WPT applications such as portable electronic devices, phone chargers, and rotating machines [85]–[87]. Compared to MC-WPT, CWPT offers no core losses and a simpler and compact design with its use of advanced geometric and mechanical structures of the coupling capacitors [88]. CWPT systems are also superior in safeguarding against electromagnetic field exposure by containing almost all of the electric flux inside the dielectric materials [14], and its electric field's direction is controllable [89]–[92]. In [89], the CWPT system is able to achieve an efficiency of 84% at 30 W power level with 5 mm air gap. The CWPT system in [93] uses inductors in series with the capacitors to allow for both high voltage and low current operation unlike IPT. The size of the coupling capacitors and the distance between the two plates characterizes the level of power transfer in the system. Hence, CWPT offers high performance for small air gap applications [94]. CWPT is largely lacking due to inadequate power capacity at larger air gap distances [95] and voltage constraints [88], [89] compared to MC-WPT options excluding PMPT. In [88] utilizing the restriction of small air-gap in CWPT, the authors have proposed the use of EV's bumper as a receiver for receiving charging at 83%

efficiency with less than 1 kW power and 540 kHz operating frequency. In contrast, authors in [96] suggest high capacitance coupling designs for CWPT systems to enable high power EV charging with larger air gaps.

2.2.2 Far-Field Wireless Power Transfer

A. Short Wavelength Wireless Power Transfer

Optical waves, ultrasonic waves and microwaves have been researched for long distance WPT. According to [97], the basic principle of operation involves converting the electrical energy to be transmitted into optical energy, ultrasonic or microwaves to travel through the air, and the receiver upon reception converts it back into electrical energy for use.

i) Optical Wireless Power Transfer (OWPT)

It provides the highest power density WPT compared to existing technologies, but more research needs to be conducted to prove safe operation for commercial deployment in all kinds of environments [98], [99]. Due to its optical nature, it is inherently free of flux guidance. Researchers in [100] have proved 84% efficient WPT at 30 kW with an impressive air gap of 1 mile. The OWPT system using optical antenna embedded within the solar panel is proposed in [99] to increase the output power efficiency of a solar panel by 40% compared to regular solar panels. A design for optical WPT using light fidelity (Li-Fi) for WPT in ad-hoc vehicular networks is proposed due to Li-Fi's inherent characteristics of safety, efficiency and high speeds, but laboratory testing is yet to be done [101]. A hybrid system in [98] is presented that achieves 150 mw optical power with 10 MHz data transmission, but the system has less than 20% overall WPT efficiency. These systems are promising with large distance operation, but are not mature enough for reliable performance in high power applications.

ii) Ultrasonic Transcutaneous Energy Transmission (UTET)

This is highly inefficient and costly to build, deploy and maintain. But, it is suitable for non-radiative applications that require multi-device charging like smart and personal devices with the help of non-directive field [88][102]. In [103], only a poor 39% WPT efficiency was achievable with 360 mW power at a distance of 30 mm, while in [104] no more than 25% WPT efficiency was possible. The paper in [102] attempts at increasing the power efficiency of UTET systems with the proposed spider clamp method, and compared against the traditional silver epoxy attachment method the experimental results demonstrated an overall 28% increase in power transfer efficiency.

iii) Microwave Radiation WPT (MR-WPT)

It has diverse applications ranging from monolithic microwave integrated circuits to solar power satellites [105]–[107] due to its ability of reemitting power as either directive or nondirective and freedom from proper alignment in both near and far field operations. Unfortunately, it is inefficient and vulnerable to field exposure. In [106], the system was able to achieve 59.2% efficiency at 10 kW power level with an air-gap of 1.2 m, whereas the system presented in [108] achieved a dismal 5.01% at 250 mW power level within 1.0 m distance.

Table 2.1 below summarizes and compares the different WPT technologies in terms of the type of WPT technology, performance characteristics like efficiency, power level, electromagnetic interference and frequency of operation, cost-effectiveness, design complexity, and suitability level for WEVCS. It is clearly understood from Table 2.1 that RIPT systems are highly suitable for high power and efficient WPT applications like CAEV charging. Hence, RIPT is widely used to develop wireless charging systems for EVs and are considered in the development of future ITS applications like charging scheduling.

Table 2.1: Comparison of all existing WPT technologies for WEVCS applications.

Field of Operation	Near-Field				Far-Field		
WPT Technology	**IPT**	**RIPT**	**PMPT or MG-WPT**	**CWPT**	**OWPT**	**MR-WPT**	**UTET**
Coupled Type/Power Carrier	Magnetic Coupled			Capacitive Coupled	Short wavelengths		
Power Efficiency	High ≥95%	Medium to High ≥95%	Medium to Low ≤81%	Medium to Low ≤84%	Medium to Low ≤84%	Low ≤39%	Medium to Low ≤59%
Power Level	Medium to High	Medium to Low	Medium to Low	Low	Medium to Low	Medium to Low	Medium to Low
Electromagnetic Interference Level	Medium	Low	High	Medium	Low	Low	Low
Range of Operational Frequency (kHz)	[10, 50]	[10,50]	[0.05,0.500]	[100,600]	[4 x 10^{11}, 7.5 x 10^{11}]	[3 x 10^{6}, 3 x10^{8}]	[0.002, 1.2x 10^{7}]
Cost-effectiveness	Medium to High	Medium to High	High	Low	Medium to High	Medium to High	Medium to High
Design Complexity	Medium	Medium	High	Medium	Medium	Medium	Medium
Suitability for WEVCS	High	High	Medium to Low	Medium to Low	Medium to Low	Low	Low

2.3 Wireless Electrical Vehicle Charging Systems

2.3.1 Static Wireless Charging

SWC requires minimal participation of parking from the EV driver to receive charging, and this ultimately eliminates the risk of tripping over cables or getting electric shocks like in CC. Figure 2.2 shows a typical SWC system that has a primary coil either installed above or below ground with additional power converters and circuits that comprise a ground assembly

(GA). The receiving coil is installed under the EV's chassis that after receiving energy converts it from AC to DC to charge the battery with the help of a power converter. The latter complete circuit along with some wireless communication network, power control, and battery management system makes up the vehicle assembly (VA). The GA and VA communicate with each other to ensure safe operation and transfer of power over the designated air gap. The charging times are highly dependent on the type of WPT system used, power level chosen, air gap and the charging pad size. SWC systems are typically installed in home garages and parking lots.

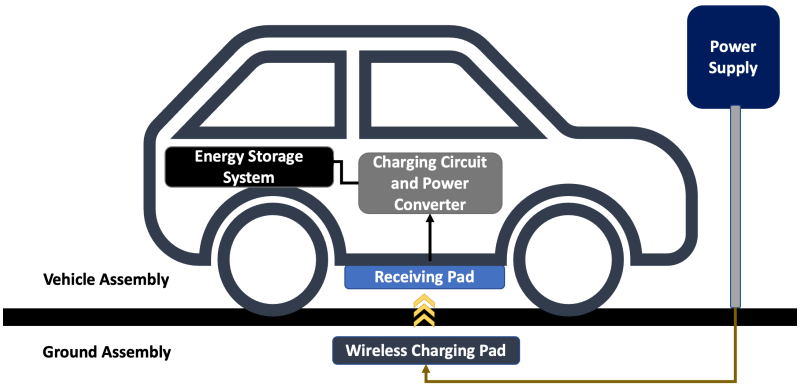

Figure 2.2: Overview of the basic SWC system.

In [109], a parallel tuned WPT system with a geometrically optimized circular resonator is proposed that can transfer power over an air gap of 0.20 m at 85% efficiency. Reference [110] proposes a SWC system with double D coils, which allows for a charging area that is four times larger than that provided by circular coils given the same cost and dimensions. Authors in [111] discuss EV charging system that employs asymmetric resonator, and in fast-charging mode this WPT system can achieve 15 kW output power over 0.15 m air gap with 0.20 m vertical and 0.40 m horizontal displacement from the charging pad. A current/constant voltage (CC/CV) charging of the battery in SWC system is presented in [112] with high misalignment tolerance. The system in [112] is controlled by a primary controller without any communication channel, and is able to control CC/CV well even when misalignment occurs due to mutual inductance estimation. With the usage of resonant frequency, the latter system makes no compromise on the WPT and efficiency, and promises practical application.

Control modules in wireless charging systems take load variation, overvoltage and overcurrent into account to make necessary adjustments with feedback assistance from the battery. The control module in [113] may even stop charging the battery to ensure safe operation. Control strategies in WEVCs have the objectives to regulate constant DC output

voltage and maximizing efficiency tracking. A control strategy based on load-phase angles is presented in [111] to supply a controllable output voltage to charge different EVs over larger air gaps with high tolerance to misalignments. This strategy enables tracking optimum operating frequency point even as the mutual inductance varies [111]. Typically, a controllable rectifier and DC-DC converters are used to easily regulate output voltage. Maximizing the system efficiency is a challenge due to aging components, different component tolerances, mistuning and load variations [113]–[117]. To maintain maximum efficiency point, usually frequency tracking, impedance matching and DC-DC conversion at one side of WPT is considered. For simplicity in high-power applications, frequency is kept at constant to follow operation in allowable bandwidths like in [118]. Single-side control is being researched due to its simplicity, reliability and low cost by eliminating vehicle sensors and using real-time calculation for load status [119]–[121]. Power control method at the transmission side is presented in [122] for optimal operating frequency where the receiving side regulates output voltage using reactive power compensation to save costs for the simple and compact wireless EV charger.

In [123], a prototype static wireless charger was built to charge EVs in UK parked on the streets, parking lots and home based on their modelling of a 500 W wireless charger to achieve an efficiency of 75% with strategic safety and operational testing. This initial model in terms of efficiency was not very impressive. However, it was able to demonstrate on a very small scale that SWC can mitigate several effects of wired EV charging like voltage violations, over-currents and system losses specifically in the UK. A modelling study is conducted in [124] for determining the design trade-offs in electrifying the shuttle buses at Zion National Park, Utah, USA, with the National Renewable Energy Laboratory's WPTSim tool. The tool enabled determination of required battery capacity based on rated power at variable number of charging locations. It revealed SWC option is significantly better than overnight CC option in terms of cost if installed at the terminus of the route. Other costs saving measures presented included reducing battery sizes, incorporating charging time in the route schedule, and using cheaper WPT system components.

Many SWC systems for commercial use and revamping the public transportation have been made, tested and sold for public use. One of the popular SWC systems available for sale is WiTricity's DRIVE 11 [125] that has scalable charging rates of 3.6-11 kW to support new and upcoming EVs with 10-25 cm air gap. DRIVE 11 has equivalent performance to Level 2 CC, and claims maximum power efficiency of 94% with high misalignment tolerance of ± 10 cm horizontal and ± 7.5 cm vertical [126], [127]. Another popular SWC system that served

half the North American EV market is Evatran's Plugless L2 Wireless charging system [128]. Plugless L2 Wireless has a charging rate of 7.2 kW with 84-90% efficiency, an air gap of 10 cm with 17.8 cm ground clearance, and a transmission pad that can be only installed above ground unlike WiTricity's DRIVE 11 [129], [130]. Plugless L2 Wireless is the first WEVCS installed on a production fleet of European Driverless Shuttlebuses, and it is also the first to support Chinese EVs with its 10 cm air gap [131]. Wireless Advanced Vehicle Electrification (WAVE) states that it's the only one that commercially offers both SWC and QWC systems of up to 250 kW, and are developing 500 kW and 1 MW inductive WPT systems [132]–[134]. WAVE's first prototype and first US use of WPT in transportation application [134] was called Aggie Bus, a campus bus at Utah State University. Aggie Bus charged wirelessly at bus stops with power of 25 kW at 20 kHz over an air gap of 15-25 cm with 90% efficiency [132], [135]. These SWC systems have gone through rigorous testing in the real-world and are inching closer to become the option for EV charging everywhere. Specifically, these SWC systems could be utilized in building large scale charging network infrastructures at lower costs for IoT enabled ITS applications like charging scheduling and trip planning of CAEVs.

2.3.2 Dynamic Wireless Charging

SWC still takes a lot of time to charge. The EV also needs to stay stationary during the duration of charging, and the driving range of the EV is usually not very long. Hence, DWC systems are an attractive alternative that entails charging EVs in motion. DWC systems can reduce battery size and increase the driving range for an overall increase in EV charging and driving experience. The general DWC system design involves installing coils underneath the road for GA, and a receiving coil mounted under the EV as part of the VA. The transmitting coils are driven usually by high frequency current. Thus, turning the ordinary road into a power track ready to transmit power wirelessly to oncoming EVs with the receiving coils installed.

The credit for the first working prototype of DWC system [136] is given to the research-project Partners of Advanced Transit and Highways (PATH) of University of California [137]–[139] that started in the 1980s and continued until 1990s. The DWC system designed in [139] was able to transfer power at 60 kW over an air gap of 2-3 inches. An efficiency of 60% similar to a comparative SWC system was achieved for the DWC system as can be seen in Figure 2.3 (a) for velocities of 24 km/h and 18 km/h at high power levels. Figure 2.3 (b) analyzes the DWC of the bus at the first driving cycle (100% charging) and fifth driving cycle (30% charging). It is observed that the average power coupled to the bus increases as the battery level decreases, since it can accept larger charging currents. It is also proven that the WPT is

independent of vehicle velocity, and the lateral misalignment had very little effect on overall system efficiency [140]. However, performance of the DWC system was not impressive enough to translate it into a commercial product.

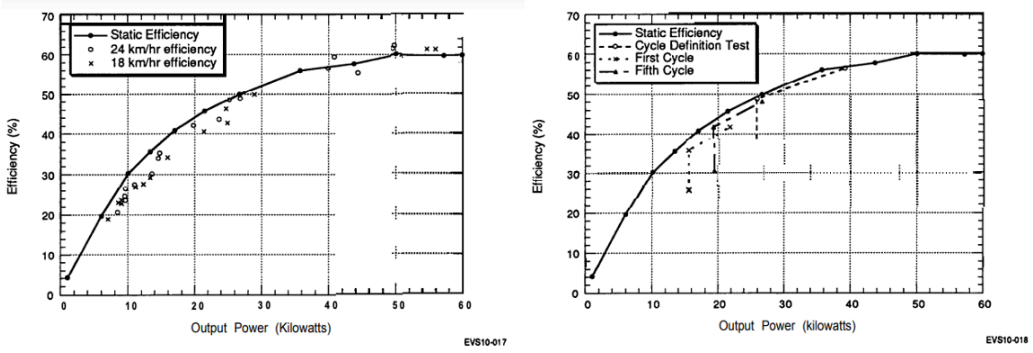

(a) (b)

Figure 2.3:(a) System efficiency as a function of output power-short dynamic tests and (b) System efficiency as a function of output power-driving cycle tests [139] .

Oak Ridge National Laboratory (ORNL) in the US in 2013 decided to build a prototype for demonstrating WPT for in-motion EVs [141] by laying circular shaped coils in series on a power track. A pick-up coil was installed underneath the in-motion EV, and the testing revealed that this initial system could receive charging at the power level of 2.2 kW with 74% efficiency. In [142], the ORNL in-motion WPT system for an on-campus modified Toyota Prius plug-in vehicle is investigated for power transfer efficiency at different air gaps as can be seen in Figure 2.4. The results confirmed that the power transfer efficiency maximizes with decreasing air gap, as the coupling coefficient increases between the coils. It is noted that the ORNL's DWC system at 125 mm air gap achieved power transfer efficiency of 97%. ORNL has also been doing research towards QWC and DWC systems for mass public transit [133], [143]. In 2018, the researchers at ORNL demonstrated a 120 kW WPT system for EVs that delivered 6 times the power of their previous ORNL WPT technology [144], [145]. The newer system co-optimized with latest silicon carbide power electronic devices is comparable in performance to CC systems by transferring power at 97% efficiency over an air gap of 6 inches [144], [145].

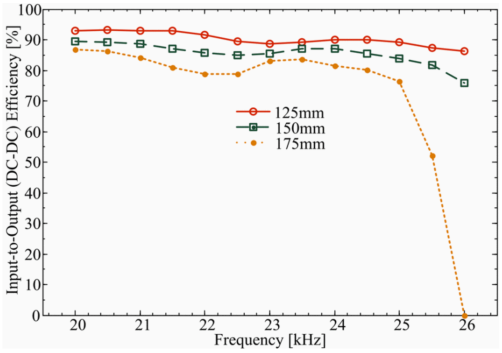

Figure 2.4: Effect of coil spacing on power transfer efficiency [142].

Korea Advanced Institute of Science and Technology (KAIST) in South Korea is often credited in literature for demonstrating the first feasible commercial DWC system for EVs in 2009 [146]. The DWC system used I-type pick up coils and U-type power supply rails to increase the air gap to 17 cm for WPT, and achieved the maximum output power of 60 kW with 72% efficiency. This DWC system was further developed into On-line EV (OLEV) system that specifically used Shaped Magnetic Field Resonance (SMIRF) technology [147]–[149] to help magnify electric waves and boost power transfer efficiency, and it was deployed in four locations in South Korea soon after its launch [147], [150]. Since 2012, two OLEV buses have been serving as shuttle busses at the KAIST campus in Daejeon [151], [152]. Reeling on their success, the authors in [146]–[149] modified the OLEV DWC system with an increased air gap of 20 cm and 83% maximum WPT efficiency, and deployed OLEV for eight electric buses with six power charging lanes in Gumi, South Korea [152].

In [153], key design and economic parameters of the OLEV system are analyzed for the closed environment commercial operation of the shuttle buses at KAIST. The first sensitivity analysis explored the optimal battery size against the battery costs as can be seen in Figure 2.5 (a). As the battery cost increased, the optimization model designed in [153] made suggestions of WPT systems with smaller battery sizes and more power transmitters. However, as the battery cost falls below $400, the model suggests a larger battery which has sufficient charge to eliminate the need for DWC. Next, it is depicted in Figure 2.5 (b) that as the cost of wireless power transmitter increases, the optimal number of power transmitter decreases and the optimal battery size increases. It is noteworthy that increasing battery size rather than increasing the length of the power transmitters is considered more cost efficient, as the power demand at the bus stations is more than farther down the route. The analysis of the number of shuttle buses in the closed operational environment revealed that increasing shuttle buses requires more batteries, and will increase the battery costs as can be seen in Figure 2.5 (c). The optimization model, as a result, tries to find a solution with smaller battery sizes and more power transmitters with increased length to be cost-efficient. Figure 2.5 (d) illustrates the fact that increasing the current stopping time of the shuttle for charging at the stop will increase the number of power transmitters, as the total length of power transmitter decreases. The latter will also result in a decrease in the battery size. So, it is more cost efficient to install smaller power transmitters at the bus station where more energy can be supplied. This designed general MIP model can be extended, and can serve as a heuristic for different transportation systems in the future.

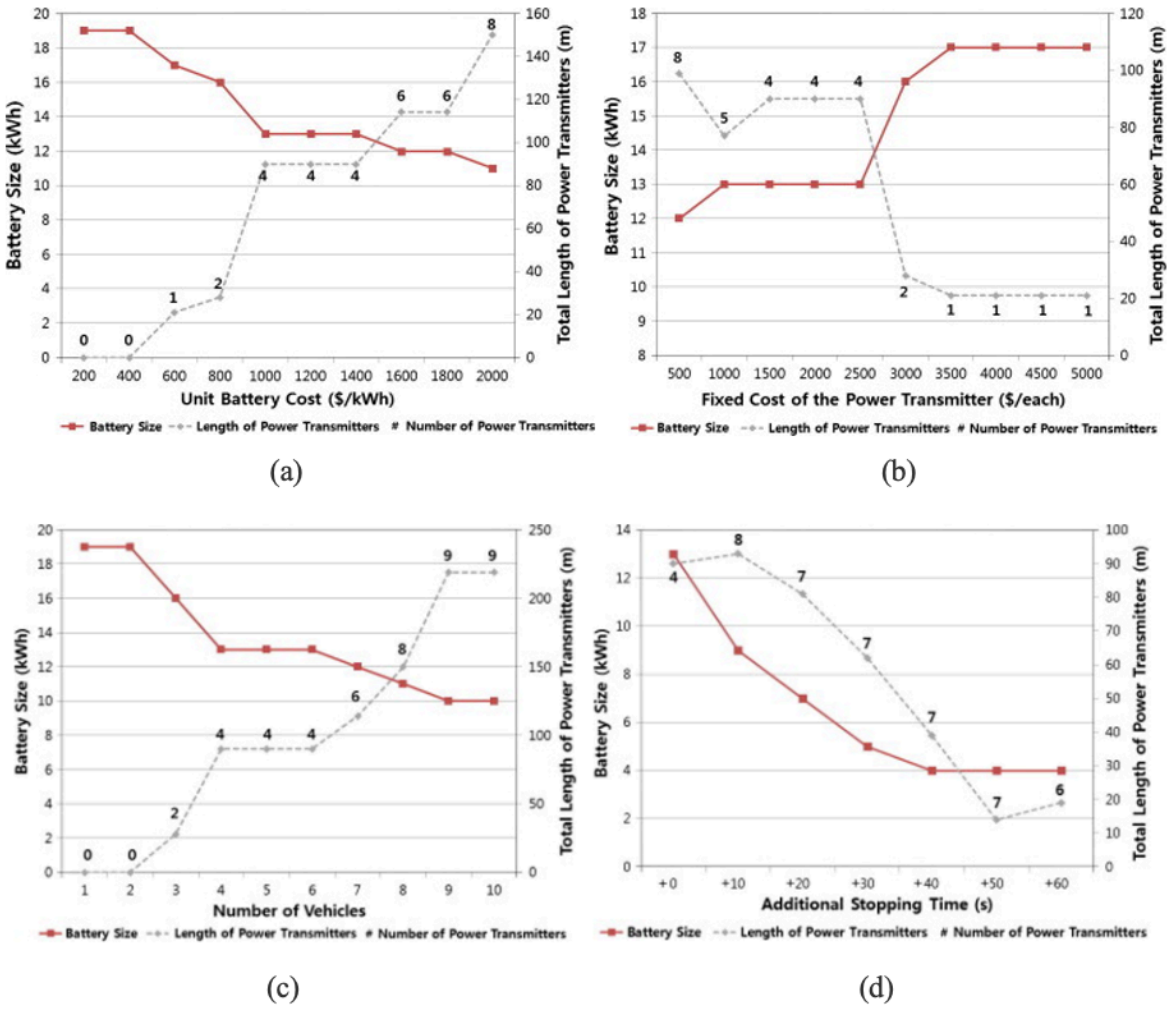

Figure 2.5: Sensitivity analysis for varying (a) unit battery cost, (b) unit inverter cost/unit inductive cable cost, (c) number of operating shuttles and (d) the stopping time of the designed dynamic wireless charging system of OLEV [153].

Recently, KAIST and Khalifa University (KU) in UAE in a joint-research effort have conducted in [154] a magnetic simulation and lab prototyping of SWC and DWC systems of length 1.4 m and 5.0 m for power lines, respectively. They were able to successfully achieve the maximum power efficiency of 90.8% for SWC and 85% for DWC prototypes in lab with maximum 12.7 kW output power when the EV was centered with 23 cm air gap. [155].

The process of wide deployment of this complex DWC technology has been costly and time-consuming, but it is defended as being the step in the right direction and worth the effort in [155]. Regarding the deployment, in general, the acceptance is relatively slow due to the lack of the standards in this field and application area of WPT systems for CAEVs. With lack of specifications and commercial DWC systems, even the design and construction of its track layout need to be carefully considered for creating efficient and safe DWC systems for CAEVs.

A. Track Layout

DWC systems create a continuous or pulsed wave of magnetic field for the EV over long sections of road. Roads transferring power wirelessly to the vehicles are often referred to as electrified roads, charging lanes or charging tracks. Now, the transmitting side of the DWC system can be constructed in two ways as depicted in Figure 2.6 (a) long tracks and Figure 2.6 (b) array of wireless charging pads (WCPs) track or segmented coil track.

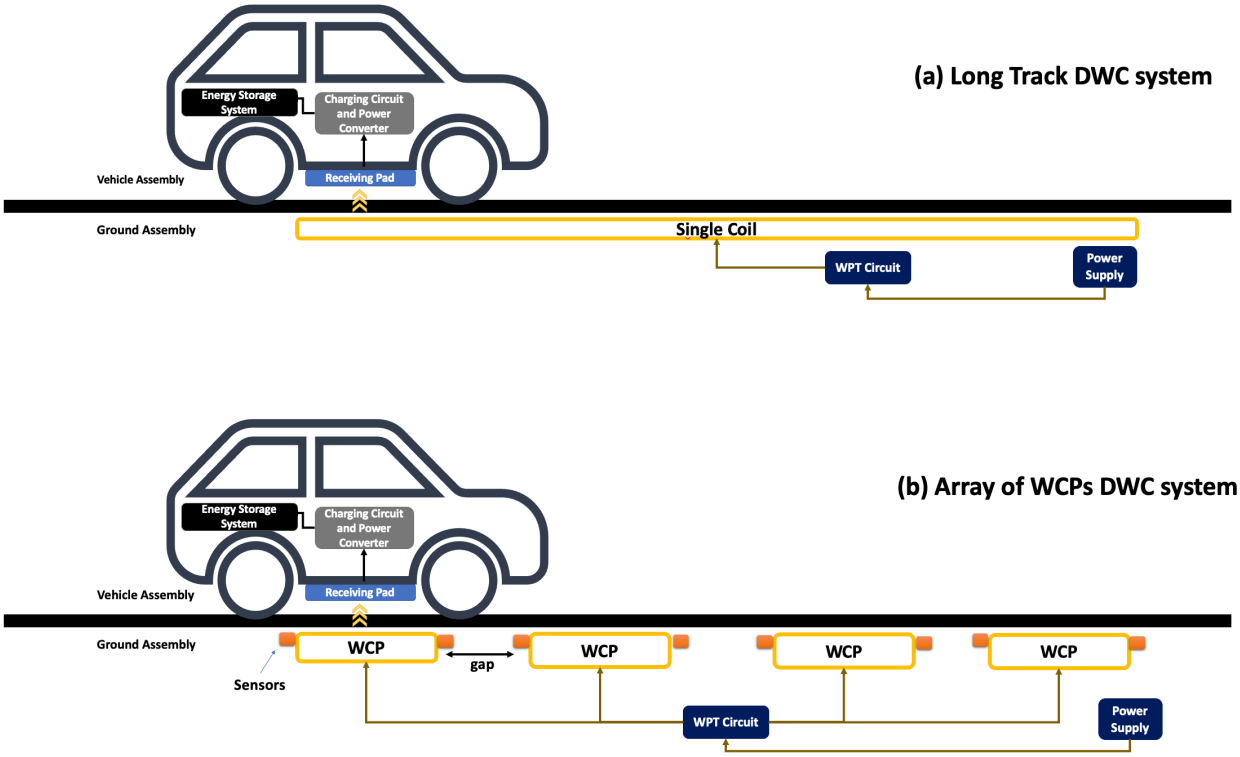

Figure 2.6: Overview of a DWC system with (a) Long Track and (b)Array of WCPs.

i) Long Tracks

The long track [156] is made up of one single coil that is as long as the power-track and the receiving coil is comparatively much smaller. The long track DWC systems have a simplistic design whose mutual inductance with the receiving coil is maintained approximately at constant, thus making it quite easy to control. In literature, this design has been widely researched and reported.

The main goal of any WPT system is to maximize power transfer efficiency. The long track DWC system in [157] has an inverter, regulator, rectifier, power lines and receiving coil configured together with the optimized magnetic core to deliver 100 kW power over an air gap of 26 cm with 80% efficiency. Authors in [158] with a similar setup as [157] achieve 95% efficiency by adding a T-type tuned topology to the WPT system. On the other hand, [159] uses an I-type long power source track of 0.1 m width to provide 27 kW power over a 0.2m air

gap with 74% efficiency. Additionally, the latter system can handle lateral misalignment tolerance of 0.24 m. Next, the S-type power source track in [160] with a 0.2 m air gap achieves a better misalignment tolerance of 0.3 m in contrast to the I-type DWC track of [159]. The need to have a power track with smaller width and increased air gap for WPT led to authors in [159] to experiment and alternate magnetic poles in the direction of EV travel. But, the latter objective was achieved at the cost of receiving coils in the EV experiencing fluctuations in the voltage induced. Researchers in [161] try to address the voltage fluctuations by creating a long power track that has a DQ-power source, so that the output voltage in maintained at constant by alternating the magnetic poles along the track in the D-phase and the Q-phase.

A long power track is high inefficient [162], [163]. The receiver only occupies a small part of the track while the entire track remains active at all times even when no EV is present. In response to this drawback, the array of WCPs track or segmented-coil track was devised.

ii) Array of Wireless Charging Pads track

The array of WCPs track [156] is made up of segmented-coils or WCPs that are usually as large as the receiving coil and are laid in series on the road with little to no gap between each WCP. This type of track activates WCPs that detect a vehicle and deactivates others [162]. As a result, it has significantly better system efficiency than long single-coil track design [162]. This design also suppresses electromagnetic field radiations from inactive WCPs [164].

Newer research advocates the use of WCPs for DWC tracks. Optimization of DWC system parameters utilizing WCPs or coil segments are discussed in [156], [163]–[166]. In [156], the transfer efficiency, air gap and gap between WCPs is increased by using a double-spiral repeater to achieve WPT efficiencies in the range of 60-81% at air gaps of 2.2 cm and 0.74 cm. The latter's optimization parameters of choice were operating frequency, number of WCPs to be activated at a time, gap between WCPs and loading condition. Taking a similar approach, authors in [166] conclude that to achieve maximum power efficiency an optimal DWC track can be constructed by analyzing the relationships between parameters like power utilization, length of the track, vehicle speed and overall efficiency. Meanwhile, [164] proposes the use of DD resonators with finite element method, and varies the resonators size to determine the gap between WCPs and the dimension of each resonator for best performance. Authors in [163] have conducted an analysis to optimize activation of WCPs. It is revealed in [163] that switching-on the coil when the receiving coil has a large air gap with the transmitting unit reduced power losses and electromagnetic field radiations. The latter prevents the peak values of switching voltage and current from surpassing the tolerance range and becoming a safety

hazard. The neighboring effect of activated WCPs on deactivated WCPs is investigated in [165] and the findings are used to create a 2.4 kW miniature DWC prototype with controllable WCP activation and deactivation. The experimental 1.4 kW DWC system in [162] achieves a DC-DC load WPT efficiency of 89.78%, and is considerate of cross-coupling among the WCPs. Authors in [167] achieved a power output level of 2.34 kW with 91.3% efficiency with a set up similar to [162]. The DWC system in [168] enables all WCPs to be driven by a single power source, and automatically distributes equal power among all WCPs. The design in [168] also helps in reducing both power loss and electromagnetic field radiation.

Long-track based DWC solutions [169] charge vehicles using continuous magnetic field. They are usually up to 240 m long, and some solutions have tracks that are only 40 mm wide. Their advantage is that they use only one inverter for a single track, and there is no need to come up with a complicated scheme or use array of sensors to turn the charging tracks ON and OFF. The drawback of such a solution is that the inverters required to drive these tracks have a very high voltage-amperes rating, and high voltage must be managed by adding series compensation. They operate only at low frequencies of 20–40 kHz, whereas the SAE J2954 standards committee has agreed on a stationary charging frequency of 85 kHz for stationary EVs [169]. For the new DWC to be compatible with existing static charging systems, it should also be operable at 85 kHz. So, the length of the track will need to be shortened to a few meters due to voltage limitations and higher AC copper losses for operation at 85 kHz.

To design a new DWC system, using array of WCPs would be a better alternative to long-tracks. The WCP array are sequentially pulsed ON and OFF as an EV drives over them. The use of separate inverters for the individual WCPs in an array can allow operation at lower voltage-amperes. This array based track solution is also less likely to couple power into unwanted loads, and is more efficient since not all WCPs are ON all the time. In a highway scenario, the vehicle typically travels at 100 km/h. If assumed that each WCP can power a vehicle for over 1 meter, then the WCP will have to be ON for approximately 36 ms for each vehicle at such speeds. For good charging synchronization, authors in [169] claim that the WCPs should turn ON within 5 ms of an EV's arrival and turn OFF within 5 ms of its departure. The disadvantage of this solution is that it uses multiple inverters each for a WCP, and schemes or techniques are required to detect vehicles and their misalignments for safe transfer of power wirelessly. So, the choice of WCPs will make DWC and SWC systems future proof. However, they dictate the need for techniques to detect CAEVs and their misalignment on WCPs.

2.3.3 Wireless Charging System Features: Foreign object detection, Misalignment detection and Communication

In [170], a marker-free approach to detect lateral coil-misalignment for DWC system is implemented using a tunneling magnetoresistive (TMR) sensor array. The small sized TMR sensor array in-plane with receiving coil is used to detect magnetic field generated by the primary coil installed underground. It also helps detect coil-misalignment position by analyzing the output amplitude of the TMR sensors. Existing solutions for detecting the location of the vehicle's receiving pad often rely on extra hardware such as additional detection coils, sensors and filters. These methods require additional hardware that adds extra cost and complexity to the system design. Ideally, these additional systems should be minimized to ensure a cheap and robust in-ground system. Hence, senor less solutions are explored. In [169], a method of detecting a vehicle is proposed that utilizes variations in the free resonant current developed in neighboring WCPs in response to small variations in coupling between WCPs. The latter system also makes use of the increasing coupling between the WCP and the approaching vehicle's pad for detection. These variations in the free resonant currents are detected by the current sensors that are already present to monitor and control the ground WCP current for activation and deactivation. This proposed method of [169] is also able to detect the vehicle's pad if it is unenergized.

To protect the WCPs from malfunctions and uphold user safety, the transmitting system needs to be equipped with sensors or a system to distinguish between EVs and other foreign objects. Foreign object detection and EV detection systems can help switch on power transmission only when needed, thus making the DWC system sustainable and economically attractive in the long-term. Systems in [171]–[173] use sensors and cameras to detect foreign objects. Cost-effective ways involve relying on quality factor of receiving pad [173], but this only works with SWC systems with no misalignment tolerance. Reference [174] uses a multi-coil non-overlapping transmitting pad to detect foreign objects by noticing variations in magnetic field and voltage difference in sensing coils across the pad. EV detection systems are often used in combination with foreign object detection systems. EV detection is specially needed in DWC systems with multiple coils or WCPs. The multi-coil system of [175] uses one coil for ordinary WPT and second for detecting EVs with an offset in the direction of travel, and a detection coil is also added to the receiving pad. Other cost-effective approaches include phase differences between voltage and current in transmitting pads [176] or using RFID [177] to detect a single EV with speed limitations for proper operation.

DWC systems could employ various real-time roadside information all together like measurements of vehicle misalignment and speed, and vehicle-side information like driver input. In [178], an intelligent Vehicle Detection and Information System (VDIS) is proposed that implements a misalignment-tolerant DWC system. VDIS helps the DWC controller adjust the power transfer to achieve misalignment tolerance by accurately estimating the lateral misalignment. It could deploy an emergency shutdown in case a foreign object is detected on the electrified track with the help of real-time image processing. It helps the driver improve the alignment of the vehicle with the charging track by displaying the lateral misalignment information wirelessly on the display inside the vehicle, and allows the driver to initiate or terminate charging. This designed prototype is successfully tested on a dynamically charged 25-kW electric bus in [178].

The communication between the transmitter and the receiver is also essential in both SWC and DWC systems. The charge receiving side needs to detect the transmitter and send request for charging, and the transmitting side should be able to receive and accept the request to initiate charging only when it is safe to do so that is no foreign objects are present. The transmitter may even communicate to the receiving vehicle the status of charging and any misalignments detected to ensure optimal delivery of charging. Two-way communication technologies for SWC that are extensively being used and researched includes ZigBee, Dedicated Short Range Communication (DSRC) and cellular communication like LTE and 5G [179]–[187]. DWC involves very fast moving vehicles, so low-latency, long-range and real-time communication technologies like Wi-Fi, DSRC or RFID are considered alone or in combination. Though, 5G is the best amongst the three in terms of coverage and latency [180], [186], [187]. DSRC is the most used in safety applications with low latencies [182]. A combination of technologies may also be used for communication that involves wired connections with road side units (RSUs) like in [181] and even fog computing may be deployed like in [183].

DWC has the potential to increase the driving range of EVs without putting the EVs in downtime. The WPT can happen in motion by using wireless charging lanes, but the distribution of power among the EVs on a single lane at an instance is a novel and complex problem that is addressed in [188]. The system of [188] balances the state of charge (SoC) of the EVs by continuously collecting information about the EVs and scheduling their power distribution. Vehicle to fog communication protocol is used to reduce communication latency, computational overhead, and network congestion. The system allocated separate channels for each EV to communicate with the local controllers. The experimental results proved this

system improves localization and balances power efficiently amongst all EVs, and it could be extended to include DWC over complete route from source to destination.

So, to propose a wireless charging infrastructure for ITS applications that is both sustainable and future proof features like misalignment detection, EV detection and communication need to be included for safe and proper deliver of charging to CAEVs. Further, the proposed charging network infrastructure should also be independent of specific hardware and communication technologies. Thus, enabling an implementer to make hardware choices based on design goals like cost, performance, etc.

2.3.4 Charging Infrastructure: Installation and Allocation

Selecting a place to install or build a wireless charging station is not an easy task, as it can have huge economic and environmental impacts. The allocation problem often uses available logistical insights to support decisions in placement and distribution of the charging infrastructure. The optimal allocation of wireless charging systems is a complex problem that is often solved by using algorithms and mathematical optimization techniques. These optimization techniques may directly determine the final location or may be an intermediate step in determining the final placement of the wireless charging systems. For optimal allocation, the optimization techniques may consider goals of cost-effectiveness, travel-time, charging needs, traffic density, traffic flow, vehicle speeds, etc. The problem of allocation can be solved either on the local level or the global level. At the local level, the focus of the allocation problem is kept to a specific road route. On the other hand, at the global level, the focus of the allocation problem takes into consideration surrounding traffic environment and behaviors or moves to a higher-level of a suburb, city or a country.

Authors in [189] and [82] suggest optimal locations for wireless charging facilities at minimum total investment cost. Reference [189] is a pioneering approach in finding the optimal placement of limited number of wireless charging facilities by considering the limited number of locations while also maximizing traffic flow. The prior formulates the problem using mixed integer non-linear programming (MINLP), and later a global optimal solution is proposed through the developed solution. Liked-oriented set covering location modeling approach is adopted in [82] for optimal allocation of DWC infrastructures while meeting travel requirements between cities, and it proves that DWC eliminates the need for larger batteries. However, the study in [82] was unrealistic, as it ignored the traffic environment and human choice of charging stations in favor of strict cost minimization. Researchers in [190] argued

that optimization of WPT can reduce CO_2 emissions by 8%, but the break-even analysis revealed that profits can be made only after 20 years.

Studies in [191] and [192] optimize layout of DWC lanes in a cost-effective manner. The model in [191] is the first to address the trade-off between charging needs and travel time by considering the driver's choice of speed. Since, slower speeds allows more time and charging on the lanes. The network-based modeling framework and algorithm in [192] is able to minimize costs by choosing routes that are all feasible, but assumes that EVs arrive at the final destination above a set battery charging threshold.

SAEVs with automated WPT charging infrastructure in [193] used agent-based modeling to reduce fleet-level per-mile travel cost. The simulation examines the operation of SAEVs under various vehicle range and charging infrastructure scenarios in a gridded city modeled roughly after the densities of Austin, Texas, USA. It also determines the number of charging stations needed for full service of the SAEV fleet. Simulation results proved that fleet size is highly dependent on charging infrastructure and vehicle range.

Table 2.2 compares the surveyed papers on wireless charging infrastructure's allocation problem based on vehicle type, algorithm and optimization approach, main goals, performance metric and test set up. It is clear from Table 2.2 that placement of charging networks can have a significant impact on the volume of CAEVs that the charging network will service, and will eventually have an effect on the return on investment, profits, and even the environment. Further, systems that schedule charging and plan trips for CAEVs will need to consider the placement of charging networks to meet their goals like minimizing wait times, travel times, traffic congestion, etc.

Table 2.2: Summary of wireless charging infrastructure's allocation.

Ref.	Vehicle type	System/ Algorithm and optimization approach	Main goals	Performance metric	Test set up
[189]	EV	MINLP and a solution method is developed to obtain the global optimal solution of the linearized program	To locate a given number of wireless charging facilities for EVs out of a set of candidate facility locations for capturing the maximum traffic flow on a network.	Number of located facilities, % of captured flow, link traffic flow	Numerical experiments are presented to demonstrate the model validity
[82]	EV	Liked-oriented set covering location modeling approach with time and battery constraint requirements	Optimal allocation of DWC infrastructures while meeting travel requirements between cities	Total system cost, vehicle range and cost, yearly cost of additional range of EVs	Simulation: A Mathematical Programming Language (AMPL) and the CPLEX 12.4 solver on California freeways
[190]	EV	Genetic algorithm	To optimize the rollout of DWC infrastructure both spatially and temporally in order to minimize life cycle costs, GHG, and energy burdens.	Life cycle assessment is based on three key sustainability metrics: costs, GHG emissions, and energy burdens	Break even cost analysis: Case study of arterial roads in Washtenaw County in Michigan, USA
[191]	EV	A new user equilibrium model to describe the equilibrium flow distribution across a road network where charging lanes are deployed with active set algorithm.	Trade-off between charging needs and travel time by considering the driver's choice of speed Optimize the locations of charging lanes for a given budget	Travel time, recharging time, cumulative energy recharged, energy consumption	Numerical examples are presented based on the Nguyent–Dupius and Sioux Falls networks
[192]	EV	Network-based modeling framework and algorithm and modeled as n integer programming problem	Minimize cost by choosing routes that are all feasible for placement of the wireless charging lanes	Average final SoC, number of routes ending with final SOC below a given value, number of infeasible routes	Simulation experiments with Manhattan network
[193]	SAEV	Agent-based modeling and greedy algorithm	To reduce fleet-level per-mile travel cost and determine the number of charging stations needed for full service of the SAEV fleet	Fleet-level per-mile travel cost, fleet size, average wait time, average trip distance, vehicle capital and operational costs	Simulation on a gridded city of Austin, Texas, USA

2.3.5 Charging Reservation: Scheduling, Billing and Payment of Charging

Commercialization of the WEVCs will ultimately entail billing the users for their charging requests. Billing policies and schemes along with pricing electricity will become critical in the operation of the reservation system. The existing literature suggests that both a flexible billing policy and a secure payment system are needed for successful deployment of WEVCSs in the real-world.

The nature of DWC dictates a CAEV user request to be serviced and billed sequentially. This puts the CAEV user's privacy and security at risk, as their current location and personal information can be retrieved from the payment and billing systems. Authors in [194] and [195] address this concern by proposing real-time and secure payment systems.

In [194], a light-weight and secure payment protocol using low-cost operations like XOR, concatenation and symmetric encryption for DWC of EVs is presented. The vehicular cloud of this system is comprised of a key distribution center, energy provider, bank and trusted authority. All the cloud entities communicate securely using symmetric keys with the EVs through RSUs over 5G high-speed network. The anonymity and location privacy with traceability of the EV users is achieved with the help of the trusted authority. The trusted authority registers the EV users and authenticates them for initiating charging and billing the bank accounts at the end of the highway lane. Instead of WCPs, [194] uses energy segments that are inherently more inefficient meaning that the EV user will never receive the exact requested charging. These energy segments end up billing the EV users unfairly, as the payment system is not secure against free-riders. In the context of DWC, free-riders are EV users that tail behind or slightly in front of the authenticated EVs to steal charging from the turned ON and authenticated energy segments.

On the other hand, [195] uses light-weight cryptosystems to secure the EV communication to the bank, charging service provider and the RSUs. An efficient technique is developed to enable the charging service provider to share secret keys with the RSUs, and the RSUs to share keys with the WCPs. Each EV maintains an account in the bank, and the account is used to buy anonymous coins for pre-payment of charging. Meanwhile, this pre-payment anonymously authenticates the EV to the charging service provider. As part of their hierarchical authentication, the EVs then authenticate themselves to the RSUs, and finally to the WCPs over the wireless channel to receive charging. However, this anonymity compromises traceability of the EV users, and the pre-payment means that the EV user may be billed unfairly due to the inefficient nature of wireless charging.

Researchers in [196] address the free-rider issue by using compensation-prepaid token and detecting battery power levels periodically of the in-motion EVs. Further, the service provider can obtain compensation if it can prove that an EV is a free-rider. However, this system relies on a tamper proof OBU for honest reporting of the battery levels.

EV users with range-anxiety face challenges like searching for charging stations and planning their trips to accommodate recharging at those charging stations. Reference [197] addresses this concern by proposing the use of A* search algorithm for finding the shortest optimal and lowest cost route to the destination while considering charging reservations. It uses SWC, DWC and QWC systems for charging EVs. RFID tags are installed at various points across the city, and are used for EV authentication and efficiently billing the EV's charging based on time duration. This paper makes no mention of the procedure or protocol for the actual

charging and billing of the EVs, although it does stand out for considering three different wireless charging technologies. Nonetheless, it provides the EV user with options of using certain charging stations along its route with no automated requests and reservations being made for the user.

The WCPs are known to have limited computational and communication resources. In [198], charging tickets are introduced with time stamps to allow for mutual authentication between the EV and the charging station's WCP for pre-paid DWC. It eliminates the need of a third party by using blind signature for charging request to maintain EV's anonymity and location privacy. The verification of the hash chain at charging pads requires computing simple hash operations, which are computationally fast and efficient. Once authenticated, the EVs and the WCPs have a secured session for encrypted communication of EV charging information. The system is protected against double spending of charging tickets, and can inadvertently protect the user from paying for free-riders.

Inadequate charging infrastructure is cited as the major adoption barrier of EVs in [199]. IoT connectivity between the EVs and the CC stations is advocated without any third-party intervention. It enables private exchange of information between the EVs and the charging stations to achieve efficient EV load forecasting. The application in [199] alerts the EV user for the need to charge, and looks up and recommends available and nearest charging stations for reservation with consideration to economic costs and reduced charging time. This system eliminates the need of complex information exchange environment, as it relies on GPS and publicly available websites. The charging stations are chosen manually by the EV user; hence, making it more private. The amount of energy consumed to charge the EV and its cost is only kept between the charging station and the EV user. Further, congestion is avoided at the charging stations by looking at real-time status of its availability. This system presents recommendations for CC stations, but is neither automatic nor dynamic in fulfilling charging requests.

In [200], a real-time metering and wireless charging system consisting of identification equipment, charging software, watt-hour meter and the OBU installed on the EV is presented. A charging control unit and a watt-hour meter installed at high frequency power inverter of the charging segment is also part of the system in [200]. To realize billing of wireless charging session, a billing strategy that is composed of electricity fee and service fee is introduced. The billing takes into account power loss, construction cost, operation costs, the road congestion and the electricity load. The EV authenticates with the database using its OBU, and once authenticated with sufficient funds it is allowed to enter the charging lane to receive real-time

metered charging. This system requires a certain road-section be reserved for wireless charging and does not protect against free-riders. It is also does not provide anonymity and location privacy, and does not detail the communication or handshake protocol needed to initiate a charging session.

2.3.6 Optimization of Charge Schedules and Trip Routes

Wireless charging systems are being developed for the autonomous future. In this completely automated future, it is proposed that the vehicles will be shared for the AMoD trips to gain from both the economic savings and environmental benefits. However, from a societal and security point of view, potential customers may be comfortable sharing rides with colleagues and friends, but not with complete strangers, and same goes with parcels. New methods and algorithms may need to be developed to match customers with shared riders using rating and profiling systems. The AMoD systems that use shared CAEVs require techniques to optimize their charge schedules and routes, as the CAEVs need to be kept operational till they reach their intended destination. Most of the literature on joint optimization of charge schedules and routes consider wired charging, but these techniques can be directly applied to SWC due to their static nature and extended to DWC with some modifications.

Reference [4] solves the problem of routing EVs for MoD applications jointly with charge scheduling using battery swapping and wired charging. The main objective was to maximize EVs utilization. The latter is achieved for a medium scaled network of EVs using optimal mixed integer programming (MIP) formulation. To increase the scale of operation, a non-optimal incremental MIP algorithm and a non-optimal greedy scheduling algorithm are proposed. Both non-optimal solutions quality is improved using tabu search-based local search technique. Another proposed algorithm also takes into account randomness in online future MoD requests of EVs. All proposed algorithms are empirically tested with real-world data. It is found that the non-optimal greedy algorithm with large battery capacity EVs using both battery swapping and wired charging performed significantly better than the optimal MIP algorithm. However, with smaller battery capacity EVs, the incremental MIP generated better solutions than the greedy algorithm. Optimal algorithm is deemed the best, but it is limited to medium scale operations. The online algorithm was able to achieve up to 90% operation of the optimal while neglecting variables like trip cancellations, delays, accidents, etc. Finally, the algorithms could be improved by factoring in shared CAEVs and the stochastic nature of the MoD operation.

For EVs in [201], the joint optimization of routing and charge scheduling is achieved using MILP with V2G communication. This system decides when and where energy exchange will take place with the grid for maximizing total revenue. Using the IEEE 37-node test feeder, it was experimentally proved that slight changes in driving patterns related to movements and charging and discharging patterns can improve overall network operation and significantly increase energy transfer. Reference [202] also approaches the same problem jointly using MILP but for SAEVs. The latter system ran two model-predictive control algorithms in parallel to optimize both charging and transport service at longer and shorter time scales, respectively. Its goal was to minimize waiting times and electricity costs. The model was also tested experimentally using transport survey data and electricity prices from a case study in Tokyo to successfully reduce charging costs without significantly impacting waiting times. V2G is deemed inefficient for current cost structures of power and battery, but in the long run can prove cost effective with higher variability in price profiles. Both [201] and [202] prove that EVs or SAEVs can become effective energy storage for the grid and make the grid more robust and less congested. Other features like which charging stations are available, and other grid characteristics like frequency regulation and operating reserve can be taken into account for global optimization.

Using MILP, the optimization of maintenance costs and extra charge hours for fleet of EVs to deliver packages along the delivery route is presented in [203]. The latter model jointly finds the delivery route with a charge schedule that considers the average speed, battery level, number of deliveries for each EV, battery performance, and traffic road uncertainties. The cost effectiveness of the system in [203] makes it suitable for analysis and economic planning of EVs by transport sector and companies.

EVs over long journeys require multiple stops for charging, and fast charging is seen as an solution due to shorter charging times. However, fast charging may overload the stations during on-peak hours with several EVs charging at the same time. Reference [204] tries to offset the overlap of charging demand by optimizing the EVs charging and routing with improved chrono-SPT (ICS) algorithm under real-time pricing policy. Additionally, a simply-charge-control algorithm is applied to reduce computation complexity and achieve optimal cost.

Table 2.3 summarizes the joint optimization of routes and charge schedules based on vehicle type, algorithms, main goal and test setup. It can be noted that existing literature does not really consider DWC and SWC, and focuses on operational cost minimization and maximization of profit or total revenue.

Table 2.3: Comparison of joint route and charge optimization of EVs.

Ref.	Vehicle Type	System/ algorithm and optimization approach	Main goal	Test setup
[4]	EVs	Optimal MIP, non-optimal incremental MIP, non-optimal greedy algorithm	Maximizing EVs utilization	Empirically tested with real-world data
[201]	EVs	MILP with V2G communication	Maximizing total revenue	Experimentally proved on IEEE 37-node test feeder
[202]	SAEVs	MILP, two model-predictive control algorithms in parallel	Minimizing waiting times and electricity costs	Tested experimentally using transport survey data and electricity prices from a case study in Tokyo
[203]	EVs	MILP	Optimization of maintenance costs and extra charge hours	Simulation
[204]	EVs	ICS algorithm under real-time pricing policy, and the simply-charge-control algorithm	Offsetting the overlap of charging demand	Simulation

Now, these WEVCSs are still under research and development, and new trends to realize this technology for wider proliferation and deployment are highlighted in the next section.

2.4 Future Trends of Wireless Charging Systems

All these efforts to boost EV production will ultimately increase the load on the power grid and its distribution networks. Many grid management techniques and additional power compensation techniques like renewable energy sources are presented as solutions. However, bi-directional power transfer or more specifically WPT is a new avenue that is being explored as the solution to this problem. The V2G power transfer concept is an attractive idea that enables an EV to sell back its stored charge from the battery and supply the power to the grid by discharging during peak times. The wireless V2G [205]–[207] involves the installation of bi-directional power converters installed at both the transmitter and the receiver. These bi-directional DC-DC converters operates in step-down mode when it charges the battery bank, and boosts to increase power level upon discharge. The entire process is autonomous, safe and enables the EV to act as a back-up mobile energy storage device.

In late February 2020, ORNL successfully demonstrated a 20 kW bi-directional wireless charging system [208] installed on a United Postal Services (UPS) Plug-in hybrid EV (PHEV) delivery truck. The system transferred power with more than 92% efficiency over an 11 inch air gap to the UPS PHEV's 60 kWh battery from the grid. It would take about 3 hours to charge its 60 kWh battery while a wired charging system would take twice as much time. This bi-directional technology is designed to be fully compliant with the grid's power quality standards of the US, and about 50 PHEVs' batteries could provide energy storage at the

megawatt scale. It is a first of its kind project with high bi-directional power transfer for higher ground clearance vehicles.

With the proliferation of wireless sensor networks (WSNs), a lot of research is being done for charging of the small battery powered sensor nodes. The problem addressed in [209] of charging small sensor nodes is very similar in nature to SAEVs charge schedule problem. Mobile wireless charging vehicles (MWCVs) are advocated by authors of [209] for periodically charging the sensor nodes to minimize charging costs for prolonged battery life of sensors. The latter technique can be extended for SAEVs. Like WSNs, for SAEVs charging factors like EV's traveling route and speed, range, period and power of charging have to be considered. Charge scheduling schemes are classified based on different aspects like the number of MWCVs, charging range of MWCVs including single-to-single or single-to multiple charging schemes, charging cycles of periodic or on-demand charging schemes, and optimization goals of the charging schemes that focus on the node network. All these aspects of the WPT charging schemes for sensors in WSNs can serve as the basis for the development of WPT charging schemes for SAEVs.

V2V charging schemes are gaining popularity for mobile, fast and flexible charging of EVs without the need of expensive charging facilities or changes to road infrastructure. Both systems in [210] and [211] employ V2V charging schemes while battling against communication loads and computation complexities. These systems aim to achieve optimal matching of discharging vehicle or mobile energy disseminator (MED) with the EV that needs charging. Study in [210] uses mobile edge computing to maintain reliable charging information at low communication costs. The prior system locally and globally coordinates charging based on traveling time and charging time to dynamically choose optimal traveling route and best pair for V2V charging. Similarly, reference [211] optimally routes EVs with bus MEDs. It uses constraint logic programming and a graph-based shortest path algorithm to minimize total travel time and queue wait times. IPT WPT is used in [211] for V2V charging to extend travel range and conserve travel time. Further, the combination of wireless MEDs and wired charging stations is proved to be four times more efficient than wired charging stations. Authors in [212] address the efficiency gains discovered in [211] of using MEDs. They propose MEDs as backup to wired charging stations for handling the increase in charging demand of EVs. The scheduling of mobile charging stations to different static charging stations is proven to be NP-hard, as a result two heuristic algorithms are proposed in [211]. The slotMCS-Allocation algorithm performs better than the reduced-slotMCS-Allocation algorithm in terms of the number of EVs charged, but is computationally expensive. To be future proof and cost effective

in long run, these systems can be improved by combining the MEDs with magnetic resonance SWC and DWC stations.

The placement of receiving charging coil in the wheel motors instead of underneath EV chassis is an interesting approach first presented in [213]. The first In-Wheel Motor (IWM) wired charging was not put to practical use due to possibility of cables disconnecting, as a result integrating WCPs was deemed attractive for boosting adoptability. The IWM receives its power wirelessly from the vehicle body, and can also be powered directly from power-transmitting coils in the road. Since the motor is subject to vibrations while driving, the preferred method of WPT is magnetic resonance coupling that is robust to misalignment of the transmitter and receiver coils. The first generation Wireless IWM's (W-IWM1) first trial unit achieved 3.3 kW per wheel and 88% DC-DC efficiency from the chassis side to the wheel side with coil to coil gap of 100 mm. The second trial unit W-IWM2 is presented in [214] with a Lithium-ion Capacitor (LiC), power management system, and circuit on its wheel side for high power and efficient DWC. The latter's second trial in the real-world is expected to upgrade the DC efficiency from 88% to 96% with the added bonus of range extension while driving. The development from second to third generation W-IWM3 was reported with experimental results in [215]. The bench test results for the W-IWM2 with the coil to coil gap of 100 mm revealed efficiency of 92.37% with the DC input power of 12.532 kW at 89 kHz frequency on the road side. Furthermore, the real vehicle test results on a DWC road also obtained similar results. Further, the W-IWM3 EV was designed to be more compact. All the components for charging and driving of the W-IWM3 including the rectifier, inverter, motor, their control circuit, and liquid cooling system, are placed inside a wheel. Thereby, the overall EV can have a much smaller chassis for improved motor output and maximum torque. Finally, a medium sized passenger vehicle with 17 inch wheels is designed and tested in [215]. From the second to third generation, the size of the vehicle-side coil is reduced by 53% and the size of the road-side coil is reduced by 61%. The air gap between the transmitter and receiver coils was 50 mm, and the W-IWM3 achieved an output of more than 18 kW with a DC-to-DC efficiency of 95.1%. The overall charging power is increased by 66%, and the loss of the coil is reduced by 45% form the second to third generation of the charging system design.

Another unique approach is presented in [216] for WPT that uses stretchable coils. It addresses the charging efficiencies and absence of universal charging systems for available EVs. The stretchable WPT system (SWPT) uses thin and stretchable inductive coils fashioned in serpentine shapes to provide stretchability in charging of different EVs. The transmitting coil is hung over the EV that is adjustable for varying the transmission distance based on the

vehicle, and the receiving coil is installed on the EV's roof to receive charge. This system demonstrated feasibility with two EVs that were able to maintain stable performance and charging efficiencies of above 50% with bendable and stretchable coils. The capability of the coils was improved with optimized design of windings, which decreased resistance through fabricating treble strand serpentine copper traces. This novel approach is thought provoking and demonstrates a new way of delivering power wirelessly to EVs. It claims to be universal by working on any EV model, and can be used in applications where installation on the ground might not be possible, for instance, for safety reasons.

2.5 Research Challenges and Future Opportunities of Connected and Autonomous Electric Vehicles

To realize a sustainable and smart ITS that is wirelessly powered, the optimistic forecasts and excitement about the shared CAEVs as a new market must be weighed against existing technological, social and economic realities. The challenges to the realization of AMoD systems operated with a fleet of shared CAEVs can be broadly put into three main categories that help identify future opportunities. The barriers to wider adoption with complex solutions are discussed in the following sub-sections.

2.5.1 Range-Anxiety and Charging Infrastructure

Average EV range is difficult to measure, but according to estimates it falls somewhere between 100-300 miles [217]. Lower temperatures can significantly reduce EV's battery range [218]. According to the survey in [219], approximately 50% of all prospective car buyers in the US agreed that lower purchase prices and longer EV driving ranges would be effective in driving up adoption rates. Range anxiety is the nervousness a consumer of an EV feels due to the limited driving range afforded by the small batteries [12]. This fear serves as one of the biggest obstacle to EV adoption. The available literature and policy makers have come up with their own responses to this widely accepted psychological issue. Though, the apparent response has been to look into ways to increase the range.

Range anxiety of consumers is deemed irrational in [220], as 98% of trips taken by US EV drivers are under 50 miles that can be easily travelled by the smallest battery capacity EVs. It may seem that the obvious solution is increasing the battery size, but larger batteries are costly and take more time to charge. Further,the heavy battery will also take a toll on the driving range. Tesla and other companies are trying to make affordable batteries, since lithium-ion battery costs declined by 73%, from $1,000 per kWh to $270 per kWh in only seven years

[220]. Another popular approach to address range concerns is expanding the charging network infrastructure.

Longer trip EV drivers are usually concerned with planning a route with known charging stations. Two-thirds of drivers who end up buying an EV prefer grocery stores for charging when away from home [219]. Additionally, EVs take a long time to charge which is influenced by the electrical current and the battery size. Fast-charging can be used, but it puts the EV battery at risk of overheating. Wireless charging technology is also a great solution, but it is still not widely deployed and standardization activities are in progress. A survey in 2017 found that US consumers were spoiled by the 121,000 gas stations, in contrast to the mere 16,000 charging stations of which not all are compatible with available EV's on the market [220]. The wider impression is that charging stations are not sufficient, when in fact the existing ones are a reachable distance from one another. Changing public perceptions will require efforts in awareness as well as investment in expansion of both wired and wireless charging systems. Current charging stations are not enough to meet projected demands that require $6 trillion of investment [221]. About 75% of US EV owners have access to charging facilities in comparison to only 40% in China and 30% in Europe [222]. Thus, indicating the lack of charging infrastructures in urban areas where people do not own private chargers. Further, EV charging standardization efforts are underway with legislation introduced in Europe to give non-exclusive access to chargers and their information [223]. Specification on type of charging equipment, the ideal number of charging points, the charging point distribution, location, and providers are discussed in [223] for Europe.

In [12], it is highlighted that the usual further investment in public charging facilities and awareness programs fail to address the main concern of consumers invoking reactionary rhetoric. For instance, deployment of expensive charging facilities may drive away EV consumers and give rise to another reactionary rhetoric namely charger anxiety that is the psychological fear of charging on the right time at the right facility. Though several charging reservation systems are in development, policymakers may consider spreading awareness like Nordic countries where the EV policies entail focusing on socioecological barriers including cost of ownership. Norway increased its EV adoption rate by incentivizing consumers using non-monetary benefits like free tolls, ferries and parking, thus bypassing the range anxiety. In the US, the federal government has allowed tax credits of up to $7,500, and in China up to $8,500 tax exemptions are given to drive up EV purchases [220]. Netherlands offers more complicated financial schemes like taxation based on CO_2 emissions [220]. In Ontario, Canada the Used EV Incentive Program and the Scrappage EV Incentive Program offers up to $1000

towards the purchase of used EV and PHEVs, and the federal government offers point-of-sale incentives of $2,500 to $5,000 for purchasing or leasing an EV [224]. This may go beyond tax credits to include vouchers, reductions in vehicle registration fees, lower charging rates, and high-occupancy vehicle lane exemptions amongst others. These examples illustrate the power of government policies to shape consumer behavior, but these incentives may be phased out after consumers are hooked like the taxation exempts in Denmark by 2022 [220].

Political actors may also want to keep perpetuating range anxiety to secure the oil industry and internal combustion engine manufacturers. In addition, range anxiety may be promoted to avoid personal changes like purchasing EVs that may damage their identity. Overall, diagnosing rhetorical range anxiety may be vital for other countries to cost-effectively implement EV policies and avoid over-investment into public charging infrastructure that can not effectively eliminating range anxiety [225]. As the range anxiety is comprised of technical, psychological, and rhetorical aspects, the policy solution should address all three aspects.

2.5.2 Urban Planning: Road and Transport Infrastructure

Through the convergence of automation, electrification and ride-sharing technologies, SAEVs have the power to significantly transform urban development, planning policies and lifestyle. The autonomy can push for a more human-centered city planning with more walkable city practices while also accommodating changes for smooth operation of CAEVs. The main challenge arises for city planners who according to [226] are ill-prepared for disruptions brought on by the CAEVs in the imminent future. These urban planners, transport planners and government alike will need to take smart and proactive decisions to take advantage of the urban extension. The new opportunities and challenges of land-use will need to be explored in the automated future. The cities should be better prepared for CAEVs through appropriate and timely policies, planning, investments and guidelines. Both community and government support will be required to realize smart urban autonomous mobility systems.

The SAEVs can easily operate like taxis, public transport or parcel delivery services. The perceived opportunities presented by the commercialization of SAEVs in mobility as a service (MaaS) or AMoD systems include reduced driver, delivery, transport and travel costs as well as associated hiring, training and insurance costs [227], [228]. Agent-based modelling in [229] claims that 11 internal combustion vehicles can be replaced by one SAEV, thus discouraging traditional car ownership. Authors in [230], [231] optimistically predict shared ownership of CAEVs in the future. These changes come at the expense of employment of individuals especially in the automobile manufacturing, driving and repair industry [232].

Layoffs in driver licensing, traffic policing and insurance sales are to be expected [233]. For those displaced and seeking jobs, government can compensate them with pay packages. More importantly, the government as well as the automotive industry can invest and offer training for other jobs in new sectors created by SAEVs. The opportunities for employment in construction of parking and charging facilities, roads and highway modification construction and IT product and services are expected to rise by 15% [234].

Other perceived benefits may include increased comfort and interest in longer trips, and reduced traffic congestion and parking demand. The agent-based model in [235] reveals that up to 90% of parking demand can be decreased at a low market penetration rate of 2% with shared autonomous vehicles (SAVs). The planners can promote tech and transit oriented developments as well as tackle transport related social exclusion by replacing traditional parking spaces with neighborhood parking zones or collective multistory garages in the inner-city districts [236]. The saved off-street parking spaces could increase urban density by being repurposed for residential and commercial development, or converted into bus lanes, cycle lanes, or new public spaces [227], [228]. Further enabling longer commutes at lower cost, SAEVs can increase accessibility in remote areas with low-cost houses, render public transport useless, and will also consequently decrease rent in central urban districts [227], [233], [237]–[239]. The latter can create urban sprawl that seems to be the biggest challenge for urban policy and planning. Hence, presenting an urgent need for research into modelling the impacts of CAEVs in our cities, and then developing policies and actions to address these challenges.

Integration of cooperative SAEV fleet control technology like platooning and lane changing can help increase road capacity by five times [240], and enable wider deployment of autonomous delivery and public transport services. With increased road capacity, re-evaluation in planning of roads may be required before investing large sums of money. Further, any new ITS and level of service projects will need to be assessed for compatibility with SAEV fleets [241]. In an ideal condition, where all the vehicles are fully autonomous, highway capacity might increase to 100% [242]. As a result, road infrastructure may need new design methodologies. For instance, [243] advised that the width of the roads might be made narrower for CAEVs that are more accurate in their lateral control. The recommendations to face the SAEV challenges in [241] include planning paint markings for pavement distinction, planning radio and ITS messages and warnings for CAEVs, and choosing DSRC locations for traffic signals.

CAEVs are expected at the latest by 2060 to fully contribute to energy conservation efforts [244]. The operation of SAV fleet is proven to increase fuel efficiency and limit GHG

emissions, as the cooperation reduces rapid acceleration and deacceleration while cruising at average speeds [227]. Reference [245] verifies the reduction in CO_2 emissions due to SAVs that replaced private cars, taxis and public transport system in Lisbon, Portugal. More importantly CAEVs by 2030 are predicted to more aggressively reduce GHG emissions than other alternatives [246]. Regardless, the energy consumption and emissions cannot be attributed to the operation of the vehicles alone. As a result, all the available estimations are not very accurate. Factors like the manufacturing of the autonomous vehicles, their design, operation, choice of energy, and the policies on which these vehicles operate all indirectly affect the overall energy consumption and emissions [247]. Government also plays a huge role in promoting eco-friendly vehicles with policies and incentives like tax rebates.

2.5.3 Public Perception: Safety, Liability and Security

Ensuring safety without hindering innovation is a huge challenge. Carefully defining rules, requirements, standards and policies is considered an appropriate response to promote innovation in autonomous mobility while holding all CAEV manufacturers to the same standards. However, there is still debate on standardization and establishing a common legal ground for the design, manufacturing, testing and deployment of CAEVs. Authorities may follow "binding regulation", "non-binding regulation" or "granting exemption", where both the "binding regulations" and "exemption under conditions" are legally binding for manufacturers to ensure safety during testing [248]. Technical developments particularly flourish under "exemption under conditions", as it poses legal flexibility and uncertainty for manufacturers. For instance, Dutch Vehicle Authority (RDW) granted exemptions to CAEVs from certain laws under certain conditions for testing on public roads with test specific conditions once all the functionalities to be tested are passed on test track [249]. On the other hand, "non-binding regulation" serve as testing guides while allowing manufactures to adapt and adjust with technological advancements [237]. The US National Highway Traffic Safety Administration (NHTSA) under national policy [250] and the UK Department of Transport (DoT) under its code of practice [251] exercise "non-binding regulations" for test and deployment regulations of CAEVs on public roads. Further, the UK DoT also addresses the requirements about the test driver [251].

Nevertheless, no 100% guarantee with empirical proof of CAEVs safety exist [252], as the existing literature on CAEV's safety against crashes assumes expert estimates and forecasts with assumed CAEV deployment and market penetration scenarios. The German In-Depth Accident Study (GIDAS) [253] and NHTSA [254] crash databases claim that over 93% of all

crashes can be attributed to human error, and with the elimination of human drivers it is thought that the crashes would not occur. In support, [252] forecasts that increased automation can decrease crashes by 10%, 50%, 71% and 100% by 2020, 2050, 2060 and 2070, respectively. These studies seem to neglect the potential risks of software failure, hardware failure, failure of CAEVs artificial intelligence to perceive the surrounding traffic environment, controller malfunctioning, viruses and cyber-attacks that may make the CAEVs vulnerable to collisions.

As new crash risks emerge, the accident related costs like medical and legal costs, insurance and administrative costs, emergency service costs and property damages can be minimized effectively with the government enforced safety rules and regulations carried out by high level CAEVs [228]. Data obtained through OBUs can provide sufficient details of a collision to determine "at-fault" party and other liability decisions with high degree of precision [255]. CAEVs can accurately identify the accident related factors, and accelerate the insurance payout and legal litigation costs. But, a bigger subject of debate in CAEV accidents is legal accountability between the owner, manufacturer and the driver at autonomy level 3. Reference [256] argues that robotic and automated systems do not have their own consciousness, and such systems human programmers and developers should be held accountable if the system in question was created with the intent to harm human life. In California, USA, the Californian draft autonomous vehicle Express Terms suggests holding CAEV manufactures responsible for accidents, and advocate for CAEVs covered by proper insurance [248]. However, authors in [256] claim that vehicle operators that try to counteract risk of autonomous systems should have limited liability. For instance, the Dutch law plans to hold the possessor of CAEV liable for development risks [248]. The UK proposal in [257] discussed first party insurance option for the victim, where the victim can claim from the insurer regardless of liability, and the insurer can claim from the manufacturer if held liable. The major concern exists in slowing down innovation, as disinterest of insurance companies in covering high risk CAEV will increase if the liability of the collisions shifts to manufacturers [248]. The proposed solutions in [248] include limiting number of claims and getting government to encourage insurance for CAEVs.

CAEVs equipped with OBUs that retain travel data might be vulnerable and have serious impact on information privacy of the vehicle owners. Privacy mainly relates to control over autonomy, information, and surveillance when it comes to CAEVs [255]. Reference [258] advocates for manufacturers being held responsible if CAEV fails to comply with laws associated with protection of personal data. Personal information privacy can be violated as CAEVs collect, store, share, manipulate, sell, or destroy data under no regulations or disclosure

control [259]. There should be rules and laws on the purpose, ownership, accessibility and shareability of the collected data, as having information about previous and future trips can compromise the CAEV user's privacy as well as personal security and well-being. CAEV privacy is a challenge that can become a factor in resistance to wide deployment if no rules and regulations are laid out to insure protection of private information. One of the main cause of CAEV failure is predicted to be cyber-attacks and software and hardware defects. Hence, the onboard systems should be equipped with defense layers that can ward off inadvertent attacks and can automatically and effectively respond to system failures. Mainly, the cybersecurity system should safeguard on-board data storage and data sharing, and government should propose self-regulating policies to control communication, privacy and cybersecurity of CAEVs with experimentations [260]. Following the laid out government policies, the CAEVs cybersecurity requirements should be considered at the system design level to insure a well-protected and secured system [261].

2.6 Conclusion

This chapter presents an overview on the WEVCSs from a technological and social perspective. On the technological front, the chapter started by summarizing all the important and recent advancements of WPT technologies. The SWC and DWC systems' literature is reviewed to highlight the system design, architecture and features, allocation techniques, charge scheduling, and CAEV route optimization methods. Next, the future trends of WEVCSs include bi-directional charging options like V2G and sharing charging using V2V, and novel placements of receiving coil like the wheel's rotor in EV or the roof. Lastly, the main challenges to wider adoption of shared CAEVs including range-anxiety and charging infrastructure, urban planning, and public perceptions of safety, reliability and liability are addressed from the technological, environmental, social and economic perspectives. More importantly, WEVCSs can help make shared CAEVs a reality with automation and ease of charging, and will ultimately shift the paradigm of urban transportation.

Chapter 3 System Architecture and Handshake Protocol

3.1 Introduction

System architecture is considered crucial for laying out the plan for system implementation. It entails detailing the organization, structure, understanding, and negotiations that helps different parts of the system to communicate and work together as a whole. The main focus of this chapter is to present the proposed system architecture and the accompanying handshake protocol that would enable wired and wireless charging networks to seamlessly communicate with one another. This chapter will also define the system entities and propose accompanying light-weight message frames for communication between the CAEVs and the system. Two real-time charge metering billing schemes are also presented. The chapter also aims at highlighting the IoT application for ITS that can employ and benefit from the presented system architecture and handshake protocol.

This chapter's section 2 details the proposed design of the three-layer CN hierarchy. Next, the handshake protocol that works well with the system design is presented in section 3 with definition of system entities. Further, section 3 presents light-weight message frames and fair billing schemes for CAEV charging reservations. Section 4 presents the system cycle of the CAEV charging reservation and trip planning system that can be realized using the proposed architecture and protocol for the ITS application. Finally, section 5 concludes this chapter.

3.2 Proposed Design of the Three Layer Charging Network Hierarchy

The presented architecture is novel, as it aims to operate with both existing wired and future wireless charging systems including SWC and DWC systems. The wired and wireless charging systems should also be able to interoperate with one another. Hence, a hierarchical and layered approach is adopted to enable seamless communication between several CNs of different type. The hierarchy introduces efficiency and control into the design, as it dynamically distributes a single charging request over CNs of different types. Decentralized decision making is avoided, as it would slow down processing of requests, make it difficult to track the CN accountable for scheduling and certain CNs may be prioritized unfairly. Next, layers allow for all types of CNs to have similar architecture and features, and introduces uniformity in design. The latter also ensures expandability, as future CNs can be added easily.

3.2.1 Charging Network Hierarchy

This system design enables static wired charging network or CC network (CCN), DWC network (DWCN) and SWC network (SWCN) to communicate with one another as well as allow for dynamically fulfilling large charging requests by automatically distributing the request over different types of available charging networks (CNs). To achieve the latter, the hierarchy of CNs for communication is proposed. The CN hierarchy in Figure 3.1 has a CN head (CNH) that contains information about all the existing types of CNs, and manages and maintain all the connected CNs of different types. The dynamic charging network has only one type that is DWCN in this system, and the static charging networks are of two types: 1) CCN and 2) SWCN. DWCNs have electrical vehicle supply equipment (EVSE) that control an array of WCPs typically embedded beneath roads to facilitate in-motion charging, whereas the SWCNs have EVSEs that typically control one WCP usually installed at parking locations to enable a CAEV to park and charge for longer durations. CCNs like SWCNs are static in nature and only have EVSEs. CCNs enable CAEVs to receive charging after parking and plugging-in to EVSEs usually for longer durations.

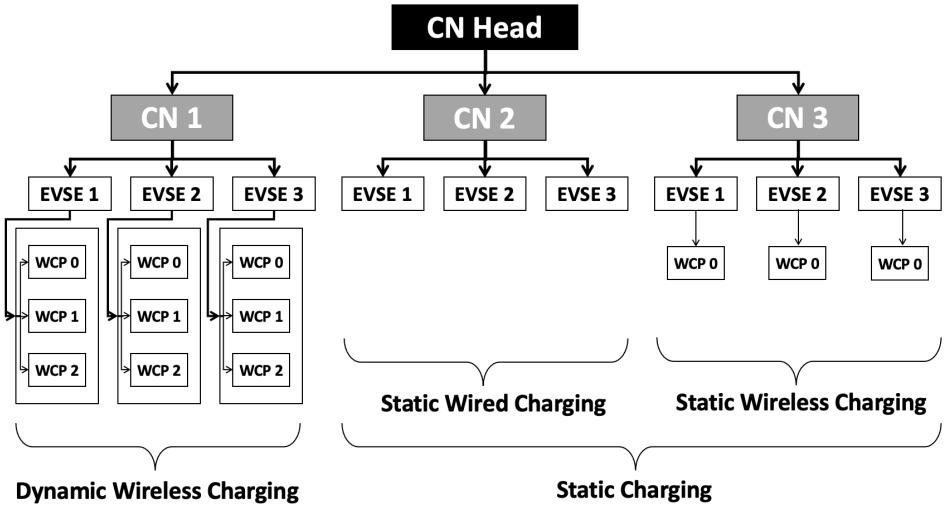

Figure 3.1:Charging Network Head manages the three types of charging systems.

The CCN infrastructure is very prevalent today. This thesis is focused on implementing and simulating the less prevalent wireless charging options. Usually, WCPs are installed on a highway lane in DWCNs and installed at a parking lot in SWCNs. The presented wireless charging system aim to work with existing standard wired charging infrastructures like the ones at Caltech adaptive charging network (ACN) and Jet Propulsion Laboratory (JPL) located in California [262].

3.2.2 Three Layers

The three different CN types are all implemented to operate with the following proposed three-layer system design:

Layer 0 - Vehicle Layer: It is composed of CAEVs and EVSEs that are wired in CCNs and wireless for DWCNs and SWCNs, and can communicate with one another using V2G. Additionally, in the DWCN, the EVSE is connected to an array of WCPs that are embedded under a highway lane. In SWCN, the EVSE is only connected to one WCP that may be installed above ground or below ground at static locations like parking lots. Each WCP comes equipped with an RFID sensor for detecting and authenticating a vehicle and sensors for detecting and reporting vehicle body misalignment and speed errors. The static CNs that include the CCN and SWCN may have queues of a certain size per EVSE to allow CAEVs to wait in line for their turn to receive charging.

Layer 1 - Fog Layer: This layer is composed of one or more RSUs that act as gateways between the lower and upper layers. The DWCN system has one RSU for each EVSE with an array of WCPs, and has several RSUs installed along a long highway lane for the moving CAEV to communicate easily with the above or lower layer with V2I. On the other hand, the SWCN and the CCN have only one RSU due to their static nature. Importantly, the RSUs of different CNs or the same CN can communicate with one another.

Layer 2 - Cloud Layer: This layer is composed of entities that require heavy processing, power and storage, and is shared by all CNs. The cloud entities include the Key Distribution Center (KDC), Bank, Energy Service Provider (ESP) and Energy Distribution Center (EDC). The role of each of the four main cloud entities is described below:

a) KDC: It enables symmetric encryption, and allows access to two or more entities by generating a unique session key for establishing a secure connection over which data is shared and transferred. The Bank, EDC and ESP as well as the RSUs are all registered with the KDC.

b) Bank: The CAEV users register and open a bank account in person with a minimum set opening balance. The Bank will act as the middle-man between the EDC and the CAEV to anonymously and securely complete Credit Points (CPs), a virtual currency, purchase and sales transactions.

c) ESP: It is responsible for generating and supplying power to the CN and its EVSEs with the help of an EDC. There can be one or more ESPs each with their own methods of generating and supplying energy.

d) EDC: It is an entity that manages both the payment and the distribution of the energy provided by one or more ESPs. The EDC will be responsible for distributing CPs in exchange

for actual money to the CAEV user. These encrypted CPs are used as virtual currency to pay for requested charging reservations. Each CP is defined to be sold at a determined fixed rate, for example, 1 CP can be sold at the rate of $1.00. Next, the EDC is also responsible for communicating with the CNH via the ESP to check the status and availability of the EVSEs for making the requested charging reservations.

The system design for CCN, SWCN and DWCN can be seen in Figure 3.2, Figure 3.3 and Figure 3.4, respectively. Figure 3.1 puts the interaction between the wired and wireless CNs into perspective.

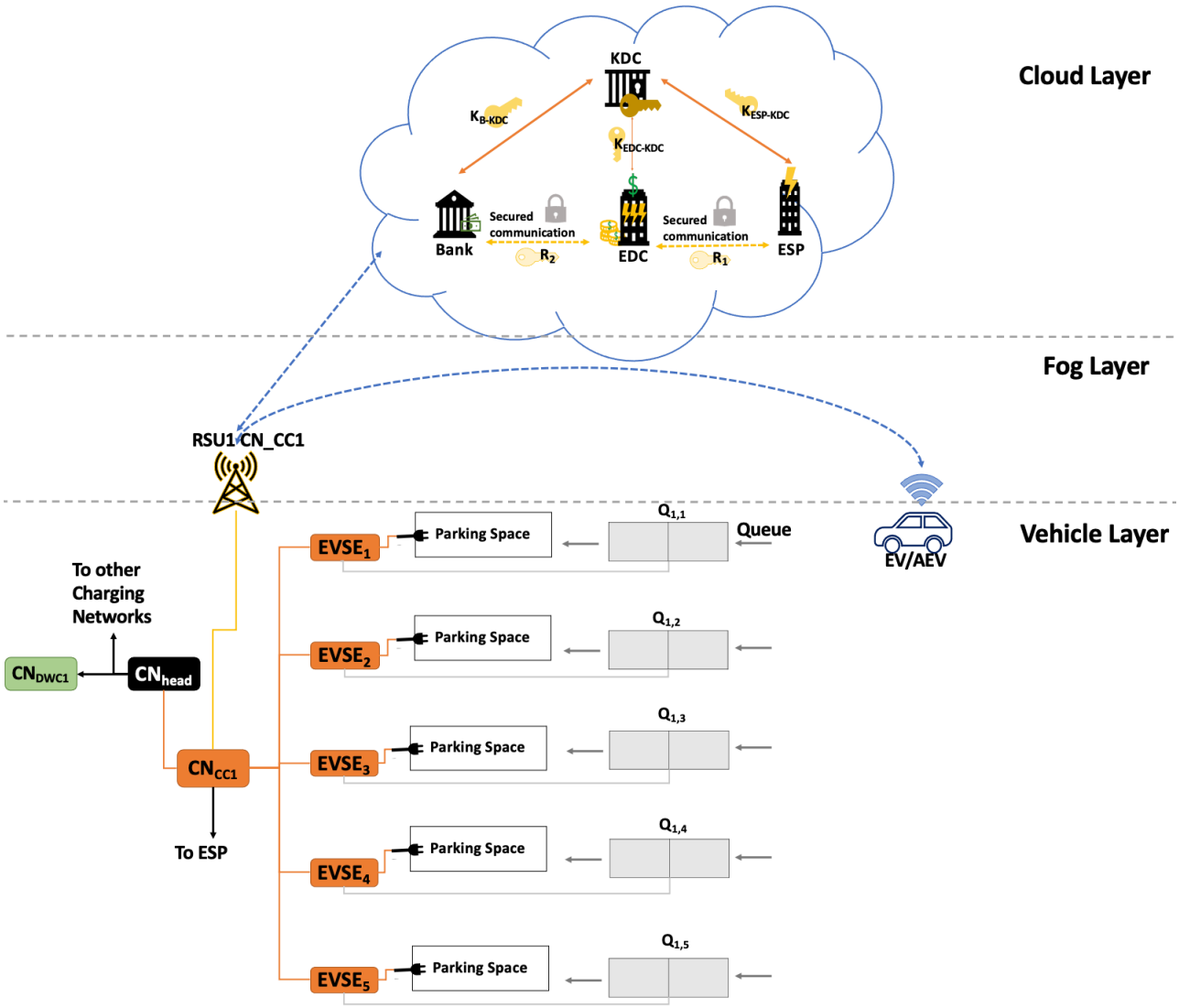

Figure 3.2: CCN following the proposed three-layer hierarchical design.

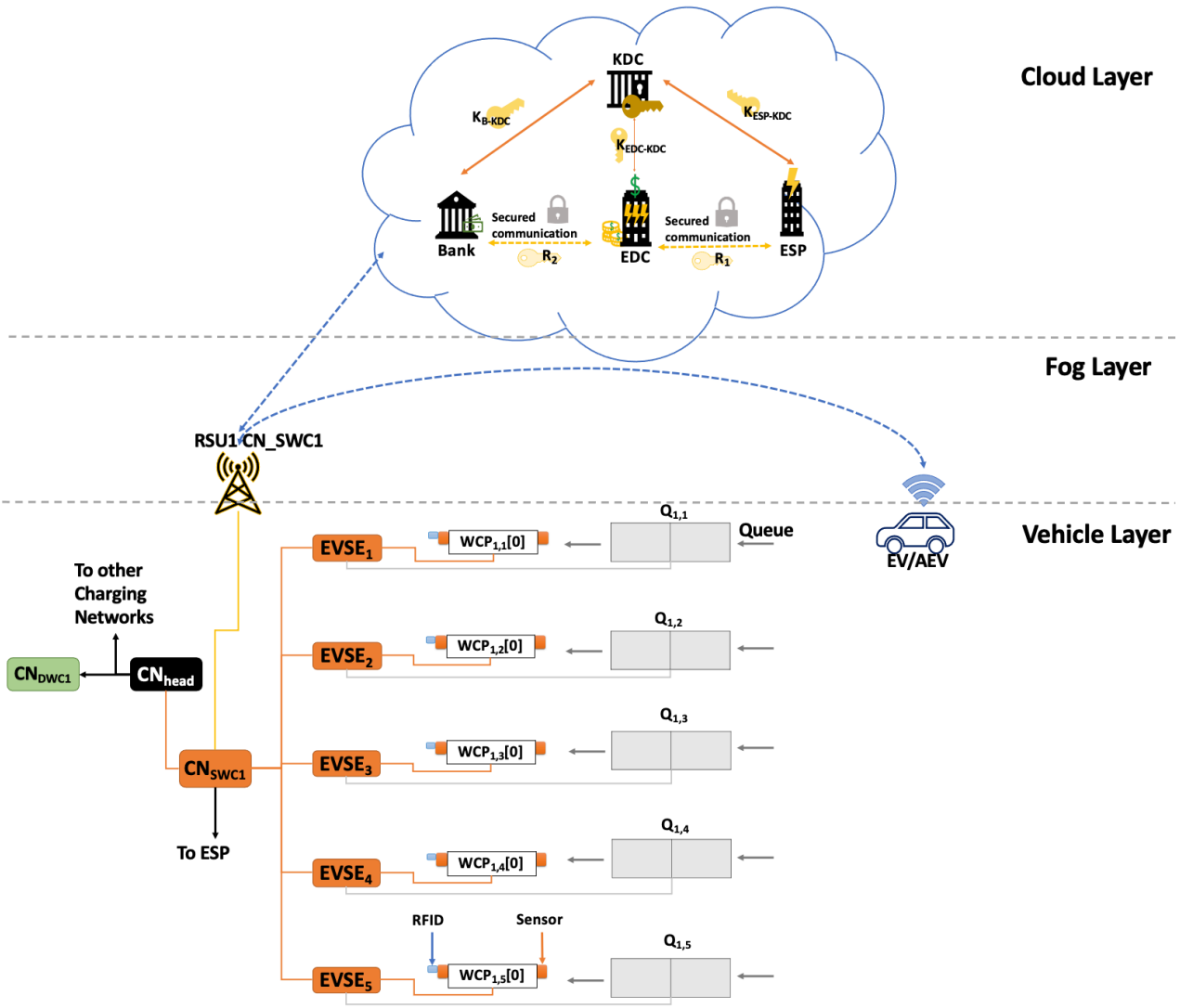

Figure 3.3: SWCN following the proposed three-layer hierarchical design.

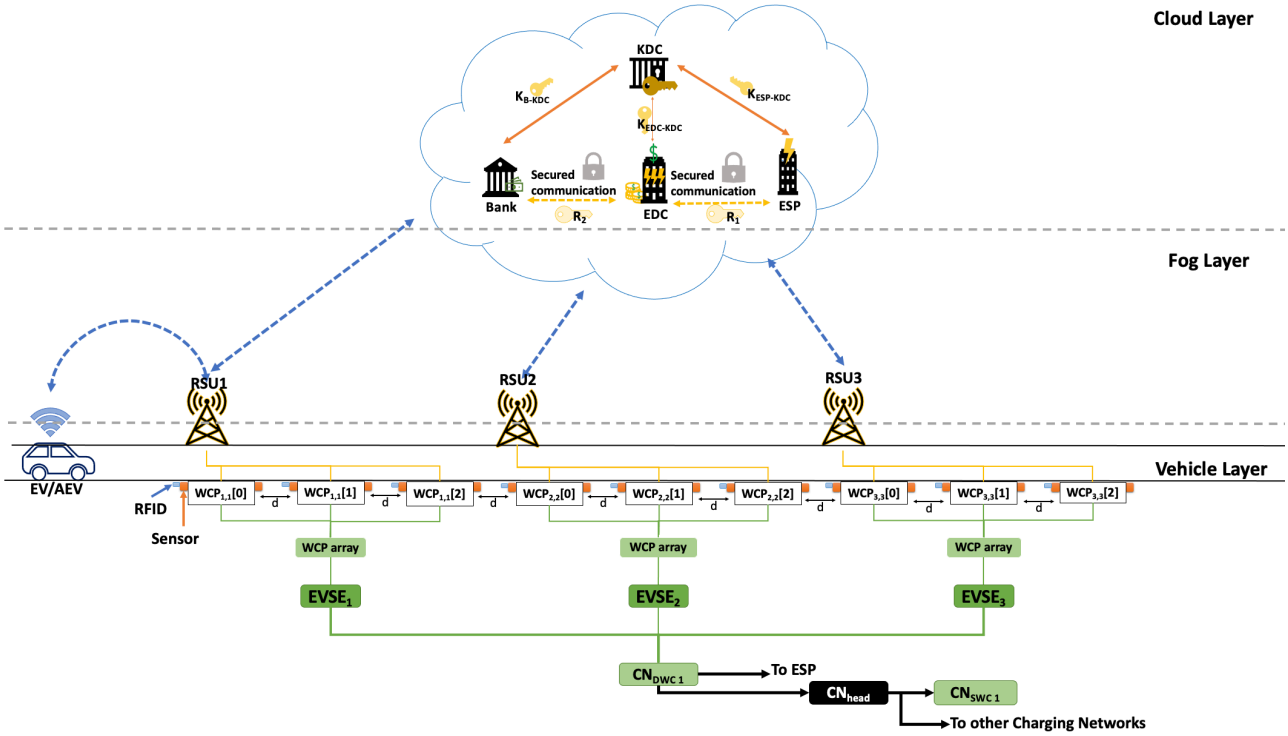

Figure 3.4: DWCN following the proposed three-layer hierarchical design.

3.3 Proposed Handshake Protocol

This section describes the proposed handshake protocol that works in tandem with the proposed three-layer hierarchical CN system to enable communication between a CAEV and the CN. It can enable IoT applications like requesting charging reservations.

3.3.1 System Entity Definitions

Besides the cloud entities that included the KDC, Bank, EDC and ESP, the basic system entities and their roles are described below:

a) Battery: Every CAEV is equipped with the industry standard lithium-ion battery that can be charged using both wired charging systems and wireless magnetic resonance charging systems.

b) EVSE: The electric energy supply equipment controls the charging current of a CAEV for charging. The correct charging current is set based on the maximum current the charger can provide as well as the maximum current the CAEV can receive. In CCN, they communicate with the CAEVs directly, whereas in wireless charging the EVSE communicate via the WCPs to ensure proper and safe delivery of charging. Safety is ensured by stopping power supply if the charger is not correctly connected in CCNs and if the CAEV is not properly aligned on the WCPs in the SWCNs and DWCNs. Thus, preventing battery damage, electrical shorts and fire.

c) WCP: They have a short-range communication module like RFID for direct communication with the CAEV in wireless charging systems. They are connected and controlled by EVSEs. These WCPs are also equipped with misalignment detection sensors and speed detection sensors to ensure expected reserved charging is delivered to the CAEV. These WCPs may be installed above or below ground of a parking lot or garage, for example, in SWCNs and are installed underground of highways and roadways in DWCNs.

d) CAEV: It is powered by a lithium-ion battery, and is equipped with an OBU, GPS and sensors to record relevant information for a single charging reservation like arrival time, departure time, estimated departure time, current speed, current SoC, CAEV range, CAEV battery efficiency, and requested energy. The CAEV user may manually send a charging request or the CAEV may automatically detect the current SoC and send a charging request to the nearby RSU in a reservation request message frame. These CAEVs are also equipped with low-latency and fast wireless communication technology like LTE or 5G for seamless V2I communication. CAEVs include location and navigation information to carry out self-driving actions like driving itself to the reserved EVSEs of the allocated CNs following the proposed confirmation reservation frame's information. Additionally, each CAEV user registers their CAEV with the Bank to open an account with virtual currency called CPs.

e) Account: Each CAEV user is mandated to open a bank account in-person with a set opening balance. The in-person registration ensures a more secure system, as the CAEV user passes through background checks. Further, the account adds a layer of privacy and security by keeping the CAEV user's current location and identity private, and the use of virtual currency like CPs also enables secure payments for IoT applications. For example, this account enables payment transactions for reserved charging sessions to the EDC, as well as for any penalties if enabled by the implementer for late arrivals, late departures, accidents and inappropriate behavior like blocking EVSEs. The bank account enables the user to securely buy as well as sell CPs to the EDC through an RSU at a set rate, and even buy CPs on credit.

f) CPs: They are a form of virtual currency that are encrypted with a unique ID to add a layer of protection and avoid forgeries. These CPs help maintain anonymity of the CAEV user and enable location privacy and secure payments for the charging reservations. These CPs are purchased by the Bank from the EDC at a defined selling rate, for example, $1.00 per CP. The CPs can also be sold back to the EDC by the CAEV based on the defined buying rate of the EDC, and can also be transferred to other CAEV user account's if the option is enabled by the implementer.

g) RSU: They are strategically placed for wide coverage in a given area and are accompanied by all CNs. They make up the Layer 1 - Fog Layer of the proposed system. They act as secure gateways that can process the incoming CAEV messages from the Layer 0 - Vehicle Layer and pass it on to the Layer 2 - Cloud Layer and vice versa. They receive and process the incoming charging requests, report confirmation of reservations as well as report misalignment and speed issue errors back and forth from the CAEVs to the EVSEs of the CN. Each CN has its own RSU type with a unique ID. The SWCN and the CCN have only one RSU, whereas the DWCN has multiple RSUs spread across the highway for the in-motion CAEV to maintain connectivity.

3.3.2 Bank Account

Every CAEV user will need to register and open an account with the Bank in person to purchase CPs. The latter virtual currency would enable the system to keep the CAEV user's location and identity private while adding a layer of security and privacy to the system. The account ID will not have any association with the CAEV ID, and will not carry or share information regarding the CAEV's current location and identity. Further, the account's use of virtual currency also eliminates access and use of actual monetary currency by the IoT system applications. These CPs may have value only in context of the IoT system applications that employ them as acceptable means of payment. Thus, enabling the CAEV user to pay off bills for the charging session securely while upholding privacy.

A. Account Registration

The CAEV user must go to the Bank in-person and open an account with a set minimum balance of, for example, $100.00. Then, it is safe to assume that each CAEV with its unique ID comes registered with the Bank and has a minimum initial balance of $100.00. Hence, a registered account is mandatory for the CAEV to operate in the proposed system. Further, the in-person registration with the Bank makes the system more secure. Since, the account registration procedure with the Bank often involves in-person meeting and thorough background checks. The account registration is advocated to be independent from the CAEV itself. So, the CAEVs can be shared without any change in its payment operation where by the current CAEV user may login and pay for their charging sessions. In the future, if multiple users are carpooling, then each passenger using their account can be billed equally for the charging sessions and penalties if any.

B. Account Access

The CAEV user may wish to get their account information like the total number of transactions, type of transactions, the current balance in both dollars and CPs and amount in credit and debit, etc. The CAEV user can gain access to their bank account by communicating with the Bank via a nearby RSU. The communication link can be secured thanks to the KDC provided one-time session keys. CAEV user may login with its credentials and the Bank may then enable it access and provide the information it seeks. The Bank may put limits on the number of account transactions in a day, the minimum amount in the account, the maximum and minimum amount for transactions in dollars and virtual currency, and may even charge a fee for carrying out certain transactions or charge a fee for processing transactions on certain times of the day.

C. Account Transaction Types

After gaining access to the bank account, the CAEV user account can carry out four main types of bank transactions at minimum: 1) Debit, 2) Credit, 3) Buying CPs and 4) Selling CPs. The CAVE user's bank account carries out debit transactions when depositing and withdrawing money from the account or transferring money to other bank accounts. The money is specially deposited into the account when the CPs are sold back to the EDC and are debited by the Bank when CPs are purchased. The credit type transactions are carried out when the CAEV user wishes to borrow money from the Bank to assist in buying CPs. The system may automatically borrow money from the Bank when the CAEV user account requesting for a charging reservation does not have sufficient funds to book charging sessions or to pay bills for the charging sessions. Thus, preventing the charging reservation system from declining the request of a CAEV user with insufficient funds. Credit option even helps pay off charging session bills. A maximum limit for borrowing money from the Bank may be set by the account holder or the Bank. The CAEV user can they pay off the credited amount at a later date to the Bank. Next, the CAEV user may wish to purchase CPs to pay off bills for charging sessions now or in the future. The Bank acts as an intermediary between the CAEV user and the EDC to enable purchase of unique and encrypted CPs at the selling rate set by the EDC, for example, 1 CP is sold at the rate of $1.00 by the EDC to the Bank. Again, the communication link between the cloud entities, Bank and the EDC, and the CAEV user via the RSU can be secured using one-time session keys of the KDC, for instance. The CAEV user may first login to their account to gain access. After successful authentication by the Bank, the CAEV user can then use the account to place an order to buy CPs. The account will carry out the buying CPs

transaction, for example, by buying 100 CPs from the EDC at its fixed selling rate of let's say $1.00 per CP. The EDC will then create and assign unique and encrypted CPs to the account, and the account will then be appropriately debited for $100.00 for the 100 CPs. During the buying of CPs, if the CAEV's account does not have sufficient monetary funds, then the account will automatically borrow the exact amount of money from the Bank in a credit transaction prior to the buy CP transaction. Fourth transaction type is the selling of CPs, and it entails the CAEV account selling a number of its CPs back to the Bank. The CAEV user may wish to sell back their CPs to the EDC, for example, to pay off their account's credit bills. Let's say the EDC buying rate is $1.00 per CP. Then, the selling CP transaction will take the number of CPs the user wishes to sell let's say 50. These 50 unique and encrypted CPs are sold back to the EDC only when the EDC ensures that they are not forgeries, have not been used and were created by an authorized EDC. EDC then buys back the authenticated CPs and the CAEV user account will then be debited with $50.00 in this case. The EDC may then resell the CPs to other CAEV user accounts. If forgeries are found, the EDC may file a complaint and the Bank may block the CAEV user account for further investigation.

Figure 3.5 shows the CAEV securely communicating with the Bank and the EDC via the RSU using KDC assigned one-time session keys. The CAEV user after gaining access to the account may carry out actions like logging in to the account, checking balance and buying and selling CPs as depicted in Figure 3.6.

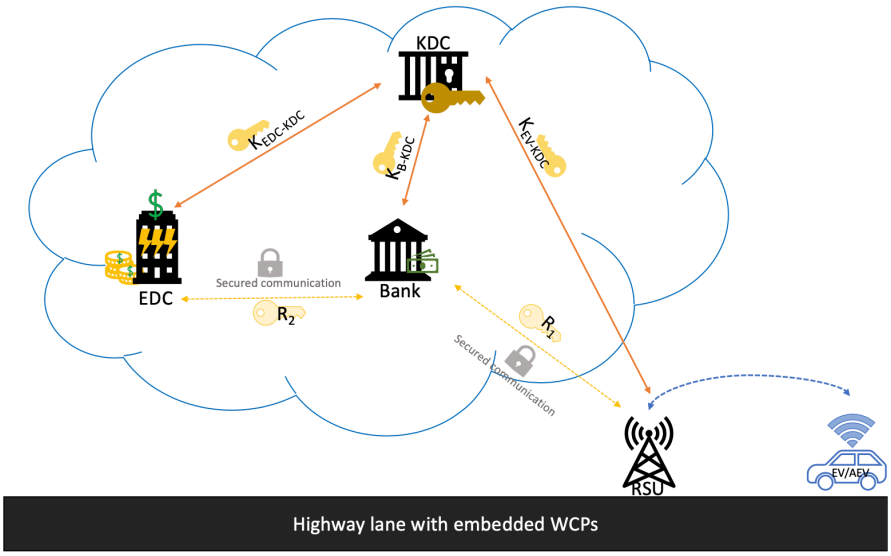

Figure 3.5: Secure communication between the vehicle and the cloud.

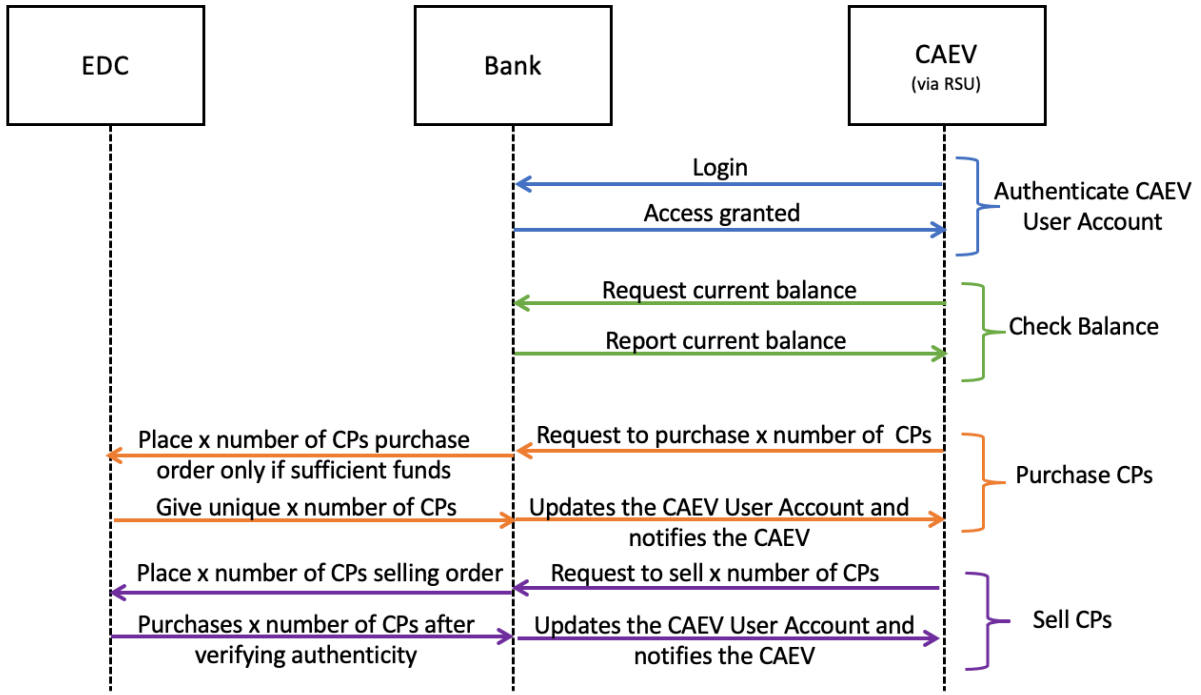

Figure 3.6: The CAEV user account authentication, balance checking and purchasing and selling of CPs.

3.3.3 Proposed Light-weight Message Frames

Message frames are proposed to enable a CAEV to request a charging reservation over the proposed system architecture and receive a confirmation for a charging reservation.

A. Reservation Request Message Frame

The reservation request message frame, F_{req}, is created to enable a CAEV to communicate via a nearby RSU with a charging reservation system that employs the presented system architecture. The F_{req} is designed to be light-weight and secure by only carrying information that is essential to request a charging reservation. No information about the CAEV's identity is recorded. The frame is then designed to contain the current speed (curr_speed), current SoC (curr_SoC), requested SoC (req_SoC), and the current balance (curr_balance) of CPs at minimum. Additional details may include CAEV's disclosure of its current location (source_ID) and the intended destination (dest_ID) as well as arrival time (time_arr) and departure time (time_dept). These additional message contents can help the system to plan a shortest route for the CAEV's trip with the charging reservations considered. The message frame contents sent from the CAEV to the RSU can be seen highlighted in gray, and the RSU added fields can be seen highlighted in blue in Figure 3.7 (a). The RSU adds its own ID, RSU_ID, and location ID, loc_ID, to the message to help estimate the CAEVs location on a map besides CAEV's own disclosure of its location. To maintain anonymity of the user and the CAEV, the CAEV is assigned a randomly generated unique reservation request ID

(req_ID) by the RSU for every charging reservation request message generated. Then, this F_{req} is forwarded to the EDC. The EDC may then do the necessary processing and add contents to the request message frame that includes the type of CNs (type_CN), the req_SoC from each CN type and the estimated CAEV charging duration (dur) at the CN. The latter message contents are highlighted in yellow in Figure 3.7 (b). The message frame can then be used to look up EVSE availabilities and make the best reservations possible for the CAEV over the CNs to fulfill the charging request.

req_ID	1234
curr_speed (km/h):	45
curr_SoC:	0.25
req_SoC:	**0.75**
curr_balance:	100
source_ID	0007
dest_ID	0015
time_arr	12:45:00
time_dept	15:00:00
RSU_ID	0001
loc_ID:	0007

(a)

req_ID:	1234
curr_speed (km/h):	45
curr_SoC:	0.25
req_SoC:	**0.75**
curr_balance:	100
source_ID	007
dest_ID	0015
time_arr	12:45:00
time_dept	15:00:00
RSU_ID:	0001
loc_ID	0007
type_CN:	[CN_DWC, CN_SWC]
	CN_DWC:
	req_SoC: 0.30
	dur: 20
	CN_SWC:
	req_SoC: 0.15
	dur: 35

(b)

Figure 3.7:The reservation request message frame that is processed by the (a) RSU and the (b) EDC.

B. Reservation Confirmation Message Frame

The proposed reservation confirmation frame, $F_{confirm}$, is returned back to the EDC by the CNH and then finally reported to the CAEV via the RSU to confirm the reservation of EVSEs at the CNs that will best fulfill the CAEV's original charging reservation request. This frame at minimum will contain the reservation confirmation ID (confirm_ID), reserved CN IDs (CN_ID), their EVSE IDs (EVSE_ID), and their respective location IDs (loc_ID) and their reservations' start time (start_time) and end time (end_time). This is reported back to the CAEV from the EDC through the RSU as can be seen in Figure 3.8 (a) where the blue highlighted fields carry RSU information like RSU_ID and its loc_ID and the yellow highlighted fields are specifically generated by the EDC. The confirm_ID is the same as the req_ID for the CAEV from its F_{req}. The latter enables traceability for the CNH while keeping

the CAEV's user information private. It can also allows the CNH to know the exact amount of charging is going to be fulfilled by each CN's reserved EVSE. The minimal $F_{confirm}$ can be seen depicted in Figure 3.8 (a). Additional information can be added to the frame like the allocated reserved time duration (alloc_time) at the EVSE, the requested SoC (req_SoC) reserved to be delivered by the CN (req_SoC) and the type of CN (type_CN). The reserved start and end times with the desired SoC to be delivered for each EVSE reservation can be included as well or removed based on the level of privacy of information by the implementer. For the system, the confirm_ID is sufficient for a CN to retrieve details for the reservation of a CAEV. The CN IDs and the EVSE IDs enable navigation to the CN's EVSE. The added details can be seen in Figure 3.8 (b). As a design choice, the detailed $F_{confirm}$ in Figure 3.8 (b) can be sent to the EDC while the EDC trims the details like allocated reservation time, start and end times, and requested SoC for more privacy and efficiency, and sends the trimmed frame in Figure 3.8 (a) to the RSU for acknowledging the successful confirmation of the reservation request. Finally, the RSU can communicate to the CAEV the approval or acknowledgement of the request with this $F_{confirm}$.

confirm_ID:	1234	
RSU_ID	0001	
loc_ID:	0007	
	CN_ID:	3002
	loc_ID	0003
	start_time	13:30:00
	CN_ID:	2002
	EVSE_ID:	2009
	loc_ID	0002
	start_time	14:00:00
	end_time	14:35:00

(a)

confirm_ID:	1234	
RSU_ID	0001	
loc_ID:	0007	
type_CN:	[CN_DWC, CN_SWC]	
	CN_DWC_ID:	3002
	req_SoC:	0.30
	loc_ID	0003
	start_time	13:30:00
	CN_SWC_ID:	2002
	EVSE_ID:	2009
	loc_ID	0002
	req_SoC:	0.15
	alloc_time:	35
	start_time	14:00:00
	end_time	14:35:00

(b)

Figure 3.8: The confirmation reservation frame for (a) CAEV and (b) EDC.

3.3.4 Requesting a Charging Reservation

A CAEV will communicate the F_{req} that includes the req_SoC to the closest RSU using V2I communication to request for a charging reservation. The RSU of Layer 1 after adding its own ID and location to the F_{req} will forward the frame, see Figure 3.7 (a), to the Layer 2's EDC to make reservations for one or more charging sessions at one or more CNs. The RSU's location ID can help approximately estimate the CAEVs location with respect to the CN if the CAEV user does not wish to disclose the CAEV's exact location. The request message received

by the EDC is enough to first check that the requesting CAEV has sufficient funds or CPs to purchase the desired or requested SoC. If funds are not sufficient, the CAEV's ability to take credit from the Bank is ensured to proceed else the request returns to the CAEV with a negative acknowledgement. If the CAEV's account is approved for sufficient funds, then the EDC communicates with the ESP to look up EVSE availabilities for charging with the help of the CNH. The charging reservation system employing the proposed system architecture will dynamically divide the request over one or more types of CNs. Specially, if the CN type, for example, the DWCN, can only fulfill part of the charging request due to constraints of maximum SoC it can provide. The charging reservation system can even have an integrated trip planning system to enable the charging reservation system to look up EVSE availabilities in CNs that are close in proximity and along the CAEV's trip route. The joint charging reservation and trip planning can save computation costs by narrowing the number of CNs to look up for availabilities, and may result in a more optimal and intelligent charging reservation for the requesting CAEV. The final message frame communicated by the EDC to our proposed CNH via ESP can be revisited in Figure 3.8 (b).

Figure 3.9 shows the CAEV sending a charging reservation request with the proposed frame with two cases. In case 1, the CAEV's charging reservation request does not go through due to insufficient funds, and the EDC reports this error to the CAEV. Then, the CAEV can get credit from the Bank or terminate the request. In case 2, the CAEV's charging request is approved by the EDC, and the EDC starts looking up available EVSEs for charging reservation with the help of the ESP and the CNH.

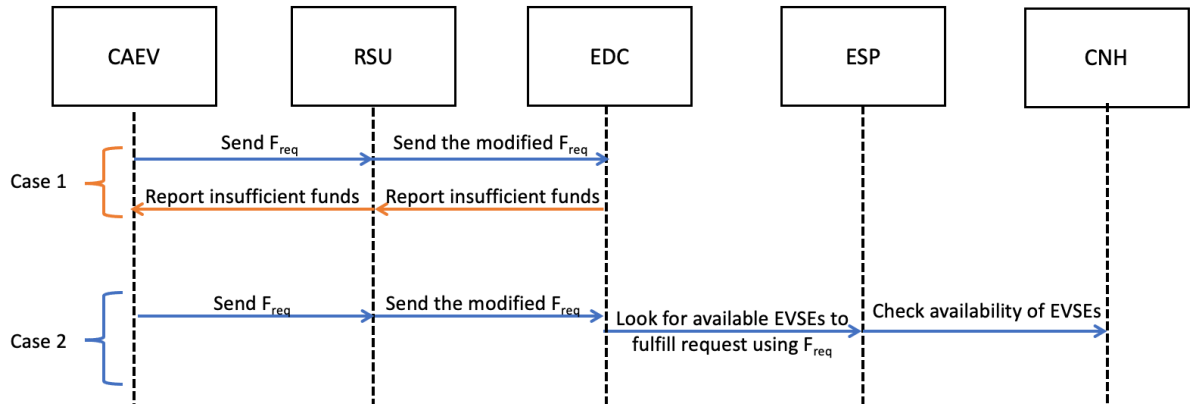

Figure 3.9: CAEV sends the charging reservation request.

3.3.5 Confirming a Charging Reservation

The EDC had sent the F_{req} to the CNH via the ESP to look up available EVSEs for charging reservation. So, the CNH waits back for the list of EVSE availabilities from all or selected CNs close to CAEV's reported current location or trip route. The CNH will then report

the list of availabilities to the EDC via the ESP to select the best possible EVSEs for reservation in fulfilling the charging reservation request. The EVSE selection can be based on the first available EVSE that can provide the maximum SoC to the CAEV in the estimated charging time. Other selection parameters that may be set all together or individually can include minimizing waiting times, travel times, pricing, charging duration, etc. After selecting the EVSEs based on the set parameters, the EDC will send the message to the CNH via the ESP to reserve the chosen EVSEs. The CNH reports back the acknowledgement for successful reservations of EVSEs at the CNs to the ESP. The ESP notes the locations of the EVSEs and the reserved start time and end time of the charging, and reports it to the EDC. This information is used by the EDC to create the $F_{confirm}$ to be delivered to the CAEV. As a design choice, either the detailed frame illustrated in Figure 3.8 (b) is reported to the CAEV or the trimmed down frame for added security that is illustrated in Figure 3.8 (a) is reported back to the CAEV via the RSU for confirmation of a successful charging reservation.

Figure 3.10 illustrates the CAEV sending a F_{req} , the system looking up all available EVSEs in all CNs, selecting the EVSEs to best fulfill the request, making the EVSE reservations and reporting back the confirmation to the CAEV. So, the request for a charging reservation has been approved and acknowledged with the $F_{confirm}$. Now, the establishment of the charging session for initiation of charging is discussed in the following section.

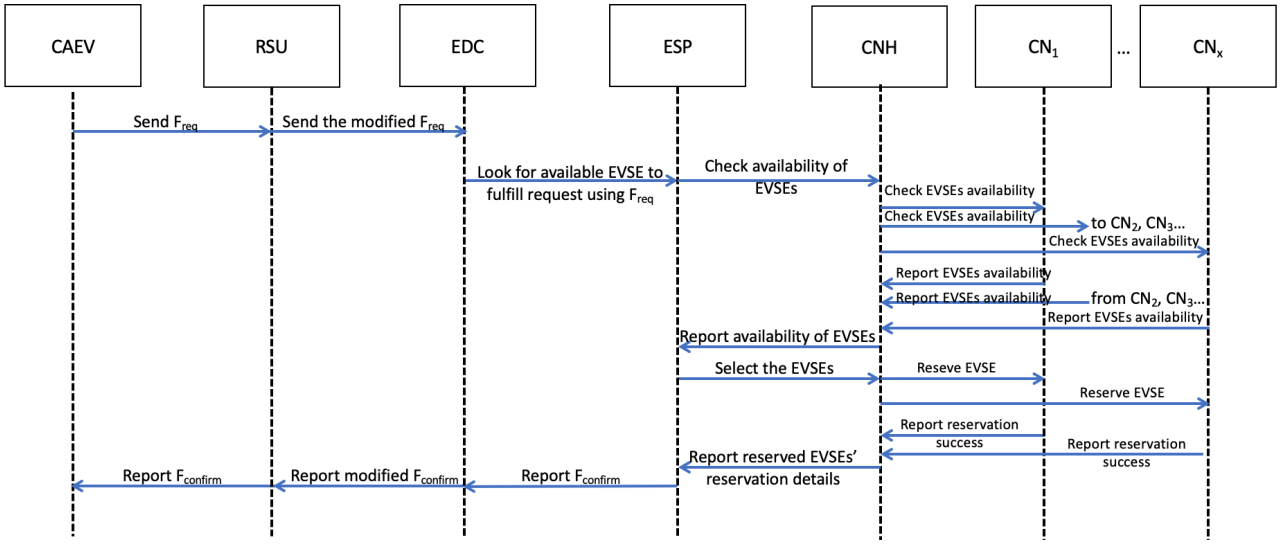

Figure 3.10: CAEV user sends the charging reservation request frame and receives the confirmation frame.

3.3.6 Establishing a Charging Session: Authentication, Synchronization and Charging

In CCNs, the CAEV is authenticated by exchanging the confirm_ID from its $F_{confirm}$ with the EVSE. The power is then supplied to the CAEV only if it is properly connected to the EVSE and has a charging reservation at the current time. On the other hand, in wireless CNs,

the CAEV is detected by the WCP's sensors and upon contact it exchanges the confirm_ID from its $F_{confirm}$. The WCP will then communicate this ID with its EVSE. If the confirm_ID is in the EVSE's reservation list, then the EVSE will start supplying power by turning the WCP ON when the CAEV is detected else the WCP remains OFF. To ensure vehicle authentication for an approved charging session specifically in wireless CNs, the following three options can be explored:

Option 1: Using RSUs

Approach 1: Communicating with the reserved EVSE

The CAEV communicates its confirm_ID with the RSU that is wired to one EVSE in DWCNs and all EVSEs in CCNs and SWCNs. This RSU keeps a list of the charging reservation confirmation IDs for all the EVSEs in static CNs and for an EVSE to which it is wired in DWCN. If the reservation confirmation ID is in this reservation list, then the EVSE is communicated the information to be ready for the CAEV. In CCNs, the EVSE will then simply start supplying power once the CAEV plugs in for charging. In wireless CNs, the EVSE immediately turns ON the WCP for the incoming CAEV. The sensors on the WCPs detect the vehicle, and supply the power for the duration the CAEV is in contact with the WCP. Additionally, in DWCN as the CAEV leaves the current WCP, the next WCP is signaled to be triggered ON by the EVSE. This approach assumes that on the DWC lane the CAEVs are not overtaking one another as each WCP only detects the CAEV and does not authenticate it. Importantly, this approach assumes that the CAEV will repeatedly send messages to each RSU that it passes by for authentication, and synchronizing and starting the charging session. Since, it is assumed that each DWCN's RSU connected to a unique EVSE only stores information about its reservations. This process is depicted in Figure 3.11 for the first RSU encountered by the CAEV on a DWC lane. The RSU signals the EVSE to activate connected WCPs, and supply power once the authenticated CAEV is detected.

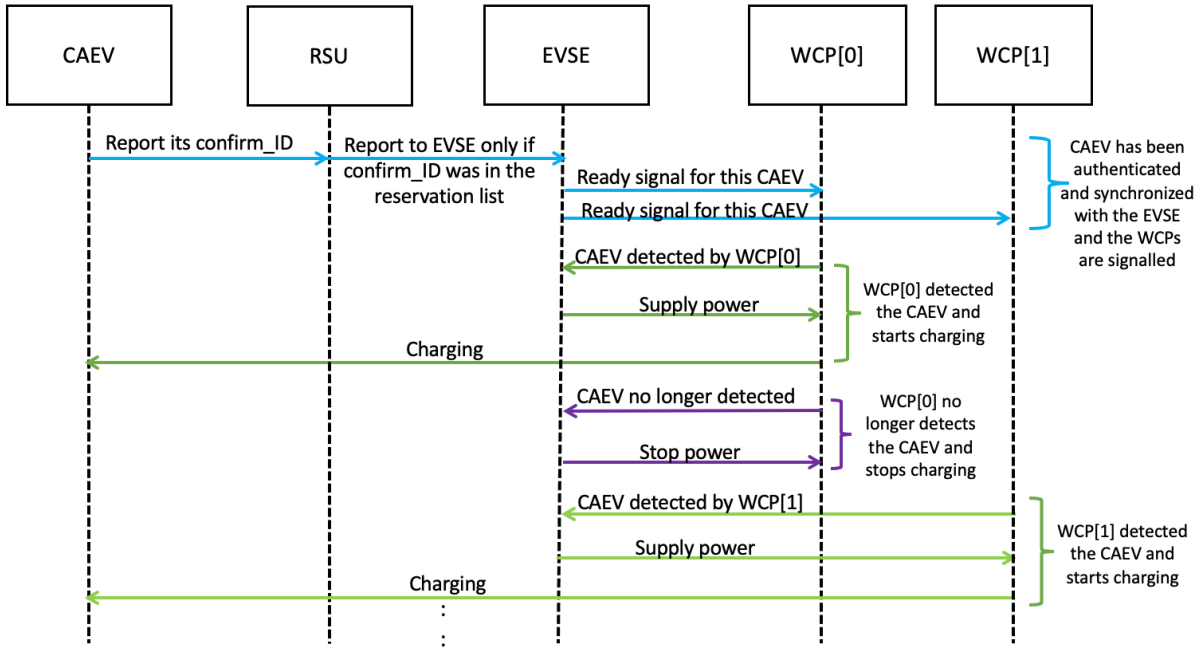

Figure 3.11: CAEV establishing the charging session with EVSE communication via the RSU.

Approach 2: Communicating with the CN

The RSU receives from the CAEV its confirm_ID and it communicates it to its CN. If the reservation exists, then the static CNs signal their EVSE to be ready. In case of DWCN, the CN will use the RSU's loc_ID to approximate the CAEV's location with respect to the DWC lane. If the CAEV is close to the EVSE, then the EVSE is activated to supply power to the oncoming vehicle that will be detected by the sensors of the WCPs of this EVSE. Again, this approach assumes CAEVs are not overtaking one another in the DWCN lanes. In Figure 3.12, the CAEV encounters the RSU of the DWCN and it will prepare all reserved EVSEs of that CN to expect an oncoming CAEV by sending a signal to all the reserved EVSEs. So, this approach is very similar to Approach 1: Communicating with the reserved EVSE except the CN is involved, and a CAEV does not need to exchange multiple messages with each RSU it encounters to ready an EVSE for an oncoming CAEV.

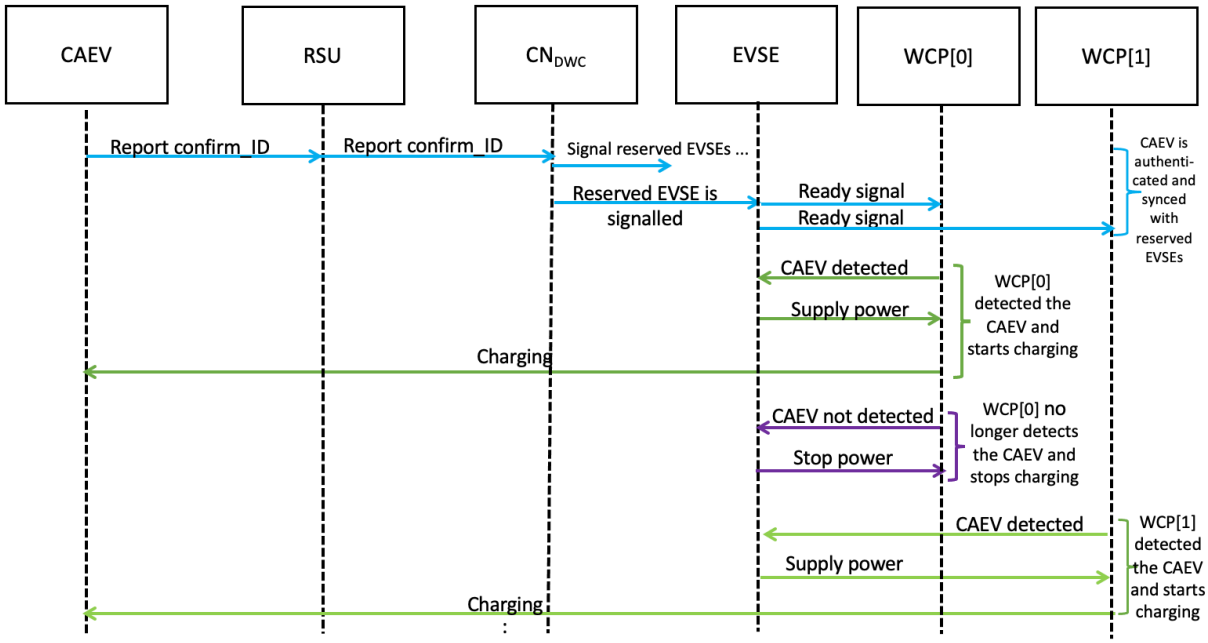

Figure 3.12: CAEV establishing the charging session with CN communication via the RSU.

Option 1 at large cannot avoid free-riders or those that tail behind an authenticated CAEV to steal charging in DWNCs. Since, each EVSE authenticates a CAEV and not the WCPs for charging synchronization. The WCPs only detects the presence of a CAEV and starts supplying power. Also, this option makes it difficult to report error messages like speed and misalignment in time to the moving CAEV in DWCNs.

Option 2: Using RFIDs for direct EVSE communication

In CCNs, the CAEV plugs in to the EVSE, and communicates its confirm_ID to the EVSE using RFID. If the reservation exists, then the EVSE will start supplying power to the CAEV. In wireless CNs, the CAEV is detected by the WCP's sensors and upon contact it exchanges its confirm_ID using RFID. The WCP will communicate the confirm_ID with the EVSE, and if it is in the list, then the EVSE will supply power to the WCP for charging the CAEV. Additionally, this synchronization is done for each WCP in DWCNs, so that the CAEV user can leave the lane and re-enter before a set timer expires. This is depicted in Figure 3.13. Here, the CAEV is synchronized and authenticated for each WCP before being supplied power. Despite the repeated synchronization at each WCP, using only RFID communication for in-motion charging means that the CAEV might soon drive out of communication range of a WCP. This means that the CAEV will not be able to receive immediate error messages about speed and misalignment issues.

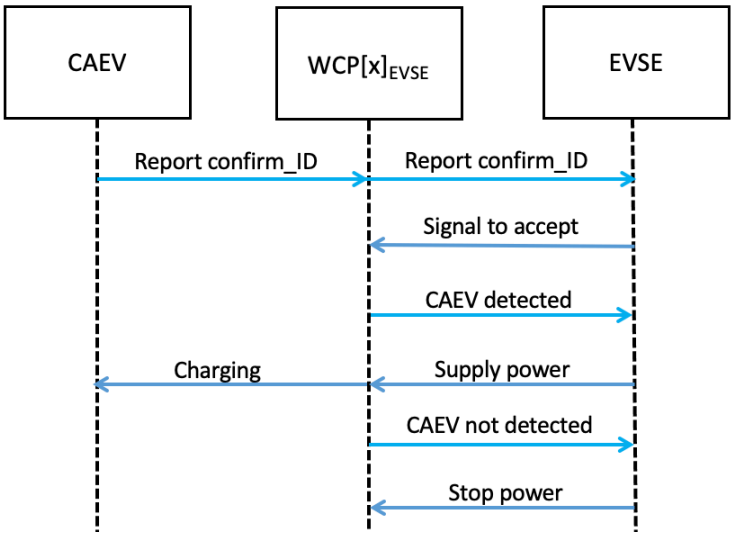

Figure 3.13: CAEV communicates with WCP for charging session establishment.

Option 3: Using both the RSUs and RFID communication

This implementation option combines both options 1 and 2. The initial authentication of the CAEV with the EVSE via an RSU occurs to prepare it for an oncoming vehicle. In CCNs, the CAEV can then just go plug in and use RFID to authenticate and synchronize itself to start receiving charging. In wireless CNs, the RFID communication between the CAEV and the WCP only occurs if the EVSE that contains that WCP is expecting a CAEV. The CAEV's interaction with each WCP is used to synchronize charging, and also to report errors like speed and misalignment. Both SWCN and DWCN use RFID communication to report the error messages immediately to the CAEV. However, if the CAEV is out of range of WCP's RFID communication in DWCNs, then the RSU of the next EVSE on the lane can report the error message to the CAEV. This can be seen depicted in Figure 3.14.

This option stops repeated exchange of messages with each RSU in DWCNs, as the CN will already signal the reserved EVSEs to be prepared for the oncoming vehicle. Further, it also limits the CAEV from sending messages to each WCP encountered. Only the WCPs of EVSE that is signaled to be ready will be open to receive messages and detect vehicles at low power supply, and full power is supplied once the reserved CAEV is detected and authenticated.

This is the best option out of all three, as it allows for misalignment and speed error detection in wireless CNs. It even allows the CAEV to leave and enter the DWCN lane if needed. Most importantly, it prevents free-riders from stealing charging from authenticated CAEVs on DWCN lanes. As a result, this option is highly recommended for implementation and design of a future proof system.

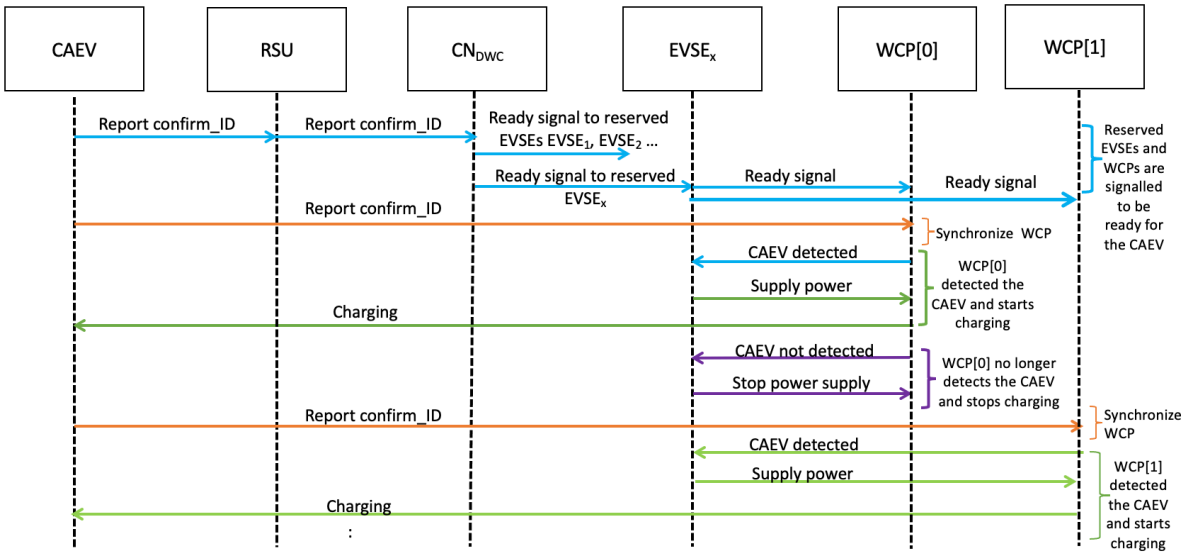

Figure 3.14: CAEV establishes the charging session using RSUs and WCPs.

A. Misalignment Error and Speed Error Detection and Reporting

Charging is only delivered in wireless CNs if the CAEV is parked on the WCP within the alignment tolerance range. If the CAEV is not properly aligned on the WCP as detected by the sensors, the CAEV's OBU is immediately reported to correct the alignment for receiving proper charging. The latter reporting is done either using RFID if the CAEV is within the WCP's range in SWCNs and DWCNs or with RSU if the CAEV is out of WCP's range in DWCNs. Error detection and reporting is done for each WCP in the DWCN lane, so the vehicle has the freedom to leave and re-enter the lane before a time-out expires. This also enables the DWCN to avoid free-riders.

Now, consider the scenario where the CAEV is authenticated with the WCP, but it is not detected by the particular WCP due to misalignment. The WCP will report to the CAEV that it is not being detected. It may suggest moving right or left based on other sensor readings as part of a feedback system with the driver until properly aligned. The Case 1 depicted in Figure 3.15 shows the WCP directly reporting the error to the CAEV with RFID. In Case 2, the CAEV is assumed to have driven past the WCP's communication range, so the misalignment message is reported to the CAEV via the RSU. Case 3 occurs where both the WCP and the RSU are used to report the error to the CAEV, as the CAEV while in range of the WCP was not able to correct its alignment and the RSU had to be used to continue reporting the error until the correction is made. It should be noted that the error is reported continuously as part of the automated driving feedback system until the CAEV corrects its alignment to receive charging.

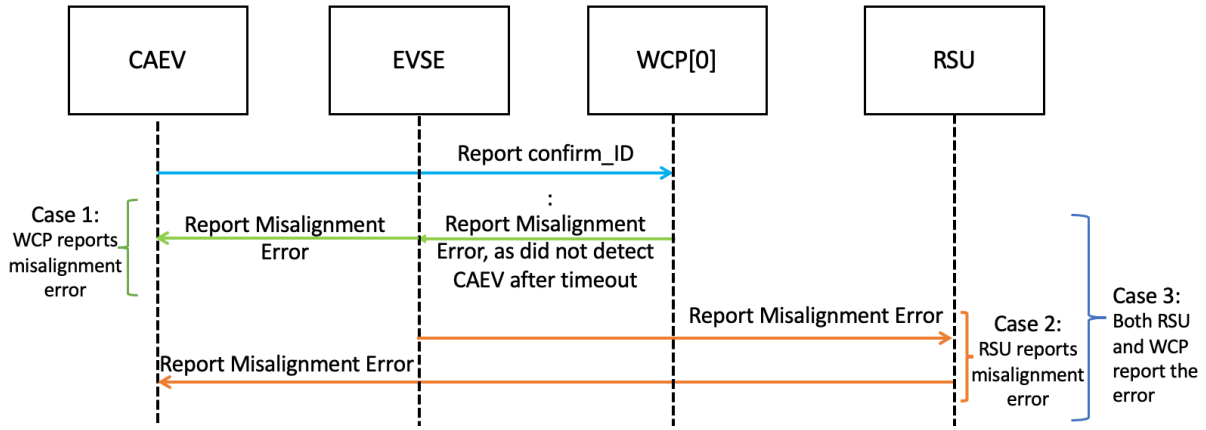

Figure 3.15: Detecting and reporting CAEV misalignment error.

Besides misalignment, in DWCN the CAEV's speed is detected continuously and is reported as a feedback to the CAEV's OBU for correction if outside the set range. Now, consider the case where the CAEV is authenticated and detected by the WCP. The WCP is supplying power, but the CAEV does not receive charging due to the CAEV moving too fast or too slow. The CAEV's report of charging received is not matching with the amount WCP supplied. Hence, the speed issue is detected by checking the current CAEV speed reported to the RSU. The proposal to increase or decrease speed is communicated to the CAEV by the WCP with RFID, RSU or both as can be seen in Figure 3.16 Case 1, Case 2 and Case 3, respectively. In Case 1, the WCP is able to report to the CAEV within the communication range, whereas in Case 2 the RSU reports the error to the CAEV that is now past the WCP's communication range. Case 3, however, uses both WCP and the RSU assuming that the CAEV has not corrected the error while it was within the range of WCP's communication and it continues reporting the error via the RSU.

Another option for detecting no charging received would be to wait for a fixed timer, after sending the authentication and detection message. If the timer expired, then the CAEV that did not receive the charging during the period will contact with the WCP and RSU with its speed and verify if the speed needs to be reduced, increased or maintained for the current and next WCPs as can be seen in Figure 3.17. The error is then reported back to the CAEV by the WCP, RSU or both as depicted with Case 1, Case 2 and Case 3, respectively. Alternatively, both the charging report method depicted in Figure 3.16 and the timer expiration method depicted in Figure 3.17 can be combined. So, before the timer expires the charging report can be checked to ultimately report the CAEV's OBU to correct its speed. This combined procedure could be used as a backup in case of speed sensor failure.

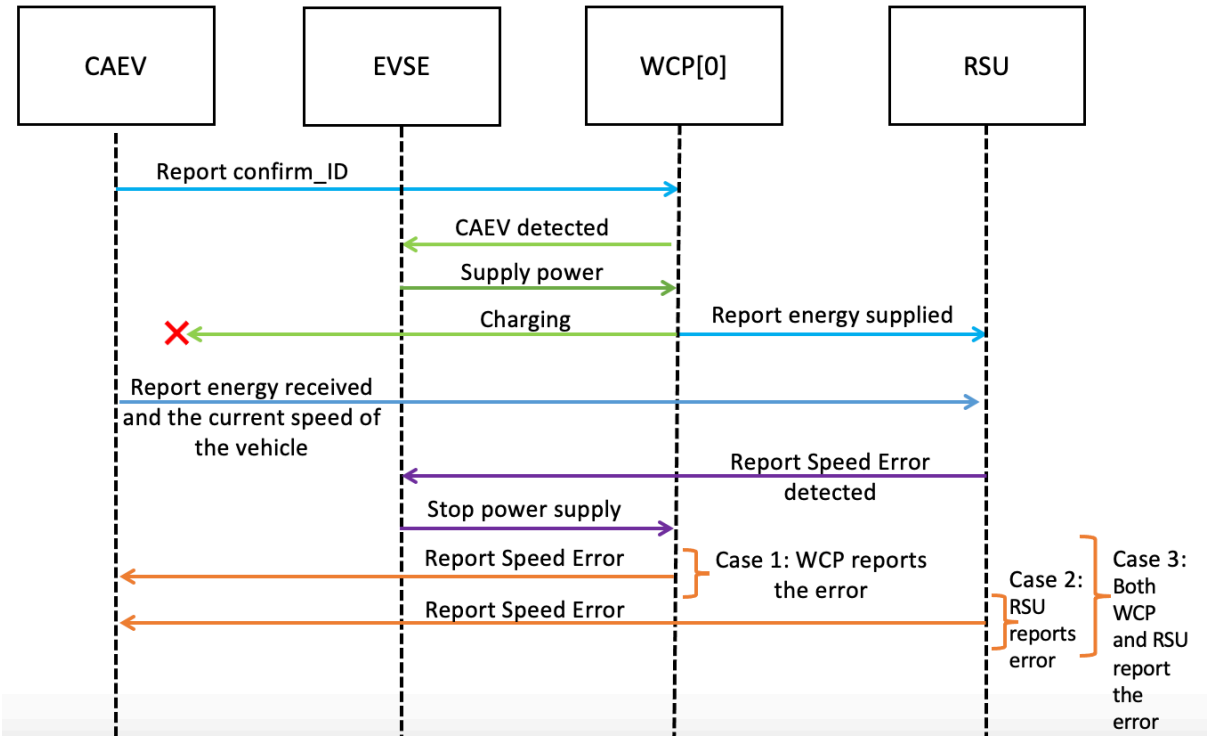

Figure 3.16: CAEV speed error reporting using energy delivered reports from the CAEV and the EVSE.

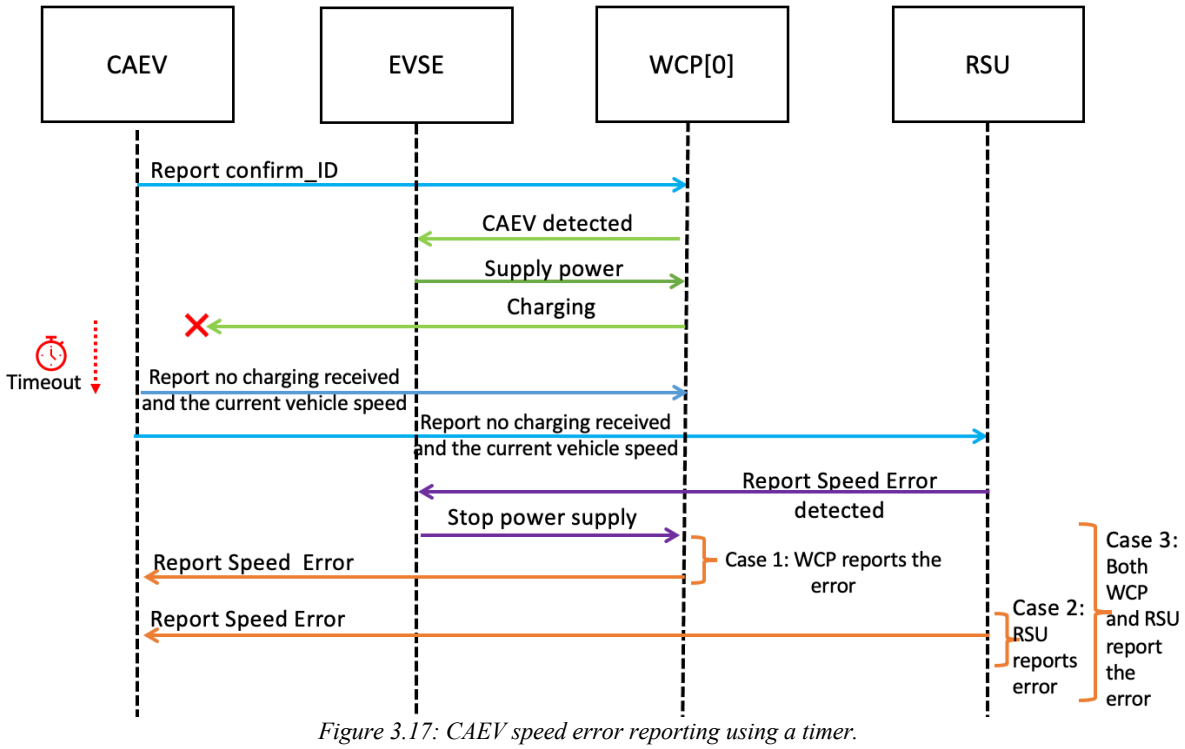

Figure 3.17: CAEV speed error reporting using a timer.

3.3.7 Real-time Charging Metering and Billing Schemes

The CAEV's OBU keeps track of how much kW per ms or µs is received by the battery from the EVSE in the CCN and from the WCP in SWCNs and DWCNs. The charging delivered by the EVSE of a CN to the CAEV is metered in real-time. Based on the Time of Use (TOU) electricity billing model, the EDC can then fairly bill the vehicle with the real-time metered

charging data, and the CPs will then be automatically deducted from the CAEV user account to reflect the change. Fair billing means that the CAEV user account is charged exactly for the amount of electrical energy the CAEV received. One of the following two proposed approaches can be adopted for billing CAEVs for the charging received:

A. Pay Per Charging Session

A charging session is defined by the charging duration for which the CAEV receives continuous charging from a reserved EVSE in static CNs and multiple reserved EVSEs in DWCN. The pay per charging session means paying for the entire charging session. In other words, the CAEV user's CPs are deducted whole at the end of the reserved charging session.

The EVSE may conclude that a charging session is completed when the CAEV is unplugged in CC or the WCP's sensor detects that the CAEV has left in SWC and DWC on or before the end time of the charging reservation. If the CAEV leaves charging before the end of the charging session, a timer may be used to enable the CAEV to resume charging before the timer expires and the session is ended. The EVSE delivers charging to the CAEV, and the metered charging is reported in real-time to the EDC via RSU. At the end of the session, the RSU forwards the request of computing the final bill to the EDC. The EDC computes the final payment in CPs using TOU and reports it to the CAEV. The CAEV is then immediately billed by the EDC, after ensuring that it is being charged for the energy received by its battery. Finally, the CAEV user's bank account reflects the change in CPs while the EDC keeps a record of the anonymous charging session as paid. The charging session is anonymous, as the EDC does not keep record of the actual CAEV user for privacy purposes. The payment for a charging session using pay per charging session method is depicted in Figure 3.18 where it is assumed the charging session has just ended and the RSU requests the EDC to compute the bill. For simplicity, the RSU contacting the Bank to access CAEV user's account is not shown in Figure 3.18.

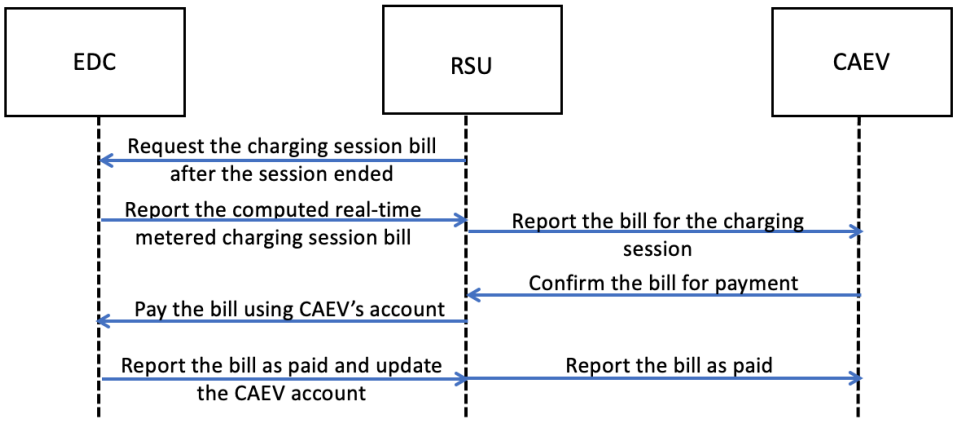

Figure 3.18: CAEV's charging session payment using pay per charging session method.

B. Pay Per Energy Unit

The idea is to pay for each energy unit received by the CAEV's battery. So, the rate of each energy unit charged will have to be defined. For example, 1 energy unit or "pulse" that could be a kW will cost 1 CP. Then, the CAEV's battery upon successfully receiving a burst or surge of energy unit will be automatically billed for that energy unit right away by the EDC via RSU in real-time. The latter is done repeatedly until the charging session is completed as can be seen in Figure 3.19. The EVSE as soon as it finishes delivering an energy unit of charging, it reports it to the EDC via the RSU. The EDC automatically creates the bill and reports it to the CAEV. If the CAEV does not agree with the report, then it may send an error message or a negative acknowledgement to further investigate the issue. Otherwise, the CAEV pays the bill via its account to the EDC, and this entire process keeps on repeating for each energy unit delivered until the end of the charging session.

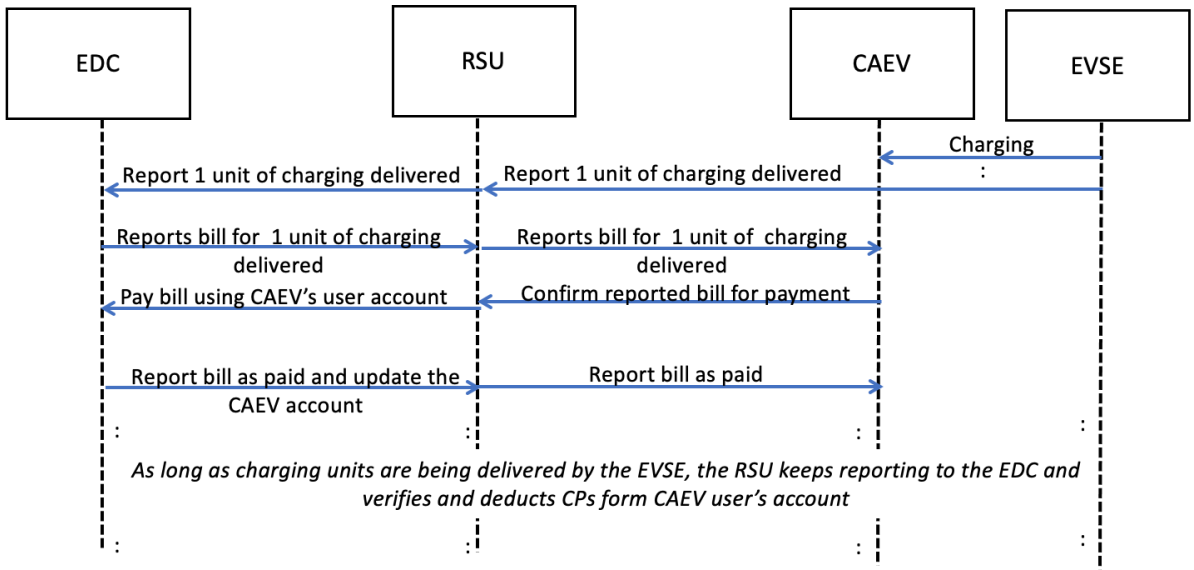

Figure 3.19: CAEV's charging session payment using pay per energy unit method.

Both these billing schemes can easily deal with unusual CAEV behaviors like early departures from the reserved EVSE, blocking a WCP, accidents on DWC lanes and transferring CPs. In case of early departures or "incomplete" charging sessions that are unable to deliver the reserved SoC to the CAEV, the presented billing schemes will fairly bill the CAEV's account only for the charging delivered. The CAEV obtaining charging from DWCN lanes might still want to resume charging after leaving the lane to give way to another CAEV or to bypass an obstacle caused by an accident on the lane. To enable such CAEVs to resume charging during the reserved charging session, a set timer might be used. If the timer expires, the CAEV will need to re-establish the charging session in DWCNs. The timers for charging session continuation can then be used for SWCNs and CCNs as well. Now, if the CAEV is

blocking a WCP or EVSE, then the system will bill the CAEV fairly for the charging delivered and the EVSE's power supply will be immediately stopped. Additionally, the system may choose to fine the CAEV for every time unit the CAEV blocks the WCP or EVSE. For arriving late for a reservation or cancelling a reservation close to the reserved time, CAEV users may be charged set number of CPs.

CPs may be awarded to promote good driving behaviors and encourage usage of certain DWC highway lanes or CNs that have less traffic or are farther away. CAEV users may transfer CPs to their friends or other CAEV users via EDC, but the anonymity feature will be sacrificed. Since, the sender and the receivers CAEV IDs may be required for transfer. However, a solution to the latter problem could be assigning temporary IDs to maintain anonymity. The CPs belong to the CAEV and the system can choose to disallow its transfer or sharing for security reasons.

C. Dealing with Unpredictable Circumstances

i) Late, Early and On-time Arrivals

When the CAEV arrives to the CN on time for its charging reservation, it can simply drive up to the EVSE and receive its expected SoC for the reserved charging duration. However, it may be the case that the CAEV might arrive early or late for the reserved charging due to unpredictable conditions like high traffic density, accidents, construction works, detours, etc. To deal with early and late arrivals, the reserved EVSE of the CN might have to make certain reservation updates.

In DWCN, the issue of late and early arrivals is not a big concern. Since, the CAEV whenever it enters the DWCN lane for charging will have to travel the complete path at an average constant speed to receive reserved charging. The time slots reserved for charging on DWCN lanes can even be booked multiple times given the capacity of the DWCN lane to serve one or more CAEVs for charging at once with an expected maximum set by the DWCN.

In case of SWCN and CCN, the early and late arrivals need to be dealt with in a proper manner as these static CNs have EVSEs that have waiting queues for CAEVs. The two main cases are discussed below:

Case 1: *CAEV arrives at the CN earlier than the reservation start time*

Case 1.a: Reserved EVSE is free

CAEV can park and receive charging right away. The EDC is notified as well as the CNH, so that the EVSE's reservation information can be updated.

Case1.b: Reserved EVSE is busy serving another CAEV

If the reserved EVSE is busy, then the CAEV will have to be queued in line to wait until its actual reserved time. The system implementer can also take another approach in that the CAEV will get a new reservation in the same CN for an EVSE that is free in the current time or has less wait time than its current reservation. After gaining approval of the CAEV user, the new reservation will be made and the previous reservation will be cancelled with zero or some penalty. If the next free EVSE is the same as the one reserved, then the CAEV is queued for that EVSE. If the newly reserved EVSE is free, then the reservation information is updated after cancelling the previous one, and the CAEV will park to receive its charging. If the newly reserved EVSE also requires some wait time less than the original reservation, this CAEV will be queued for this newly reserved EVSE. The system will always chooses the EVSE with the least wait-time.

Case 2*: CAEV arrives at the CN later than the reservation start time*

The system may attempt at preserving the original charging reservation of the CAEV, and the EVSE keeps on waiting for the CAEV to arrive unless CAEV sends a cancellation message. If the CAEV arrives, then the CAEV goes and charges during the on-going reserved time while the remaining charging requested may be accommodated by making another charging reservation request. It should be noted that at any time the CAEV can cancel a or leave a reservation.

Another approach can be postponing the original charging reservation of the CAEV. The charging reservation is delayed by a fixed amount and may be assigned another EVSE if needed, while another CAEV reservation can be pushed forward by the reserved EVSE. When the CAEV finally arrives, then it according to the updated reservation may be considered early and follow Case1.b where the reserved EVSE is busy in servicing another CAEV. If on time, then the CAEV will just go park and start receiving charging.

Further, the system can combine both approaches and have a fixed timer that waits for a CAEV to arrive as the reservation time starts. After this timer expires, the RSU of the CN may automatically send a message to the CAEV inquiring about its wish to preserve, postpone or cancel the charging reservation

ii) Accidents on Dynamic Wireless Charging Network Lanes

The accidents on the DWCN lane can occur anywhere with a probability of P_a, and the CAEV may choose to end or skip the charging session with a probability of P_s . The sensors of the WCPs can detect blockage, inappropriate behaviors and accidents with foreign object detection techniques, and the on-ground highway patrol officers if deployed can report

accidents and remotely close off the affected sections of the lane with ± X m for buffer. All the WCPs that fall in the closed off section will be deactivated and the other remaining active WCPs can carry the load of the remaining charging. The CAEV users can choose to cancel or resume their charging reservation after bypassing the accident affected area. If the accident occurs while the CAEV was receiving charging, then the CAEV will be notified of the situation with the choice to end the session or resume it after bypassing the affected area. Additionally, all other CAEVs that are headed towards the DWCN lanes affected by the accident can be notified and given the option to cancel or book another charging session at another CN or at the same CN at a later time. Alternatively, the system implementer may decide to take an easier approach of completely closing off the DWCN lane and compensate the CAEVs for cancellation with CPs or booking another charging reservation.

3.4 Proposed System Cycle of the Charging Reservation and Trip Planning System

The proposed handshake protocol and the proposed architecture can be employed in making many IoT charging applications a reality. One such IoT application for ITS is the joint charging reservation and trip planning system for CAEVs. The system cycle and its six main phases are detailed below, and it can be utilized to plan and implement the system for ITS.

1. *Driving Phase:* The CAEV is driving towards its destination from an arbitrary point following the shortest route possible. The CAEV on its AMoD trip will make stops at EVSEs of the CNs to obtain charging based on prior reservations.
2. *Charging Request Phase:* The CAEV's SoC has fallen below a threshold on its way to a destination, so it reports a reservation request frame to the system via a nearby RSU. The reservation request frame holds the information about CAEV's current state and the desired trip destination. The RSU will then forward this request frame to the system only if the CAEV's bank account ensures its ability to pay for the possible charging reservation.
3. *Charging Scheduling and Trip Planning Phase:* This phase involves processing the CAEV's reservation request frame that came via an RSU to schedule charging at CNs that are close in proximity and along the shortest possible trip route. It primarily involves searching for all available EVSEs at CNs that can best fulfill the CAEV's charging request. The system aim to minimize travel costs, wait times, charging payments and battery consumption with the EVSE search.
4. *Charging Reservation and Route Confirmation Phase:* After shortlisting the availabilities of EVSEs at CNs in close proximity and on the shortest trip route, the system will then choose and reserve EVSEs that can deliver the most of the requested charging in the

requested timing. The system then confirms the reservation to the CAEV by reporting a reservation confirmation frame via the RSU.

5. *Waiting Phase:* The CAEV user has to wait in queue if its early for a charging reservation at static CNs like SWCN and CCNs. The CAEV faces this phase when the system is not able to update the reservation for the early arrival at the EVSE of SWCNs and CCNs.
6. *Charging Phase:* It is where the actual charging takes place. This phase is comprised of several parts. First, the charging session is established by authenticating a CAEV to ensure that no imposter steals a reservation. Second, the CAEV is synchronized with the EVSE for proper and safe delivery of charging using misalignment sensors and speed detection sensors. The latter sensors are used to report CAEV's violation to safe charging delivery parameters set by the CN like being out of range of the WCP's misalignment tolerance or not following the cruising speed range on a DWC lane. Third, the actual charging is metered in real-time and delivered to the CAEV. Fourth, this real-time metering by the system and the CAEV enables two-types of billing schemes for fair and secure payments. Fifth, the CAEV after paying travels towards its destination or the next CN on its planned shortest route.

Figure 3.20 shows the flowchart of the charging reservation and trip planning system from the point the CAEV requests a charging reservation and trip planning to the point it arrives at the destination of the trip. The system cycle starts with a CAEV requesting for a charging reservation. It then proceeds to the system scheduling charging along with a shortest route for the trip to the requested destination, then the system confirms the reservation and route of travel. The CAEV then drives to different CNs to receive charging until it reaches the destination following the planned shortest route by the system. It should be noted that if the CAEV arrives early at static CNs like CCNs and SWCNs, then the CAEV may need to enter a waiting phase to wait for its reservation time to receive charging.

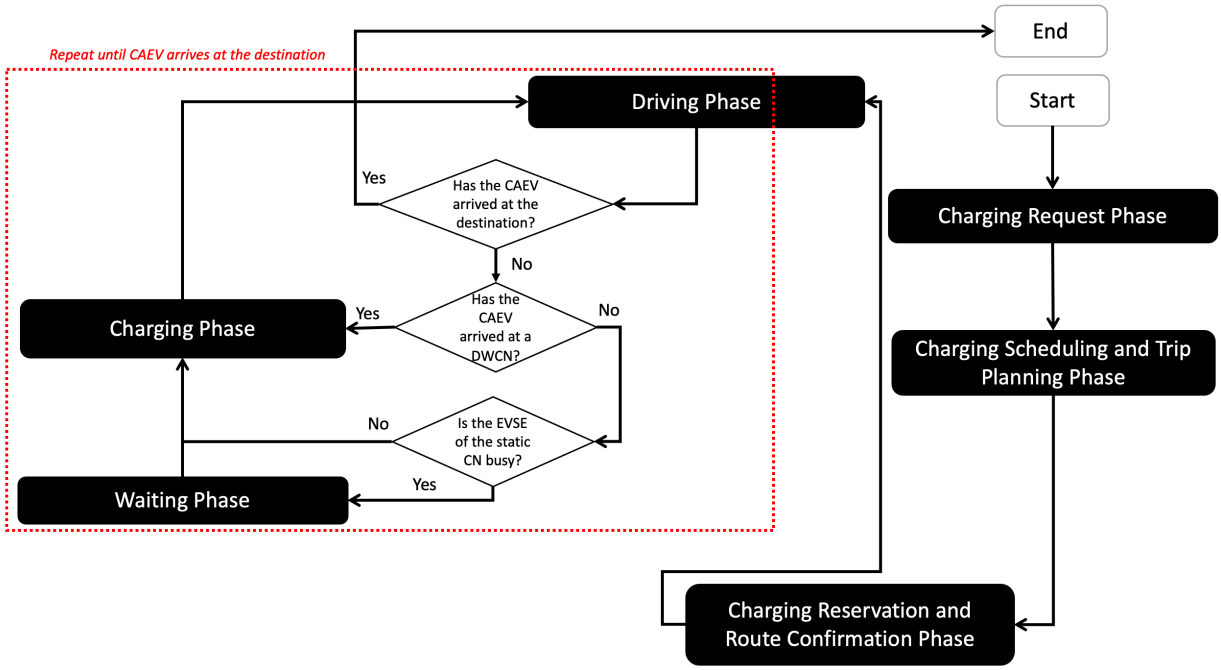

Figure 3.20: Flowchart of the charging reservation and trip planning system phases.

3.5 Conclusion

In this chapter, the system architecture and design of a three-layer CN hierarchy is proposed that enables wired and wireless charging networks to interoperate and potentially work with existing and future international charging standards. The accompanying handshake protocol, light-weight message frames and real-time metering billing schemes makes this hardware independent proposed system very powerful to realize IoT applications. This chapter helps pave the way for realizing the presented system architecture and protocol for an IoT application like joint charging reservation and trip planning for CAEVs. Next, chapter details the software implementation of the discrete-event simulator that can realistically simulate, generate results and help analyze the operation of the charging reservation and trip planning system for ITS.

Chapter 4 Simulation Architecture, Design and Implementation

4.1 Introduction

The charging reservation and trip planning system proposed will process charging reservation requests and trip planning of CAEVs on a given map. The problem formulated here is of CAEVs getting a charging reservation and shortest route planned for their trips while minimizing costs, travel and wait times and overall battery consumption. The latter addresses the problems of a range-anxiety compelled CAEV user going out unplanned to get charging. These problems include the CAEV user encountering traffic congestion along the way, and suffering long waiting times once it finds a CN. The discrete event simulation is considered appropriate for implementing the proposed system, as it will enable the study of the internal interactions of the complex charging reservation and trip planning system and its sub-systems. The system modelled employs the presented three-layer charging network hierarchy and accompanying handshake protocol, message frames and payment schemes. Therefore, the model simulation will allow for observing the system behavior and resulting outputs due to changes in environment and internal variables like service times of charging networks to evaluate overall system performance. Moreover, the simulation approach will allow experimentation of new design or policies to improve the system through model building while saving time and money.

This chapter's section 2 discusses the simulation model's conceptualization and translation. Section 3 details the simulation architecture and design by discussing each module that comprises the simulator and presents the overall logic of the simulator and its events. The simulated events and phases and the algorithms used in the simulator are discussed in Section 4. The DWCN design specification tool is highlighted in Section 5. Section 6 concludes this chapter.

4.2 Simulation Model Conceptualization and Translation

To construct the conceptual model, the structure of the charging reservation and trip planning system is created. The internal entities of the system are realistically modelled CAEVs coming from the external environment like cities and even houses or parking lots with finite population as set by system analyst. It can be assumed that the CAEVs coming into the system from the environment have no limit that is the arrival rate remains unaffected by the departure of the units, and that no CAEV is rejected by the system. Poisson process is assumed for modelling arrivals of CAEVs because of assumption of large numbers of CAEVs and their

independent arrivals. The interarrival times of CAEVs follow the exponential probability distribution function. The service times of the CNs and the EVSEs is influenced by the charging rate of the EVSE and the CAEV, and the wait times are affected by the early or late arrival of CAEVs at the CN due to unpredictable traffic conditions.

In this system, the essential elements included are the finite calling population for the CAEVs, the arrival time of the CAEVs defined by interarrival time distribution, the service time of the CNs determined by the CAEV and the EVSE charging rate, the travel time of the CAEV to the CN locations and the queuing discipline followed by CCNs and SWCNs. The CCN and the SWCN have EVSEs with buffers of size 2 for allowing 2 CAEVs to wait in line when they are early for a reservation. The service rate and the arrival rate of the CAEVs is balanced by the reservation system to avoid having an unstable or an explosive system with long waiting lines and waiting times. The main states to be tracked include number of CAEVs in the overall system, number of CAEVs serviced by the overall system, number of CAEVs serviced by each CCN, SWCN and DWCN, number of CAEVs still in each CCN, SWCN and DWCN, waiting time of CAEVs in each CCN, SWCN and DWCN, throughput of each CN, proportion server idle time of each CN, and the total payment, travel time, wait time and battery consumption of the CAEV for the charging reservation and planned shortest trip route. The time taken to process the charging reservation and trip planning requests is considered negligible, as that part is independent of the CAEV's actual start and end of the trip and charging statistics. A CAEV could easily request a charging reservation and trip planning well in advance of the actual start time of its trip.

It should be noted that the data collection for this system to be modelled cannot be done, as it does not exist in the real-world yet. The idea of this simulator is to simulate how this system would behave when it should be implemented in the real-world. Hence, the distributions of interarrival times of CAEVs is random and follows the exponential probability distribution function. The service time distributions of EVSE of the CN are realistically determined by the charging rate of the EVSE and the CAEV modelled. The length of waiting lines under varying conditions of EVSEs at a CN is affected by the CAEV's arrival to the charging reservations that can be modelled by the exponential probability distribution function.

Python, a high level object-oriented programming language, is chosen for simulation and model translation. The choice is influenced by popularity, simplicity, ease of use, availability of numerous resources and libraries, and the flexibility to implement one's own higher level logic to meet the model requirements. This choice of high level language allows for implementing the event scheduling worldview, and keep track of all the states, entities,

attributes, events and activities while advancing the system clock. The driving, departure and arrival events can be designed in detail, and the rand() functions from the numpy library allow for generation of interarrival time and service time with random samples from the desired probability distribution functions like exponential distribution. More importantly, keeping track of all the states and attributes allow for generating reports and generalizing the simulation results using statistical functions. However, one major drawback of using python is the time consumption, as a lot of the event-scheduling worldview specific methods, data structures and required functions have to be created from scratch.

4.3 System Simulation Architecture and Design

The discrete event simulator implementing the charging reservation and trip planning system follows an object-oriented architecture. Object-oriented programming like python helps model complex things as reproducible simple structures that can be used across programs. These object information is protected through encapsulation. Further, this approach enables modelling physical objects as closely as possible, and allows extensions for future modifications and use cases. Class-specific behavior is also enabled through polymorphism and debugging is easier with classes containing all applicable information within them. The problem at hand is subdivided into classes. Each entity of the proposed system is modelled in python files by one or many classes. This can be seen depicted in Figure 4.1. The simulation model is coded in python and the python files are placed in subdirectories named cloud, network and models. These subdirectories are stored in the main directory named simulator. All python files and the classes are discussed in the next section in detail.

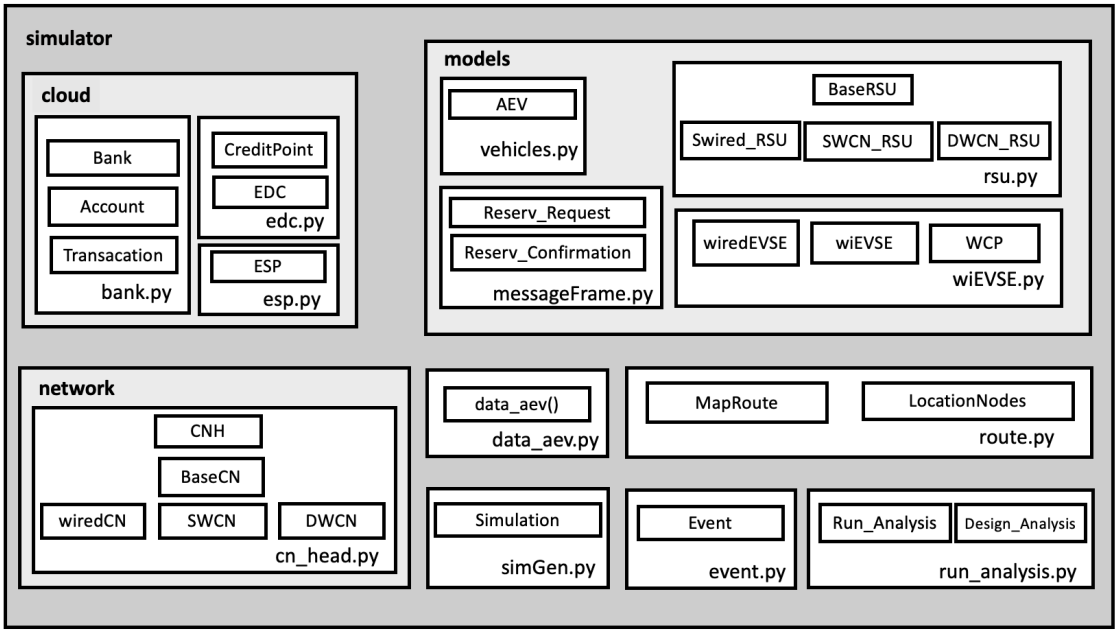

Figure 4.1: Overview of the simulator file organization.

4.4 System Module Definitions

4.4.1 Cloud Entities

The cloud subdirectory as the name suggests holds the python files for the cloud entities that include Bank, EDC and ESP. For real-world implementation of KDC, libraries like kdcproxy and kerbose can be utilized. To keep the information visible for evaluation and analysis in the simulation, the encryption of message frames exchanged is ignored.

A. Bank

The bank.py file models the Bank entity and contains the Bank, Account and Transaction classes. The Bank class can be instantiated with a unique institution code and location ID. Additionally, the Bank's name, set minimum opening balance, and maximum and minimum transaction amounts are also set. The Bank keeps track of registered accounts and the CAEVs registered with dictionaries, and also maintains a dictionary of closed accounts. It should be noted that in python a dictionary is a collection of stored data in key and value pairs which is ordered, changeable and does not allow duplicates. The Bank for statistical purposes also keeps track of total credited amount, debited amount, total number of CPs bought and sold and total number of credit, debit and buy and sell CP transactions created and processed. The Bank has several accounts and each account can have one or more transactions. So, the CAEV users register and open an account with the Bank with a set minimum balance using the register_AEV() method. The Bank can get hold of an account using the get_AEV_account() method, and the get_AEV() and get_AEV_from_account() methods can be used to get the registered CAEV from the account ID alone. The status of the account can be verified using the is_registered_Account() method, and the is_closed_Account() method can be used to check if the account is closed. The process_transaction() method is used to process transactions for the given account ID, and the Bank processes four main types of transactions. First, the credit transaction is carried out by the credit_account() method that credits the given Canadian dollars (CAD) amount for the given account ID. Second, the debit_account() debits the given amount in CAD or CPs to the identified account. Third and fourth types of transactions are buying CPs from EDC and selling CPs to the EDC, respectively. It should be noted that the buying of CPs from the CAEV user's account will automatically lead to debiting of the account for payment, and the selling of CPs to the EDC will automatically lead to crediting to the account for the sale.

Now, each registered CAEV user has an account which is created using the Account class. The Account class enables the CAEV user to pay for charging sessions securely using

CPs that it could buy from the EDC and sell to the EDC via the Bank. The Account is characterized by its unique ID, CAEV's ID, opening date and closing date of the account if any, time of account creation, total number of transactions carried out by the account, list of transactions, current balance and list of CPs, the Bank ID to which the account is registered and the status of the account as active, inactive or suspended. Its credit() and debit() methods are called by the Bank to credit and debit the account, respectively, when a transaction is processed.

The Transaction class is used to create objects of type Transaction for an Account object, and the Bank processes or creates transactions for the accounts. The attributes of a Transaction object include the unique transaction ID, account ID, amount for transaction, date of transaction, transaction type's ID and the EDC ID that is contacted to buy and sell CPs. The start_transaction() method is called by the Bank's process_transaction() for a particular account to start processing the transaction based on the transaction type.

B. Energy Distribution Center

The edc.py file contains the classes EDC and CreditPoint. The EDC class models the EDC that is part of the cloud entities of the three-layer CN system design. It is responsible for setting rates of selling as well as buying CPs for the CAEV users with their bank accounts. Since EDC creates unique CPs for sale, it maintains a list for the CPs created, issued and used. The total number of CPs created, used and issued are also tracked. Additionally, a list on charging reservation requests, charging reservation confirmations and paid charging reservation is maintained. Further, the total number of charging reservation requests, charging reservation confirmations and paid charging reservations is also tracked. EDC's make_reservationRequest() method communicates with the CNH via the ESP to make a charging reservation and report back its confirmation to the CAEV. The method cancel_reservationRequest() can be used to cancel the reservation request, and the cancel_confirm_reservation() method cancels the CAEV's confirmed charging reservation. The method createCP() creates the CPs, verifyCP() verifies the CP for authenticity, removeCP() removes a CP that is a forgery, and issueCP() creates and assigns CPs to the Bank. The buyCPs() method enables the Bank to buy the CPs for the CAEV user's account, and the sellCPs() method enables the Bank to sell the number of CPs requested by the CAEV user's account. EDC is responsible for billing the CAEVs for their charging sessions using one of the two proposed payment schemes. The report_energydelivered() method is used for real-time metering of each charging unit delivered. The report_final_energydelivered() function reports

the charging delivered before the end of the charging session, and the report_final_energydelivered_wcp() reports the charging delivered before CAEV's last contact with the WCP. The report_PerEnergyUnitBill() and the calculate_PerEnergyUnitBill() are used to implement pay per energy unit billing scheme. On the other hand, the report_chargeSessionBill() and the calculate_ChargeSessionBill() are used to implement the pay per charging session billing scheme. To fairly bill real-time charge metering with TOU, the Ontario's peak times from [263] for summer and winter and the power supply rates based on the year simulated are used. The latter is obtained with the get_rate() method. The paymentCPs() method called by the payBill() method enables the CAEV user account to pay for the charging session in CPs to the EDC and allows the charging session to be marked off as paid.

The CreditPoint class models CPs that are to be used as virtual currency by the CAEVs to pay for their charging sessions. They are distributed only by the EDC, and each CP has a uniquely generated CP ID, a creator ID to identify the EDC responsible for its creation, date of issue, issuing Bank ID, status ID of it being newly created, issued or used, and a verified status that guarantees its authenticity.

C. Energy Service Provider

The esp.py file contains the ESP class. It models the ESP cloud entity and as the name implies it is responsible for supplying energy to the different CNs connected to a CNH. The ESP requests the CNH for possible availabilities of EVSEs to reserve a charging session. It also reserves selected EVSEs, and reports the booking confirmation back to the CAEV via the EDC. An EDC can have one or more ESPs each with its own unique source of generating power. An ESP class is characterized by a unique ID and location ID. It also holds the information of the CNH ID, total number of CNs powered, total number of EVSEs and CNs powered, and total power generated for each CN type and for all CNs. The request_avail_CNs() method requests for all available CNs that can fulfill the charging reservation request. The request_avail_EVSEs() calls the prior method to look up available EVSEs in available CNs to fulfill the charging reservation request. The choose_EVSE() method then selects the EVSEs to reserve from the list returned by the request_avail_EVSEs() based on maximizing delivery of charging that is requested, time of the actual charging session, and proximity of CNs to the CAEV's location and shortest trip route. The latter method's selection of EVSEs will minimize traveling time, waiting time, charging payments and battery consumption. The reserve_EVSE() method actually reserves the chosen EVSE and returns back the confirmation. The

cancel_EVSE_CN_reservation() cancels the charging reservation at an EVSE of a CN by taking in the reservation confirmation ID, EVSE ID and CN ID. The request_CNs() gets the list of CNs, request_reserved_EVSEs() returns the list of reserved EVSEs of all CNs, and request_resevred_EVSEs_typeCN() gets the reserved EVSEs of all CNs of a particular type. The timeToCharge() method computes the total time the EVSE of CCN and SWCN will take to deliver the requested SoC based on charging rate of CAEV and the EVSE, and it also identifies the exact start and end times for booking timeslots for the charging reservation. The timeToCharge_DWC() method is like timeToCharge() method but for DWCN. The start_power_CN(), stop_power_CN(), start_power_EVSE(), and stop_power_EVSE() methods as the name suggest start and stop power supply to CN or ESVE. The activate_EVSE() method supplies low power for activation of EVSE, and deactivate_EVSE() function stops power supply completely at deactivation of EVSE.

4.4.2 Network

A. Charging Network Head

This charginghead.py file models three different types of CNs, and it also models the CNH entity that controls the connected CNs of same and different types. It specifically contains the parent class BaseCN whose children are the wiredCN, SWCN, and DWCN, and the CN_head class. The BaseCN is an abstract class that describes the infrastructure of the three-layer CN that will deliver charging with its EVSEs and will hold charging reservation information for each of its EVSEs. Its main attributes are a unique CN ID, location ID, total number of EVSEs, dictionary of EVSE objects, and the type of CN. The activateEVSE() and deactivateEVSE() as the name suggests activates and deactivates a particular EVSE of that CN for charging. The startPower_EVSE() and stopPower_EVSE() are invoked by the ESP to fully supply power for charging a CAEV and fully shutting down the power supply of an EVSE, respectively. The check_avail_EVSE() method is called by the ESP to look up charging reservation availabilities of EVSEs for the given start and end time. Since it is an abstract class, the latter methods are defined and not implemented.

The wiredCN class overrides BaseCN class methods and adds its own unique methods. It inherits BaseCN's attributes and adds the attribute of the CN's designated RSU. It implements all of the BaseCN's methods. Further, it adds the check_EVSE_reservation() method to verify if the given reservation exists for an EVSE of the CN. The pac_EVSE() method enables the CAEV to park and receive charging from the EVSE given that the EVSE is available as checked by the status_EVSE() method else the CAEV is queued or detoured.

An early arrival CAEV is queued if there is space in the queue else the CAEV is suggested to park somewhere else and come back when there is space in the queue or it is time to receive charging using the reserv_early() method . The is_aev_queued() method is used to check if a certain CAEV is in the queue of a particular EVSE. The make_reservation_EVSE() method is used to reserve an EVSE for a particular time duration, and is invoked by the CNH.

Like the wiredCN, the SWCN class inherits from the BaseCN class. It like the wiredCN class has only one designated RSU, but also maintains a dictionary of WCPs that are controlled by the EVSEs. It implements all the methods of the BaseCN and has all the same additional methods as the wiredCN class to deliver charging using EVSEs, make reservations and process early CAEV arrivals. Since it is a SWCN, the methods activateWCP() and deactivateWCP() are added to activate and deactivate a WCP for delivering charging to a CAEV, respectively.

The DWCN class also inherits from the BaseCN class. It models the DWCN, and has a dictionary of WCPs and their location coordinates for installation on a highway as well a dictionary of RSUs that are installed along the highway. Additionally, a DWCN object will also hold information about gaps between each WCP installation, average CAEV cruising speed, the length of the track, WCPs and EVSEs, the time to cover the distance of WCP, EVSE and track with the average cruising speed, and the value of EVSE voltage. This class like the wiredCN and SWCN has methods to check and make EVSE reservations, verify EVSE reservations and its availability, activate and deactivate WCPs and EVSEs, and start and stop power supply to EVSEs. Further, it has the dac_EVSE() method to enable a CAEV to drive and receive charging from the track. This latter method invokes the accident() method to simulate accidents based on the set probability, and the decision() method simulates the CAEV's probability to skip or resume charging after bypassing the accident zone. The calculate_param_reqSoC() method is used to compute the charging rate and the amperage for the EVSEs of the DWCN to deliver the requested SoC.

The CNH class models the CNH entity that controls and manages one or more CNs of different types, and enables seamless communication between the CNs for enabling IoT applications for ITS. It allows the EDC and the ESP to communicate with the different CN types. Its attributes include the unique CNH ID, ID of the ESP powering all the CNH managed CNs, dictionary of CNs, and the set threshold of charging delivery in percentage for each CN type. Since it is an entity that manages all the CNs, it has a lot of getter and setter methods to retrieve and set information of CNs, EVSEs, WCPs and RSUs. The all_available_EVSEs(), all_available_EVSEs_CN() and all_available_EVSEs_typeCN() enables the EDC and the ESP to check for charging reservation availabilities of all EVSEs in all CNs, all EVSEs in a CN,

and all EVSEs of all CNs of a particular type, respectively. On the other hand, the all_reserved_EVSEs(), all_reserved_EVSEs_CN() and all_reserved_EVSEs_typeCN enables retrieving reservation information of all EVSEs of all CNs, all EVSEs in a CN and all EVSEs of all CNs of a particular type, respectively. The make_reservation_EVSE_CN() is used to make a charging reservation at an EVSE of a CN and is invoked by the EDC via ESP. The cancel_EVSE_reservation() enables cancelling a charging reservation at an EVSE of a CN.

4.4.3 Models

A. Message Frames

The messageFrame.py module has two classes that model the proposed reservation request and confirmation frames. The reservation request frame is modelled by the Reserv_Request class that is used to create message frame objects that are securely communicated between the CAEV and the cloud entities via the RSU. It contains reservation information like reservation request ID, arrival and estimated departure times of the CAEV relative to the system, current balance in CPs, current CAEV battery SoC, CAEV speed and requested SoC, and the current location and destination location for the CAEV's AMoD trip. The RSU that receives this frame may then add its own ID and location whereas the EDC and the cloud entities will then process it to add details for looking up charging reservation. The class has only setter and getter methods. Similarly, the Reserv_Confirmation class is used to create the reservation confirmation message frames instantiated by the EDC to return back the reservation confirmation, and includes information like confirmation ID that is the same as the request ID for traceability of the reservation. It also contains charging reservation information like the type of CN, CN ID, EVSE ID and location, start and end times of the reservation and total charging duration. This frame is later on used by the system to also keep track of the actual start and end time of the charging sessions, the real-time metered charging bill and its status of paid or unpaid, and the actual charging delivered by each charging session. It has only setter and getter methods.

B. Road Side Unit

The rsu.py module models the RSUs for the different CN types. The BaseRSU class is the base class that models RSUs that are part of the Layer 1 of the proposed three-layer CN hierarchy. The class is characterized by a unique RSU ID and location ID, ID of RSU's CN, the RSU type that is the same as its CN type, CNH ID, EDC ID and Bank ID. The methods check_credit(), verify_CP(), purchase_CP(), sell_CP(), refill_CP() are used to check the CAEV user account's balance, verify the authenticity of CPs, buy CPs, sell CP and buy set amount of

CPs, respectively. The report_energy() and report_final_energy() methods are invoked by EVSEs to real-time meter the charging delivered to the CAEVs. The method report_bill() reports the bill from the EDC to the CAEV, and the pay_bill() method enables the CAEV user's account to pay the EDC for the charging session. The verify_reservation() and verify_request() is used to check if the CAEV's charging reservation and its request exists, respectively. The cancel_reservation() allows a CAEV to cancel a reservation, and the cancel_request() enables cancellation of a request by a CAEV.

Now, the SWired_RSU class models the behavior of a RSU that belongs to a CCN. It inherits from the BaseRSU class and has its own unique CCN ID and CCN location ID. It also has a make_reservation() method to make reservation at EVSEs of a specific CCN. Similarly, SWC_RSU models behavior of an RSU that belongs to a SWCN and inherits from the BaseRSU class. It also has its own unique SWCN ID and SWCN location ID. Additionally, it has the method make_reservation() method to make a reservation at the SWCN's EVSEs. Further, the SWCN's RSU is also responsible for reporting speed and misalignment errors to the CAEVs using the report_speedERROR() and the report_misalignERROR(), respectively. Finally, the DWCN_RSU class models the RSUs of the DWCN and inherits from the BaseRSU class as well. It has a unique DWCN RSU ID and DWCN RSU location ID, and has methods for the reporting of speed errors and misalignment errors along with making reservations at EVSEs. Further, it has a report_final_energy_wcp() method that is exclusive to the DWCN RSU. The latter method enables a CAEV departing from a WCP to report the final amount of charging received for fair real-time metering of charging.

C. EVSE

The wiEVSE.py module is responsible for modelling two main type of EVSEs of the three different types of CNs presented. First, the wiredEVSE class models the wired EVSEs of the CCN. It has attributes like the current pilot signal, CAEV connected, wired EVSE ID, CN ID, type of CN, RSU ID, list of available time slots for charging reservation, list of reservations and reserved time slots, current status of availability, queue, and the set EVSE voltage. It also hold information about the total energy delivered, total number of CAEVs serviced and the list of total amount of energy delivered per charging reservation. The verify_AEV() and authenticate_AEV() methods verifies the charging reservation and authenticates the CAEV before delivering the charging to the CAEV. The activateEVSE() method prepares the EVSE to deliver charging to the CAEV, then the turnON() with powerON() method actually delivers the charging to the CAEV. The deactivateEVSE() method safely stops charging. The

powerOFF() method shuts off power supply to the EVSE by the ESP. The queueAEV() method queues the CAEV if there is space in the EVSE's queue and the dequeueAEV() method deques the CAEV form the EVSE's queue. The is_vehicle_plugged() method is used to check if a CAEV is connected before supplying power to deliver charging. The check_availability() and the reserve_availability() methods are used to check for charging reservation availabilities and booking the charging reservation at an EVSE invoked by the CNH for a CN. The verify_reservation() method can be used to check if the reservation exists for a CAEV at an EVSE.

The wiEVSE class models the EVSEs of wireless CNs, and control an array of one or more WCPs. It has the same attributes like the wiredEVSE class, but also includes a dictionary of WCPs and the set total number of WCPs for an array. It has all the methods that a wiredEVSE class has to make charging reservations. The class object authenticates, synchronizes and delivers charging to a CAEV using turnON_swc() and powerON_swc() methods in SWCNs and turnON_dwc() and powerOn_dwc() method in DWCNs. It should be noted that the queueing and dequeuing methods are exclusive to SWCNs. Further, the activateEVSE() and deactivateEVSE() invoke the activate() and deactivate() methods of this class object's WCPs to prepare them for delivering charging to the authenticated CAEV.

The WCP class models the WCP, and one or more WCPs are part of a wiEVSE object to model a wireless EVSE for SWCN and DWCN. It has attributes like a unique WCP ID, installation position coordinates relative to the road length, dimensions of the WCP, reservation list, RSU ID, CN ID, EVSE ID, average vehicle speed for safe charging delivery, and activation status. The turnON_swc() and turnON_dwc() methods of the WCP are invoked by its EVSEs to deliver charging after authentication and verification of the CAEV. It also has methods like detect_speedERROR() and detect_misalignERROR() to detect speed and misalignment issues, respectively. It uses report_speedERROR() to report the speed issue error to the CAEV, and the report_misalignERROR() reports the misalignment error to the CAEV. The latter methods are part of the automated driving feedback system, and report errors continuously until the errors are corrected for safe charging delivery.

D. Connected and Autonomous Electrical Vehicle

The vehicles.py module has an AEV class to model a CAEV. It holds information about the CAEV model like model name, year and month, vehicle body type, manufacturer name, manufacturer continent, and market price of the new vehicle in CAD and British Pounds. The CAEV's efficiency, range and charge acceptance rate is also defined to realistically model a

CAEV. The data_AEV() method in the data_aev.py file helps generate realistic CAEV objects with the EV data from the online EV database [264]. Additionally, the start and end times, start and end location IDs of the desired AMoD trip, current vehicle speed, current balance in CPs, battery's current SoC, current charging rate, total energy delivered for the reservation, coordinates of the CAEV's position relative to the road, and path to travel for the trip are also part of the attributes of the AEV object. The CAEV has its own unique ID and can have one or more user accounts associated with it like in carpooling or family use cases. The sendRequest_chargeSession() method requests for a charging reservation and trip planning via the closest RSU from the system. The registerAEV() method enables a CAEV user to register and open an account with the Bank. The sell_CPs() and purchase_CPs() method is used to place CP sales and purchase order, respectively, via the current CAEV user's bank account. Its report_bill() method is invoked by the EDC via the RSU to report the bill for a charging session. The correctSpeedError() and the correctMisalignError() methods enable the CAEV to correct its speed and misalignment, respectively, until the RSU stops reporting the error and the CAEV starts receiving proper and safe delivery of charging. Importantly, its charge() method is called by the EVSE to deliver charging to its own battery. It should be noted that the battery of the CAEV is modelled by the Linear2StageBattery class of the acnsim library [265], and as the name suggests it realistically models the charging of battery.

4.4.4 Simulation

A. Shortest Route Computation for Trip Planning

The route.py module models the shortest route computation for the CAEV's AMoD trip, and the Dijkstra's algorithm used is inspired by [266]. It has the LocationNodes class that models a location node representing a park, apartment building, mall, office, school, etc. or a CN. Its attributes include the location name, location ID, and index ID for accessing the node. It also has all the usual setter and getter methods. The MapRoute class is used to build a graph of a map, and calculates the shortest route from a source to the destination for a CAEV that wants to obtain charging along the way of its AMoD trip. Its attributes include setting the graph of the map as undirected or directed, two dimensional matrix representing the map, and list of location nodes of type LocationNode. The create_map() method enables the simulator to create a symmetric map with two main areas connected by the given number of DWCN highway lanes, and the SWCNs and CCNs are equally distributed between the two areas. The nodes are connected using the connect() method with travel path costs defined by the implementer. The calculate_route() that invokes the dijkstra() method uses the Djikstra's algorithm to compute

the shortest path from one location node to another with the least travel cost. The print_route() method prints out the detailed path that the CAEV may follow to complete its trip.

B. Simulation Events

The simulator uses a future event list (FEL) to drive the discrete event simulation. The entire simulation is traced with a simulation clock where each integer count is equal to a minute. The sim_event.py module has the Event class that models an Event object that is fetched from the FEL to process at the simulation run time. The FEL has ordered objects of type Event with the latest timed Event object on top. The Event object holds information like the event type, time in minutes, reservation confirmation frame, CAEV and the source and destination ID. There are seven main type of events that are described below:

1) Driving Event: It drives a CAEV from one location node to another location node by computing the shortest driving path between the two nodes with the calculate_route() method of the MapRoute object. The source and destination of the route is determined from the CAEV's $F_{confirm}$. It deducts the battery charge of the CAEV based on CAEV's efficiency and distance travelled to simulate battery consumption. Upon arrival at a CN, this event will automatically generate an arrival event of that CN type and append it to the FEL of the simulator. However, when a CAEV arrives at the final destination, no other event is automatically generated and the CAEV's trip is declared successfully completed as can be seen in Figure 4.2.

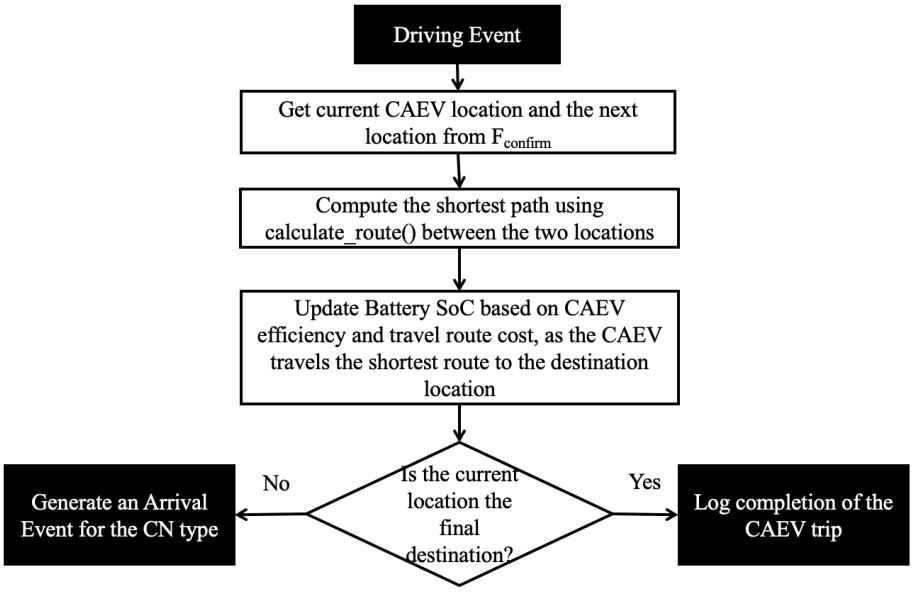

Figure 4.2: Flowchart of processing a driving event.

2) Arrival Event for CCN: This event involves simulating a CAEV arriving at the CCN to obtain charging from the reserved EVSE. It will first evaluate whether the CAEV is on-time, early or late for the reservation. If the CAEV is on-time or late, then the CAEV

establishes a charging session and plugs into the EVSE to obtain charging until the end of the reserved time. However, if the CAEV is early, then the CAEV will either be queued, detoured or given an earlier charging reservation of equal duration at the same EVSE. Additionally, early arrival of CAEV will automatically lead to generation of another arrival event for the same CCN to process the CAEV when it is on-time with the updated reservation. After processing the arrival event, the departure event for CCN is automatically generated and placed in the FEL. This can be seen depicted in Figure 4.3.

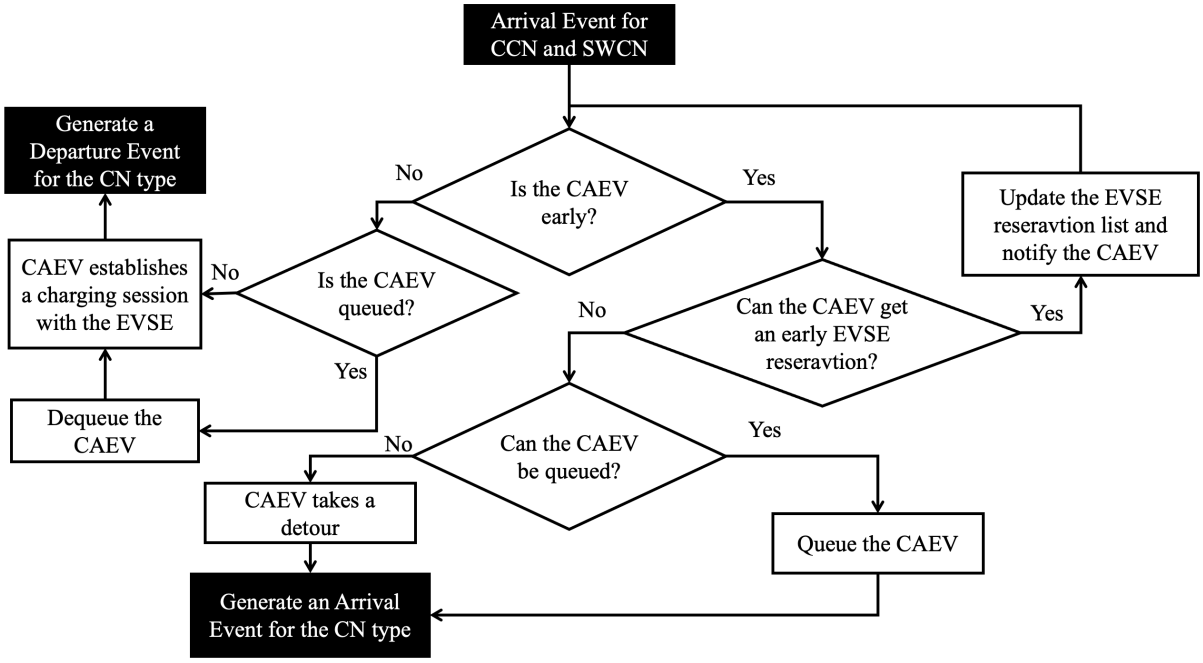

Figure 4.3: Flowchart for processing an arrival event for CCN and SWCN.

3) Departure Event for CCN: This event, illustrated in Figure 4.4, involves the CAEV actually receiving charging with real-time metering and paying for the charging session based on the billing scheme chosen by the implementer or analyst of the simulator. After receiving charging and paying the bill, the CAEV leaves the CCN. Then, the driving event is automatically generated based on the information in its $F_{confirm}$.

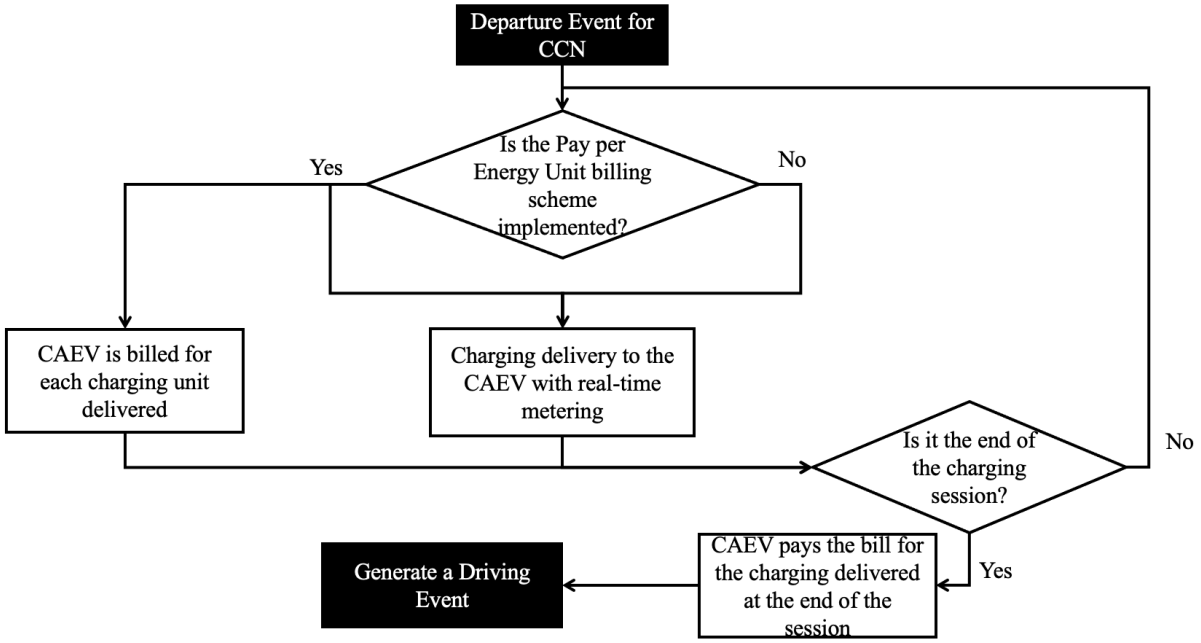

Figure 4.4: Flowchart for processing a departure event for CCN.

4) Arrival Event for SWCN*:* This event process is the same as the arrival event of CCN but is for SWCNs, as can be seen in Figure 4.3. The CAEV upon arrival is evaluated for establishing a charging session based on early, on-time or late arrival. Then, the CAEV is plugged in for on-time and late arrivals. The CAEV is queued, detoured or obtains an updated reservation with automatic generation of another arrival event for early arrivals. If the CAEV was plugged-in to obtain charging, then this event will also automatically generate the departure event for the SWCN.

5) Departure Event for SWCN: This event is the same as the departure event for CCN in its process but occurs for SWCNs. Additionally, charging is only delivered to the CAEV if the CAEV is properly aligned otherwise the continuous reporting of misalignment error occurs as part of the automated driving feedback system for correction. After receiving wireless charging and paying the bill, the CAEV leaves the SWCN, and the driving event is automatically generated based on the information in its $F_{confirm}$. This is depicted in Figure 4.5.

6) Arrival Event for DWCN: This event involves a CAEV entering the charging lane to receive charging by establishing a charging session, and its actual arrival time is noted. The departure event is automatically generated and added to the FEL as can be seen in Figure 4.6.

7) Departure Event for DWCN: The charging session is established and the charging is only delivered after ensuring the CAEV is moving within the speed and the misalignment tolerance range. Otherwise, the CAEV's speed and misalignment errors are reported and

corrected by the CAEV as part of the automated driving feedback system to receive safe and proper delivery of charging. The charging is being real-time metered and the CAEV is fairly billed. During this event, based on the probability set an accident may occur on the charging lane. Based on the decision probability, the CAEV may leave or resume charging after by passing the blocked-off accident area of the charging lane. After end of the charging session and completing payment, the CAEV departs the charging lane. The driving event is automatically generated based on the $F_{confirm}$ information and is added to the FEL as can be seen in Figure 4.7.

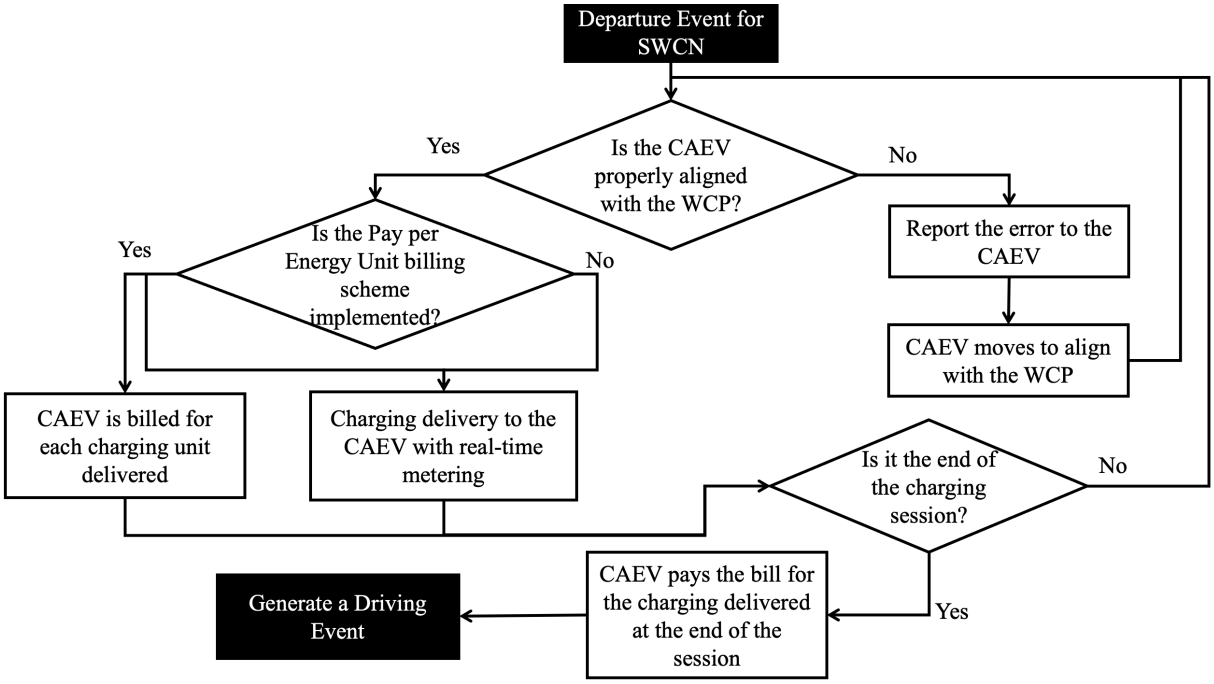

Figure 4.5: Flowchart for processing a departure event for SWCN.

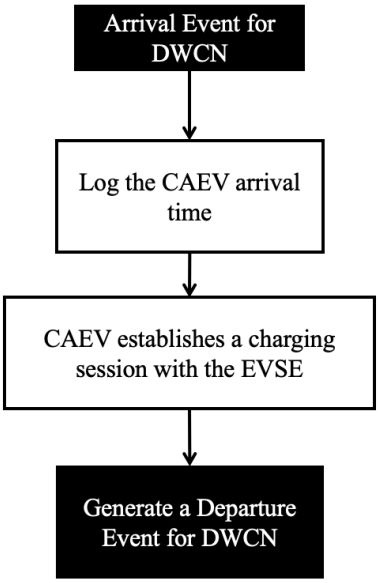

Figure 4.6: Flowchart for processing an arrival event for DWCN.

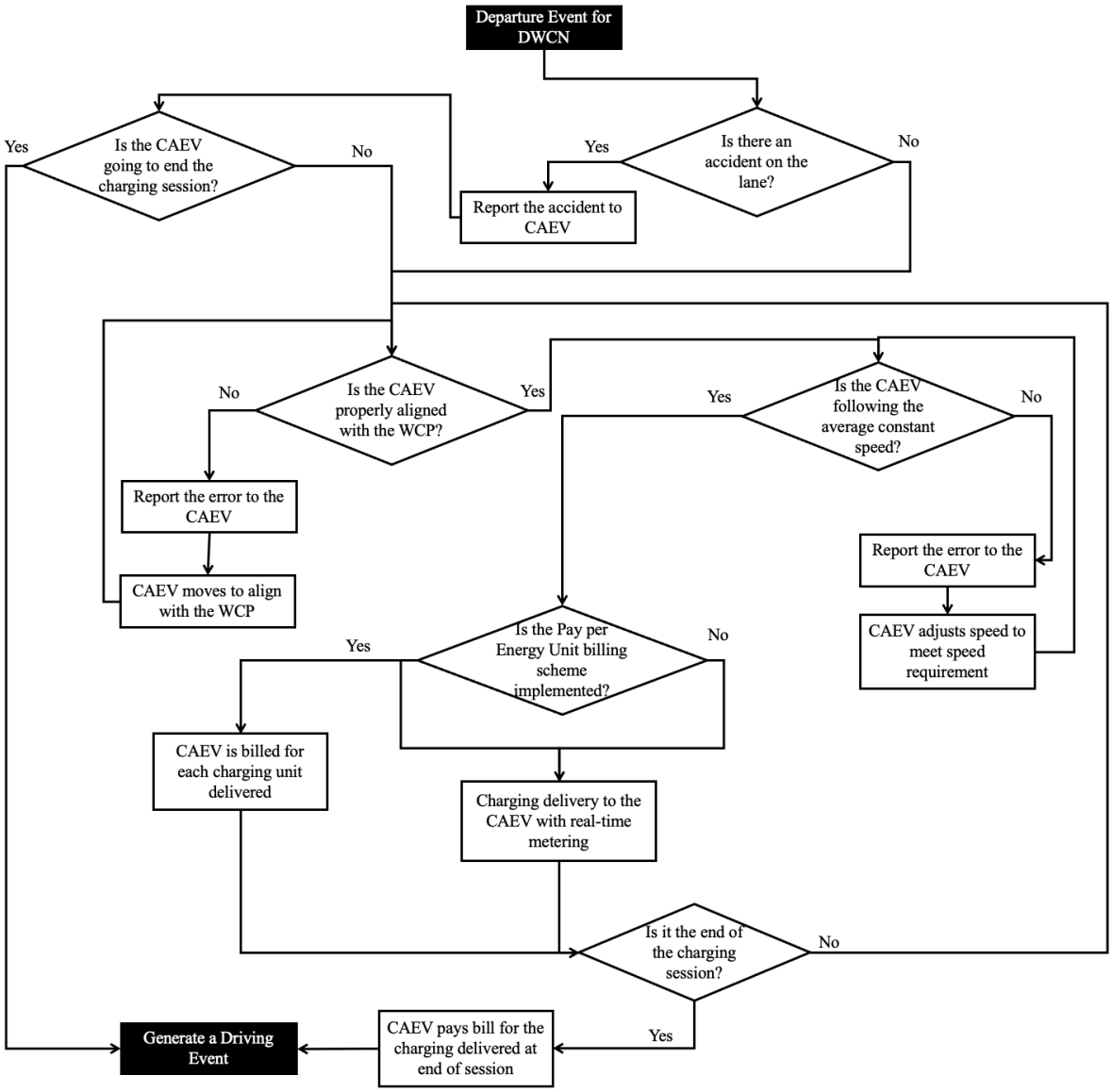

Figure 4.7: Flowchart for processing a departure event for DWCN.

C. Simulator

The simGen.py module has the Simulation class that is responsible for running all the above mentioned modules and objects of the classes together to simulate the proposed charging reservation and trip planning system for CAEVs. This Simulation class is characterized by holding pointers to objects of type Bank, EDC, ESP and the CNH. It has the simulation clock, start and end date of the simulation, number of days for simulation run, total period of simulation run in minutes, the FEL and the map on which CAEVs will be simulated. It will keep track of the total number of CAEVs in the system and in each CN, total number of CAEVs serviced by the system and by each CN, total number of each CN type and CAEVs, list of location IDs of each CN based on map areas, and total number of CAEV arrivals and CAEV departures of the overall system and each CN. It also collects statistics like the wait times,

throughput, average service time, proportion server idle time, server utilization and system times for the overall system and each CN. First, the setup() function is called to set up the simulation run by taking in information like number of map areas, number of each CN type, number of CAEVs, dimensions of each WCP and the gap between each WCP installation, threshold of SoC delivery for each CN type and the start and end date of the simulation with time slot duration for the charging reservations. The setup() method then sets up the simulation by creating the cloud entities using the class method create_cloud_entities(), and then creates the map with the create_map() method for the given number of CCNs, SWCNs and DWCNs. CCNs are created with generate_wiredCN() method, SWCNs are created with generate_SWCNs(), and DWCNs are created by calling the generate_DWCN() method. Additionally, DWCNs are built with the help of the DWCN design specification tool method called WCP_param_recomm(). The given number of CAEVs are then created with generate_AEV() using the list_type_aev(). Each CAEV that arrives in the system requests for a charging reservation and trip planning. The request is formulated in a F_{req} with a randomly generated SoC request and start and end locations for the requested AMoD trip. The charging reservation is then made following the handshake protocol, and a $F_{confirm}$ is returned via the RSU that is used to generate the driving event to be appended to the FEL. Finally, the run_sim() method is called by setup() function to start the simulation.

Now, the run_sim() method is where the actual simulation of the charging reservation and trip planning system begins. The latter extracts events based on the current simulation run time and processes them. The time advance subroutine starts by looking at the FEL. The imminent event with the lowest time is chosen. The simulation clock is then advanced to the imminent event time, and the event either an arrival, departure or driving event is executed and processed. In the event subroutine, system states and entity attributes are updated, statistical data is collected, and future events are generated and placed on FEL. The type of event is evaluated and accordingly the process function for each event type is called. It should be noted that each arrival event may either generate a departure event or another arrival event in case of CCNs and SWCNs when the CAEV arrives early. The departure event leads to the automation generation of the driving event, and the driving event leads to the automatic generation of arrival event in case of arrival at a CN. It is noteworthy that the driving event upon reaching its destination just logs the CAEV's trip as completed and generates no further events for that CAEV. The event generation method for each event type are created to create event objects and append to FEL. The events are generated for each CAEV using the information in the

$F_{confirm}$. Next, the simulation's current clock is compared with the total run time to decide on the termination of the simulation. The time-advance subroutine and the event process sub-routine are repeatedly executed until termination or no more events are left in FEL. After a simulation run, statistics are automatically generated and printed in a file named "test_res.txt" using the generate_STAT() method along with the plots for CAEV's travel times, wait times, battery consumption, charging reservation costs, and comparison between charging requested, reserved and actually delivered per CAEV. The overall simulator flowchart can be seen in Figure 4.8. The simulation results are used for verification of the code and are discussed in length in the next chapter.

4.4.5 System Run Analysis

The run_analysis.py file has the Run_Analysis class. It helps collect statical data from independent replications or simulation runs. It calculates confidence interval (CI) and prediction interval (PI) for each statistical parameter chosen for evaluation, and attaches a degree of confidence to the generated results. It logs statistical data like wait times, throughput, average service time, proportion server idle time, server utilization and system times for the overall system and each CN for given number of simulation runs. The collect_data() method collects the data for the given simulation set up with random generator seeds that are farther apart for independent simulation runs, and the calc_stats() method takes the data collected for independent simulation runs and attaches CIs and PIs to each statistic Finally, the print_stats() prints the results into a text file of a specified name.

Next, the Design_Analysis() class enables comparing two different simulation system set ups to evaluate which design is better. This class holds statistics for independent simulation runs with common random numbers (CRN) for each simulation design set up by calling the collect_data() method of the Run_Analysis() object. It also computes the comparison statistics with CIs and PIs by calling its own calc_print_data() method to compute and print the results in a specified text file. The results generated and their computation formulation is discussed in Chapter 5.

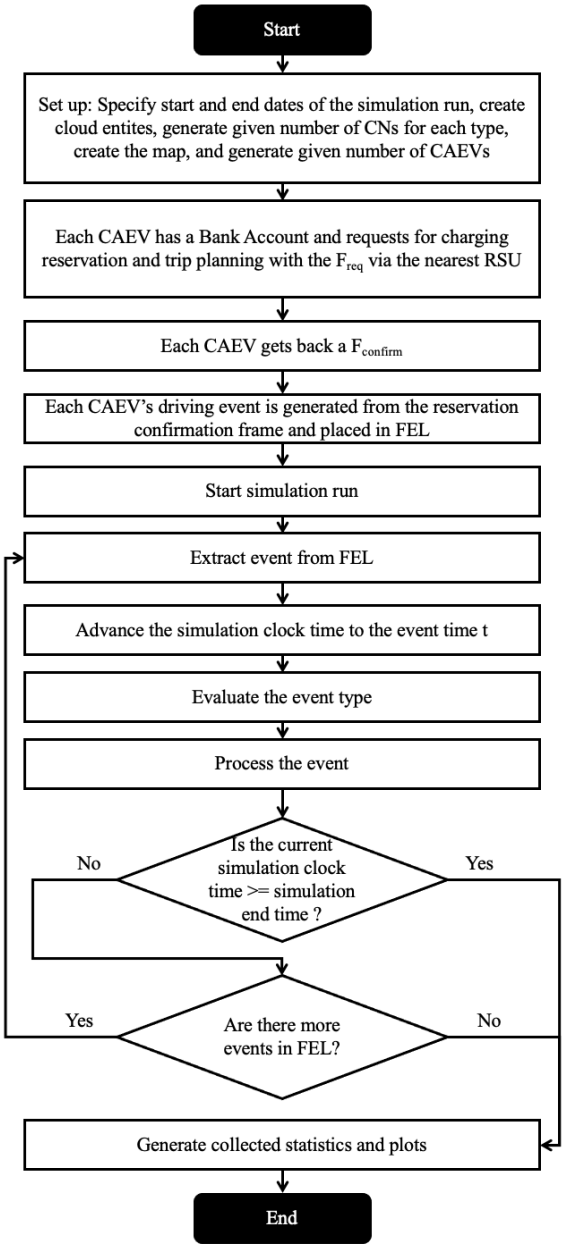

Figure 4.8: Flowchart of the overall simulator.

It should be noted that this designed simulator can not only work independently but can work with other simulators like ACN-Sim [45] whose architecture can be seen in Figure 4.9. The wiEVSE class can extend the ACN-Sim's EVSE class, and the AEV class can extend its EV class and use the Battery class to model the lithium-ion battery.

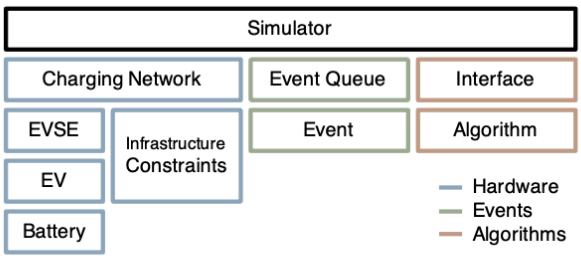

Figure 4.9: Architecture of the ACN-Sim [45].

4.5 Simulation System Event Phases Implementation

Consider a CAEV user that decides to travel from an arbitrary point to a desired destination, and the OBU of the CAEV detects that the charge of its battery has fallen below a set threshold of let's say 25%. The CAEV needs to complete the trip in the shortest time and lowest cost before running out of charging. So, its OBU automatically sends the F_{req} via the closest RSU using V2I to reserve EVSEs close in proximity and along the shortest route to the destination. Thus, minimizing CAEVs waiting times at the CNs, travel costs and battery consumption. The programmed handshake protocol, system design and algorithms to simulate the system event phases in detail are described next.

4.5.1 Shortest Route Trip Planning

To calculate the shortest route for the CAEV trip, Dijkstra's algorithm is used. This designed system can work with any real-world map design. For simulation analysis and proof of concept, the CNs are placed on an automatically generated interconnected map that has two areas or cities each with two sub-areas or towns as can be seen in Figure 4.10. Let's say the area on the left is area 1, A_1, and the area on the right is area 2, A_2. The symmetric map created with the create_map() of MapRoute object automatically places in each area's first sub-area or town half of the CCNs and in the second town half of the SWCNs. The two areas are connected by two DWCN highways. The physical locations of all the CNs have been labelled on the map along with other possible arbitrary pick up points and destinations of the CAEV trips. In this Figure 4.10 map, the location nodes that may represent a mall, school, apartment, etc., in A_1 sub-area 1, A_{11}, and sub-area 2, A_{12}, are $L_{A_{11}} = \{7,8,9,10,11,27\}$ and $L_{A_{12}} = \{17,18,19,20,21,29\}$, respectively. Similarly, the location nodes in A_2 sub-area 1, A_{21}, and sub-area 2, A_{22}, are $L_{A_{21}} = \{12,13,14,15,16,28\}$ and $L_{A_{22}} = \{22,23,24,25,26,30\}$, respectively. The CN location nodes in A_1 sub-areas are $Cl_{A_{11}} = \{1\}$ and $Cl_{A_{12}} = \{5\}$, in A_2 sub-areas are $Cl_{A_{21}} = \{2\}$ and $Cl_{A_{22}} = \{6\}$, and connecting both areas is $Cl_{A_1A_2} = \{3,4\}$. So, $n_{A_{11}} = L_{A_{11}} \cup Cl_{A_{11}}, n_{A_{12}} = L_{A_{12}} \cup Cl_{A_{12}}, n_{A_{21}} = L_{A_{21}} \cup Cl_{A_{21}}$ and $n_{A_{22}} = L_{A_{22}} \cup Cl_{A_{22}}$ denote sets of all map nodes in each area's sub-area. The routes connecting all nodes within a sub-area are labelled x, those connecting the two sub-areas are labelled y and the ones connecting the area to another area via the DWCN are labelled z. The values for these routes are used for minimum route calculation, and can be as simple as depiction of the distance of the route or as complex as the cost of travelling the route that is a combination of traffic density, distance, etc.

The map information helps make reservations for EVSEs in CNs that are either closer in proximity to the CAEV or along the route to CAEV's destination. The latter helps reduce or

eliminate wait times at the static CNs. The system computes shortest routes to the CNs, from CN to other CNs or the final destination by choosing routes with minimum overall travel costs. The travel costs considers total distance travelled in meters and CAEV's battery consumption determined by its efficiency and range ratings. The system analysts can choose to set modelled CAEV range and efficiency ratings specified by Electric Vehicle Data Base (EVDB), New European Driving Cycle (NEDC), Worldwide Harmonized Light-Duty Vehicles Test Procedure (WLTP), Environmental Protection Agency (EPA), or the CAEV manufacturer. Since the system calculates the path after each stop at the CN, the system can dynamically update the computed best route at the time of departure from the current location to factor unpredictable conditions like accidents and traffic congestions. As a result, the overall trip will not only have minimum travel costs and battery consumption costs, but also will complete the trip in the shortest amount of time possible and avoid traffic congestions. Further, the charging reservation will help in minimization of wait times and payments. The CAEVs battery consumption, B_{cons}, from travel using efficiency, B_{effic} , and route cost, C_{route} , can be calculated using (4.1), and (4.2) updates the current battery level, B_{curr}, of the CAEV.

$$B_{cons} = C_{route} * B_{effic} \tag{4.1}$$

$$B_{curr} = B_{curr} - B_{consum,}, where\ B_{consum} \leq B_{max} \tag{4.2}$$

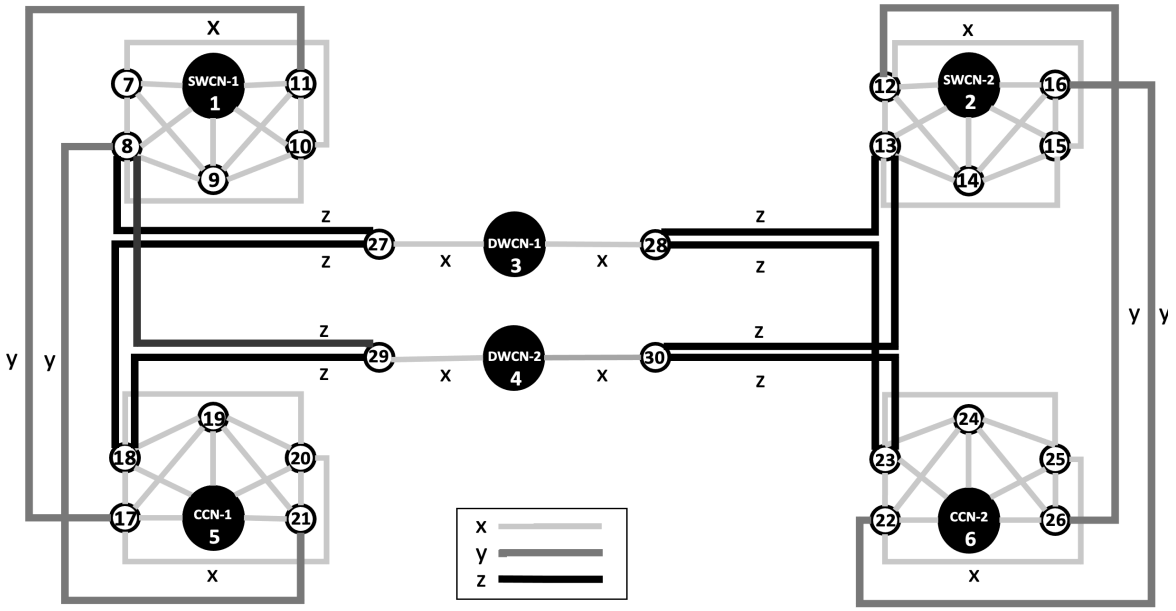

Figure 4.10: Symmetric map for trips with placements of CNs.

4.5.2 Requesting a Charging Reservation

The CAEV via the closest RSU communicates with the EDC to request for a charging reservation and trip planning as can be seen illustrated in Figure 4.11 by calling its sendRequest_chargeSession() method. It should be noted that CAEV requests are scheduled

on a first-come-first-serve basis. The request is carried in the F_{req} that is modelled by object of type Reserv_Request.The RSU adds its own ID and location ID to the message to help estimate the CAEVs location with respect to the map besides CAEV's own disclosure of the current location and intended trip destination, and calls its own make_reservation() method. To maintain anonymity of user, the CAEV is assigned a randomly generated unique reservation request ID (req_ID) by the RSU for every charging reservation request. Then, this F_{req} is forwarded to the EDC, and the EDC calls its make_reservationRequest() method. The request message received by the EDC is enough to first check that the requesting CAEV has sufficient funds or CPs to purchase the desired or requested SoC. After the CAEV's account is approved for sufficient funds, the EDC communicates with the ESP to look for available EVSEs in CNs that are within the vicinity of the CAEV and along the route to the final destination. The latter is done by invoking ESP's request_avail_EVSE() method. The EDC dynamically distributes the request of charging reservation for the requested SoC based on the set thresholds of CNs, the CN locations as well as estimated times the CAEV can spare at each CN to receive the requested SoC. Basically, the system dynamically divides the charging request over one or more types of CNs considering if a DWCN lane falls on its path to the destination and if the requested SoC is more than one EVSE at a CN can provide. Algorithm 1 (see Figure 4.12) is designed to dynamically distribute charging requests.

Now, the system considers two main things for dynamically distributing the charging request over different types of CNs. First, the RSU type that forwarded the request, and second, the source and destination or the possible traveling regions of the route that the CAEV will travel. RSU types are the same as the three CN types. So, the type of RSU from which the request is received helps identify that the CAEV is near which type of CN and the location IDs of the RSU as well as the CAEV's own current location and trip destination disclosure helps narrow down the search of CNs to areas that the CAEV will travel through. As explained earlier, the symmetric map is divided into two main areas or cities composed of two sub-areas that are interconnected by two DWCN lanes. If the CAEV is travelling within the same sub-area, then the subset of CNs that are within it are used to look up for availabilities. Similarly, if the CAEV is travelling within the same area, then the CNs that fall in the two sub-areas along the route of the CAEV are considered. The latter can be seen in Algorithm 1's lines 21-35 and lines 36-50 in Figure 4.12 for requests received from SWCN and CCN RSUs or CAEV's having trips within the same area. However, if the CAEV is travelling from one area's sub-area to the other area's sub-area, then the CNs that are within the two sub-areas are considered along

with the DWCN lanes that are connecting the two areas.Lines 1-20 of Algorithm 1 in Figure 4.12 are employed to achieve the latter. Moreover, the looking up of EVSEs and CNs for reservation is also then based on the idea of location and RSU types. Logically, partial or full charging reservation requests are fulfilled by DWCNs only when the CAEV in the system is going to the other area and will be utilizing the DWCN highway lane on its route. This knowledge of CN locations and the RSU location and types helps distribute the charging reservation request more intelligently and at lower computation costs by significantly narrowing the area of search.

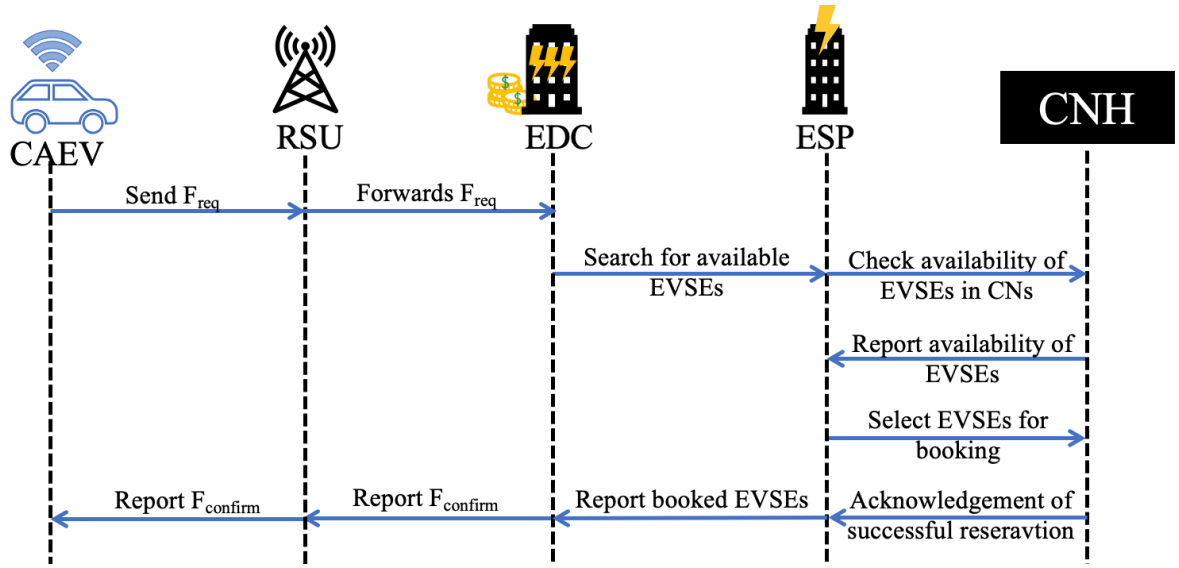

Figure 4.11: CAEV sending a charging reservation request and receiving back a confirmation.

Let's assume, the maximum SoC fulfillment threshold set for DWC is set at 40 % of CAEV battery capacity, and for SWC and CC is set at 100 % of CAEV battery capacity. Thn suppose a CAEV user has requested a SoC of 60 % of its 100 kWh battery capacity that is 60 kWh of charging is requested. The CAEV wants to travel from A_{11} to the A_{22}, then the CNs in those specific sub-areas along with the DWCN highway lanes that fall on the route given by $Cl_{A_{11}} \cup Cl_{A_{22}} \cup Cl_{A_1A_2}$ will be considered for searching EVSE availabilities. The EDC after receiving the request of 60 kWh of charging will use Algorithm 1 in Figure 4.12 to create a query for search that is dynamically distributed over different CN types. In accordance with the algorithm, the lines 1-20 will take the request and fulfill the 40 kWh over DWCN and the leftover SoC over the SWCN or CCN whichever type of CNs fall on the path to the destination. Algorithm 2 and Algorithm 3 in Figures 4.13 and 4.14, respectively, are used to estimate the time of charging at the EVSE of the DWCN and static CNs, respectively.

Algorithm 1 Dynamic Distribution of Charging Reservation Request over Different CN Types

If CAEV's trip source and destination are in opposite A_x or RSU Type == DWCN **then**
  If ($SoC_{req} \geq th_{DWC}$) **then**
    $T_{DWC}^{dur} = Computed\ using\ Algorithm\ 2$
    Add to F_{req} the SoC_{req} and T_{DWC}^{dur} to look for all available $DWCN \subseteq Cl_{A1A2}$ EVSEs that can fulfill the request
    $SoC_{DWC}^{left} = SoC_{req} - th_{DWC}$
    If ($SoC_{DWC}^{left} \leq th_{SWC}$)**then**
      $T_{SWC}^{dur} = Computed\ using\ Algorithm\ 3$
      Add to F_{req} the SoC_{DWC}^{left} and T_{SWC}^{dur} to look for all available $SWCN \subseteq (Cl_{Axy} \cup Cl_{Axy})$ EVSEs that can fulfill the request
    else
      $SoC_{SWC}^{left} = SoC_{DWC}^{left} - th_{SWC}$
      If ($SoC_{SWC}^{left} \leq th_{CC}$)**then**
        $T_{CC}^{dur} = Computed\ using\ Algorithm\ 3$
        Add to F_{req} the SoC_{SWC}^{left} and T_{CC}^{dur} to look for all available $CCN \subseteq (Cl_{Axy} \cup Cl_{Axy})$ EVSEs that can fulfill the request
      else
        $SoC_{CC}^{left} = SoC_{SWC}^{left} - th_{CC}$
        Add to F_{req} the SoC_{CC}^{left} as portion of charging that cannot be fulfilled
      endif
    endif
  endif
endif
If CAEV's trip source and destination are in A_x and RSU Type == SWCN **then**
  If ($SoC_{req} \leq th_{SWC}$)**then**
    $T_{SWC}^{dur} = Computed\ using\ Algorithm\ 3$
    Add to F_{req} the SoC_{req} and T_{SWC}^{dur} to look for all available $SWCN \subseteq Cl_{Ax}$ EVSEs that can fulfill the request
  else
    $SoC_{SWC}^{left} = SoC_{req} - th_{SWC}$
    If ($SoC_{SWC}^{left} \leq th_{CC}$)**then**
      $T_{CC}^{dur} = Computed\ using\ Algorithm\ 3$
      Add to F_{req} the SoC_{SWC}^{left} and T_{CC}^{dur} to look for all available $CCN \subseteq Cl_{Ax}$ EVSEs that can fulfill the request
    else
      $SoC_{CC}^{left} = SoC_{SWC}^{req} - th_{CC}$
      Add to F_{req} the SoC_{CC}^{left} as portion of charging that cannot be fulfilled
    endif
  endif
endif
If CAEV's trip source and destination are in A_x and RSU Type == CCN **then**
  If ($SoC_{req} \leq th_{CC}$)**then**
    $T_{CC}^{dur} = Computed\ using\ Algorithm\ 3$
    Add to F_{req} the SoC_{req} and T_{CC}^{dur} to look for all available $CCN \subseteq Cl_{Ax}$ EVSEs that can fulfill the request
  else
    $SoC_{CC}^{left} = SoC_{req} - th_{CC}$
    If ($SoC_{CC}^{left} \leq th_{SWC}$)**then**
      $T_{SWC}^{dur} = Computed\ using\ Algorithm\ 3$
      Add to F_{req} the SoC_{CC}^{left} and T_{SWC}^{dur} to look for all available $SWCN \subseteq Cl_{Ax}$ EVSEs that can fulfill the request
    else
      $SoC_{SWC}^{left} = SoC_{CC}^{req} - th_{CC}$
      Add to F_{req} the SoC_{SWC}^{left} as portion of charging that cannot be fulfilled
    endif
  endif
endif
Return F_{req}

Figure 4.12: Algorithm 1 for dynamic distribution of charging reservation request over different CN types.

In Algorithm 2 and Algorithm 3, the duration of one time slot, ts_{dur}^{CN}, in minutes has to be defined. The charging period, T_{CN}^{dur} , in static CNs is identified by computing the maximum charging rate at which the CAEV can receive the charging, and the total number of time slots, N_{ts}, that will be required to achieve the desired charging. N_{ts} is then converted to minutes based on the definition of one time slot, and then the estimated start time, T_S^{CN}, and end time,

T_E^{CN}, are computed by adding the T_{CN}^{dur} to the T_S^{CN}. However, the constraint is that if the T_E^{CN} of charging is more than the estimated departure time, T_{tdept}, of the CAEV, then T_{tdept} will be used to mark the end of the charging session's duration in making a reservation. The latter condition may occur when the CAEV's charging acceptance rate or the EVSE's charging rate is not high enough to fulfill the CAEV's requested SoC in the requested charging duration. In case of DWCN, only the time slot is assigned. No calculation for N_{ts} is conducted, as each CAEV needs to travel over the entire length of the DWCN lane to receive its charging. The fixed value of ts_{dur}^{CN} is indicative of the prior fact. In other words, charging reservation passes or session tickets of fixed charging durations are supplied in DWCNs. Since, the entire DWCN lane cannot be reserved for one CAEV. A maximum limit for the number of CAEVs that can be on the highway DWC lane at the same time or for the same session ticket can be defined to avoid traffic congestion.

Algorithm 2 Estimating Charging Duration for DWCN

1:	T_E^{CN}=$T_S^{CN} + ts_{dur}^{CN}$
2:	**if** $(T_E^{CN} > T_{tdept})$ **then**
3:	T_E^{CN}=T_{tdept}
4:	**endif**
5:	T_{CN}^{dur}=$T_S^{CN} + T_E^{CN}$
6:	**return** T_{CN}^{dur} , T_S^{CN}, T_E^{CN}

Figure 4.13: Algorithm 2 for estimating charging duration for DWCN

Algorithm 3 Estimating Charging Duration for SWCN and CCN

1:	$N_{ts} = \left(\frac{SoC_{req}}{B_{max} * 60}\right) * \frac{1}{ts_{dur}^{CN}}$
2:	$T_{CN}^{dur} = ts_{dur}^{CN} * N_{ts}$
3:	T_E^{CN}=$T_S^{CN} + T_{dur}^{CN}$
4:	**If** $(T_E^{CN} > T_{tdept})$ **then**
5:	T_E^{CN}=T_{tdept}
6:	**endif**
7:	T_{SWC}^{dur}=$T_S^{CN} + T_E^{CN}$
8:	**return** T_{CN}^{dur} , T_S^{CN}, T_E^{CN}

Figure 4.14: Algorithm 3 for estimating charging duration for SWCN and CCN.

The Algorithm 1 modified F_{req} with new fields like type of CN, the requested SoC and estimated charging duration helps narrow the search of the EVSEs for charging reservation. This F_{req} is then forwarded by the EDC to the ESP to look for all the available EVSEs in CNs that are in the selected sub-areas along the CAEVs possible shortest route, and are also available is the estimated time range to deliver the requested SoC. The ESP calls the CNH that manages all the CNs. CNH calls each CN located within the narrowed sub-area, and searches availabilities through the EVSEs of the CNs using its request_all_available_EVSEs() method within the estimated charging duration. The logic of search involves adding all EVSEs that are available starting from or after the estimated start time of charging to the estimated end time

of charging into a list. The list of availabilities is then reported back to the ESP by the CNH as can be seen illustrated in Figure 4.11.

4.5.3 Confirmation of a Charging Reservation

The ESP upon getting the list of available EVSEs in CNs will have to make the best selection of one or more EVSEs for one or more reservation with the shortest possible route. The selection's goal is to minimize the overall travel costs, battery consumption and wait times of the CAEV on its shortest route to the destination. The latter is partially achieved by making the selection among the EVSEs that are close in proximity and along the possible route of the CAEV's trip destination. It should be noted that the exact route for the CAEV is computed only after the CNs are selected. The final selection of EVSEs now comes down to one or more EVSEs that can best fulfill the originally requested SoC within the estimated CAEV arrival and departure times. So, the first available EVSE in the list that can provide the maximum charging within the estimated charging stay duration of the CAEV is selected for reservation using the choose_EVSE() method of the ESP. Then, the selected EVSEs and their CNs are notified of the reservation request with ESP's reserve_EVSE() that invokes CNH's make_reservation_EVSE_CN(), and the successful reservation confirmation signal is sent back to the EDC as can be seen in Figure 4.11. The ESP notes the locations of the EVSEs and the reserved start time and end time of the charging and reports it to the EDC. This information is used by the ESP to create the $F_{confirm}$ modelled by the Reserve_Confirm object. Finally, the RSU communicates to the CAEV the approval or acknowledgement of the request with a $F_{confirm}$. The confirm_ID is the same as the req_ID for the CAEV that requested a charging reservation. The latter enables traceability for the CNH while keeping the CAEV's user information private. It also allows the CNH to know what amount of charging will be delivered by CN's reserved EVSE. For the system, the confirm_ID is sufficient to retrieve details for the reservation of a CAEV. The CN and EVSE location IDs enable navigation to the CN's EVSE.. The entire procedure of requesting a charging reservation and obtaining a confirmation for a CAEV can be seen depicted in Figure 4.11. So, the request for a charging reservation has been confirmed. Now, the CAEV following the $F_{confirm}$ will need to drive on the computed shortest trip route to the reserved EVSEs of CNs and obtain their requested SoC.

4.5.4 Establishing a Charging Session

A. Authentication and Synchronization for Charging

The CAEV communicates its unique confirm_ID with the RSU of the CN once it is close in proximity as can be seen in Figure 4.15 using its pac() method for SWCN or CCN and

dac() for DWCN. The CN and RSU are identified by the CAEV by matching the location ID of the CN and the RSU that were supplied in the $F_{confirm}$. If the confirm_ID is in the CN's reservation list, then the reserved EVSE is activated using CN's activateEVSE() method and is supplied power with startPower_EVSE() method. In the CCN, the EVSE is activated to be prepared for the incoming CAEV and supply the reserved power via the plug for the reserved charging duration. In SWCN, the EVSE relays the activation signal and the CAEV's confirm_ID to its WCP that will supply power to the authenticated CAEV. In DWCN, all the EVSEs and their corresponding arrays of WCPs are sent a signal for activation along with the confrim_ID of the oncoming CAEV to supply the reserved power.

The initial synchronization of the CAEV with the EVSE occurs to prepare it for the oncoming vehicle. In static CNs, the CAEV goes and parks at the free and expecting EVSE for its reserved charging session. The CAEV in CCN plugs-in for its charging session. If the CAEV's confirm_ID communicated to the EVSE via RFID exists in the EVSE's reservation list, then the charging session begins and the CAEV is supplied power for the reserved charging duration. In wireless CNs, the RFID communication between the CAEV and the WCPs only occurs if the EVSE that contains those WCPs is activated and expecting the CAEV. Only the WCPs of EVSE that is signaled to be ready will be open to receive the confirmation IDs and detect vehicles at low power supply, and full power is supplied once the expected CAEV is detected. So, the CAEV's interaction with each WCP is used to synchronize charging, and also to report speed errors or misalignment issues to the CAEV user immediately. Specifically, the CAEV is detected by the WCP's sensors and upon contact it exchanges its confirm_ID. The WCP will communicate the confirm_ID with the EVSE, and if it is in the list, then the EVSE will supply the power to the WCP to charge the CAEV for the reserved charging duration the CAEV is in contact with the WCP. This synchronization is done for each WCP in DWCN, so the CAEV user can leave the lane and re-enter before a time-out expires. As depicted in Figure 4.15, the CAEV is synchronized and verified for each WCP before being supplied power. It should be noted for CCNs the actions depicted of EVSE and WCP in Figure 4.15 are combined and carried out by a wired EVSE alone.

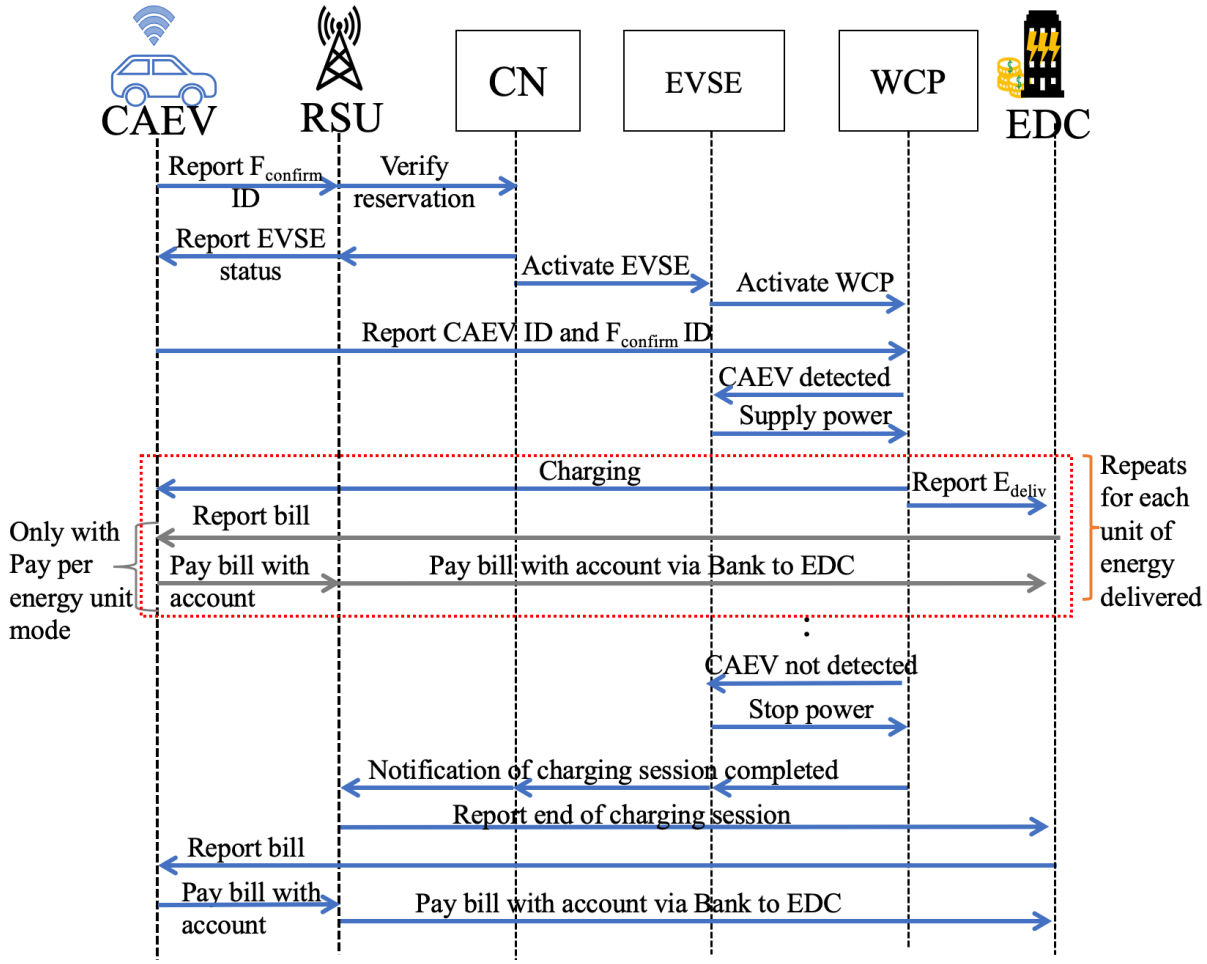

Figure 4.15: CAEV managing a charging session.

B. Misalignment Detection and Speed Detection

In SWCN, the CAEV needs to be parked and properly aligned whereas in the DWCN the CAEV has to be aligned as well as maintain a set constant speed to receive charging. However, if these alignment and speed conditions are not met in wireless CNs, then the CAEV will not receive its requested reserved SoC in a proper and safe manner. To solve the issue of misalignment and speed errors, the system has an automated driving feedback system implemented by Algorithms 4 and 5 in Figures 4.16 and 4.17, respectively. In wireless charging systems, the automated driving feedback system checks for both misalignment and speed errors and will not deliver charging until the set misalignment tolerance and speed tolerance conditions of the CN are satisfied. The WCP reports to the CAEV that it is not being detected and is misaligned by a calculated value. Then, the CAEV will start to move the vehicle left or right or even backwards and forwards by a certain steering rate, r_{steer}, until the feedback system reports that the CAEV is within the misalignment tolerance range. Parallelly, the feedback system with its sensors detects the speed of the CAEV. For SWCN, the speed of the CAEV needs to be 0 km/h, and if the vehicle is detected to be moving then the WCP with its

RFID communication reports this to the CAEV. Then, the CAEV will start reducing the speed of the CAEV at a certain rate, r_{acc}, and once the feedback system of reporting detects the speed reaching within the range of tolerance the reporting stops. Similarly, for DWCN the feedback system reports the speed issue error by WCP's RFID communication but also uses the RSUs given that the CAEV might accelerate away from the WCP's range of communication. The feedback system will keep on reporting the error until the CAEV maintains a constant speed within the tolerable set range for safe charging delivery. Once both the speed and misalignment tolerance conditions are met, the system can start delivery of charging. In the process of charging delivery, this feedback system keeps on monitoring and ensuring that the CAEV is receiving charging within the safe operating conditions and constraints.

Algorithm 4 Misalignment Detection in SWCNs and DWCNs

1:	**while** $(pos_y \; is \; not \; in \; [(W_S^y + W_{tol}^y), (W_E^y - W_{tol}^y)] \;)$ **do**
2:	Report speed error to the CAEV through RFID communication or via the closest RSU if the CAEV is not in RFID's communication range
3:	CAEV's OBU upon receiving the report will steer left or right the CAEV by a factor of r_{steer} to update pos_y
4:	**end while**
5:	**while** $(pos_x \; is \; not \; in \; [(W_S^x + W_{tol}^x), (W_E^x - W_{tol}^x)] \;)$ **do**
6:	Report speed error to the CAEV through RFID communication or via the closest RSU if the CAEV is not in RFID's communication range
7:	CAEV's OBU upon receiving the report will steer left or right the CAEV by a factor of r_{steer} to update pos_x
8:	**end while**
9:	**continue** with the charging operation

Figure 4.16: Algorithm 4 for misalignment detection in SWCNs and DWCNs.

Algorithm 5 Speed Error Detection in SWCNs and DWCNs

1:	**while** $(v_{curr} \; is \; not \; in \; [(S_{CN} + S_{tol}), (S_{CN} - S_{tol})])$ **do**
2:	Report speed error to the CAEV through RFID communication or via the closest RSU if the CAEV is not in RFID's communication range
3:	CAEV's OBU upon receiving the report will increase or decrease the CAEV's v_{curr} by a factor of r_{acc}
4:	**end while**
5:	**continue** with the charging operation

Figure 4.17: Algorithm 5 for speed error detection in SWCNs and DWCNs.

It should be noted in DWCN lanes a stretch of road before the WCPs is kept for calibration purposes, so that this feedback system can maintain CAEV's constant speed and misalignment tolerance conditions before cruising into the stretch of road that has the activated WCPs. Thus, allowing the feedback system to later on quickly correct any abnormal CAEV driving behavior without losing its reserved charging.

4.5.5 Delivery and Real-time Metering of Charging

A. Battery Management System and Charge Delivery

After successful authentication and synchronization, the EVSE starts to deliver charging in the reserved duration compatible with the CAEV's charging acceptance rate. For realistic simulation, we like [267] advocate the use of linear two-stage battery model for charging, and oppose the idealized modelling in (4.3) that unrealistically assumes that the CAEV's battery will follow the given pilot signals exactly.

The linear two-stage battery model [268] approximates the roughly piecewise linear charging process used for lithium-ion batteries. Its charging rate, $\hat{r}(t)$, is given by (4.4). The $r(t)$ is the pilot signal passed to the battery, $\bar{r}$ is the maximum charging rate of the on-board charger, $\hat{e}(t)$ is the difference between the capacity of the battery and the energy stored in it at time t, SoC is the state-of-charge of the battery, and th marks the transition from the bulk stage to the absorption stage of the charging process. All charging rates are positive, as only battery charging is considered. The first stage called bulk charging lasts from 0 to between 70 to 90 % SoC where the current draw, neglecting changes in pilot, is nearly constant. The second stage called absorption is distinguished by the linear decrease in charging current while the battery voltage stays constant. The latter behavior is illustrated in plot of Figure 4.18 from [267] to reveal its realistic depiction of charging behavior compared to the idealized model and the real-world battery charging data. It can be seen that the real charging rate of an EV is often strictly lower than the pilot signal and decays as the battery approaches 100% SoC. The battery's actual charging rate depends on the pilot signal as well as the vehicle's on-board charger, its SoC, and other environmental factors. So, this piecewise linear model is a very good approximation of the real-world charging behavior.

$$\hat{r}(t) = \min\{r(t), \bar{r}, \hat{e}(t)\} \tag{4.3}$$

$$\hat{r}(t) = \begin{cases} \min\{r(t), \bar{r}, \hat{e}(t)\} & if\ SoC \le th \\ \min\{\dfrac{(1-SoC)\bar{r}}{1-th}, r(t)\} & otherwise \end{cases} \tag{4.4}$$

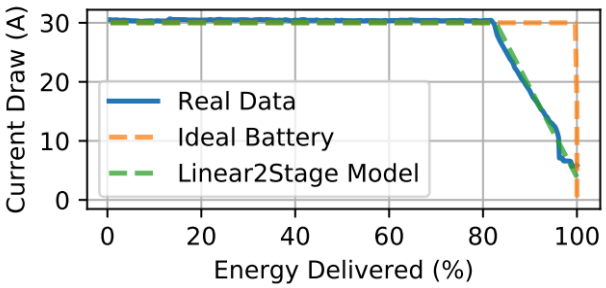

Figure 4.18: Comparing the real battery data, ideal battery model and the linear-two-stage model [267].

Both the battery and its battery management system are modelled. The charge method is designed to take in a pilot signal as well as the voltage of the EVSE and the duration of the timestep. It then calculates the actual charging rate of the battery and updates the battery's internal state. The charge method loops from start time of CAEVs arrival, T_{tarr}, that may be greater or equal to reserved start time, T_S^{CN}, to the reserved end time, T_E^{CN}, or CAEV's departure time, T_{tdept}, for delivering charging.

B. Fair Billing Schemes and Payments

Now, when charging is being delivered to the CAEV each energy unit delivered by the EVSE of the CN, E_{deliv}, is reported via the RSU to the EDC for real-time metering. The EDC then applies the Ontario Energy Board's TOU electricity billing pricing rate by breaking down the time, day, month and year of energy delivery, EDC then starts logging the total E_{deliv} data for computing the bill for charging. Besides the EDC's real-time metering of charging, the CAEV also keeps track of how much kW per ms or μs is received by the CAEV's battery from the WCPs or the plug to ensure fair billing. Fair billing means that the CAEV is charged exactly for the actual charging received. The real-time metering of charging is accompanied by our two proposed payment schemes to fairly bill the CAEV either in real-time as charge is being delivered or at the completion of the charging session at the CN. One of the two proposed approaches can be adopted for billing CAEVs for their charging sessions as depicted in Figure 4.15. The pay per charging session enables billing the CAEV at the end of the charging session using calculate_chargeSessionBill() and report_chargeSessionBill() to calculate and report the bill from the EDC to the CAEV, respectively. On the other hand, the pay per energy unit enables billing the CAEV for each unit of charging delivered by calculating the bill using calculate_PerEnergyUnit() for each kW delivered and reports the bill from the EDC to the CAEV with report_PerEnergyUnit(). Further, the bill is also computed and reported at the end of the charging session for any leftover charging that is less than the defined energy unit. For example, if the CAEV received 45.8 kW and the energy unit was defined as 1 kW, then the user after being billed for every energy unit that is 45 kW in total will also be billed for the leftover charging that is 0.8 kW at the end of the charging session. As a result, the CAEV is billed fairly. The CAEV pays the bill using EDC's payBill() method, and the EDC keeps a record of the anonymous charging session as paid. The charging session is truly anonymous, as the EDC does not keep record of the actual CAEV user for privacy purposes.

C. Payment Calculations

Since the system has been real-time metering the charging delivery, the EDC has information of how much charging in kW has been delivered to the CAEV. For each bill reporting, the total amount of energy delivered, E_{deliv}, is converted to CAD, C_{CAD}, using the appropriate TOU pricing rate, r_{energy} as can be seen in (4.5). Based on the defined purchase rate of the CPs, r_{CP}, the EDC converts the C_{CAD} to cost in CPs, C_{CP}, using (4.6). This computed C_{CP} is then reported to CAEV for charging payment. If the CAEV does not agree with the report, then it may send an error message or a negative acknowledgement in both payment options for

recalculation of the bill. Once the CAEV agrees with the report, the CPs are then automatically deducted from the CAEV's account to reflect the change.

$$C_{CAD} = E_{deliv} * r_{energy} \tag{4.5}$$

$$C_{CP} = \frac{C_{CAD}}{r_{CP}}, where\ C_{CAD} \geq r_{CP} \tag{4.6}$$

4.5.6 Late and Early Arrivals

When the EVSE is ready to service the CAEV, then the CAEV can drive to it and start the charging session. However, when the CAEV arrives early or late to the EVSE certain updates to the reservation may be made.

For DWCN, the issue of late and early arrivals is not that big as the CAEV has a session ticket or reservation along with possible one or more CAEVs for the same time slot. The DWCN is designed to accommodate a certain number of CAEVs for simultaneous charging without congestion. The system has assigned reservations to let's say only 75% of total DWCN capacity for the same time slot. So, if the CAEV is a bit early or late, it can still enter and receive charging. The reservation information of true arrival and true departure of the charging session maintained by the EDC will be updated accordingly for later traceability. However, in case of SWCN and CCN the early and late arrivals need to be dealt with in a proper manner using Algorithm 6 in Figure 4.19.

In static CNs, two main cases of arrivals have to be dealt with that are early and late arrivals as depicted in Algorithm 6. For early arrival cases lines 37-42 in Algorithm 6 (see Figure 4.19), the system will have to allow the CAEV to receive charging at an earlier time or wait in the queue if there is place else the CAEV is detoured to come back at the reserved time. The appropriate reservation updates have to be made by the EDC to update the reservation list of this reserved CN and its EVSE as depicted in lines 1-36 of Algorithm 6 in Figure 4.19. So, if the CAEV has arrived earlier than its reservation at the EVSE, and the EVSE has earlier time slots available that are of the same reserved charging duration, then the CAEV's reservation can be updated to an earlier time. Then, the old reserved time slots are either passed on to any CAEVs next in line in terms of reservation or are made available for all future CAEV reservations. Another possible case is that the EVSE has time slots available for earlier time but it's not of an equivalent charging duration, then the CAEV's currently reserved time slots continuity with the available EVSE time slots is checked. If there is continuity among the earlier available time slots and the reserved time slots of the CAEV and their combination results in greater or equivalent charging duration, then the combined time slots are used to replace and update the charging reservation. If there are any leftovers, then they may be

assigned to the next CAEV in line, if any, using the same earlier arrival logic again. After the evaluation for reservation update, the CAEV may park right away for reserved charging, queued or sent to detour if the queue has no space. Detouring involves allowing the CAEV to wait in the parking lot or even roam around to let the CAEV user run other chores. In the case of late arrivals, lines 45-47 of Algorithm 6 in Figure 4.19 are executed. The CAEV can just go and park at the EVSE to receive charging mid-way of the reservation. The system may impose penalties and the CAEV as expected would not receive the fully received SoC from this reserved EVSE. The system instead of automatically preserving the charging reservation can choose to send a message to check up on CAEV. The CAEV user can choose to cancel or postpone the reservation for a penalty if imposed by the implementer .

Algorithm 6 Processing CAEV Arrivals at SWCNs and CCNs

1:	**if** $(T_{tarr} < T_S^{CN})$ **then**
2:	**If** $(EVSE_{reserv}\ has\ ts_{avail} < T_{tarr})$ **then**
3:	add the ts_{avail} to ts_{extrac}
4:	sort ts_{extrac} in ascending order
5:	**If** $(ts_{extrac}\ has\ continuity\ with\ ts_{reserv})$ **then**
6:	combine ts_{extrac} and ts_{reserv} into ts_{extrac}
7:	sort ts_{extrac} in ascending order
8:	**If** $\left(T_{dur}^{ts_{extrac}} == T_{dur}^{CN}\right)$ **then**
9:	swap ts_{extrac} with ts_{reserv}
10:	update the $EVSE_{reserv}$ and notify the CAEV
11:	**elseif** $\left(T_{dur}^{ts_{extrac}} > T_{dur}^{CN}\right)$ **then**
12:	add time slots from ts_{extrac} to ts_{reserv} that have T_{dur}^{CN}
13:	add leftover time slots in ts_{extrac} to ts_{left}
14:	update the $EVSE_{reserv}$ and notify the CAEV
15:	**If** $\left(Q_{EVSE_{reserv}} is\ not\ empty\right)$ **then**
16:	make ts_{left} available for the next CAEV
17:	**else**
18:	add ts_{left} to the ts_{avail}
19:	**endif**
20:	**endif**
21:	**else**
22:	**If** $\left(T_{dur}^{ts_{extrac}} == T_{dur}^{CN}\right)$ **then**
23:	swap ts_{extrac} with ts_{reserv}
24:	update the $EVSE_{reserv}$ and notify the CAEV
25:	**elseif** $\left(T_{dur}^{ts_{extrac}} > T_{dur}^{CN}\right)$ **then**
26:	add time slots from ts_{extrac} to ts_{reserv} that have T_{dur}^{CN}
27:	add leftover time slots in ts_{extrac} to ts_{left}
28:	update the $EVSE_{reserv}$ and notify the CAEV
29:	**If** $\left(Q_{EVSE_{reserv}} is\ not\ empty\right)$ **then**
30:	make ts_{left} available for the next CAEV
31:	**else**
32:	add ts_{left} to the ts_{avail}
33:	**endif**
34:	**endif**
35:	**endif**
36:	**endif**
37:	**If** $(T_{tarr} < T_S^{CN})$ **then**
38:	**If** $\left(Q_{EVSE_{reserv}} has\ space\right)$ **then**
39:	add CAEV to the queue
40:	**else**
41:	detour CAEV
42:	**endif**
43:	**elseif** $(T_{tarr} == T_S^{CN})$
44:	park CAEV to begin charging session
45:	**elseif** $(T_{tarr} > T_S^{CN})$ **then**
46:	park CAEV to begin charging session and penalize for missed time slots
47:	**endif**

Figure 4.19: Algorithm 6 for processing CAEV arrivals at SWCNs and CCNs.

4.6 Dynamic Wireless Charging Network Design Specification Tool

The DWCN are not yet available for public use, and there are no standards available to follow for its construction and operation. Hence, a novel design specification tool implemented as WCP_param_recomm() method is designed to take in parameters like number of EVSEs, N_{EVSE} , to be installed, length of track, l_{track}, in meters, length and width of a WCP in meters, l_{WCP} , and gap in meters, g_{WCP} , that need to be maintained between each WCP installation. Other input parameters include EVSE's charging rate in kW, r_{charge} , at which the battery of a CAEV is charged, the voltage at which an EVSE operates, and the vehicle speed tolerance that can be afforded to safely supply the promised charging to a CAEV in motion.

Equations (4.7) to (4.13) represent formulas by the tool to calculate the total number of WCPs, N_{WCP}, that need to be purchased, required number of WCPs per EVSE, N_{WCP}^{EVSE}, calculated length of track with WCPs installed, recommended average speed, v_{recomm}, to receive charging from the track, time it will take to drive over the track in minutes, T_{track}, and the total charging, C_{track}, the track can deliver in the track's travel time, respectively. Additional features that the design specification tool can calculate includes length of each EVSE with WCPs installed, time to driver over a WCP and an EVSE in minutes, energy that can be delivered by an EVSE, WCP and the track in kWh, total number of EVSEs and WCPs needed to deliver 1 kWh of energy to a vehicle in motion, total ampere needed for EVSE's operation, recommended maximum energy threshold in kWh for the track and its EVSE and WCPs, the exact location of each WCP installment in meters, and the recommended time slot in minutes to use for reservations.

The design specification tool is designed and tested in python version 3.9, and it is a tool that can be used both independently in recommendations for real-world construction and with a simulator that simulates our proposed system. It can help analyze and predict performance of DWCNs in a smart city. The design specification tool analysis can be seen in APPENDIX A.

$$N_{WCP} = \frac{l_{track}}{l_{WCP} + g_{WCP}} \tag{4.7}$$

$$N_{WCP}^{EVSE} = \frac{N_{WCP}}{N_{EVSE}}, where\ N_{EVSE} > N_{WCP} \tag{4.8}$$

$$calculated\ N_{WCP} = N_{WCP}^{EVSE} * N_{EVSE} \tag{4.9}$$

$$l_{EVSE} = l_{WCP} * N_{WCP}^{EVSE} \tag{4.10}$$

$$calculated\ l_{track} = l_{EVSE} * N_{EVSE} \tag{4.11}$$

$$T_{track} = \frac{calculated\ l_{track}}{v_{recomm}} \tag{4.12}$$

$$C_{track} = T_{track} * r_{charge} \tag{4.13}$$

4.7 Conclusion

In this chapter, the charging reservation and trip planning system with the proposed CN hierarchy, protocols and messages is translated into an operational simulation model. In other words, the conceptual model is realized using the python programming language. This simulator specifically addressed issues of unplanned trips and searching for charging stations like traffic congestion, battery consumption, long waiting times and charging times of CAEVs.

The simulation model building is not linear but an iterative process. So, its implementation was comprised of repeated modifications. The knowledge gained during the designing and implementation of the simulation model was of great value in making improvements in the system under investigation. Informational, organizational and environmental changes of the presented system can now be emulated, and the effect of these alterations on the simulation model's behavior can be observed to answer "what if" questions. Further, new hardware design, physical layouts, transportation systems could be tested without commitment of expensive resources. Overall, this designed simulator can help in understanding how a system actually works rather than how we as analysts and implementers think it would work.

Since the overall goal is to have a simulation model with increased accuracy and credibility, the next chapter discusses the verification and validation of the system with increased confidence in generated results. Moreover, the simulation approach allows experimentation of new design or policies to improve the system through model building while saving time and money. Hence, other alternative design choices are explored next to balance cost and performance of the overall system like having more or fewer number of EVSEs per CN.

Chapter 5 Results and Discussion

5.1 Introduction

Verifying and validating the simulation model is a difficult yet necessary task to ensure credibility of generated results. The overall goal is to have a simulation model with increased accuracy and credibility to give the implementers and analysts confidence in the results generated for making real-life decisions. This simulation model building process is not a linear but an iterative process. So, the prior comprises of repeated modifications to the simulation model where the conceptual and operational models are compared against each other while performing verification and validation techniques. Once the system is verified and validated, it is run to generate results and conduct an output analysis. The output analysis enables examination of generated statistics to predict absolute performance of the system with the chosen evaluation parameters. Further, the output analysis is also used to conduct comparison with other system designs for estimation of relative performance, and determination of best system design for an analyst or implementer, for example.

This chapter is organized to discusses the proposed simulated model's verification and validation in sections 2 and 3, respectively. Section 4 presents the simulation model's set up, run and generated results. The parameters chosen for evaluating the system are defined in section 5. Section 6 discusses the results of the output analysis of the simulated model and its alternative system designs to reveal the best system design for implementation. The proposed system design's novelty is highlighted in section 7 by comparing it with somewhat similar existing systems in literature. Finally, section 8 concludes this chapter.

5.2 Model Verification

Verification of the simulation model involves ensuring that the conceptual or proposed model in Chapter 3 is correctly translated into the operational model or simulation model of Chapter 4. Since verification is concerned with building the model correctly, the conceptual model is compared to the implementation or computer representation.

Firstly, debugging and code correction is done using python's print statements and VSCode integrated development environment's Run and Debug Tool with its break points and logging options to help trace behaviors of methods. It ensured proper behavior is programmed and executed. After the debugging process, the written python code successfully compiled and ran. Hence, it is concluded that the system simulation with its assumptions and abstractions, input parameters and logical structures are implemented correctly. The event processing

flowcharts in Figure 4.2 to 4.7 and algorithms 1 to 6 besides reflecting implementation logic were a very good way of quickly rechecking, verifying and debugging the simulation operation. If the simulation did not seem to behave in a desired manner, that part of the logical flow was stepped through for debugging and correction. Thus, enhancing the credibility of the simulation logic.

Another way the simulation is verified is by checking the output for reasonableness under a variety of settings for the input parameters. The latter is done by printing out current counts or number of CAEVs in each system component or CN at the current time for tracing and debugging during the initial phase of testing and implementation. The generate_STAT() function of the Simulation object prints out the selected current count statistics to evaluate and analyze simulation run results successfully.

The long-run measures of simulation performance are also calculated like server utilization, average number of components in system (L) and average time spent in the system. The long-run statistics are often computed using theories and formulas and then compared to simulated counterparts for verification. The main objective of the simulation is to estimate the mean measure of performance such as mean response time that cannot be computed analytically. So, Chapter 6 of [269] states if the simulation results predict the average response time or utilization correctly, then all other parameters estimated are highly confident to be correct as well. Otherwise, if the model is wrongly predicting the parameters, then the confidence in the estimation of the other parameters lowers even when they are not directly related. Following the analytical approach, the conservative law or the Little's Law is used for verification. The Little's Law calculation can be found in APPENDIX B.1. It is ensured that for each CN and the overall system the Little's Law computed and calculated L match. Thus, increasing the overall credibility of all other results produced by the simulation.

Evaluating the statistics for different total simulation run times with the same seed, helped detect the mistakes in the code logic, data initializations, CN initialization states, as well as CN operation. Further, checking for output reasonableness with tracing was a quick way to detect major errors like expecting 50 CAEVs that enter the system to be serviced will also leave the system by end of the simulation run. This process of adding current counts, total counts, and printing out statistics as well as traces made the simulation model self-documenting. Thus, enabling an outsider or an analyst to understand the evolution of the states, entities, parameters and attributes over time.

All three classes of verification techniques were used to verify the simulation model. These included the common-sense techniques like flowcharts, algorithms, reasonableness, and

analytical calculations through documentation and traces. After successfully verifying that the code is correct, the next step is to check whether the operational model is truly reflective of the real-world model that is being simulated. In other words, the model is built correctly, but it needs to be checked if it is the correct model.

5.3 Model Validation

The goal of validation is to end up with a model that mirrors the true system behavior close enough to be considered as a credible substitute for making real-life decisions by experimenting with the system, analyzing its behavior, and predicting system performance under specified conditions. Validation is achieved through the iterative calibration of the model that involves comparing the model with the real-world system repeatedly. In each iteration, the discrepancies between the two systems are utilized to gain insight and make necessary modifications or re-calibrations for bringing the behavior of the two systems close together. Eventually, the model accuracy will reach the desired level of acceptability or closeness to the real-world system being modelled. Realistically, no model can ever be truly and completely reflective of a real-world system under study, since the real-world is not very deterministic. Also, every iterative change in the calibration of the model increases the cost, time and effort. These factors need to be taken into account to decide what level of accuracy is needed and could be afforded.

The presented simulated system to be validated has no real user beyond the designer, implementer and the evaluator yet. In other words, a real-world counterpart for this system does not exist yet. However, if this model were mirroring a real-world CN and trip planning facility, then the manager of the system would require a credible model created within time and budget constraints to make decisions like building more CNs or installing more EVSEs. The validation procedure follows the following three steps: 1) Building the model with high face validity, 2) validating model assumptions and 3) comparing the model input output transformations with the corresponding input-output transformations of the real system. In the case of this thesis, the system being modelled is realistic yet an imaginary one designed to learn its behavior were it to be deployed in the real-world, and as expected no complete real-world inputs and outputs exist. The discussion of validation is done when applicable in the context of evaluation of the proposed simulated system with the first two steps including face validity and assumptions. The last step cannot be carried out, as no real-world system exists for collecting input and output data from observations.

The basic idea of face validity is that from inception the model should be designed to appear reasonable on its face to the user groups that are knowledgeable about the real system being simulated. The potential users like the designer, implementer, analyst and evaluator are involved in the construction of the model from its conceptualization to its implementation by having various discussions. The user inputs are successfully used to increase the expected degree of realism from the model through reasonable assumptions specified in the model requirements of Chapter 3. The critique from the user group aided in the calibration process, and their insights helped identify discrepancies in the initial version of the model. Since the first version is almost always never correct, the identified discrepancies are used to make corrections to the model. For example, considering the possibility of late and early arriving CAEVs and its effect on charging reservations and considering the possibility of accidents on the DWCN lanes. The involvement of the user group increases the model's perceived validity. In the real-world, this perceived validity is taken seriously, and allows the manager and other future potential user groups to willingly rely in the system for making actual real-life decisions. Besides involving user groups to check for face validity, sensitivity analysis can be used. For instance, a sensitivity analysis test was conducted to verify that increasing the arrival rate of CAEVs did increase the number of CAEVs in the system or in the queue, and expectantly also increased the server utilization of the CNs. The latter expectant observation of model behavior upon changing an input parameter like throughput is learnt from experience and observations of similar or same real-world systems. Since, the model developer and the evaluator alike have an idea about the direction the output results would take when a certain input parameter is changed. It is almost always too expensive and time consuming to vary all the possible input variables to conduct many sensitivity tests. If the real system output data were available for some input parameters, objective scientific sensitivity tests could have been conducted using statistical techniques like the error difference between the expected output value and the value outputted by the model.

Next, model assumptions were validated. First, structural assumptions involves inquiring how the system actually operates and making simplifications and abstractions of reality. In the case of this proposed model, most structural assumptions were discussed in Chapter 3. The main requirement was to implement the proposed three-layer CN hierarchy to enable different CN types to communicate seamlessly with one another for enabling IoT applications for ITS like the charging reservation and trip planning system. Another assumption was that the CAEVs are modelled realistically using real-world data like efficiency, range and battery consumption statistics, and the lithium-ion battery's wired and wireless charging are

modelled using the linear two stage battery model. These CAEVs are assumed to randomly arrive or originate within a location on the system map like a mall, office, house, etc., with a randomly generated demand for charging and AMoD trip that will be requested to the proposed and simulated system. In other words, it is assumed in the real-world the CAEV user's leaving a location like their home garages and parking lot of mall or office will request for their AMoD trip with charging. Other structural assumptions like having each EVSE with a queue of size 2 for CAEVs that are early for their charging reservations, WCPs having RFID, misalignment and speed sensors for enabling the misalignment and speed error correction of CAEVs, the two areas in the map are connected by DWCN lanes that are constructed using the DWCN recommendation tool, and each CN having a set number of EVSEs were all specified in Chapter 3. These structural assumptions are usually verified by comparing the model to the real-world system, but the absence of one left reliance on the designer's feedbacks, expectations and the proposed system design and architecture.

Second, data assumptions are based on collection of reliable data and correct statistical analysis of the data. Data collection for this system to be modelled cannot be done, as it does not exist in the real-world yet. The idea of this simulator is to simulate how this system would behave were it to be implemented in reality. Hence, the distributions of interarrival times of CAEVs is random and follows exponential probability distribution function. The service time of EVSE of the CN are realistically determined by the charging rate of the EVSE and the CAEV modelled, and the length of waiting lines under varying conditions of EVSEs at a CN is affected by the CAEV's late and early arrivals to the charging reservations that can be modelled by the exponential probability distribution function. Further accidents on roads are modelled following probability statistics of Ontario's road accident.

5.4 Simulated System Set up and Run

The proposed three-layer CN hierarchy along with the handshake protocol is simulated in python version 3.9 on a computer with 2.9 GHz Dual-Core Intel Core i5 Processor for proof of concept and evaluation of the charging reservation and trip planning system. For analysis and evaluation purposes, 500 total number of AEVs, N_{AEV}, are randomly generated and realistically modelled using the EV database in [264] with manufacturer range and battery charging efficiency values.

Each CAEV models an industry standard lithium-ion battery using the linear two-stage battery model that can be charged using both wired charging system and wireless magnetic resonance charging systems. These CAEVs have [20-50 km/h] variable moving speed and

initial battery capacity that is randomly generated to be in the range of 25% to 70 % of the original battery capacity, and are initialized on the symmetric map of Figure 4.10 at random locations. Their desired trip destinations are also randomly chosen locations on the map.

The original arrival times of CAEVs entering the system are randomly generated following an exponential probability distribution function. The CAEVs send a request for charging reservation in the range of 30 to 100% of battery capacity along with their intended destination trips. The CAEV travels the planned shortest route, and the battery consumption is computed using (4.1). The system also simulates late or early arrivals by adding a randomly generated time value from exponential probability distribution function with λ=3 to account for unpredictable traffic conditions like congestion, construction work and accidents along the route among others.

This simulator is designed to work independently but its results can be fed into other simulators like ACN-Sim [45]. The simulation setup is kept simple for proof of concept and to give a clear analysis of the proposed system and protocol. This simulator is capable of handling much larger loads of over 10,000 realistically modelled CAEVs that can be simulated to run over several days on a larger map for a large scale and detailed CN reservation and trip planning system analysis.

The simulator setup used can be seen in Table 5.1 where the simulator is run for two days with two CCNs, two SWCNs and two DWCN lanes of 20 km each. The CNs are placed on the symmetric interconnected map of Figure 4.10 that is automatically generated by the system, and Dijkstra's algorithm is used to calculate shortest routes on the map. The Ontario's road accident probability [270] is used to set accident probability, P_a, to 1/189.59 with the probability of a CAEV skipping the charging session, P_s, set to 1/2. The billing scheme is set to pay per charging session and the Ontario Energy Board's TOU pricing [263] is applied. The length of WCPs for SWCN are set to 10 m whereas the ones used for DWCN are set to 120 m. The fixed values for SWCN and CCN used mimic the commercially available and researched CNs parameters [45], [271]. Since DWCNs do not exist in the real-world for public use, our simulator builds a custom DWC infrastructure from given parameters for realistic testing, see Table 5.1, using the proposed DWCN design specification tool. Each time slot duration , $\mathrm{ts}_{dur}^{\mathrm{CN}}$, for CNs is kept to be 10 minutes long, and based on N_{days} = 2 days simulation run the number of time slots created per EVSE of a CN can be computed using (5.1) to generate N_{ts} = 288 time slots per EVSE.

$$N_{ts} = N_{days} * \frac{24\ hrs}{day} * \frac{60\ min}{hr} * \frac{1\ ts}{\mathrm{ts}_{dur}^{\mathrm{CN}}} \quad (5.1)$$

In the simulation, each of the randomly generated 500 CAEVs' OBU uses V2I to communicate with the nearby RSUs to request for a charging session along the shortest route to their destination. The requests are fulfilled by the charging infrastructure using V2I and V2G communication following the proposed handshake protocol as the CAEVs complete their trips. The recorded results for one simulation run can be seen in Table 5.2.

Table 5.1: Simulation parameters for the first system.

Simulation Parameters	
Simulation Start Date	2020-01-01
Simulation End Date	2020-01-02
Total Simulated Days	2
Total Simulated Time (minutes)	2880
Billing Scheme	Per Session
Per CP rate (CAD)	0.01
TOU Ontario Energy Board Electricity Rates Effective Date	2019-11-01
Off peak price (cents per kWh)	10.1
Mid-peak price (cents per kWh)	14.4
On-peak price (cents per kWh)	20.8
Total Number of CCNs	2
Total Number of SWCNs	2
Total Number of DWCNs	2
Per Reservation Time Slot (minutes)	10
Total Number of CAEVs	50
Total Number of Charging Reservations	50
EVSEs per CN	20
EVSE Minimum Rate (Ampere)	16
EVSE Maximum Rate (Ampere)	200
Queue Length for CCNs and SWCNs per EVSE (vehicles)	2
CCN Setup	
Per EVSE Voltage (Volts)	240
SWCN Setup	
Per EVSE Voltage (Volts)	240
Per EVSE WCPs	1
Length of WCP (meters)	10
DWCN Setup	
Per EVSE Voltage (Volts)	480
Length of Track (meters)	20,000.00
Per EVSE WCPs	8
Length of a WCP (meters)	120
Width of a WCP (meters)	2.0
Gap Between WCPs (meters)	0.5
Average Vehicle Speed (km/h)	79.92
Total Number of WCPs Installed	160
Length of Track with WCPs Installed (meters)	19,279.5

It can be seen that the average per vehicle battery capacity is 68.445 kWh with an average per vehicle efficiency of 0.175 kWh/km and an average per vehicle range of 363.11 km. The average waiting time for CAEVs that were either too early or late for a reservation at a SWCN is 8.28 minutes and for a CCN is 2.59 minutes. The average distance travelled for a trip is 0.713 km as can be seen in Figure 5.1. The average battery consumption per CAEV on a trip is calculated to be 0.125 kWh as can be seen in Figure 5.2, and the average per vehicle payment for a charging reservation is 2.642 CAD that is equivalent to approximately 264 CPs as can be seen in Figure 5.3. Figure 5.4 shows the SoC that was requested originally by a

CAEV, the SoC that was reserved and the SoC that was actually received by a vehicle. For each charging request made, the charging reservation reserved 99.41% of the original SoC requested. On average, 90.25% of the charging is delivered finally to a CAEV from its charging reservation. The 9.75% loss of charging promised can be accounted for by late CAEV arrivals, early CAEV departures, accidents, alignment and speed issues in WPT, CAEVs cancelling reservations and EVSE's inefficiency.

So, the average waiting times at static CNs are successfully minimized and the travel costs are kept at minimum for the vehicles to consume the lowest possible battery levels compared to manual and random searching for EVSEs by vehicles. Further, this simulator allows to build and test DWCNs realistically before real-world implementation, thus saving cost and time.

Table 5.2: Simulation results of the first system.

Simulation Results	
Total Number of Requested Trips with Charging Requests	500
Total Number of Completed Trips with Charging Reservations	500
Total Energy Supplied (kWh)	13109.72
Total Payment Collected (CPs)	132098.00
Total Payment Collected (CAD)	1321.08
Total Number of Paid Charging Reservations	500
Total Number of Unpaid Charging Reservations	0
Overall Per Vehicle Statistics	
Average per Vehicle Battery Capacity (kWh)	68.445
Average per Vehicle Battery Charge Acceptance Rate (kW)	11.4694
Average per Vehicle Battery Efficiency (kWh/km)	0.175
Average per Vehicle Range (km)	363.11
Average Waiting Time per Vehicle at SWCNs (minutes)	8.28
Total Number of Vehicles Waited at SWCNs	187
Average Waiting Time per Vehicle at CCNs (minutes)	2.59
Total Number of Vehicles Waited at CCNs	115
Average Travel Cost Per Vehicle (meters)	713.40
Average Battery Consumption per Vehicle Trip (kWh)	0.125
Average Per Vehicle Payment of a Charging Reservation (CAD)	2.642
Average Per Vehicle Requested SoC Fulfilled by each Reservation (%)	99.41
Average Per Vehicle Reserved SoC Delivered by each Reservation (%)	90.25
DWCN Statistics	
Total Number of Vehicles Serviced by DWCN-1	259
Total Energy Delivered by DWCN-1 (kWh)	5818.10
SWCN Statistics	
Total Number of Vehicles Serviced by SWCN-1	101
Total Number of Vehicles Serviced by SWCN-2	86
Total Charging Delivered by SWCN-1 (kWh)	2068.40
Total Charging Delivered by SWCN-2 (kWh)	1855.39
CCN Statistics	
Total Number of Vehicles Serviced by CCN-1	51
Total Number of Vehicles Serviced by CCN-2	64
Total Charging Delivered by CCN-1 (kWh)	1344.04
Total Charging Delivered by CCN-2 (kWh)	2023.79

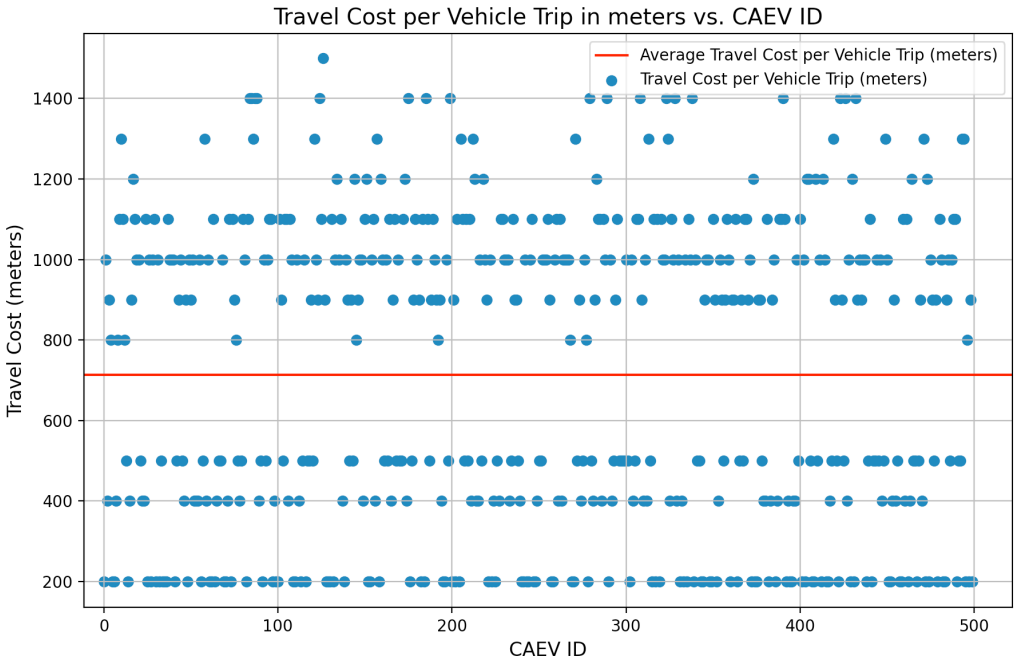

Figure 5.1: Travel Cost per Vehicle Trip in meters.

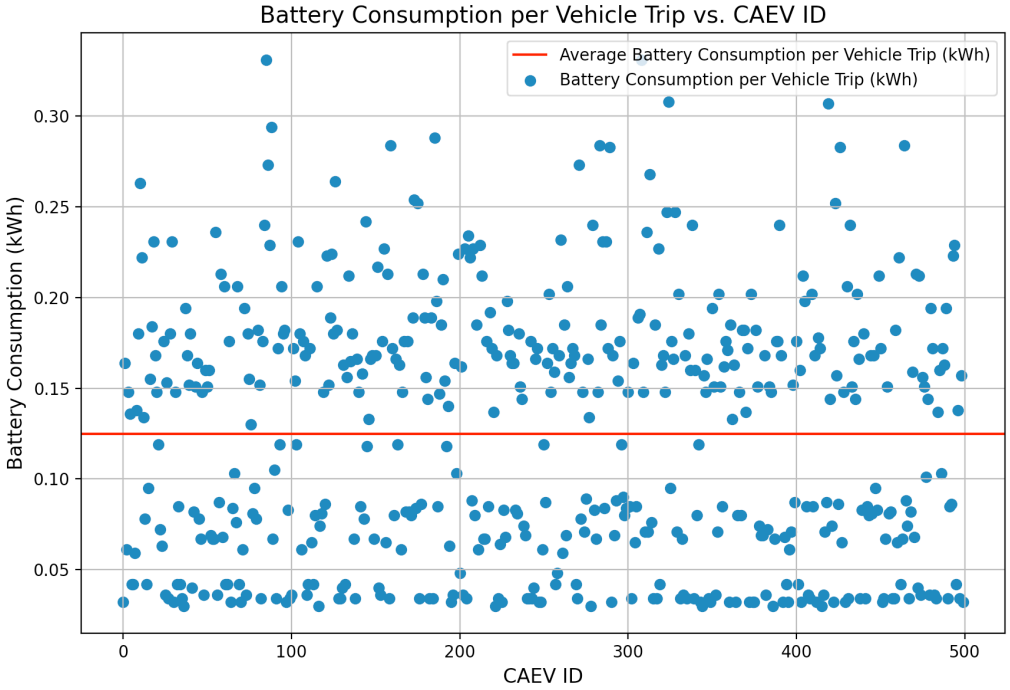

Figure 5.2: Battery Consumption in kWh per Vehicle Trip.

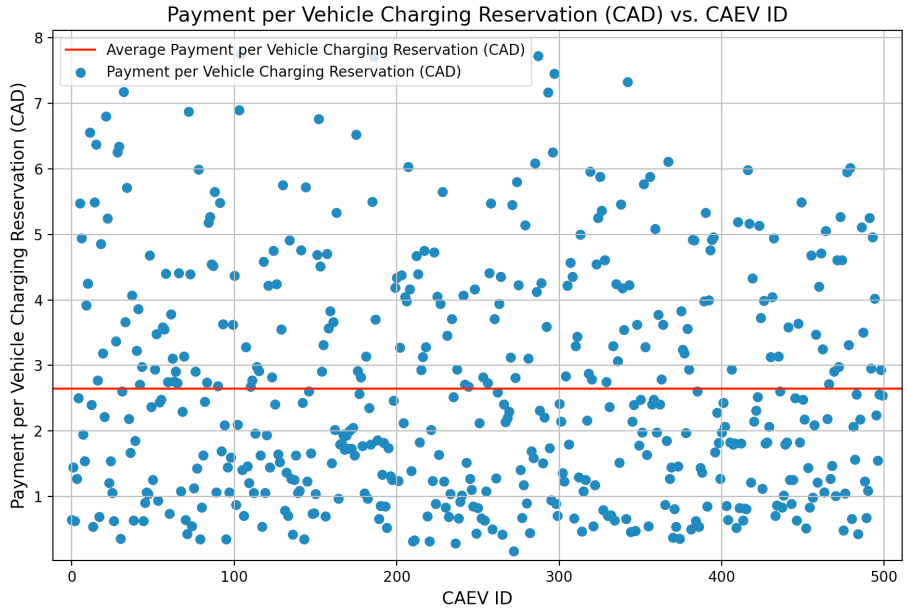

Figure 5.3: Payment per Vehicle Charging Reservation in CAD.

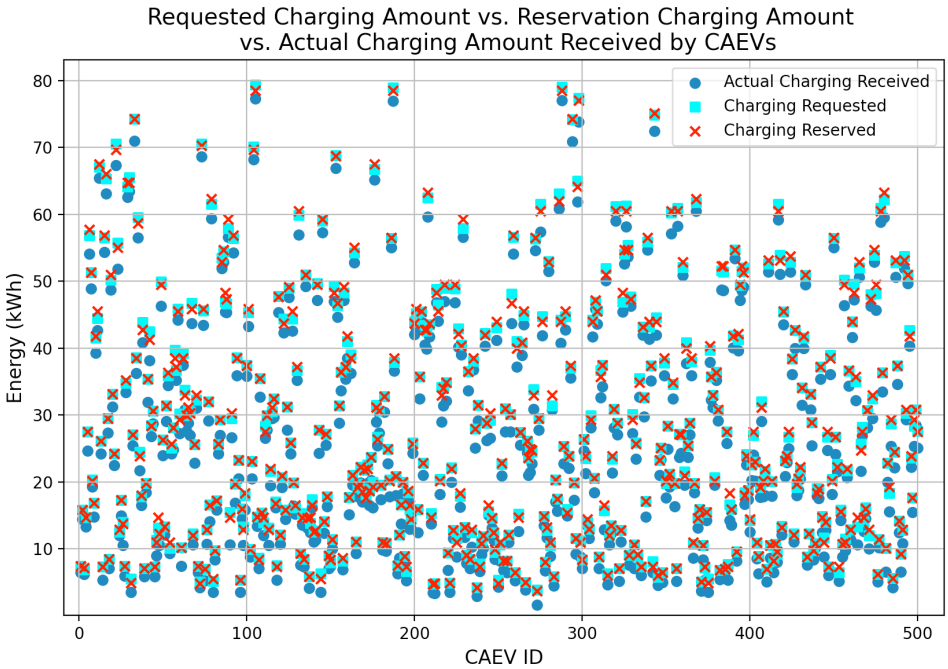

Figure 5.4: The charging requested, reserved and received per Vehicle.

5.5 System Evaluation Parameters

To help evaluate and verify the system set up, the performance estimation parameters that are computed are defined below:

a) Average Waiting Time per CAEV (T_Q): It is the average time the CAEV spends in the queue of a CN waiting for its service turn. The average waiting time is computed by dividing the total number of CAEVs serviced by the CN, N_D, divided by the total time, Q, that all CAEVs spent waiting in the queue of the CN as can be seen in (5.2).

$$T_Q = \frac{1}{N_D}\sum_{i=1}^{N_D} Q_i \tag{5.2}$$

b) Throughput (λ): It is also known as departure rate. It is used to measure how many CAEVs are processed by a system or CN in one time unit. It is usually defined as the ratio of the number of departures, N_D, divided by total simulation time T as can be seen in (5.3). The unit of throughput is CAEVs per time unit (CAEV/min). Since one CN has c multiple servers in parallel or EVSEs, the modified equation (5.4) is used.

$$\lambda = \frac{N_D}{T} \tag{5.3}$$

$$\lambda = \frac{N}{c * T} \tag{5.4}$$

c) Average Service Time per CAEV (T_s): It is computed by dividing the total server busy time B by the total number of departures N_D as can be seen in (5.5). Equation (5.6) reveals that B is equal to summing together all the service time, T_i, for the i^{th} CAEV that departed.

$$T_s = \frac{B}{N_D} \tag{5.5}$$

$$B = \sum_{i=1}^{N_D} T_i \tag{5.6}$$

d) Server Utilization (ρ): It is the proportion of simulation time during which the server or CN is busy. It is the product of its throughput and the average service time per CAEV, T_s. This can be mathematically expressed by (5.7).

$$\rho = \lambda T_s \tag{5.7}$$

e) Proportion Server Idle Time (β): It is proportion of the time during which the server is not processing any CAEVs, and it is basically 1 minus the server utilization as defined in (5.8).

$$\beta = 1 - \rho \tag{5.8}$$

f) Average System Waiting Time (w): It is also known as the response time or delay. It is the total time the CAEV spends in the system or CN that includes the waiting or queuing time and the service time. So, w can be computed using (5.9) where W_i is the time spent in the system by the i^{th} simulated CAEV and N_A is the number of arrivals.

$$w = \frac{1}{N_A}\sum_{i=1}^{N_A} W_i \tag{5.9}$$

In our system set up of Table 5.1 with one simulation run, the evaluation statistics for the CNs with reservations and the overall system are collected as can be seen in Table 5.3.

Table 5.3: Validation statistics for simulation run of first system.

Validation STATs	
CCN-1	
Total Number of Vehicles Serviced by CCN-1	51
Total WaitingTime for CCN-1	106
Average Waiting Time per CAEV for CCN-1	2.07843
Throughput for CCN-1	0.031835
Total service time for CCN-2	7339
Average service time per CAEV for CCN-1	143.90196
Total system waiting time for CCN-1	7445
Average system waiting time for CCN-1	145.98039
Computed Little's Law for CCN-1	4.64732
Calculated Little's Law for CCN-1	4.64732
Server Utilization for CCN-1	0.22906
Proportion Server Idle Time for CCN-1	0.77094
CCN-2	
Total Number of Vehicles Serviced by CCN-2	64
Total Waiting Time for CCN-2	191
Average Waiting Time per CAEV for CCN-2	2.98438
Throughput for CCN-2	0.037647
Total service time for CCN-2	11086
Average service time per CAEV for CCN-2	173.21875
Total system waiting time for CCN-2	11277
Average system waiting time for CCN-2	176.20312
Computed Little's Law for CCN-2	6.63353
Calculated Little's Law for CCN-2	6.63353
Server Utilization for CCN-2	0.32606
Proportion Server Idle Time for CCN-2	0.67394
SWCN-1	
Total Number of Vehicles Serviced by SWCN-1	101
Total Waiting Time for SWCN-1	948
Average Waiting Time per CAEV for SWCN-1	9.38614
Throughput for SWCN-1	0.065584
Total service time for SWCN-1	11352
Average service time per CAEV for SWCN-1	112.39604
Total system waiting time for SWCN-1	12300
Average system waiting time for SWCN-1	121.78218
Computed Little's Law for SWCN-1	7.98701
Calculated Little's Law for SWCN-1	7.98701
Server Utilization for SWCN-1	0.36857
Proportion Server Idle Time for SWCN-1	0.63143
SWCN-2	
Total Number of Vehicles Serviced by SWCN-2	86
Total Waiting Time for SWCN-2	600
Average Waiting Time per CAEV for SWCN-2	6.97674
Throughput for SWCN-2	0.0527607
Total service time for SWCN-2	9161
Average service time per CAEV for SWCN-2	106.52326
Total system waiting time for SWCN-2	9761
Average system waiting time for SWCN-2	113.5
Computed Little's Law for SWCN-2	5.98834
Calculated Little's Law for SWCN-2	5.98834
Server Utilization for SWCN-2	0.28101
Proportion Server Idle Time for SWCN-2	0.71899
DWCN-1	
Total Number of Vehicles Serviced by DWCN-1	260
Throughput for DWCN-1	0.18005
Total service time for DWCN-1	2340
Average service time per CAEV for DWCN-1	9.0
Total system waiting time for DWCN-1	2340
Average system waiting time for DWCN-1	9.0
Computed Little's Law for DWCN-1	1.6205
Calculated Little's Law for DWCN-1	1.6205
Server Utilization for DWCN-1	0.08102
Proportion Server Idle Time for DWCN-1	0.91898
Overall System STATs	
Total number of AEV arrivals	500
Total number of AEV departures	500
Throughput	0.29412
Total system waiting time	44247
Average system waiting time	88.494
Computed Little's Law	26.02765
Calculated Little's Law	26.02765

It can be seen in Table 5.3 clearly that the analytically calculated L matched the simulation computed L for all CNs and the overall system. Thus, verifying the simulation successfully. The throughput of CCNs compared to SWCNs is low, but it is expected as the number of CAEVs serviced by the CCNs is also low. The DWCN has the highest throughput, as it services the greatest number of CAEVs that is 260 out of the 500 in this case. The CCNs have the lowest waiting times compared to SWCNs, and this could be because the CAEVs arriving to the SWCNs were earlier than their reservation times and had to be queued with no earlier reservation timeslots available for a new reservation at the reserved EVSE. The proportion of time the CNs are busy processing the CAEVs is approximately between 0.2 and 0.4 for CCNs and SWCNs, and it is expected to be low because multiple servers or EVSEs in total 10 are working in parallel in each CN. Thus, distributing the total load of the CN and explaining their low overall proportion idle time. Further, the charging reservations are made in advance, and each EVSE of a CN is basically servicing the CAEVs based on the reserved time slots. The EVSE only has to do further processing to deal with any early arrival to evaluate for queuing or pushing the reservation to an earlier time for better accommodating the CAEV user and improving their overall experience. Finally, the average service time has to do with the reservations made and can be affected by CAEVs late arrivals that only get service from their time of arrival to their time of departure. The CAEV may even choose to abandon their reservation mid-way due to accidents or cancel their reservation all together. Thus, affecting the average service time per CAEV. However, in this case no accidents had occurred.

Now, basing an evaluation on a single run of the simulation is not enough to draw any meaningful conclusions. Hence, an output analysis is conducted for this simulation set up along with comparison with other alternative system set ups.

5.6 Output Analysis

The developed model is classified as a non-terminating simulation. The nature of the charging reservation and trip planning system is continuous where charging reservation scheduling and AMoD trip planning of CAEVs can be carried out for days. The simulation is run from time 0 to analyst specified simulation end time, T_E, with specified initial conditions. It's also known as a steady-state system, and its steady-state behavior needs to be studied for analyzing the output data independent of the initial conditions or bias. To do so, the chosen performance output evaluation parameters discussed earlier need to be estimated.

Output analysis involves examining the generated simulation data to predict the system performance, and compare with performance of other systems. The absolute performance of

the developed system is estimated. The output data is random in nature, since the input variables were themselves generated using random generators. Hence, statistical analysis of generated outputs is required when different random streams for the inputs will lead to different random outputs.

The initialization conditions of the developed model is an issue, as it can influence the output data causing bias. For example, this simulation model starting empty that is with no CAEVs to process, may service initial set of vehicles faster. The initial conditions will influence the waiting times of the first few components and the autocorrelation of the observations will carry the error to the rest of the data as well. The initial conditions need to be chosen intelligently else they can affect the long-run or steady-date performance measurements. The initial bias or output bias can be easily removed by allowing the implementer or analyst to either discard the collected statistics up to a certain simulation time or by setting intelligent initial conditions. The absence of a real-world system leads to the use of dividing the simulation run into two phases. The first phase from time 0 to T_0 is called the initialization phase, and the phase from T_0 to T_0+T_E is called the data collection phase. The identification of T_0 =228.71 minutes that is representative of steady-state behavior is done by adopting the Welch's method from Chapter 11 of [269]. The length of T_E for data collection phase is set as two days that is long enough to guarantee precise estimation of response variables in the long-run behavior of the system.

Additionally, the output variable under study let's say Y, is considered an independent random variable with unknown distribution. After running one replication, we get n observations for n number of CAEVs. But, the observations within a replication are considered autocorrelated, since the departure of a single CAEV can affect the submission of the next CAEV and its waiting time. So, the classical independent statistical methods cannot be directly applied for statistical analysis of the output data. Instead, the simulation is run for several replications to get data across replications that is independent and enables application of classical independent statistical methods indirectly. Let the performance of the simulated system measured be the parameter θ, and the set of simulation experimental results be the estimator $\hat{\theta}$. The precision of the error of the estimator $\hat{\theta}$ can then be measured by its standard error, by the width of the performance parameter θ or by finding its confidence or prediction interval widths. In other words, the goal of statistical analysis is to estimate these standard errors and CIs of the performance parameters to indicate the degree of confidence of 95% in the predicted output responses of the simulation.

We have chosen performance parameters for analysis that are defined in the earlier section for each CN and the overall system. The precision of the error of the estimator $\hat{\theta}$ can then be measured by its standard error or by the interval width of the performance parameter θ. There are two type of intervals: 1) Confidence intervals (CI) are known as the measure of error and 2) Prediction intervals (PI) are known as measure of risk. Both intervals assume that the output data produced by the simulation model can be represented well by a probability model. The APPENDIX B.2 details the method used for computing point estimators of output parameters and their CIs and PIs.

5.6.1 Absolute Performance and Relative Performance

The absolute performance of the developed system with 10 EVSEs per CN called S1, is estimated first, and later alternative systems with 20 EVSEs referred to as S2, and 5 EVSEs per CN referred to as S3, are analyzed and compared with S1. The remaining set up of the simulation systems S1, S2 and S3 is the same as Table 5.1. It should be noted that statistics for the CNs with reservations like the two CCNs, two SWCNs, and a DWCN are generated along with the overall system for analysis and evaluation.

A. Results

Data is collected for precise estimation of measures of performance for the current system with 10 EVSEs per CN, S1, and its alternative systems S2 and S3 with 20 EVSEs and 5 EVSEs per CN, respectively. Each system setup is first run 10 times and then 30 additional times to reduce the overall error and have better evaluation and estimation of parameters. The alternative systems, S2 and S3, cannot be compared truly with S1 by just looking at the performance estimators, as the response or output variables contain random variation. Common random numbers (CRNs) for conducting statistical analysis with correlated sampling technique is used to determine whether the observed differences are due to differences in design or merely the random fluctuation inherent in the simulation models being compared. This CRN technique reduces the variance of the estimated difference of the performance measures and provides a more precise estimation of the mean difference for a given sample size n compared to independent sampling technique. So, the point estimator data is collected for system designs S1, S2 and S3 for R=10 and R=40 replications for total simulation run time of 2 days using the CRN technique. Tables 5.4 to 5.9 show side by side absolute performance data collection of the three systems for CCN-1, CCN-2, SWCN-1, SWCN-2, DWCN-1 and the overall system respectively. The point estimation data with CIs is plotted for CCN-1, CCN-2, SWCN-1,

SWCN-2, DWCN-1 and the overall system in Figures 5.5 to 5.10, respectively, for visual comparison.

Now, the comparison of two system designs is deemed easier than comparison of multiple systems simultaneously. So, the S1 system is compared with the S2 system and then with the S3 system as can be seen in Table 5.10 to 5.12 for CCNs, SWCNs and DWCN and the overall system, respectively. The main goal of these simulation experiments was to obtain point and interval estimates of the difference in mean performance like $\theta_1 - \theta_2$, where θ_1 is the parameter for the first system and θ_2 is the same parameter for the second system to be compared with the first. The CRN technique helps compute the CI of $\theta_1 - \theta_2$, and drawn meaningful conclusions for comparisons between the two systems. The CIs do not answer questions of practical significance directly, like is the true difference between the two systems large enough to make a decision about which system design to implement, but the CI does bound the true difference with probability 1-$\alpha = 0.95$ in this case. Some average differences were 0 that emphasize no difference in performance with R=10. Hence, more replications that is R=40 were computed to see a visible difference in performance if any. Thus, this comparison can help decide for a real-world designer of the system whether to build the system with double or half the number of EVSEs per CN, and help evaluate the ramifications of going with one design choice over the other.

B. Discussion

First, system S1 is compared with S2 as can be seen by the comparative data $\theta_1 - \theta_2$ with CIs collected in Tables 5.10 to 5.12. The average number of CAEVs, L, in the CCN-1 are slightly more in S2 than in S1 with strong statistical evidence and of -0.00889 average difference as seen illustrated in Figure 5.5 (d), which is expected with S2 CNs having double the capacity of S1. The overall average number of CAEVs in the system S1 at any given time is less than in S2 as can be seen in Figure 5.10 (a) with the average difference of -0.09457 noted in Table 5.12. The average waiting time per CAEV in CCN-1, CCN-2, SWCN-2 and SWCN-1 is less for S2 than in S1 as can be seen in Figures 5.5 (a), 5.6 (a), 5.7 (a) and 5.8 (a) respectively, and this could be due to the reservations of CAEVs spread out to 20 EVSEs of the same CN. So, if a CAEV arrives early, then it has a higher chance of getting an earlier reservation from the reserved EVSE, thusreducing queuing time. The proportion server idle time of CNs in S1 is less than in S2 as can be seen in Figures 5.5 (f), 5.6 (f), 5.7 (f), 5.8 (f) and 5.9 (c), as S1 is busy processing 500 CAEVs with half the number of EVSEs per CN compared to S2. The throughput of SWCN-2 of S2 have slightly higher throughput of 0.05588 than

SWCN-2 of S1 with 0.05566 as can be seen in Table 5.7 with average difference of -0.00022 noted in Table 5.11, since it has more parallel EVSEs working to service larger number of CAEVs. The latter explanation also applies to all other CNs of S2. So, the investment into doubling the capacity of EVSEs per CN can be justified if the designer expects a large traffic of over 500 CAEVs utilizing the charging reservation and trip planning system. For charging request traffic of up to 500 CAEVs, S1 system with half the EVSEs is sufficient and also enables saving costs. Perhaps, the designer can add 10 more EVSEs per CN later on when more CAEVs begin using the service. It should be noted that output analysis of relative performance between S1 and S2 with only 40 replications was able to highlight the difference in performance, but generating results with more replications and additional computing resources would make the difference more pronounced to give stronger statistical evidence and narrower CIs.

Next, system S1 is compared with S3, and the data for relative performance computed can be seen in Tables 5.10 to 5.12. The average waiting time per CAEV for CNs of S3 is less than the respective comparative CNs of S1. The throughput of CNs belonging to S1 is higher than those of S3, and the server utilization of S1 CNs like CCN-1, see Figure 5.5 (e), is less than those of S3. The latter statistical evidence is supported by the fact that S1 has twice the EVSEs per CN than CNs of S3, and having double the capacity of servicing CAEVs also reduces the workload per CN to help reduce the server utilization and increase proportion server idle time per CN. The system waiting time of CCN-1 of S3 is 149.587 minutes that is more than that of S1 with 142.834 minutes, as can be seen in Figure 5.5 (c), but the system waiting time of CCN-2 of S3 is 136.810 minutes that is less than that of S1with 146.419 minutes, as can be seen in Figure 5.6 (c). The CCN-1 of S3 is expected to have a higher system waiting time, since it has fewer EVSEs to service CAEVs and early CAEV arrivals might have to be queued with no availability of earlier reservations. However, CCN-2 of S3 having lower system waiting time compared to S1 might seem contradictory, but CCN-2 of S3 with lower number of EVSEs might not be able to accommodate large number of reservations in the first place. Thus, CCN-2 of S3 with fewer overall charging reservations might have maintained lower system waiting times compared to CCN-2 of S1 with double the capacity. The average number of CAEVs in the system at any given time of S1 CNs is more than those of S3 CNs as expected with having higher number of EVSEs per CN as can be seen in Figures 5.5 (d), 5.6 (d), 5.7 (d), 5.8 (d) and 5.9 (b), and the same is true for the overall system with higher overall system throughput as can be seen in Figure 5.10 (b). So, for the system designer S3 is only a great choice if charging request traffic is much less than 500 CAEVs. Further, the S1 and S3

relative performance output analysis data with 40 replications was sufficient to show the difference in performance. Nevertheless, having more replications and computation resources would only lead to drawing of conclusions with stronger statistical evidence.

Overall, S2 with 5 EVSEs for smaller charging request traffic is similar to S1 in performance, but S1 with 10 EVSEs per CN is a good design compromise in terms of cost and performance. For introduction of the system to market, S1 can handle traffic of up to 500 CAEVs quite easily with high throughput and minimum waiting times per CN. The implementer of the design has the flexibility to add 10 more EVSEs per CN like S3 in the future to handle growing traffic of CAEVs with the increase in popularity of the system among the users.

Table 5.4: CCN-1 validation statistics of S1, S2 and S3 systems.

CCN-1 Avg. Waiting Time Per CAEV (min/CAEV)									
R	System	S1	S2	S3	R	System	S1	S2	S3
10	Average	3.54150	3.43739	5.17564	40	Average	2.69743	2.63701	4.36636
	S^2	1.44553	1.35563	6.48371		S^2	2.34172	2.29318	9.92220
	S	1.20230	1.16432	2.54631		S	1.53027	1.51432	3.14995
	H	0.85926	0.83211	1.81979		H	0.48875	0.48366	1.00606
	CI (95%)	[2.68224, 4.40075]	[2.60527, 4.26949]	[3.35586, 6.99543]		CI (95%)	[2.20867, 3.18618]	[2.15335, 3.12067]	[3.36030, 5.37242]
	Risk	2.84983	2.75979	6.03555		Risk	3.12954	3.09694	6.44195
	PI (95%)	[0.69167, 6.39132]	[0.67760, 6.19717]	[-0.85990, 11.21119]		PI (95%)	[-0.43211, 5.82696]	[-0.45993, 5.73395]	[-2.07559, 10.80830]
CCN-1 - Throughput (CAEVs per minute)									
R	System	S1	S2	S3	R	System	S1	S2	S3
10	Average	0.03619	0.03619	0.01703	40	Average	0.03533	0.03537	0.01857
	S^2	0.00001	0.00001	0.00002		S^2	0.00002	0.00002	0.00002
	S	0.00353	0.00353	0.00460		S	0.00479	0.00479	0.00485
	H	0.00252	0.00252	0.00329		H	0.00153	0.00153	0.00155
	CI (95%)	[0.033663, 0.038710]	[0.033663, 0.038710]	[0.013743, 0.020320]		CI (95%)	[0.033795, 0.036856]	[0.033846, 0.036903]	[0.017025, 0.020122]
	Risk	0.00837	0.00837	0.01091		Risk	0.00980	0.00979	0.00992
	PI (95%)	[0.027816, 0.044557]	[0.027817, 0.044560]	[0.0061252, 0.027938]		PI (95%)	[0.025526, 0.045126]	0.025589, 0.045161]	[0.0086567, 0.028490]
CCN-1 - System waiting time (W) (Minutes per AEV)									
R	System	S1	S2	S3	R	System	S1	S2	S3
10	Average	143.50759	143.84069	152.69305	40	Average	142.83431	142.89253	149.58730
	S^2	110.35848	108.09447	232.69959		S^2	124.00628	124.44226	272.91375
	S	10.50516	10.39685	15.25449		S	11.13581	11.15537	16.52010
	H	7.50778	7.43037	10.90200		H	3.55667	3.56291	5.27636
	CI (95%)	[135.99981, 151.01537]	[136.41032, 151.27106]	[141.79105, 163.59505]		CI (95%)	[139.27764, 146.39097]	[139.32961, 146.45544]	[144.31095, 154.86366]
	Risk	24.90047	24.64373	36.15785		Risk	22.77378	22.81378	33.78516
	PI (95%)	[118.60712, 168.40806]	[119.19696, 168.48442]	[116.53520, 188.85090]		PI (95%)	[120.06052, 165.60809]	[120.07874, 165.70630]	[115.80213, 183.37246]
CCN-1 - L (AEVs)									
R	System	S1	S2	S3	R	System	S1	S2	S3
10	Average	5.18218	5.19552	2.59786	40	Average	5.04930	5.05819	2.77349
	S^2	0.27997	0.29216	0.55582		S^2	0.67898	0.67803	0.60493
	S	0.52913	0.54051	0.74553		S	0.82400	0.82342	0.77778
	H	0.37815	0.38629	0.53281		H	0.26318	0.26299	0.24841
	CI (95%)	[4.80403, 5.56033]	[4.80922, 5.58181]	[2.06505, 3.13068]		CI (95%)	[4.78612, 5.31248]	[4.79520, 5.32119]	[2.52507, 3.02190]
	Risk	1.25419	1.28119	1.76714		Risk	1.68517	1.68398	1.59062
	PI (95%)	[3.92799, 6.43637]	[3.91433, 6.47670]	[0.83072, 4.36501]		PI (95%)	[3.36413, 6.73447]	[3.37421, 6.74217]	[1.18286, 4.36411]
CCN-1 - Server Utilization									
R	System	S1	S2	S3	R	System	S1	S2	S3
10	Average	0.50538	0.25355	0.50087	40	Average	0.49536	0.24824	0.53699
	S^2	0.00258	0.00068	0.01959		S^2	0.00650	0.00164	0.02101
	S	0.05077	0.02615	0.13997		S	0.08065	0.04046	0.14496
	H	0.03628	0.01869	0.10003		H	0.02576	0.01292	0.04630
	CI (95%)	[0.46910, 0.54166]	[0.23486, 0.27224]	[0.40084, 0.60091]		CI (95%)	[0.46960, 0.52112]	[0.23532, 0.26116]	[0.49069, 0.58329]
	Risk	0.12033	0.06198	0.33177		Risk	0.16494	0.08274	0.29646
	PI (95%)	[0.38505, 0.62571]	[0.19157, 0.31553]	[0.16911, 0.83264]		PI (95%)	[0.33043, 0.66030]	[0.16550, 0.33098]	[0.24053, 0.83346]
CCN-1 - Proportion Server Idle Time									
R	System	S1	S2	S3	R	System	S1	S2	S3
10	Average	0.49462	0.74645	0.49913	40	Average	0.50464	0.75176	0.46301
	S^2	0.00258	0.00068	0.01959		S^2	0.00650	0.00164	0.02101
	S	0.05077	0.02615	0.13997		S	0.08065	0.04046	0.14496
	H	0.03628	0.01869	0.10003		H	0.02576	0.01292	0.04630
	CI (95%)	[0.45834, 0.53090]	[0.72776, 0.76514]	[0.39909, 0.599158]		CI (95%)	[0.47888, 0.53040]	[0.73884, 0.76468]	[0.41671, 0.50931]
	Risk	0.12033	0.06198	0.33177		Risk	0.16494	0.08274	0.29646
	PI (95%)	[0.37430, 0.61495]	[0.68447, 0.80843]	[0.167358, 0.83089]		PI (95%)	[0.33970, 0.66957]	[0.66902, 0.83450]	[0.16654, 0.75947]

Table 5.5: CCN-2 validation statistics of S1, S2 and S3 systems.

CCN-2 - Avg. WaitingTime per AEV (minutes/AEV)									
R	System	S1	S2	S3	R	System	S1	S2	S3
10	Average	3.55414	3.46667	3.71643	40	Average	2.89417	2.72246	3.42037
	S^2	1.51604	1.52330	1.12019		S^2	2.28036	2.47934	4.86783
	S	1.23127	1.23422	1.05839		S	1.51008	1.57459	2.20631
	H	0.87996	0.88206	0.75640		H	0.48231	0.50291	0.70467
	CI (95%)	[2.67418, 4.43410]	[2.58460, 4.34873]	[2.96003, 4.47283]		CI (95%)	[2.41186, 3.37647]	[2.21955, 3.22537]	[2.71569, 4.12504]
	Risk	2.91850	2.92548	2.50871		Risk	3.08827	3.22019	4.51212
	PI (95%)	[0.63564, 6.47264]	[0.54119, 6.39215]	[1.20772, 6.22514]		PI (95%)	[-0.19410, 5.98243]	[-0.49773, 5.94265]	[-1.09175, 7.93249]
CCN-2 - Throughput (AEVs per minute)									
R	System	S1	S2	S3	R	System	S1	S2	S3
10	Average	0.03430	0.03430	0.01739	40	Average	0.03572	0.03579	0.01826
	S^2	0.00001	0.00001	0.00003		S^2	0.00002	0.00002	0.00003
	S	0.00319	0.00319	0.00509		S	0.00443	0.00442	0.00502
	H	0.00228	0.00228	0.00364		H	0.00141	0.00141	0.00160
	CI (95%)	[0.03202, 0.036582]	[0.032022, 0.036582]	[0.013756, 0.021028]		CI (95%)	[0.0343036, 0.037131]	[0.034381, 0.037207]	[0.016655, 0.019865]
	Risk	0.00756	0.00756	0.01206		Risk	0.00905	0.00905	0.01027
	PI (95%)	[0.026739, 0.041864]	[0.026739, 0.041864]	[0.0053334, 0.0294510]		PI (95%)	[0.026665, 0.044769]	[0.0267458, 0.044843]	[0.00798596, 0.028534]
CCN-2 - System waiting time (W) (Minutes per AEV)									
R	System	S1	S2	S3	R	System	S1	S2	S3
10	Average	145.26921	145.26921	135.46056	40	Average	146.41922	146.68311	136.81044
	S^2	233.75160	233.75160	276.99875		S^2	196.34545	196.34779	264.65869
	S	15.28894	15.28894	16.64328		S	14.01233	14.01242	16.26833
	H	10.92662	10.92662	11.89453		H	4.47540	4.47543	5.19594
	CI (95%)	[134.34260, 156.19583]	[134.34260, 156.19583]	[123.56603, 147.35510]		CI (95%)	[141.94382, 150.89462]	[142.20769, 151.15854]	[131.61450, 142.00638]
	Risk	36.23949	36.23949	39.44970		Risk	28.65654	28.65671	33.27027
	PI (95%)	[109.02972, 181.50870]	[109.02972, 181.50870]	[96.010863, 174.91026]		PI (95%)	[117.76269, 175.07576]	[118.02640, 175.33982]	[103.54016, 170.08071]
CCN-2 - L (AEVs)									
R	System	S1	S2	S3	R	System	S1	S2	S3
10	Average	4.98011	4.98011	2.32062	40	Average	5.22243	5.24326	2.51385
	S^2	0.43981	0.43981	0.30552		S^2	0.59970	0.60147	0.63680
	S	0.66318	0.66318	0.55274		S	0.77440	0.77554	0.79800
	H	0.47396	0.47396	0.39503		H	0.24734	0.24770	0.25487
	CI (95%)	[4.50615, 5.45407]	[4.50615, 5.45407]	[1.92560, 2.71565]		CI (95%)	[4.97509, 5.46976]	[4.99556, 5.49096]	[2.25899, 2.76872]
	Risk	1.57195	1.57195	1.31016		Risk	1.58372	1.58606	1.63198
	PI (95%)	[3.40816, 6.55205]	[3.40816, 6.55205]	[1.01046, 3.63079]		PI (95%)	[3.63871, 6.80615]	[3.65721, 6.82932]	[0.8819, 4.14583]
CCN-2 - Server Utilization									
R	System	S1	S2	S3	R	System	S1	S2	S3
10	Average	0.48594	0.24312	0.45182	40	Average	0.51174	0.25723	0.48939
	S^2	0.00433	0.00109	0.01212		S^2	0.00564	0.00144	0.02290
	S	0.06581	0.03306	0.11008		S	0.07513	0.03793	0.15132
	H	0.04703	0.02362	0.07867		H	0.02400	0.01212	0.04833
	CI (95%)	[0.43890, 0.53297]	[0.21949, 0.26674]	[0.37315, 0.53049]		CI (95%)	[0.48774, 0.53574]	[0.24512, 0.26935]	[0.44106, 0.53772]
	Risk	0.15599	0.07835	0.26093		Risk	0.15365	0.07758	0.30947
	PI (95%)	[0.32994, 0.64193]	[0.164764, 0.32147]	[0.19089, 0.71275]		PI (95%)	[0.35809, 0.66539]	0.17965, 0.33481]	[0.17992, 0.79886]
CCN-2 - Proportion Server Idle Time									
R	System	S1	S2	S3	R	System	S1	S2	S3
10	Average	0.51407	0.75688	0.54818	40	Average	0.48826	0.74277	0.51061
	S^2	0.00433	0.00109	0.01212		S^2	0.00564	0.00144	0.02290
	S	0.06581	0.03306	0.11008		S	0.07513	0.03793	0.15132
	H	0.04703	0.02362	0.07867		H	0.02400	0.01212	0.04833
	CI (95%)	[0.46703, 0.56110]	[0.73326, 0.78051]	[0.46951, 0.62685]		CI (95%)	[0.46426, 0.51226]	[0.73065, 0.75488]	[0.46228, 0.55894]
	Risk	0.15599	0.07835	0.26093		Risk	0.15365	0.07758	0.30947
	PI (95%)	[0.358075, 0.67006]	[0.67853, 0.83524]	[0.28725, 0.80911]		PI (95%)	[0.33461, 0.64191]	[0.66519, 0.82035]	[0.20114, 0.82008]

Table 5.6: SWCN-1 validation statistics for S1, S2 and S3 systems.

SWCN-1 - Avg. Waiting Time per AEV (minutes/AEV)									
R	System	S1	S2	S3	R	System	S1	S2	S3
10	Average	9.79836	9.59217	12.03213	40	Average	8.71650	8.49172	10.09783
	S^2	6.86561	6.51399	5.44286		S^2	10.76633	9.83156	13.94191
	S	2.62023	2.55225	2.33299		S	3.28121	3.13553	3.73389
	H	1.87261	1.82403	1.66733		H	1.04799	1.00146	1.19257
	CI (95%)	[7.92575, 11.67097]	[7.76814, 11.41620]	[10.36479, 13.69946]		CI (95%)	[7.66851, 9.76450]	[7.49026, 9.49317]	[8.90527, 11.29040]
	Risk	6.21076	6.04962	5.52991		Risk	6.71038	6.41246	7.63615
	PI (95%)	[3.58760, 16.00911]	[3.54255, 15.64179]	[6.50221, 17.56204]		PI (95%)	[2.006125, 15.42689]	[2.07926, 14.90417]	[2.46168, 17.73398]
SWCN-1 - Throughput (AEVs per minute)									
R	System	S1	S2	S3	R	System	S1	S2	S3
10	Average	0.05547	0.05553	0.02662	40	Average	0.05408	0.05429	0.02720
	S^2	0.00003	0.00003	0.00004		S^2	0.00003	0.00003	0.00003
	S	0.00557	0.00569	0.00627		S	0.00576	0.00588	0.00554
	H	0.00398	0.00406	0.00448		H	0.00184	0.00188	0.00177
	CI (95%)	[0.051487, 0.059445]	[0.051463, 0.059591]	[0.022133, 0.031098]		CI (95%)	[0.052237, 0.055918]	[0.052410, 0.056164]	[0.025432, 0.028971]
	Risk	0.01320	0.01348	0.01487		Risk	0.01178	0.01202	0.01133
	PI (95%)	[0.042269, 0.068662]	[0.042048, 0.069006]	[0.011748, 0.041483]		PI (95%)	[0.042293, 0.065861]	[0.042272, 0.066302]	[0.015870, 0.038533]
SWCN-1 - System waiting time (W) (Minutes per AEV)									
R	System	S1	S2	S3	R	System	S1	S2	S3
10	Average	122.04802	121.07713	127.08606	40	Average	120.33642	120.25099	117.97849
	S^2	120.77749	117.83210	314.89335		S^2	102.73793	107.37296	331.13770
	S	10.98988	10.85505	17.74523		S	10.13597	10.36209	18.19719
	H	7.85419	7.75783	12.68207		H	3.23733	3.30955	5.81200
	CI (95%)	[114.19383, 129.90221]	[113.31930, 128.83496]	[114.40398, 139.76813]		CI (95%)	[117.09909, 123.57375]	[116.94144, 123.56054]	[112.16648, 123.79049]
	Risk	26.04940	25.72981	42.06167		Risk	20.72902	21.19145	37.21497
	PI (95%)	[95.99861, 148.09742]	[95.34732, 146.80694]	[85.02439, 169.14773]		PI (95%)	[99.60741, 141.06544]	[99.05954, 141.44245]	[80.76352, 155.19345]
SWCN-1 - L (AEVs)									
R	System	S1	S2	S3	R	System	S1	S2	S3
10	Average	6.79963	6.74252	3.39828	40	Average	6.51570	6.53826	3.23103
	S^2	1.19299	1.01102	0.97997		S^2	0.89294	0.96123	0.81517
	S	1.09224	1.00550	0.98994		S	0.94496	0.98043	0.90287
	H	0.78060	0.71860	0.70748		H	0.30181	0.31314	0.28837
	CI (95%)	[6.01904, 7.58023]	[6.02392, 7.46113]	[2.69080, 4.10577]		CI (95%)	[6.21389, 6.81751]	[6.22512, 6.85139]	[2.94266, 3.51939]
	Risk	2.58895	2.38334	2.34645		Risk	1.93253	2.00506	1.84645
	PI (95%)	[4.2107, 9.38858]	[4.35919, 9.12586]	[1.05183, 5.74474]		PI (95%)	[4.58317, 8.44823]	[4.53319, 8.54332]	[1.38458, 5.07747]
SWCN-1 - Server Utilization									
R	System	S1	S2	S3	R	System	S1	S2	S3
10	Average	0.62573	0.31059	0.61493	40	Average	0.60421	0.30381	0.58969
	S^2	0.01179	0.00260	0.03405		S^2	0.00775	0.00216	0.02644
	S	0.10860	0.05104	0.18454		S	0.08802	0.04647	0.16262
	H	0.07761	0.03648	0.13188		H	0.02811	0.01484	0.05194
	CI (95%)	[0.54811, 0.70334]	[0.27411, 0.34706]	[0.48305, 0.74682]		CI (95%)	[0.57609, 0.63232]	[0.28897, 0.31865]	[0.53776, 0.64163]
	Risk	0.25742	0.12098	0.43741		Risk	0.18000	0.09504	0.33257
	PI (95%)	[0.36831, 0.88315]	[0.18961, 0.43156]	[0.17752, 1.05234]		PI (95%)	[0.42420, 0.78421]	[0.20878, 0.39885]	[0.25713, 0.92226]
SWCN-1 - Proportion Server Idle Time									
R	System	S1	S2	S3	R	System	S1	S2	S3
10	Average	0.37427	0.68941	0.38507	40	Average	0.39579	0.69619	0.41031
	S^2	0.01179	0.00260	0.03405		S^2	0.00775	0.00216	0.02644
	S	0.10860	0.05104	0.18454		S	0.08802	0.04647	0.16262
	H	0.07761	0.03648	0.13188		H	0.02811	0.01484	0.05194
	CI (95%)	[0.29666, 0.45186]	[0.65294, 0.72589]	[0.25318, 0.51695]		CI (95%)	[0.36768, 0.42390]	[0.68135, 0.71103]	[0.35837, 0.46224]
	Risk	0.25742	0.12098	0.43741		Risk	0.18000	0.09504	0.33257
	PI (95%)	[0.11685, 0.63169]	[0.56844, 0.81039]	[-0.052345, 0.82248]		PI (95%)	[0.21579, 0.57580]	[0.60115, 0.79123]	[0.077740, 0.74287]

Table 5.7: SWCN-2 validation statistics of S1, S2 and S3 systems.

SWCN-2 - Avg. Waiting Time per AEV (minutes/AEV)									
R	System	S1	S2	S3	R	System	S1	S2	S3
10	Average	10.78923	10.46810	11.62591	40	Average	9.12121	8.65890	10.73038
	S^2	6.82622	6.19042	5.73312		S^2	10.47810	10.19491	16.85941
	S	2.61270	2.48806	2.39439		S	3.23699	3.19295	4.10602
	H	1.86723	1.77815	1.71121		H	1.03386	1.01980	1.31142
	CI (95%)	[8.92110, 12.65646]	[8.68995, 12.24625]	[9.91470, 13.33712]		CI (95%)	[8.08730, 10.15507]	[7.63911, 9.67861]	[9.41896, 12.04180]
	Risk	6.19291	5.89746	5.67545		Risk	6.61995	6.52988	8.39720
	PI (95%)	[4.59632, 16.98214]	[4.57064, 16.36556]	[5.95046, 17.30135]		PI (95%)	[2.50126, 15.74116]	[2.12903, 15.18878]	[2.33318, 19.12758]
SWCN-2 - Throughput (AEVs per minute)									
R	System	S1	S2	S3	R	System	S1	S2	S3
10	Average	0.05351	0.05351	0.02490	40	Average	0.05566	0.05588	0.02782
	S^2	0.00003	0.00003	0.00006		S^2	0.00005	0.00005	0.00005
	S	0.00577	0.00577	0.00801		S	0.00715	0.00704	0.00727
	H	0.00412	0.00412	0.00573		H	0.00228	0.00225	0.00232
	CI (95%)	[0.049384, 0.0576334]	[0.049384, 0.057633]	[0.019172, 0.030628]		CI	[0.053378, 0.057946]	[0.053629, 0.058127]	[0.025495, 0.030141]
	Risk	0.01368	0.01368	0.01900		Risk	0.01463	0.01440	0.01487
	PI (95%)	[0.039830, 0.067187]	[0.039830, 0.067187]	[0.0059028, 0.043897]		PI (95%)	[0.041035, 0.070289]	[0.041479, 0.070277]	[0.012944, 0.042693]
SWCN-2 - System waiting time (W) (Minutes per AEV)									
R	System	S1	S2	S3	R	System	S1	S2	S3
10	Average	122.67448	122.85217	118.31722	40	Average	122.63046	122.91244	121.52139
	S^2	52.83814	55.43675	275.25088		S^2	81.29734	78.79288	181.40053
	S	7.26899	7.44559	16.59069		S	9.01650	8.87654	13.46850
	H	5.19496	5.32117	11.85694		H	2.87978	2.83508	4.30171
	CI (95%)	[117.47952, 127.86944]	[117.53010, 128.17334]	[106.46028, 130.17417]		CI (95%)	[119.75068, 125.51024]	[120.07736, 125.74751]	[117.21969, 125.82301]
	Risk	17.22973	17.64833	39.32504		Risk	18.43960	18.15335	27.54435
	PI (95%)	[105.44475, 139.90421]	[105.20384, 140.50051]	[78.99219, 157.64226]		PI (95%)	[104.19086, 141.0706]	[104.75909, 141.06579]	[93.97704, 149.06575]
SWCN-2 - L (AEVs)									
R	System	S1	S2	S3	R	System	S1	S2	S3
10	Average	6.56246	6.57206	2.88274	40	Average	6.80397	6.85082	3.34251
	S^2	0.61980	0.63015	0.54372		S^2	0.72043	0.75765	0.66244
	S	0.78727	0.79382	0.73737		S	0.84878	0.87043	0.81390
	H	0.56265	0.56732	0.52698		H	0.27109	0.27801	0.25995
	CI (95%)	[5.99981, 7.12510]	[6.00474, 7.13939]	[2.35576, 3.40972]		CI (95%)	[6.53288, 7.07507]	[6.57281, 7.12882]	[3.08256, 3.60247]
	Risk	1.86608	1.88160	1.74780		Risk	1.73584	1.78012	1.66451
	PI (95%)	[4.69638, 8.42854]	[4.69047, 8.45366]	[1.13494, 4.63054]		PI (95%)	[5.06813, 8.53981]	[5.07070, 8.63093]	[1.67800, 5.00703]
SWCN-2 - Server Utilization									
R	System	S1	S2	S3	R	System	S1	S2	S3
10	Average	0.59846	0.30069	0.51965	40	Average	0.63019	0.31875	0.60723
	S^2	0.00476	0.00132	0.01743		S^2	0.00652	0.00185	0.01860
	S	0.06900	0.03633	0.13203		S	0.08073	0.04298	0.13638
	H	0.04932	0.02596	0.09436		H	0.02579	0.01373	0.04356
	CI (95%)	[0.54915, 0.64778]	[0.27472, 0.32665]	[0.42529, 0.61400]		CI (95%)	[0.60440, 0.65597]	[0.30503, 0.33248]	[0.56367, 0.65079]
	Risk	0.16356	0.08611	0.31295		Risk	0.16511	0.08790	0.27892
	PI (95%)	[0.43490, 0.76203]	[0.21458, 0.38680]	[0.20670, 0.83260]		PI (95%)	[0.46508, 0.79530]	0.23086, 0.40665]	[0.32831, 0.88615]
SWCN-2 - Proportion Server Idle Time									
R	System	S1	S2	S3	R	System	S1	S2	S3
10	Average	0.40154	0.69931	0.48036	40	Average	0.36981	0.68125	0.39277
	S^2	0.00476	0.00132	0.01743		S^2	0.00652	0.00185	0.01860
	S	0.06900	0.03633	0.13203		S	0.08073	0.04298	0.13638
	H	0.04932	0.02596	0.09436		H	0.02579	0.01373	0.04356
	CI (95%)	[0.35222, 0.45085]	[0.67335, 0.72528]	[0.38600, 0.57471]		CI (95%)	[0.34403, 0.39560]	[0.66752, 0.69497]	[0.34921, 0.43633]
	Risk	0.16356	0.08611	0.31295		Risk	0.16511	0.08790	0.27892
	PI (95%)	[0.23797, 0.56510]	[0.61320, 0.78543]	[0.167407, 0.79330]		PI (95%)	[0.20470, 0.53492]	[0.59335, 0.76914]	[0.11385, 0.67169]

Table 5.8: DWCN-1 validation statistics of S1, S2 and S3 systems.

DWCN-1 - Throughput (AEVs per minute)									
R	System	S1	S2	S3	R	System	S1	S2	S3
10	Average	0.18542	0.18542	0.08627	40	Average	0.17893	0.17939	0.08928
	S^2	0.00005	0.00005	0.00037		S^2	0.00025	0.00024	0.00029
	S	0.00672	0.00672	0.01914		S	0.01566	0.01554	0.01694
	H	0.00480	0.00480	0.01368		H	0.00500	0.00496	0.00541
	CI (95%)	[0.18061, 0.19022]	[0.18061, 0.19022]	[0.072589, 0.099946]		CI (95%)	[0.17393, 0.18394]	[0.17443, 0.18435]	[0.08387, 0.094690]
	Risk	0.01593	0.01593	0.04537		Risk	0.03203	0.03177	0.03465
	PI (95%)	[0.16949, 0.20135]	[0.16949, 0.20135]	[0.040901, 0.13163]		PI (95%)	[0.14690, 0.21096]	[0.14761, 0.21116]	[0.054627, 0.12393]
DWCN-1 - System waiting time (W) (Minutes per AEV)									
R	System	S1	S2	S3	R	System	S1	S2	S3
10	Average	9.00000	9.00000	9.00000	40	Average	9.00000	9.00000	9.00000
	S^2	0.00000	0.00000	0.00000		S^2	0.00000	0.00000	0.00000
	S	0.00000	0.00000	0.00000		S	0.00000	0.00000	0.00000
	H	0.00000	0.00000	0.00000		H	0.00000	0.00000	0.00000
	CI (95%)	[9.0, 9.0]	[9.0, 9.0]	[9.0, 9.0]		CI (95%)	[9.0, 9.0]	[9.0, 9.0]	[9.0, 9.0]
	Risk	0.00000	0.00000	0.00000		Risk	0.00000	0.00000	0.00000
	PI (95%)	[9.0, 9.0]	[9.0, 9.0]	[9.0, 9.0]		PI (95%)	[9.0, 9.0]	[9.0, 9.0]	[9.0, 9.0]
DWCN-1 - L (AEVs)									
R	System	S1	S2	S3	R	System	S1	S2	S3
10	Average	1.66875	1.66875	0.77641	40	Average	1.61040	1.61449	0.80351
	S^2	0.00366	0.00366	0.02967		S^2	0.01987	0.01955	0.02325
	S	0.06049	0.06049	0.17226		S	0.14096	0.13982	0.15249
	H	0.04323	0.04323	0.12311		H	0.04502	0.04466	0.04870
	CI (95%)	[1.62551, 1.71197]	[1.62552, 1.71197]	[0.65330, 0.89952]		CI (95%)	[1.56537, 1.65542]	[1.56983, 1.65914]	[0.75480, 0.85221]
	Risk	0.14337	0.14337	0.40830		Risk	0.28828	0.28595	0.31186
	PI (95%)	[1.52538, 1.81212]	[1.52538, 1.81212]	[0.36811, 1.18471]		PI (95%)	[1.32211, 1.89869]	[1.32853, 1.900434]	[0.49164, 1.11537]
DWCN-1 - Server Utilization									
R	System	S1	S2	S3	R	System	S1	S2	S3
10	Average	0.16687	0.08344	0.15528	40	Average	0.16104	0.08072	0.16070
	S^2	0.00004	0.00001	0.00119		S^2	0.00020	0.00005	0.00093
	S	0.00605	0.00302	0.03445		S	0.01410	0.00699	0.03050
	H	0.00432	0.00216	0.02462		H	0.00450	0.00223	0.00974
	CI (95%)	[0.16256, 0.17120]	[0.081275, 0.085599]	[0.13066, 0.17990]		CI (95%)	[0.15654, 0.16554]	[0.078492, 0.082958]	[0.15096, 0.17044]
	Risk	0.01433	0.00717	0.08166		Risk	0.02883	0.01430	0.06237
	PI (95%)	[0.15254, 0.18121]	[0.076268, 0.090607]	[0.073623, 0.23694]		PI (95%)	0.13221, 0.18987]	[0.066426, 0.095023]	[0.098328, 0.22307]
DWCN-1 - Proportion Server Idle Time									
R	System	S1	S2	S3	R	System	S1	S2	S3
10	Average	0.83313	0.91656	0.84472	40	Average	0.83896	0.91928	0.83930
	S^2	0.00004	0.00001	0.00119		S^2	0.00020	0.00005	0.00093
	S	0.00605	0.00302	0.03445		S	0.01410	0.00699	0.03050
	H	0.00432	0.00216	0.02462		H	0.00450	0.00223	0.00974
	CI (95%)	[0.82881, 0.83745]	[0.91441, 0.91872]	[0.82010, 0.86934]		CI (95%)	[0.83446, 0.84346]	[0.91704, 0.92151]	[0.82956, 0.84904]
	Risk	0.01433	0.00717	0.08166		Risk	0.02883	0.01430	0.06237
	PI (95%)	[0.81879, 0.84746]	[0.90939, 0.92373]	[0.76306, 0.92638]		PI (95%)	[0.81013, 0.86779]	[0.90498, 0.93358]	[0.77693, 0.90167]

Table 5.9: Overall system validation statistics of S1, S2 and S3 systems.

Overall - Throughput (AEVs per minute)									
R	System	S1	S2	S3	R	System	S1	S2	S3
10	Average	0.29347	0.29347	0.14143	40	Average	0.28427	0.28492	0.14607
	S^2	0.00009	0.00009	0.00116		S^2	0.00054	0.00049	0.00088
	S	0.00946	0.00946	0.03401		S	0.02326	0.02220	0.02972
	H	0.00676	0.00676	0.02431		H	0.00743	0.00709	0.00949
	CI (95%)	[0.28670, 0.30023]	[0.28670, 0.30023]	[0.11712, 0.16574]		CI (95%)	[0.27684, 0.29170]	[0.27782, 0.29201]	[0.13658, 0.15556]
	Risk	0.02243	0.02243	0.08062		Risk	0.04757	0.04541	0.06078
	PI (95%)	[0.27104, 0.31589]	[0.27104, 0.31589]	[0.060807, 0.22205]		PI (95%)	[0.23670, 0.33185]	[0.23951, 0.33032]	[0.085289, 0.206845]
Overall - System waiting time (W) (Minutes per AEV)									
R	System	S1	S2	S3	R	System	S1	S2	S3
10	Average	83.42580	83.31560	82.35259	40	Average	85.82445	85.95655	84.82824
	S^2	16.60597	15.20225	23.62549		S^2	17.60427	18.90669	30.97989
	S	4.07504	3.89901	4.86061		S	4.19574	4.34818	5.56596
	H	2.91233	2.78652	3.47375		H	1.34008	1.38877	1.77771
	CI (95%)	[80.51347, 86.33813]	[80.52908, 86.10212]	[78.87883, 85.82634]		CI (95%)	[84.48437, 87.16453]	[84.56779, 87.34531]	83.05053, 86.60595]
	Risk	9.65910	9.24185	11.52113		Risk	8.58069	8.89244	11.38291
	PI (95%)	[73.76667, 93.08490]	[74.07375, 92.55745]	[70.83145, 93.87372]		PI (95%)	[77.24376, 94.40514]	[77.06411, 94.84899]	[73.44533, 96.21115]
Overall - L (AEVs)									
R	System	S1	S2	S3	R	System	S1	S2	S3
10	Average	24.48107	24.44839	11.64906	40	Average	24.39116	24.48573	12.38231
	S^2	1.93634	1.79726	8.11807		S^2	5.12025	4.95575	6.78908
	S	1.39152	1.34062	2.84922		S	2.26280	2.22615	0.60559
	H	0.99449	0.95811	2.03627		H	0.72271	0.71101	0.83220
	CI (95%)	[23.48659, 25.47556]	[23.49028, 25.40649]	[9.61279, 13.68533]		CI (95%)	[23.66844, 25.11387]	[23.77472, 25.19674]	[11.55011, 13.21451]
	Risk	3.29834	3.17768	6.75353		Risk	4.62763	4.55269	5.32867
	PI (95%)	[21.18273, 27.77941]	[21.27071, 27.62606]	[4.89553, 18.40260]		PI (95%)	[19.76353, 29.01879]	[19.93304, 29.03842]	[7.05364, 17.71098]

Table 5.10: CCN validation statistics comparison for S1-S2 and S1-S3 systems.

CCN-1 Avg. Waiting Time Per CAEV (min/CAEV)							
R	Systems	S1-S2	S1-S3	R	Systems	S1-S2	S1-S3
10	Avg. Diff.	0.10411	-1.63415	40	Avg. Diff.	0.06042	-1.66893
	H	0.17855	2.13702		H	0.07713	0.84161
	CI (95%)	[-0.07444, 0.28266]	[-3.77117, 0.50287]		CI (95%)	[-0.01671, 0.13755]	[-2.51054, -0.82732]
CCN-1 - Throughput (CAEVs per minute)							
R	Systems	S1-S2	S1-S3	R	Systems	S1-S2	S1-S3
10	Avg. Diff.	0.00000	0.01915	40	Avg. Diff.	-0.00005	0.01675
	H	0.00000	0.00235		H	0.00007	0.00120
	CI (95%)	[0.00000, 0.00000]	[0.01680, 0.02151]		CI (95%)	[-0.00012, 0.00003]	[0.01555, 0.01795]
CCN-1 - System waiting time (W) (Minutes per AEV)							
R	Systems	S1-S2	S1-S3	R	Systems	S1-S2	S1-S3
10	Avg. Diff.	-0.33310	-9.18546	40	Avg. Diff.	-0.05822	-6.75300
	H	0.38224	7.94366		H	0.13046	3.38563
	CI (95%)	[-0.71534, 0.04914]	[-17.12912, -1.24180]		CI (95%)	[-0.18868, 0.07224]	[-10.13863, -3.36737]
CCN-1 - L (AEVs)							
R	Systems	S1-S2	S1-S3	R	Systems	S1-S2	S1-S3
10	Avg. Diff.	-0.01334	2.58432	40	Avg. Diff.	-0.00889	2.27581
	H	0.01573	0.32779		H	0.00864	0.16727
	CI (95%)	[-0.02907, 0.00239]	[2.25653, 2.91211]		CI (95%)	[-0.01753, -0.00026]	[2.10854, 2.44308]
CCN-1 - Server Utilization							
R	Systems	S1-S2	S1-S3	R	Systems	S1-S2	S1-S3
10	Avg. Diff.	0.25183	0.00450	40	Avg. Diff.	0.24712	-0.04163
	H	0.01575	-0.06054		H	0.01285	-0.07298
	CI (95%)	[0.23608, 0.26758]	[0.06504, -0.05604]		CI (95%)	[0.23427, 0.25998]	[0.03135, -0.11461]
CCN-1 - Proportion Server Idle Time							
R	Systems	S1-S2	S1-S3	R	Systems	S1-S2	S1-S3
10	Avg. Diff.	-0.25183	-0.00450	40	Avg. Diff.	-0.24712	0.04163
	H	0.01575	0.06504		H	0.01285	0.03135
	CI (95%)	[-0.26758, -0.23608]	[-0.06955, 0.06054]		CI (95%)	[-0.25998, -0.23427]	[0.01028, 0.07298]
CCN-2 Avg. Waiting Time Per CAEV (min/CAEV)							
R	Systems	S1-S2	S1-S3	R	Systems	S1-S2	S1-S3
10	Avg. Diff.	0.08747	-0.16229	40	Avg. Diff.	0.17170	-0.52620
	H	0.12145	0.48087		H	0.13521	0.47712
	CI (95%)	[-0.03398, 0.20892]	[-0.64317, 0.31858]		CI (95%)	[0.03649, 0.30691]	[-1.00332, -0.04908]
CCN-2 - Throughput (CAEVs per minute)							
R	Systems	S1-S2	S1-S3	R	Systems	S1-S2	S1-S3
10	Avg. Diff.	0.00000	0.01691	40	Avg. Diff.	0.00008	0.01746
	H	0.00000	0.00312		H	-0.00019	0.00163
	CI (95%)	[0.00000, 0.00000]	[0.01379, 0.02003]		CI (95%)	[0.00026, -0.00011]	[0.01583, 0.01909]
CCN-2 - System waiting time (W) (Minutes per AEV)							
R	Systems	S1-S2	S1-S3	R	Systems	S1-S2	S1-S3
10	Avg. Diff.	0.00000	9.80865	40	Avg. Diff.	-0.26389	9.60878
	H	0.00000	7.00426		H	0.24022	3.83105
	CI (95%)	[0.00000, 0.00000]	[2.80439, 16.81292]		CI (95%)	[-0.50411, -0.02367]	[5.77774, 13.43983]
CCN-2 - L (AEVs)							
R	Systems	S1-S2	S1-S3	R	Systems	S1-S2	S1-S3
10	Avg. Diff.	0.00000	2.65948	40	Avg. Diff.	-0.02083	2.70858
	H	0.00000	0.47563		H	0.02098	0.25881
	CI (95%)	[0.00000, 0.00000]	[2.18385, 3.13511]		CI (95%)	[-0.04181, 0.00015]	[2.44977, 2.96739]
CCN-2 - Server Utilization							
R	Systems	S1-S2	S1-S3	R	Systems	S1-S2	S1-S3
10	Avg. Diff.	0.24282	0.03412	40	Avg. Diff.	0.25451	0.02235
	H	0.02089	0.07422		H	0.01199	0.04190
	CI (95%)	[0.22192, 0.26371]	[-0.04011, 0.10834]		CI (95%)	[0.24252, 0.26650]	[-0.01955, 0.06425]
CCN-2 - Proportion Server Idle Time							
R	Systems	S1-S2	S1-S3	R	Systems	S1-S2	S1-S3
10	Avg. Diff.	-0.24282	-0.03412	40	Avg. Diff.	-0.25451	-0.02235
	H	0.02089	0.07422		H	0.01199	0.04190
	CI (95%)	[-0.26371, -0.22192]	[-0.10834, 0.04011]		CI (95%)	[-0.26650, -0.24252]	[-0.06425, 0.01955]

Table 5.11: SWCN validation statistics comparison for S1-S2 and S1-S3 systems.

SWCN-2 Avg. Waiting Time Per CAEV (min/CAEV)							
R	Systems	S1-S2	S1-S3	R	Systems	S1-S2	S1-S3
10	Avg. Diff.	0.32113	-0.83668	40	Avg. Diff.	0.46230	-1.60917
	H	0.38608	1.20753		H	0.20792	0.84510
	CI (95%)	[-0.06494, 0.70721]	[-2.04421, 0.37085]		CI (95%)	[0.25439, 0.67022]	[-2.45427, -0.76408]
SWCN-2 - Throughput (CAEVs per minute)							
R	Systems	S1-S2	S1-S3	R	Systems	S1-S2	S1-S3
10	Avg. Diff.	0.00000	0.02861	40	Avg. Diff.	-0.00022	0.08348
	H	0.00000	0.00513		H	0.00021	0.00241
	CI (95%)	[0.00000, 0.00000]	[0.02348, 0.03374]		CI (95%)	[-0.00043, -0.00001]	[0.08107, 0.08589]
SWCN-2 - System waiting time (W) (Minutes per AEV)							
R	Systems	S1-S2	S1-S3	R	Systems	S1-S2	S1-S3
10	Avg. Diff.	-0.17769	4.35726	40	Avg. Diff.	-0.28198	1.10906
	H	0.18971	8.45149		H	0.26334	3.67420
	CI (95%)	[-0.36740, 0.01202]	[-4.09423, 12.80875]		CI (95%)	[-0.54532, -0.01864]	[-2.56513, 4.78326]
SWCN-2 - L (AEVs)							
R	Systems	S1-S2	S1-S3	R	Systems	S1-S2	S1-S3
10	Avg. Diff.	-0.00961	3.67972	40	Avg. Diff.	-0.04684	3.46146
	H	0.01153	0.63365		H	0.02534	0.28136
	CI (95%)	[-0.02114, 0.00193]	[3.04607, 4.31337]		CI (95%)	[-0.07219, -0.02150]	[3.18010, 3.74282]
SWCN-2 - Server Utilization							
R	Systems	S1-S2	S1-S3	R	Systems	S1-S2	S1-S3
10	Avg. Diff.	0.29778	0.07882	40	Avg. Diff.	0.31144	0.02296
	H	0.02335	0.08435		H	0.01221	0.03957
	CI (95%)	[0.27443, 0.32113]	[-0.00553, 0.16317]		CI (95%)	[0.29923, 0.32364]	[-0.01661, 0.06253]
SWCN-2 - Proportion Server Idle Time							
R	Systems	S1-S2	S1-S3	R	Systems	S1-S2	S1-S3
10	Avg. Diff.	-0.29778	-0.07882	40	Avg. Diff.	-0.31144	-0.02296
	H	0.02335	0.08435		H	0.01221	0.03957
	CI (95%)	[-0.32113, -0.27443]	[-0.16317, 0.00553]		CI (95%)	[-0.32364, -0.29923]	[-0.06253, 0.01661]
SWCN-1 Avg. Waiting Time Per CAEV (min/CAEV)							
R	Systems	S1-S2	S1-S3	R	Systems	S1-S2	S1-S3
10	Avg. Diff.	0.20619	-2.23377	40	Avg. Diff.	0.22478	-1.38133
	H	0.17072	2.02387		H	0.17488	0.63520
	CI (95%)	[0.03547, 0.37691]	[-4.25763, -0.20990]		CI (95%)	[0.04990, 0.39966]	[-2.01653, -0.74614]
SWCN-1- Throughput (CAEVs per minute)							
R	Systems	S1-S2	S1-S3	R	Systems	S1-S2	S1-S3
10	Avg. Diff.	-0.00006	0.02885	40	Avg. Diff.	-0.00021	0.02688
	H	0.00012	0.00389		H	0.00023	0.00183
	CI (95%)	[-0.00019, 0.00006]	[0.02496, 0.03274]		CI (95%)	[-0.00044, 0.00002]	[0.02504, 0.02871]
SWCN-1 - System waiting time (W) (Minutes per AEV)							
R	Systems	S1-S2	S1-S3	R	Systems	S1-S2	S1-S3
10	Avg. Diff.	0.97089	-5.03804	40	Avg. Diff.	0.08543	2.35794
	H	2.35812	8.77557		H	0.66289	4.47774
	CI (95%)	[-1.38723, 3.32901]	[-13.81361, 3.73753]		CI (95%)	[-0.57746, 0.74833]	[-2.11980, 6.83568]
SWCN-1 - L (AEVs)							
R	Systems	S1-S2	S1-S3	R	Systems	S1-S2	S1-S3
10	Avg. Diff.	0.05711	3.40135	40	Avg. Diff.	-0.02256	3.28467
	H	0.13825	0.48092		H	0.05660	0.24208
	CI (95%)	[-0.08114, 0.19536]	[2.92043, 3.88227]		CI (95%)	[-0.07916, 0.03405]	[3.04260, 3.52675]
SWCN-1 - Server Utilization							
R	Systems	S1-S2	S1-S3	R	Systems	S1-S2	S1-S3
10	Avg. Diff.	0.31514	0.01080	40	Avg. Diff.	0.30040	0.01451
	H	0.03796	0.07640		H	0.01388	0.03923
	CI (95%)	[0.27718, 0.35310]	[-0.06561, 0.08720]		CI (95%)	[0.28652, 0.31427]	[-0.02472, 0.05375]
SWCN-1 - Proportion Server Idle Time							
R	Systems	S1-S2	S1-S3	R	Systems	S1-S2	S1-S3
10	Avg. Diff.	-0.31514	-0.01080	40	Avg. Diff.	-0.30040	-0.01451
	H	0.03796	0.07640		H	0.01388	0.03923
	CI (95%)	[-0.35310, -0.27718]	[-0.08720, 0.06561]		CI (95%)	[-0.31427, -0.28652]	[-0.05375, 0.02472]

Table 5.12: DWCN and overall validation statistics comparison for S1-S2 and S1-S3 systems.

DWCN-1- Throughput (CAEVs per minute)							
R	Systems	S1-S2	S1-S3	R	Systems	S1-S2	S1-S3
10	Avg. Diff.	0.00000	0.09915	40	Avg. Diff.	-0.00045	0.08965
	H	0.00000	0.01568		H	0.00064	0.00780
	CI (95%)	[0.00000, 0.00000]	[0.08347, 0.11483]		CI (95%)	[-0.00110, 0.00019]	[0.08186, 0.09745]
DWCN-1 - L (AEVs)							
R	Systems	S1-S2	S1-S3	R	Systems	S1-S2	S1-S3
10	Avg. Diff.	0.00000	0.89234	40	Avg. Diff.	-0.00409	0.80689
	H	0.00000	0.14114		H	0.00578	0.07020
	CI (95%)	[0.00000, 0.00000]	[0.75120, 1.03347]		CI (95%)	[-0.00987, 0.00169]	[0.73670, 0.87709]
DWCN-1 - Server Utilization							
R	Systems	S1-S2	S1-S3	R	Systems	S1-S2	S1-S3
10	Avg. Diff.	0.08344	0.01159	40	Avg. Diff.	0.08032	0.00034
	H	0.00195	0.02500		H	0.00231	0.01121
	CI (95%)	[0.08149, 0.08539]	[-0.01341, 0.03659]		CI (95%)	[0.07801, 0.08262]	[-0.01087, 0.01155]
DWCN-1 - Proportion Server Idle Time							
R	Systems	S1-S2	S1-S3	R	Systems	S1-S2	S1-S3
10	Avg. Diff.	-0.08344	-0.01159	40	Avg. Diff.	-0.08032	-0.00034
	H	0.00195	0.02500		H	0.00231	0.01121
	CI (95%)	[-0.08539, -0.08149]	[-0.03659, 0.01341]		CI (95%)	[-0.08262, -0.07801]	[-0.01155, 0.01087]
Overall System- Throughput (CAEVs per minute)							
R	Systems	S1-S2	S1-S3	R	Systems	S1-S2	S1-S3
10	Avg. Diff.	0.00000	0.15204	40	Avg. Diff.	-0.00064	0.13820
	H	0.00000	0.02098		H	0.00091	0.01106
	CI (95%)	[0.00000, 0.00000]	[0.13105, 0.17302]		CI (95%)	[-0.00155, 0.00026]	[0.12715, 0.14926]
Overall System waiting time (W) (Minutes per AEV)							
R	Systems	S1-S2	S1-S3	R	Systems	S1-S2	S1-S3
10	Avg. Diff.	0.11020	1.07321	40	Avg. Diff.	-0.13210	0.99621
	H	0.47693	2.02783		H	0.17284	1.25386
	CI (95%)	[-0.36673, 0.58713]	[-0.95461, 3.10104]		CI (95%)	[-0.30494, 0.04074]	[-0.25765, 2.25007]
Overall System - L (AEVs)							
R	Systems	S1-S2	S1-S3	R	Systems	S1-S2	S1-S3
10	Avg. Diff.	0.03268	12.83201	40	Avg. Diff.	-0.09457	12.00884
	H	0.14109	1.43433		H	0.08419	0.92730
	CI (95%)	[-0.10840, 0.17377]	[11.39768, 14.26634]		CI (95%)	[-0.17876, -0.01038]	[11.08154 12.93615]

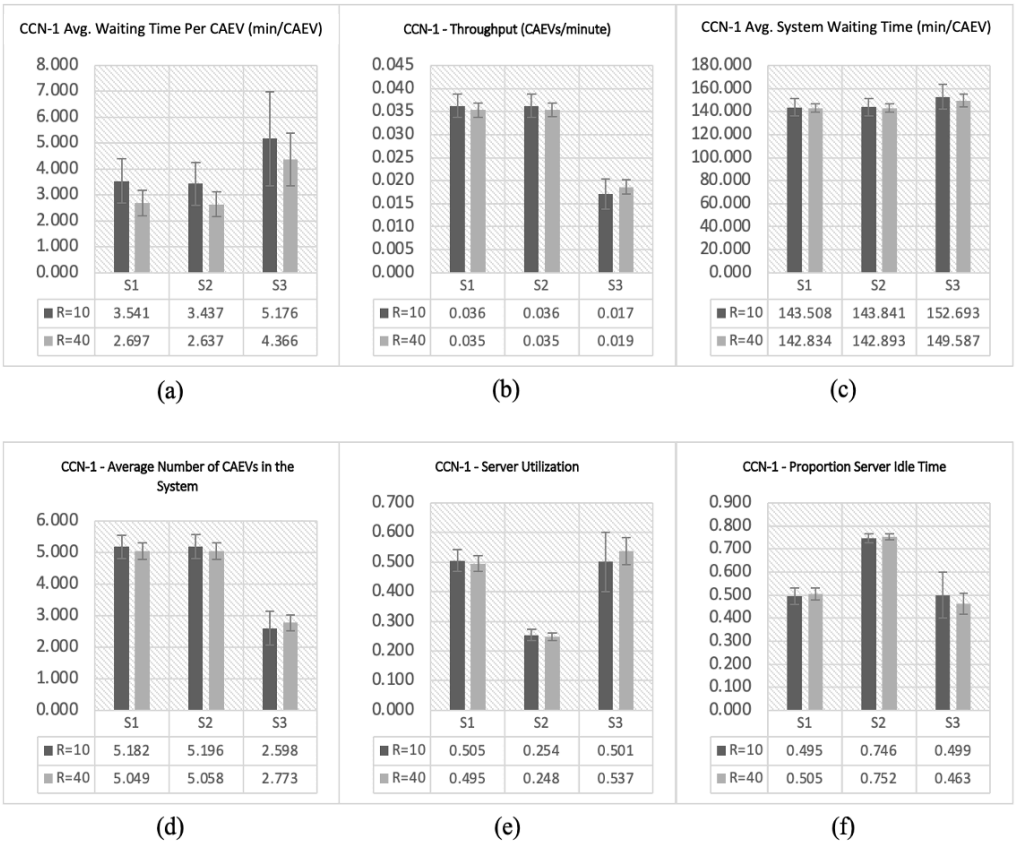

Figure 5.5: CCN-1 validation stats graphs of S1, S2 and S3 for (a) average waiting time per CAEV, (b) throughput, (c) average system waiting time (d), average number of CAEVs, (e) server utilization and (f) proportion server idle time.

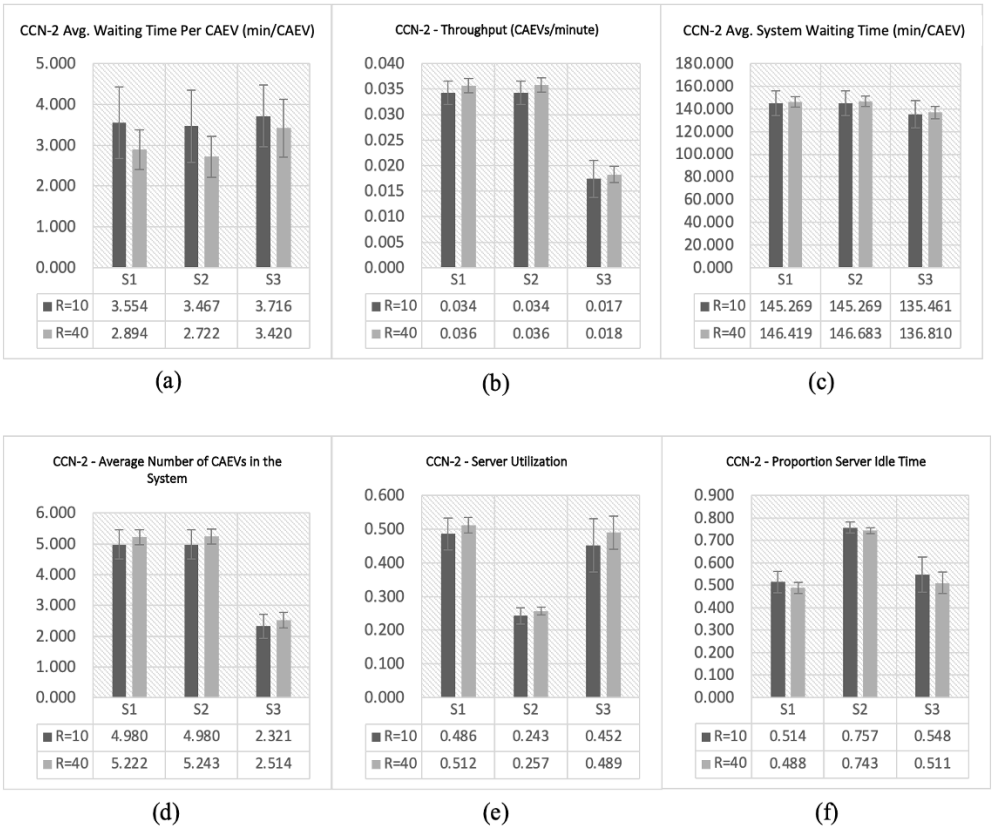

Figure 5.6: CCN-2 validation stats graphs of S1, S2 and S3 for (a) average waiting time per CAEV, (b) throughput, (c) average system waiting time (d), average number of CAEVs, (e) server utilization and (f) proportion server idle time.

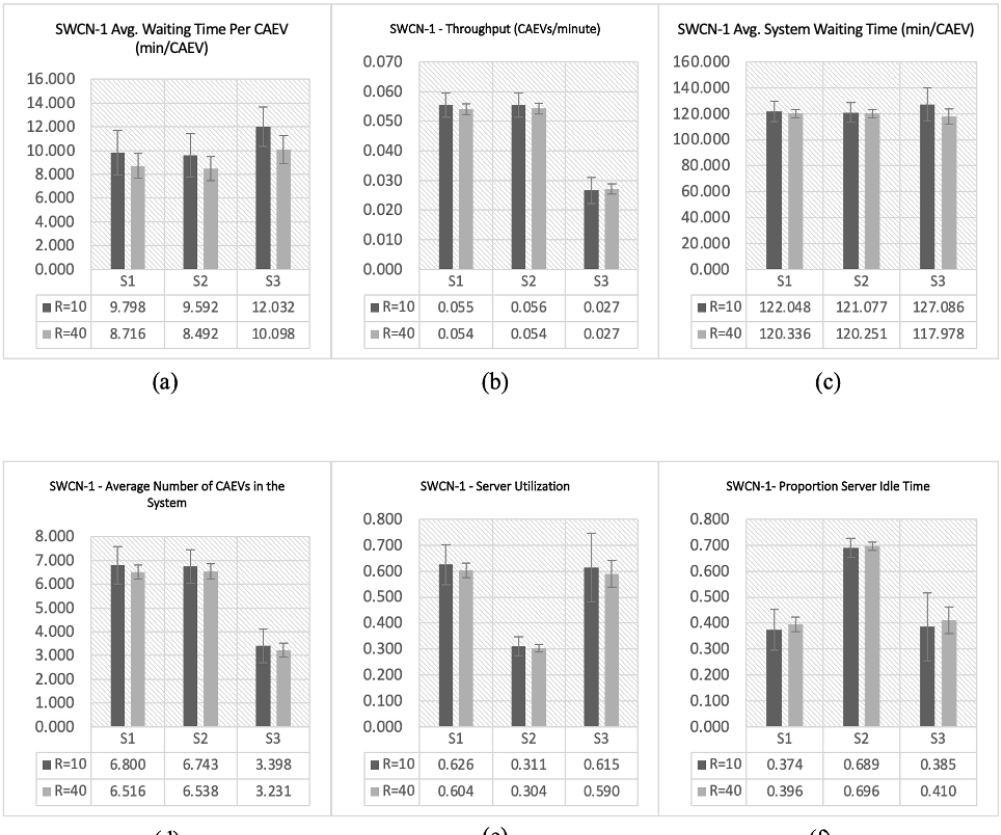

Figure 5.7: SWCN-1 validation statistics graphs of S1, S2 and S3 for (a) average waiting time per CAEV, (b) throughput, (c) average system waiting time (d), average number of CAEVs, (e) server utilization and (f) proportion server idle time.

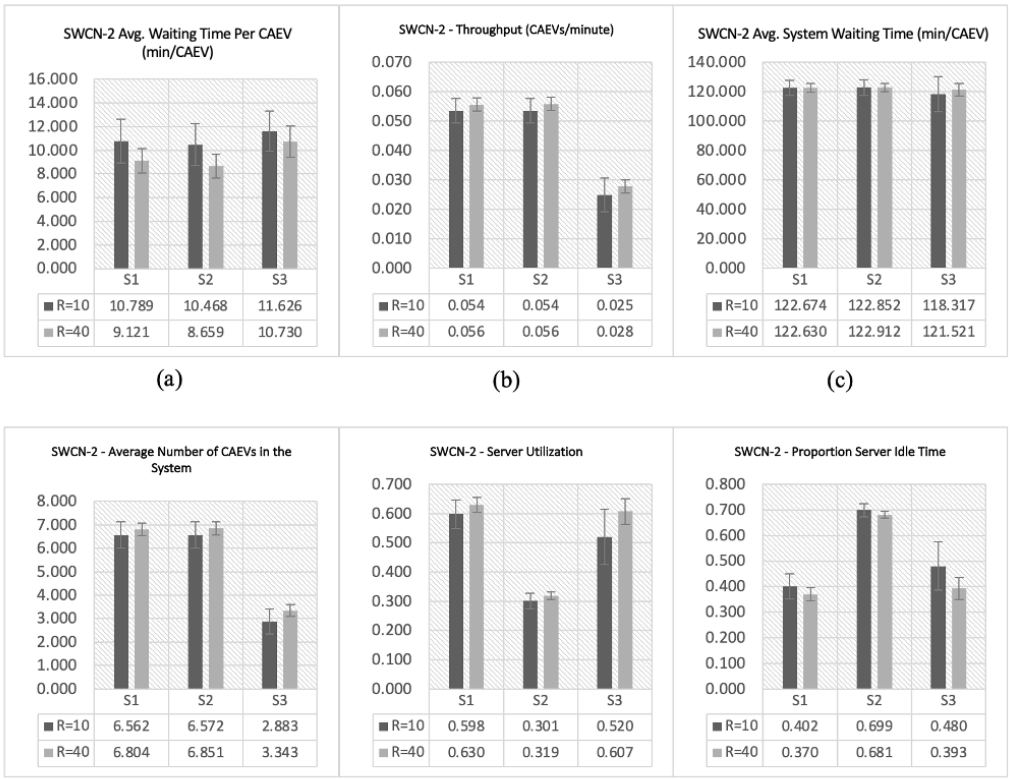

Figure 5.8: SWCN-2 validation statistics graphs of S1, S2 and S3 for (a) average waiting time per CAEV, (b) throughput, (c) average system waiting time (d), average number of CAEVs, (e) server utilization and (f) proportion server idle time.

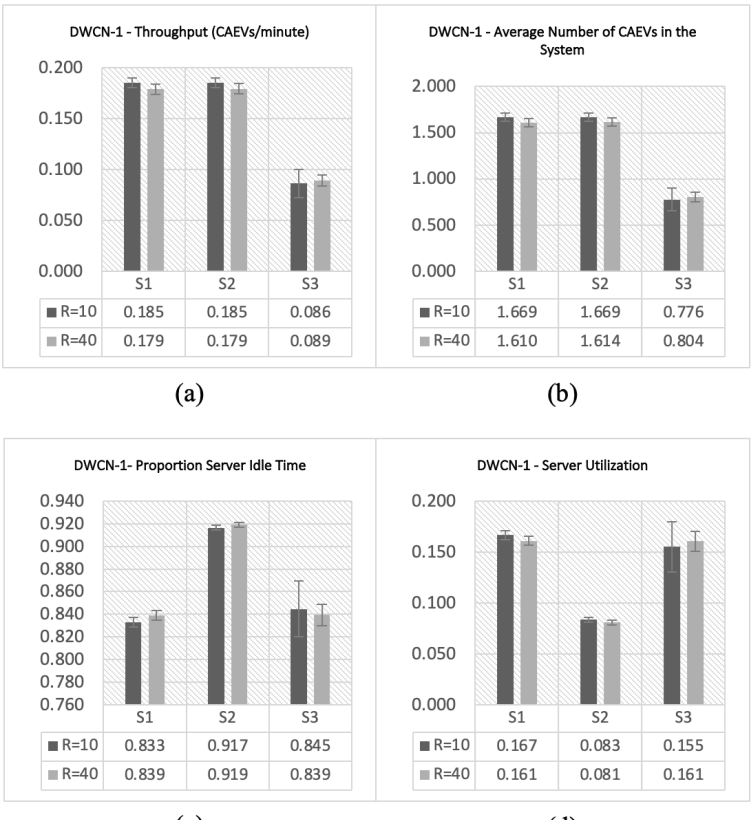

Figure 5.9: DWCN-1 validation statistics graphs of S1, S2 and S3 for (a) throughput, (b) average number of CAEVs, (c) proportion server idle time and (d) server utilization.

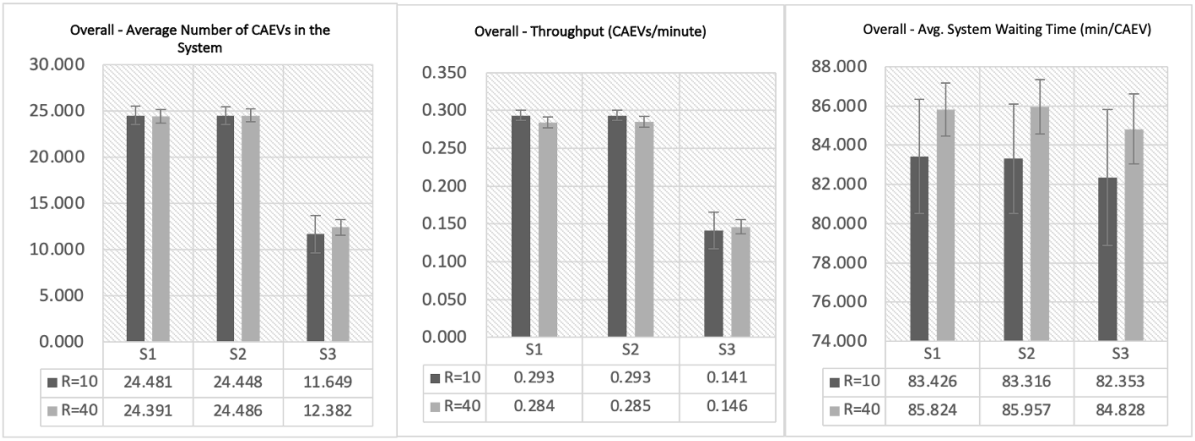

(a) (b) (c)

Figure 5.10: Overall system validation stats graphs of S1, S2 and S3 for (a) average number of CAEVs, (b) throughput and (c) average system waiting time.

5.7 Comparisons with Existing Systems in Literature

DWC involves CAEV users' requests being served and billed sequentially. Thus, putting at risk the privacy and security of CAEV users' location and personal information. Authors in [194], [195] and [200] address this concern by proposing real-time and secure payment systems. Unlike our proposed system, [194], [195] and [200] are vulnerable to free-riders and may bill unfairly due to inefficient nature of charging segments used, and do not have traceability of charging session payments to verify fairness of billing. Our proposed system also avoids free-riders and uses encrypted virtual currency to provide user anonymity and location and personal information privacy. Our integrated payment system is resistant to double spending with traceability of charging reservation payments and choice of billing schemes that use TOU based real-time metering.

As discussed earlier, the major adoption barrier of EVs is inadequate charging infrastructure. Papers [199], [272] and existing open-source and realistic simulators like Caltech's ACN-Sim [45] serve CCNs and are neither automatic nor dynamic in fulfilling charging requests. In [36], only SWC is considered.

Our proposed system is completely unique with its presentation of a novel handshake protocol and charging system design that meets the interoperability aim of the existing static CC and SWC standardization efforts with the proposed DWCN and SWCN [42]–[44]. Interestingly, the 90.25 % overall charging delivery efficiency of our reservation system meets the standardization requirements. However, it is truly incomparable, as this novel system is fulfilling charging reservation requests over three different types of CNs. It is difficult to find other models that like ours addresses variety of variables including latencies and energy consumption. The systems that exist only address some of the variables. Table 5.13 summarizes

and illustrates how our proposed system is different from already existing solutions and systems. Further, an optimal solution can be derived to compare the results as part of future work.

Our adaptive charging reservations can fairly deal with late and early vehicle arrivals by moving up or down the reservations if possible. The IoT application system employs fog and cloud computing for faster V2I and V2G communications. Importantly, using sensors the system can detect and correct vehicle body misalignment and speed issues on WCPs of wireless CNs in real-time to ensure efficient delivery of reserved charging. Noteworthy, our systems is free from the underlying hardware and communication technologies for ease of implementation.

Table 5.13: Summary of comparison between our system and existing systems.

Reference	[45]	[194]	[195]	[200]	[199]	[24]	[25]	**Ours**
CC	X				X	X		X
SWC				X			X	X
DWC		X	X	X				X
WCPs			X	X			X	X
Energy segments/lanes		X						
Location privacy		X	X					X
User anonymity		X	X					X
Automated reservations							X	X
Vehicle reservation traceability	X	X			X	X	X	X
Avoid free-riders								X
Enables overtaking in DWC								X
Misalignment detection								X
Speed error detection								X
Driver feedback system								X
Virtual currency			X					X
Prevent double spending			X					X
Secure payment and billing		X	X		X			X
Fair billing					X			X
Price flexibility		X				X		X
Fining wrong usage (e.g. blockage of WCPs/lanes, blocking an EVSE, etc.)								X
Late/Cancellation of reservation fees								X
Pre-paid charging session			X					
Pay per charging session		X		X	X	X		X
Pay per energy unit (kWh)								X
Fast vehicle authentication		X	X	X	X			X
Charging synchronization				X				X
EVSE reservation	X				X	X	X	X
Dynamic fulfillment of charging requests								X
Adaptive charging reservation								X
Compatibility with existing wired charging infrastructure and standards	X				X	X		X
Compatibility with existing wireless charging infrastructure and standards							X	X
Interoperability with wired and wireless CNs								X
Cloud computing		X			X	X	X	X
Fog computing								X
Minimize traveling time								X
Minimize waiting times						X		X
Minimize traveling distance								X
Trip Planning								X

5.8 Conclusion

In this chapter, the simulation model is verified and validated to promise credibility and accuracy of generated results. The implementation was verified using common and popular techniques like debugging, flowcharts, examining outputs for reasonableness, printing input and output parameters, tracing using print statements and self-documentation. Most importantly, the Little's Law was used to verify the overall system as well as its CNs by ensuring the computed L matched the analytical L. Validation techniques were used and discussed to make sure that the correct model presented in Chapter 3 is built. It is an iterative process that involved many calibrations. Techniques like face validity and validity of model assumptions were carried out. It should be noted that the proposed system is entirely imaginary with no input and output data available to carry out other validation techniques. The validated and verified simulation model is then set up for one simulation run and its generated results are discussed. Next, a statistical analysis of the outputs or evaluation parameters of interest under 95% CIs by performing several independent replications is conducted. The absolute measures of performance and relative performance for the original system and alternative system designs were generated and plotted to draw conclusions on system performance and determine best system design for implementation. From the output analysis of the performance parameters, it was apparent that S1 with 10 EVSEs per CN is the best design choice in terms of cost and performance for first time deployment of the novel charging reservation and trip planning system. Finally, the discussion of proposed system with existing systems in literature is presented to highlight its novelty and features.

Chapter 6 Conclusion and Future Work

6.1 Concluding Remarks

The current transportation system powered by internal combustion engines has been deemed environmentally unsustainable for the future. A rise in promotion of CAEVs by both public and private entities to reduce GHG emissions and dependance on fossil fuels has been noticed. The CAEVs can encourage generation of renewable energy for a positive environmental impact and uplift the overall quality of transportation. SAEVs with carpooling can further reduce traffic jams and transportation costs and even open up parking spaces. AMoD trips with CAEVs is a likely application to boost adoption, reduce costs associated with car ownerships and make transportation more accessible for lower income groups. However, range anxiety and longer charging times have made old fossil fuel powered car owners and potential CAEV users apprehensive.

Interestingly, the government introduced incentives, affordability, care for the environment and changing public perceptions have boosted sales and popularity of CAEVs with 245 million predicted to cruise on the roads worldwide by 2023 [31]. Hence, a need for a smart charging infrastructure is felt to accommodate the large demands of charging by these CAEVs. Further, these CAEV users might suffer from traffic jams as they randomly look for charging stations with their range-anxiety, and may also be left to deal with long charging times and waiting times at the charging stations. WPT technology coupled with CAEVs and AMoD trips has been seen as the solution to create a sustainable ITS for the future smart cities. In lieu of this, a novel three-layer hierarchical CN system design was proposed with an IoT application.

The three-layer CN hierarchy was designed to enable communication and interoperability between existing wired charging systems and future wireless charging systems and their standards to be both sustainable and future proof. The CN architecture was presented along with a handshake protocol and light-weight reservation request and reservation confirmation message frames. The protocol and the message frames enabled the proposed CN architecture to dynamically fulfill large charging requests over one or more CNs of wired and wireless types. Thus, bringing to life an IoT application like the charging reservation and trip planning system for CAEVs. The CAEVs can then use the proposed message frames over V2I and V2G communication to request and receive a charging reservation and planned AMoD trip. The system will then make reservations and plan a trip while minimizing waiting time at

charging stations, traveling cost, payment and battery consumption. It should be noted that indirectly traffic congestion was reduced by planning trips and stops at CNs with minimum travel costs and waiting times. Further, the pay per charging session and pay per energy unit billing schemes were also proposed to fairly and securely bill the CAEVs for their real-time metered charging delivery using TOU pricing. The CAEV user's privacy was maintained by paying anonymously with the proposed encrypted virtual currency called CPs. The presented automated driving feedback system ensured efficient and safe delivery of charging by detecting and reporting errors to CAEV in real-time for immediate correction. The handshake protocol's charging establishment phase with authentication and verification of CAEVs ensured fair delivery of charging, and helped avoid charge stealing or free-riders and unfair billing. More importantly, wired and some SWC systems are commercially available and their specifications and standards can be used for modelling. Since DWCN are not yet commercially deployed and no guidelines exist for their construction, a DWCN design specification tool was developed that takes in parameters and automatically builds one for realistic testing before real-world implementation.

Next, the proposed model's conceptualization was realized into a discrete event simulator with a python implementation due to the object-oriented language's features, extensive libraires and ease of use. The designed simulator enables users to simulate the proposed three-layer hierarchical CN system design with the handshake protocol on any real-world map. It simulates the driving, charging request, charging reservation and trip planning, charging reservation and route confirmation, waiting, and charging phases with arrival, departure and driving events. The simulation tool is successfully verified and validated to predict and analyze the absolute performance of existing wired CNs with wireless CNs that are to be installed with increased credibility. It can also help implementers and analysts compare alternative system design policies for making effective design and implementation choices. This charging reservation and shortest trip planning system is one of the smart city IoT applications for ITS with a significantly high charge delivery efficiency of 90.25%. The latter effectively keeps the average waiting times, travel costs and battery consumption levels for a vehicle trip at minimum compared to manual and random EVSE searches by CAEVs. It should be noted that no similar real-world system exists for true comparison of performance.

Overall, the presented charging reservation and trip planning system that employs the novel three-layer scalable CN hierarchical architecture uniquely contributes to the ongoing international standardization efforts of wireless charging systems like the ISO, IEC and SAE. Additionally, this system application maintains interoperability with existing wired charging

systems by following existing standards and guidelines of wired charging systems and SWC systems. The system design is hardware independent and can employ any fast and low-latency communication technologies and misalignment and speed detection technologies. The accompanying handshake protocol, message frames and billing schemes have privacy and security built within it from the charging request phase to charging delivery and payment. The privacy and anonymity of a CAEV user is maintained by using secure message frames that keep the identity of the requesting user anonymous. The use of encrypted CPs for payment of the charging sessions also helps safeguard the CAEV user's identity. The charging reservation traceability is maintained with the uniquely generated random ID. Moreover, the authentication and verification of CAEVs at each EVSE and WCP ensures that no other entity other than the CAEV that requested the charging receives power with fair billing of the delivered charging.

The system also takes safety of the users into account. Its ensures charging is delivered only when the CAEV is properly authenticated, verified, and positioned. For safe reception of charging, the CAEV needs to be properly plugged-in to the EVSE in CCNs. In wireless CNs, the vehicle needs to be properly aligned with the WCPs, and the DWCNs also require the CAEV to cruise at the recommended speed for efficient delivery of charging. The system can also detect accidents on DWCN lanes. It then automatically blocks the accident affected area by shutting off the WCPs. Next, it notifies the CAEVs and gives them the option to either resume or cancel their charging reservation after by passing the affected area.

Additionally, algorithms are proposed to process early and late arrivals of CAEVs at CCNs and SWCNs, charging time estimation of wired and wireless charging for a particular CAEV, distributing charging requests, and reserving charging time slots of EVSEs based on set parameters like minimum waiting time, travel costs, battery consumption and payments. More importantly, the presented IoT application stands unique in its way of fulfilling large charging requests that a single CN may not be able to fulfill alone. So, it dynamically distributes the request over one or more CNs of different types while ensuring that these CNs fall along the shortest possible route of the AMoD trip.

Now, lack of DWCNs and their standards paved way for the creation of the design specification tool that can be used alone or in combination with a simulator. It can help test and build DWCN lanes with the desired parameters, guidelines and design goals for overall savings in cost and time. Further, the simulator itself can work alone or can extend existing simulators like Caltech's ACN-Sim [45] for further system performance analysis. More importantly, this system can be used as a framework for actual implementation by charging system deployment companies and research laboratories. Wireless charging system manufacturers and car

manufacturers could be interested in manufacturing the vehicle and ground sides of the charging equipment compatible with the proposed system. Other interested parties like wireless companies, automobile manufacturers, telecommunication companies, banks, utilities, city planners, government and private agencies might be interested to invest in the proposed system for a sustainable and smart ITS.

The presented thesis work has several components that has the potential to be expanded and developed into stand-alone research work as discussed in the next section.

6.2 Future Work

The analysts and designers can use the DWCN design specification tool to build DWCNs that comply with existing standards for CAEV charging or even test new and upcoming standards. The tool can be developed further to give accurate cost estimations of installation, time estimation of construction, and estimating number of workers required with the available data and additional research work. The tool can be modified to make additional suggestions like placements of RSUs for better coverage and best allocation of the DWCN itself on a map based on chosen objectives like minimum travel time and proximity to CCNs and SWCNs, for example. Other aspects to elaborate may include optimizing the allocation and installments of WCPs, RSUs and the DWCN for efficient charge delivery at minimum cost, cost-analysis, time-analysis and break-even analysis of DWC lane construction with the given government and country guidelines, rules and regulations, and finding the optimal placement of the WCPs to maximize misalignment and speed tolerance for efficient and safe delivery of charging.

The proposed three-layer CN hierarchy and protocol could be expanded to enable bi-directional charging, and V2V communication could add the feature of CAEVs sharing charging while on the move or stationary like at parking lots or traffic jams and stops. The system can then be modified to enable fulfillment of charging requests with nearby and trusted CAEVs securely using V2V. The CAEV users could also securely sell back charging to the smart grid with V2G especially during peak times to maintain grid stability and effectively meet charging demands. The system can then be modified to dynamically fulfill requests of charging over different CNs and closely available CAEVs.

Besides mobility of people, increasing urbanization rates also seeks efficient mobility for goods. The presented system can prove crucial in the development of new logistics systems. To make transportation systems more sustainable, ecological and have better service quality, individual freight and passenger transportation streams in an urban area can be combined like [43]–[47]. Efficiency gains and challenges of people and goods sharing rides is an ongoing

research topic. So, the system can be modified to conduct joint-optimization of charge scheduling and trip planning for both people and goods. The CAEVs scheduled for a ride-sharing trip may even carry out packets for delivery if the package's final destination or intermediary stop falls on the planned route, and another vehicle may make the final delivery to the facility, pick up point or the intended destination.

The designed simulator of the proposed system can be used as a test-bed for different charging scheduling algorithms and trip planning algorithms to compare and contrast their effect on the overall performance of the system. The simulator can also be used to optimize charging scheduling while meeting charging demands, load-balancing and maintaining grid stability. Further, optimal solutions can be derived for comparing simulation results. The optimal allocation problem of the wired and wireless CNs on a given map following given rules and regulations of a city and country for the proposed architecture and system for implementation can be solved, and the solution can be fed into the simulator for further performance analysis and iterative changes. Additionally, the presented simulator by extending existing simulator's like Caltech's ACN-Sim can use Caltech's collected real-world charge scheduling data, for example, to conduct wired and wireless charging systems performance analysis. The prior can also help analyze the effect of employing the presented architecture, protocol, message frames or billing schemes with the existing charging infrastructure and systems.

To ensure privacy and security of billing and payment schemes as well as message frames in the real-world, different encryption schemes can be implemented. An in-depth security analysis for evaluating resistance against attacks can be conducted. Further, performance analysis like computation, communication and storage costs can also be done. The system for added security can be modified to use blockchain for creation and distribution of the proposed virtual currency called CPs. An analysis on choosing the best communication technology to use for exchanging the proposed message frames for requests by CAEVs can be conducted as well. A front-end and back-end application for the charging reservation and trip planning system can be developed and tested, and the collected anonymous data can then be made public for additional research with machine learning (ML).

Artificial intelligence and ML can be used to analyze large datasets and make personalized recommendations for an AMoD trip with charge scheduling. However, there is a lack of charging datasets required to train ML models, and the few that do exist like [273] and in [274] are restricted to public wired charging stations in specific geographical areas making ML models developed not applicable to other regions and wireless charging systems. Hence,

there is a need for higher dimensional data sets for further research with ML. So, datasets may be created with the proposed system for both wired and wireless CN types. Further, ML predictions for charge scheduling in minutes, days, weeks or months with the available data set and its effect on actual charging scheduling can be explored further with the proposed system. The latter maybe jointly done with trip planning. More specifically, ML can be used to predict energy consumption and costs of the CN infrastructure to help identify peak times and off-peak times in advance, and can help schedule CAEVs buying and selling of charging accordingly in bi-directional charging systems. An individual CAEV user's energy consumption behavior might be learnt and a charging scheduling algorithm may be proposed to maximize objectives like quality of experience (QoE), quality of service (QoS), grid stability, load-balancing, etc., and reduce expenses, travel costs, battery consumption, demand curve, etc. Different ML techniques like supervised learning, unsupervised learning and reinforcement learning may be used and evaluated for computational performance and overall performance improvement in the current charging scheduling and trip planning system for CAEVs.

References

[1] J. Tomić and W. Kempton, "Using fleets of electric-drive vehicles for grid support," *J. Power Sources*, vol. 168, no. 2, pp. 459–468, Jun. 2007, doi: 10.1016/j.jpowsour.2007.03.010.

[2] INRIX, "2020 Global Traffic Scorecard," *Inrix*, 2021. [Online]. Available: https://inrix.com/scorecard/.

[3] Natural Resources Canada, "Greenhouse gas emissions - Canada.ca," *Natural Resources Canada*, 2019. [Online]. Available: https://www.canada.ca/en/environment-climate-change/services/environmental-indicators/greenhouse-gas-emissions.html. [Accessed: 05-May-2021].

[4] E. S. Rigas, S. D. Ramchurn, and N. Bassiliades, "Algorithms for electric vehicle scheduling in large-scale mobility-on-demand schemes," *Artif. Intell.*, vol. 262, pp. 248–278, Sep. 2018, doi: 10.1016/j.artint.2018.06.006.

[5] UNDESA (United Nations Department of Economic and Social Affairs Population Division), "World Urbanization Prospects : The 2018 Revision," 2018.

[6] M. Densing, H. Turton, and G. Bäuml, "Conditions for the successful deployment of electric vehicles - A global energy system perspective," *Energy*, vol. 47, no. 1, pp. 137–149, Nov. 2012, doi: 10.1016/j.energy.2012.09.011.

[7] S. Kuppusamy, M. J. Magazine, and U. Rao, "Electric vehicle adoption decisions in a fleet environment," *Eur. J. Oper. Res.*, 2017, doi: 10.1016/j.ejor.2017.03.039.

[8] A. Lajunen, "Evaluation of energy consumption and carbon dioxide emissions for electric vehicles in Nordic climate conditions," in *2018 13th International Conference on Ecological Vehicles and Renewable Energies, EVER 2018*, 2018, pp. 1–7, doi: 10.1109/EVER.2018.8362390.

[9] J. Dai, M. Dong, R. Ye, A. Ma, and W. Yang, "A review on electric vehicles and renewable energy synergies in smart grid," in *China International Conference on Electricity Distribution, CICED*, 2016, vol. 2016-September, doi: 10.1109/CICED.2016.7575995.

[10] S. Sharma, A. K. Panwar, and M. M. Tripathi, "Storage technologies for electric vehicles," *J. Traffic Transp. Eng. (English Ed.*, Jun. 2020, doi: 10.1016/j.jtte.2020.04.004.

[11] O. Egbue and S. Long, "Barriers to widespread adoption of electric vehicles: An analysis of consumer attitudes and perceptions," *Energy Policy*, 2012, doi: 10.1016/j.enpol.2012.06.009.

[12] L. Noel, G. Zarazua de Rubens, B. K. Sovacool, and J. Kester, "Fear and loathing of electric vehicles: The reactionary rhetoric of range anxiety," *Energy Res. Soc. Sci.*, 2019, doi: 10.1016/j.erss.2018.10.001.

[13] "Top 20 electric vehicle charging station companies." [Online]. Available: https://roboticsandautomationnews.com/2019/05/01/top-20-electric-vehicle-charging-station-companies/22138/. [Accessed: 10-Jun-2020].

[14] "Morgan Stanley: Tesla charging station network 'competitive moat.'" [Online]. Available: https://www.cnbc.com/2019/02/12/morgan-stanley-tesla-charging-station-network-competitive-moat.html. [Accessed: 10-Jun-2020].

[15] "Renault installs electric car charging stations powered by used EV battery packs - Electrek." [Online]. Available: https://electrek.co/2017/08/29/renault-electric-car-charging-stations-used-ev-battery-packs/. [Accessed: 11-Jun-2020].

[16] "U.S. Department of Transportation Announces $130 Million in Grants for Nationwide Projects to Expand Advanced, Efficient Bus Technologies | FTA." [Online]. Available: https://www.transit.dot.gov/about/news/us-department-transportation-announces-130-

million-grants-nationwide-projects-expand. [Accessed: 11-Jun-2020].
[17] "Nation's Top Transit Official Highlights $18 Million Infrastructure Investment to Improve Safety, Reliability of Colorado Bus Systems | FTA." [Online]. Available: https://www.transit.dot.gov/about/news/nations-top-transit-official-highlights-18-million-infrastructure-investment-improve. [Accessed: 11-Jun-2020].
[18] "Canada Invests in Ontario's Electric Vehicle Network - Canada.ca." [Online]. Available: https://www.canada.ca/en/natural-resources-canada/news/2020/02/canada-invests-in-ontarios-electric-vehicle-network.html. [Accessed: 11-Jun-2020].
[19] "Canada Partners With Canadian Tire To Build One of Canada's Largest EV Charging Networks - Canada.ca." [Online]. Available: https://www.canada.ca/en/natural-resources-canada/news/2020/01/canada-partners-with-canadian-tire-to-build-one-of-canadas-largest-ev-charging-networks.html. [Accessed: 11-Jun-2020].
[20] "UK government increases funding for electric charge points." [Online]. Available: https://www.cnbc.com/2020/01/21/uk-government-increases-funding-for-electric-charge-points.html. [Accessed: 11-Jun-2020].
[21] W. Sierzchula, S. Bakker, K. Maat, and B. Van Wee, "The competitive environment of electric vehicles: An analysis of prototype and production models," *Environ. Innov. Soc. Transitions*, vol. 2, pp. 49–65, Mar. 2012, doi: 10.1016/j.eist.2012.01.004.
[22] D. Paddeu, G. Parkhurst, and I. Shergold, "Passenger comfort and trust on first-time use of a shared autonomous shuttle vehicle," *Transp. Res. Part C Emerg. Technol.*, vol. 115, p. 102604, Jun. 2020, doi: 10.1016/j.trc.2020.02.026.
[23] C. D. Harper, C. T. Hendrickson, S. Mangones, and C. Samaras, "Estimating potential increases in travel with autonomous vehicles for the non-driving, elderly and people with travel-restrictive medical conditions," *Transp. Res. Part C Emerg. Technol.*, vol. 72, pp. 1–9, Nov. 2016, doi: 10.1016/j.trc.2016.09.003.
[24] I. Overtoom, G. Correia, Y. Huang, and A. Verbraeck, "Assessing the impacts of shared autonomous vehicles on congestion and curb use: A traffic simulation study in The Hague, Netherlands," *Int. J. Transp. Sci. Technol.*, Apr. 2020, doi: 10.1016/j.ijtst.2020.03.009.
[25] X. Tan and A. Leon-Garcia, "Autonomous Mobility and Energy Service Management in Future Smart Cities: An Overview," in *4th IEEE International Conference on Universal Village 2018, UV 2018*, 2019, doi: 10.1109/UV.2018.8642141.
[26] J. Wu, H. Liao, and J. W. Wang, "Analysis of consumer attitudes towards autonomous, connected, and electric vehicles: A survey in China," *Res. Transp. Econ.*, vol. 80, p. 100828, May 2020, doi: 10.1016/j.retrec.2020.100828.
[27] D. Paddeu, I. Shergold, and G. Parkhurst, "The social perspective on policy towards local shared autonomous vehicle services (LSAVS)," *Transp. Policy*, May 2020, doi: 10.1016/j.tranpol.2020.05.013.
[28] P. Machura and Q. Li, "A critical review on wireless charging for electric vehicles," *Renewable and Sustainable Energy Reviews*. 2019, doi: 10.1016/j.rser.2019.01.027.
[29] S. Chopra and P. Bauer, "Driving range extension of EV with on-road contactless power transfer-A case study," *IEEE Trans. Ind. Electron.*, vol. 60, no. 1, pp. 329–338, 2013, doi: 10.1109/TIE.2011.2182015.
[30] E. Ayisire, A. El-Shahat, and A. Sharaf, "Magnetic Resonance Coupling Modelling for Electric Vehicles Wireless Charging," in *GHTC 2018 - IEEE Global Humanitarian Technology Conference, Proceedings*, 2019, doi: 10.1109/GHTC.2018.8601806.
[31] International Energy Agency, "Global EV Outlook 2020," 2020.
[32] T. Zhang, W. Chen, Z. Han, and Z. Cao, "Charging scheduling of electric vehicles with local renewable energy under uncertain electric vehicle arrival and grid power price," *IEEE Trans. Veh. Technol.*, vol. 63, no. 6, pp. 2600–2612, 2014, doi:

10.1109/TVT.2013.2295591.
[33] J. Timpner and L. Wolf, “Design and evaluation of charging station scheduling strategies for electric vehicles,” *IEEE Trans. Intell. Transp. Syst.*, vol. 15, no. 2, pp. 579–588, 2014, doi: 10.1109/TITS.2013.2283805.
[34] Y. He, B. Venkatesh, and L. Guan, “Optimal scheduling for charging and discharging of electric vehicles,” *IEEE Trans. Smart Grid*, vol. 3, no. 3, pp. 1095–1105, 2012, doi: 10.1109/TSG.2011.2173507.
[35] W. Tang, S. Bi, and Y. J. A. Zhang, “Online coordinated charging decision algorithm for electric vehicles without future information,” *IEEE Trans. Smart Grid*, vol. 5, no. 6, pp. 2810–2824, Nov. 2014, doi: 10.1109/TSG.2014.2346925.
[36] B. Vaidya and H. T. Mouftah, “Wireless Charging System for Connected and Autonomous Electric Vehicles,” in *Proceedings IEEE Globecom2018 Workshop on Vehicular Networking and Intelligent Transportation Systems (VENITS2018), Abu Dhabi, UAE*, 2018, p. WS26.4.1-WS26.4.6, doi: 10.1109/GLOCOMW.2018.8644359.
[37] B. Vaidya and H. T. Mouftah, “Automated Reservation Mechanism for Charging Connected and Autonomous EVs in Smart Cities,” in *Proceedings IEEE VTC2018-Fall 3rd International Workshop of CorNer: Communications for Networked Smart Cities (CorNer2018)*, 2018, p. W6.2.1.1-W6.2.1.6, doi: 10.1109/VTCFall.2018.8690905.
[38] A. A. S. Mohamed, D. Day, A. Meintz, and J. Myungsoo, “Real-Time Implementation of Smart Wireless Charging of On-Demand Shuttle Service for Demand Charge Mitigation,” *IEEE Trans. Veh. Technol.*, vol. 70, no. 1, pp. 59–68, Jan. 2021, doi: 10.1109/TVT.2020.3045833.
[39] A. A. S. Mohamed, D. Day, A. Meintz, and J. Myungsoo, “Charge Management for an Inductively Charged On-Demand Battery-Electric Shuttle Service with High Penetration of Renewable Energy,” in *Conference Proceedings - IEEE Applied Power Electronics Conference and Exposition - APEC*, 2020, vol. 2020-March, pp. 873–878, doi: 10.1109/APEC39645.2020.9124145.
[40] M. A. Saleem, K. Mahmood, and S. Kumari, “Comments on ‘AKM-IoV: Authenticated Key Management Protocol in Fog Computing-Based Internet of Vehicles Deployment,’” *IEEE Internet Things J.*, 2020, doi: 10.1109/JIOT.2020.2975207.
[41] R. Hussain and S. Zeadally, “Autonomous Cars: Research Results, Issues, and Future Challenges,” *IEEE Communications Surveys and Tutorials*. 2019, doi: 10.1109/COMST.2018.2869360.
[42] SAE International, “J2954B: Wireless Power Transfer for Light-Duty Plug-in/Electric Vehicles and Alignment Methodology - SAE International,” *2019*. [Online]. Available: https://www.sae.org/standards/content/j2954_201904/. [Accessed: 11-Sep-2020].
[43] IEC, “IEC TS 61980-3:2019 | IEC Webstore,” 2019. [Online]. Available: https://webstore.iec.ch/publication/27435. [Accessed: 11-Sep-2020].
[44] ISO, “ISO - ISO 19363:2020 - Electrically propelled road vehicles — Magnetic field wireless power transfer — Safety and interoperability requirements,” *2020*. [Online]. Available: https://www.iso.org/standard/73547.html. [Accessed: 11-Sep-2020].
[45] “ACN-Sim -- An Open-Source Simulator for EV Charging Research.” [Online]. Available: https://ev.caltech.edu/simulator. [Accessed: 12-Sep-2020].
[46] Z. Mahmood, “Connected vehicles in the IoV: Concepts, technologies and architectures,” in *Connected Vehicles in the Internet of Things: Concepts, Technologies and Frameworks for the IoV*, Z. Mahmood, Ed. Springer, Cham, 2020, pp. 3–18.
[47] A. Mahdavian, A. Shojaei, S. McCormick, T. Papandreou, N. Eluru, and A. A. Oloufa, “Drivers and Barriers to Implementation of Connected, Automated, Shared, and Electric Vehicles: An Agenda for Future Research,” *IEEE Access*, vol. 9, pp. 22195–22213, 2021, doi: 10.1109/ACCESS.2021.3056025.

[48] G. Dimitrakopoulos, A. Tsakanikas, and E. Panagiotopoulos, “Latest communication advances for autonomous vehicles,” in *Autonomous Vehicles*, Elsevier, 2021, pp. 33–43.
[49] B. Feroz, A. Mehmood, H. Maryam, S. Zeadally, C. Maple, and M. A. Shah, “Vehicle-Life Interaction in Fog-Enabled Smart Connected and Autonomous Vehicles,” *IEEE Access*, vol. 9, pp. 7402–7420, 2021, doi: 10.1109/ACCESS.2020.3049110.
[50] E. ElGhanam, M. Hassan, A. Osman, and I. Ahmed, “Review of Communication Technologies for Electric Vehicle Charging Management and Coordination,” *World Electr. Veh. J. 2021, Vol. 12, Page 92*, vol. 12, no. 3, p. 92, Jun. 2021, doi: 10.3390/WEVJ12030092.
[51] V. Bobanac, H. Pandzic, and T. Capuder, “Survey on electric vehicles and battery swapping stations: Expectations of existing and future EV owners,” in *2018 IEEE International Energy Conference, ENERGYCON 2018*, 2018, pp. 1–6, doi: 10.1109/ENERGYCON.2018.8398793.
[52] H. Qi and X. Wang, “Electric bus battery-swapping system based on robots,” in *2012 2nd International Conference on Consumer Electronics, Communications and Networks, CECNet 2012 - Proceedings*, 2012, pp. 307–310, doi: 10.1109/CECNet.2012.6202178.
[53] G. Battapothula, C. Yammani, and S. Maheswarapu, “Multi-Objective Optimal Scheduling of Electric Vehicle batteries in Battery Swapping Station,” in *Proceedings of 2019 IEEE PES Innovative Smart Grid Technologies Europe, ISGT-Europe 2019*, 2019, doi: 10.1109/ISGTEurope.2019.8905586.
[54] W. Tao *et al.*, “Integrated optimal configuration of electric vehicle charging and battery-swapping station based on ordered charging strategy,” in *China International Conference on Electricity Distribution, CICED*, 2018, pp. 2237–2241, doi: 10.1109/CICED.2018.8592420.
[55] D. Zheng, F. Wen, and J. Huang, “Optimal planning of battery swap stations,” in *IET Conference Publications*, 2012, vol. 2012, no. 611 CP, doi: 10.1049/cp.2012.1846.
[56] Z. Chen, “The combination of battery swapping system and connected vehicles technology in intelligent transportation,” in *Proceedings - 2020 International Conference on Intelligent Transportation, Big Data and Smart City, ICITBS 2020*, 2020, pp. 72–75, doi: 10.1109/ICITBS49701.2020.00023.
[57] O. Erdinç, “Considering the combinatorial effects of on-site distributed generation and battery-to-X option availability in electric vehicle battery swap station operation,” *Sustain. Energy, Grids Networks*, vol. 26, p. 100472, Jun. 2021, doi: 10.1016/j.segan.2021.100472.
[58] M. Ban, Z. Zhang, C. Li, Z. Li, and Y. Liu, “Optimal scheduling for electric vehicle battery swapping-charging system based on nanogrids,” *Int. J. Electr. Power Energy Syst.*, vol. 130, p. 106967, Sep. 2021, doi: 10.1016/j.ijepes.2021.106967.
[59] A. Asadi and S. Nurre Pinkley, “A stochastic scheduling, allocation, and inventory replenishment problem for battery swap stations,” *Transp. Res. Part E Logist. Transp. Rev.*, vol. 146, p. 102212, Feb. 2021, doi: 10.1016/j.tre.2020.102212.
[60] S. LeVine, “Why Better Place failed with swappable batteries—and your cars might just use them one day,” *Quartz*, 2013. [Online]. Available: https://qz.com/88871/better-place-shai-agassi-swappable-electric-car-batteries/. [Accessed: 13-Mar-2021].
[61] D. Booth, “Motor Mouth: Is battery-swapping the future of EVs? | Driving,” *PostMedia Network Inc.*, 2020. [Online]. Available: https://driving.ca/features/feature-story/motor-mouth-is-battery-swapping-the-future-of-evs. [Accessed: 13-Mar-2021].
[62] Q. Wang, X. Liu, J. Du, and F. Kong, “Smart Charging for Electric Vehicles: A Survey from the Algorithmic Perspective,” *IEEE Commun. Surv. Tutorials*, vol. 18, no. 2, pp.

1500–1517, 2016, doi: 10.1109/COMST.2016.2518628.
[63] C. Zhang, J. Liu, Y. Xiang, Y. Liu, T. Liu, and Y. Zhang, “A coordinated charging strategy for electric vehicle considering three-phase load unbalance,” in *2017 IEEE Transportation Electrification Conference and Expo, Asia-Pacific, ITEC Asia-Pacific 2017*, 2017, doi: 10.1109/ITEC-AP.2017.8080850.
[64] S. Arora, A. T. Abkenar, S. G. Jayasinghe, and K. Tammi, “Charging Technologies and Standards Applicable to Heavy-duty Electric Vehicles,” in *Heavy-Duty Electric Vehicles*, Elsevier, 2021, pp. 135–155.
[65] R. Fachrizal, M. Shepero, D. van der Meer, J. Munkhammar, and J. Widén, “Smart charging of electric vehicles considering photovoltaic power production and electricity consumption: A review,” *eTransportation*, vol. 4. Elsevier B.V., p. 100056, 01-May-2020, doi: 10.1016/j.etran.2020.100056.
[66] T. U. Solanke, V. K. Ramachandaramurthy, J. Y. Yong, J. Pasupuleti, P. Kasinathan, and A. Rajagopalan, “A review of strategic charging–discharging control of grid-connected electric vehicles,” *Journal of Energy Storage*, vol. 28. Elsevier Ltd, p. 101193, 01-Apr-2020, doi: 10.1016/j.est.2020.101193.
[67] S. Hardman *et al.*, “A review of consumer preferences of and interactions with electric vehicle charging infrastructure,” *Transp. Res. Part D Transp. Environ.*, vol. 62, pp. 508–523, Jul. 2018, doi: 10.1016/j.trd.2018.04.002.
[68] M. Oliinyk, J. Dzmura, and D. Pal, “The impact of a electric vehicle charging on the distribution system,” *Proc. - 2020 21st Int. Sci. Conf. Electr. Power Eng. EPE 2020*, Oct. 2020, doi: 10.1109/EPE51172.2020.9269213.
[69] J. linru, Z. yuanxing, L. taoyong, D. xiaohong, and Z. jing, “Analysis on Charging Safety and Optimization of Electric Vehicles,” 2021, pp. 2382–2385, doi: 10.1109/iccc51575.2020.9344906.
[70] A. J. Qarebagh, F. Sabahi, and D. Nazarpour, “Optimized Scheduling for Solving Position Allocation Problem in Electric Vehicle Charging Stations,” in *ICEE 2019 - 27th Iranian Conference on Electrical Engineering*, 2019, pp. 593–597, doi: 10.1109/IranianCEE.2019.8786524.
[71] K. N. Qureshi, A. Alhudhaif, and G. Jeon, “Electric-vehicle energy management and charging scheduling system in sustainable cities and society,” *Sustain. Cities Soc.*, p. 102990, May 2021, doi: 10.1016/j.scs.2021.102990.
[72] N. Aung, W. Zhang, K. Sultan, S. Dhelim, and Y. Ai, “Dynamic traffic congestion pricing and electric vehicle charging management system for the internet of vehicles in smart cities,” *Digit. Commun. Networks*, Feb. 2021, doi: 10.1016/j.dcan.2021.01.002.
[73] A. Waser, “Nikola Tesla’s Wireless Systems,” *André Waser*, 2000. [Online]. Available: https://www.researchgate.net/publication/288824068_Nikola_Tesla’s_Wireless_Systems. [Accessed: 13-Mar-2021].
[74] K. W. Klontz, A. Esser, R. R. Bacon, D. M. Divan, D. W. Novotny, and R. D. Lorenz, “An electric vehicle charging system with ‘universal’ inductive interface,” in *Proceedings of Power Conversion Conference - Yokohama 1993*, 1993, pp. 227–232, doi: 10.1109/PCCON.1993.264219.
[75] General Motors, “Electric Vehicle Charger WM7200 Inductive Charger Owner’s Manual,” 1998. [Online]. Available: http://www.evchargernews.com/miscfiles/gm atv wm7200 owners manual.pdf. [Accessed: 13-Mar-2021].
[76] F. Musavi and W. Eberle, “Overview of wireless power transfer technologies for electric vehicle battery charging,” *IET Power Electron.*, vol. 7, no. 1, pp. 60–66, Jan. 2014, doi: 10.1049/iet-pel.2013.0047.
[77] Y. Chen *et al.*, “A ZVS Grid-Connected Full-Bridge Inverter with a Novel ZVS SPWM Scheme,” *IEEE Trans. Power Electron.*, vol. 31, no. 5, pp. 3626–3638, May 2016, doi:

10.1109/TPEL.2015.2456032.
[78] WiTricity, “Automotive Solutions • WiTricity,” 2020. [Online]. Available: https://witricity.com/products/automotive/. [Accessed: 05-Mar-2021].
[79] G. A. Covic and J. T. Boys, “Modern trends in inductive power transfer for transportation applications,” *IEEE J. Emerg. Sel. Top. Power Electron.*, vol. 1, no. 1, pp. 28–41, 2013, doi: 10.1109/JESTPE.2013.2264473.
[80] R. Thakur and A. NATALE, “High efficiency wireless power transmission at low frequency using permanent magnet coupling,” *Cardiol. Clin.*, vol. 27, no. 1, pp. xv–xv, 2009, doi: 10.14288/1.0067661.
[81] S. Lukic and Z. Pantic, “Cutting the Cord: Static and Dynamic Inductive Wireless Charging of Electric Vehicles,” *IEEE Electrif. Mag.*, vol. 1, no. 1, pp. 57–64, Nov. 2013, doi: 10.1109/mele.2013.2273228.
[82] M. Fuller, “Wireless charging in California: Range, recharge, and vehicle electrification,” *Transp. Res. Part C Emerg. Technol.*, vol. 67, pp. 343–356, Jun. 2016, doi: 10.1016/j.trc.2016.02.013.
[83] C. Qiu, K. T. Chau, C. Liu, and C. C. Chan, “Overview of wireless power transfer for electric vehicle charging,” in *2013 World Electric Vehicle Symposium and Exhibition, EVS 2014*, 2014, doi: 10.1109/EVS.2013.6914731.
[84] “ELIX Opens China Engineering Center in Chongqing | Business Wire,” *Business Wire, Inc.*, 2019. [Online]. Available: https://www.businesswire.com/news/home/20190320005871/en/ELIX-Opens-China-Engineering-Center-in-Chongqing. [Accessed: 14-Mar-2021].
[85] A. P. Hu, C. Liu, and H. L. Li, “A novel contactless battery charging system for soccer playing robot,” in *15th International Conference on Mechatronics and Machine Vision in Practice, M2VIP’08*, 2008, pp. 646–650, doi: 10.1109/MMVIP.2008.4749606.
[86] F. Musavi, M. Edington, and W. Eberle, “Wireless power transfer: A survey of EV battery charging technologies,” in *2012 IEEE Energy Conversion Congress and Exposition, ECCE 2012*, 2012, pp. 1804–1810, doi: 10.1109/ECCE.2012.6342593.
[87] D. C. Ludois, J. K. Reed, and K. Hanson, “Capacitive power transfer for rotor field current in synchronous machines,” *IEEE Trans. Power Electron.*, vol. 27, no. 11, pp. 4638–4645, 2012, doi: 10.1109/TPEL.2012.2191160.
[88] J. Dai and D. C. Ludois, “Wireless electric vehicle charging via capacitive power transfer through a conformal bumper,” in *Conference Proceedings - IEEE Applied Power Electronics Conference and Exposition - APEC*, 2015, vol. 2015-May, no. May, pp. 3307–3313, doi: 10.1109/APEC.2015.7104827.
[89] C. K. Chang, G. G. Da Silva, A. Kumar, S. Pervaiz, and K. K. Afridi, “30 W capacitive wireless power transfer system with 5.8 pF coupling capacitance,” in *2015 IEEE Wireless Power Transfer Conference, WPTC 2015*, 2015, doi: 10.1109/WPT.2015.7140184.
[90] J. Dai and D. C. Ludois, “Capacitive Power Transfer Through a Conformal Bumper for Electric Vehicle Charging,” *IEEE J. Emerg. Sel. Top. Power Electron.*, vol. 4, no. 3, pp. 1015–1025, Sep. 2016, doi: 10.1109/JESTPE.2015.2505622.
[91] S. Sinha, A. Kumar, and K. K. Afridi, “Improved design optimization of efficient matching networks for capacitive wireless power transfer systems,” in *Conference Proceedings - IEEE Applied Power Electronics Conference and Exposition - APEC*, 2018, vol. 2018-March, pp. 3167–3173, doi: 10.1109/APEC.2018.8341554.
[92] C. Liu, A. P. Hu, and N. K. C. Nair, “Coupling study of a rotary capacitive power transfer system,” in *Proceedings of the IEEE International Conference on Industrial Technology*, 2009, doi: 10.1109/ICIT.2009.4939623.
[93] M. Kline, I. Izyumin, B. Boser, and S. Sanders, “Capacitive power transfer for

contactless charging," in *Conference Proceedings - IEEE Applied Power Electronics Conference and Exposition - APEC*, 2011, pp. 1398–1404, doi: 10.1109/APEC.2011.5744775.

[94] J. Kim and F. Bien, "Electric field coupling technique of wireless power transfer for electric vehicles," in *IEEE 2013 Tencon - Spring, TENCONSpring 2013 - Conference Proceedings*, 2013, pp. 267–271, doi: 10.1109/TENCONSpring.2013.6584453.

[95] F. Lu, H. Zhang, H. Hofmann, and C. Mi, "A Double-Sided LCLC-Compensated Capacitive Power Transfer System for Electric Vehicle Charging," *IEEE Trans. Power Electron.*, vol. 30, no. 11, pp. 6011–6014, Nov. 2015, doi: 10.1109/TPEL.2015.2446891.

[96] D. C. Ludois, M. J. Erickson, and J. K. Reed, "Aerodynamic fluid bearings for translational and rotating capacitors in noncontact capacitive power transfer systems," *IEEE Trans. Ind. Appl.*, vol. 50, no. 2, pp. 1025–1033, 2014, doi: 10.1109/TIA.2013.2273484.

[97] A. Ahmad, M. S. Alam, and R. Chabaan, "A Comprehensive Review of Wireless Charging Technologies for Electric Vehicles," *IEEE Trans. Transp. Electrif.*, vol. 4, no. 1, pp. 38–63, Nov. 2017, doi: 10.1109/TTE.2017.2771619.

[98] A. W. S. Putra, H. Kato, and T. Maruyama, "Hybrid optical wireless power and data transmission system," in *2020 IEEE PELS Workshop on Emerging Technologies: Wireless Power Transfer, WoW 2020*, 2020, pp. 374–376, doi: 10.1109/WoW47795.2020.9291276.

[99] S. Raavi *et al.*, "An optical wireless power transfer system for rapid charging," in *Proceedings of the 2013 IEEE Texas Symposium on Wireless and Microwave Circuits and Systems, WMCS 2013*, 2013, doi: 10.1109/WMCaS.2013.6563551.

[100] D. E. Raible, "High intensity laser power beaming for wireless power transmission," *Computer Engineering*, 2008. [Online]. Available: https://engagedscholarship.csuohio.edu/etdarchivehttps://engagedscholarship.csuohio.edu/etdarchive/576. [Accessed: 14-Mar-2021].

[101] B. O. Sadiq, A. A. Olaniyan, A. A. Ibrahim, and O. S. Zakariyya, "Li-Fi: The Future Propagation of Wireless Power Transfer in Vehicular Ad Hoc Networks," in *HORA 2020 - 2nd International Congress on Human-Computer Interaction, Optimization and Robotic Applications, Proceedings*, 2020, doi: 10.1109/HORA49412.2020.9152927.

[102] H. Rezaie, A. P. Hu, H. F. Leung, and R. Cordell, "New attachment method to increase the performance of ultrasonic wireless power transfer system," in *2017 IEEE PELS Workshop on Emerging Technologies: Wireless Power Transfer, WoW 2017*, 2017, pp. 25–29, doi: 10.1109/WoW.2017.7959359.

[103] O. Shaul, S. Boaz, and S. Doron, "Non-invasive sensing of the electrical energy harvested by medical implants powered by an ultrasonic transcutaneous energy transfer link," in *IEEE International Symposium on Industrial Electronics*, 2012, pp. 1153–1157, doi: 10.1109/ISIE.2012.6237251.

[104] C. Wei, S. Surappa, and F. L. Degertekin, "Experimental verification and design guidelines for efficient ultrasonic power transfer using capacitive parametric ultrasonic transducers," in *IEEE International Ultrasonics Symposium, IUS*, 2020, vol. 2020-September, doi: 10.1109/IUS46767.2020.9251408.

[105] K. Lee, J. Kim, and C. Cha, "Microwave-based Wireless Power Transfer using Beam Scanning for Wireless Sensors," in *EUROCON 2019 - 18th International Conference on Smart Technologies*, 2019, doi: 10.1109/EUROCON.2019.8861838.

[106] N. Shinohara, Y. Kubo, and H. Tonomura, "Wireless charging for electric vehicle with microwaves," in *2013 3rd International Electric Drives Production Conference, EDPC 2013 - Proceedings*, 2013, doi: 10.1109/EDPC.2013.6689750.

[107] N. Shinohara, “Wireless charging system of electric bicycle via microwave,” in *2019 URSI Asia-Pacific Radio Science Conference, AP-RASC 2019*, 2019, doi: 10.23919/URSIAP-RASC.2019.8738144.
[108] S. T. Khang, D. J. Lee, I. J. Hwang, T. D. Yeo, and J. W. Yu, “Microwave power transfer with optimal number of rectenna arrays for midrange applications,” *IEEE Antennas Wirel. Propag. Lett.*, vol. 17, no. 1, pp. 155–159, Jan. 2018, doi: 10.1109/LAWP.2017.2778507.
[109] S. Hasanzadeh, S. Vaez-Zadeh, and A. H. Isfahani, “Optimization of a contactless power transfer system for electric vehicles,” *IEEE Trans. Veh. Technol.*, vol. 61, no. 8, pp. 3566–3573, 2012, doi: 10.1109/TVT.2012.2209464.
[110] M. Budhia, J. T. Boys, G. A. Covic, and C. Y. Huang, “Development of a single-sided flux magnetic coupler for electric vehicle IPT charging systems,” *IEEE Trans. Ind. Electron.*, vol. 60, no. 1, pp. 318–328, 2013, doi: 10.1109/TIE.2011.2179274.
[111] N. Liu and T. G. Habetler, “Design of a Universal Inductive Charger for Multiple Electric Vehicle Models,” *IEEE Trans. Power Electron.*, vol. 30, no. 11, pp. 6378–6390, Nov. 2015, doi: 10.1109/TPEL.2015.2394734.
[112] P. Tiwari and N. R. Tummuru, “Misalignment Tolerant Primary Controller for Series-Series Compensated Static Wireless Charging of Battery,” in *2019 IEEE Transportation Electrification Conference, ITEC-India 2019*, 2019, doi: 10.1109/ITEC-India48457.2019.ITECIndia2019-262.
[113] L. L. Tan, X. L. Huang, H. Huang, Y. W. Zou, and H. Li, “Transfer efficiency optimal control of magnetic resonance coupled system of wireless power transfer based on frequency control,” *Sci. China Technol. Sci.*, vol. 54, no. 6, pp. 1428–1434, Jun. 2011, doi: 10.1007/s11431-011-4380-6.
[114] Z. H. Wang, Y. P. Li, Y. Sun, C. Sen Tang, and X. Lv, “Load detection model of voltage-fed inductive power transfer system,” *IEEE Trans. Power Electron.*, vol. 28, no. 11, pp. 5233–5243, 2013, doi: 10.1109/TPEL.2013.2243756.
[115] X. Dai, Y. Sun, C. Tang, Z. Wang, Y. Su, and Y. Li, “Dynamic parameters identification method for inductively coupled power transfer system,” in *2010 IEEE International Conference on Sustainable Energy Technologies, ICSET 2010*, 2010, doi: 10.1109/ICSET.2010.5684445.
[116] W. Fu, B. Zhang, and D. Qiu, “Study on frequency-tracking wireless power transfer system by resonant coupling,” in *2009 IEEE 6th International Power Electronics and Motion Control Conference, IPEMC ’09*, 2009, pp. 2658–2663, doi: 10.1109/IPEMC.2009.5157857.
[117] J. Liu, Z. Liu, and H. Su, “A closed-loop control strategy of maximum efficiency point tracking for wireless power charging system,” in *2020 IEEE Wireless Power Transfer Conference, WPTC 2020*, 2020, pp. 395–398, doi: 10.1109/WPTC48563.2020.9295597.
[118] R. Mai, Y. Liu, Y. Li, P. Yue, G. Cao, and Z. He, “An Active-Rectifier-Based Maximum Efficiency Tracking Method Using an Additional Measurement Coil for Wireless Power Transfer,” *IEEE Trans. Power Electron.*, vol. 33, no. 1, pp. 716–728, Jan. 2018, doi: 10.1109/TPEL.2017.2665040.
[119] D. Baros, N. Rigogiannis, P. Drougas, D. Voglitsis, and N. Papanikolaou, “Transmitter Side Control of a Wireless EV Charger employing IoT,” *IEEE Access*, 2020, doi: 10.1109/ACCESS.2020.3045803.
[120] D. J. Thrimawithana and U. K. Madawala, “A primary side controller for inductive power transfer systems,” in *Proceedings of the IEEE International Conference on Industrial Technology*, 2010, pp. 661–666, doi: 10.1109/ICIT.2010.5472724.
[121] W. X. Zhong and S. Y. R. Hui, “Maximum energy efficiency tracking for wireless power

transfer systems," *IEEE Trans. Power Electron.*, vol. 30, no. 7, pp. 4025–4034, Jul. 2015, doi: 10.1109/TPEL.2014.2351496.
[122] J. M. Miller, O. C. Onar, and M. Chinthavali, "Primary-side power flow control of wireless power transfer for electric vehicle charging," *IEEE J. Emerg. Sel. Top. Power Electron.*, 2015, doi: 10.1109/JESTPE.2014.2382569.
[123] W. G. Seward *et al.*, "Modelling of Static Wireless Electric Vehicle Charging and its Impact on a Typical Gb Distribution Network," in *2019 54th International Universities Power Engineering Conference, UPEC 2019 - Proceedings*, 2019, doi: 10.1109/UPEC.2019.8893603.
[124] A. Meintz, R. Prohaska, A. Konan, A. Ragatz, T. Markel, and K. Kelly, "Analysis of in-route wireless charging for the shuttle system at Zion National Park," in *IEEE PELS Workshop on Emerging Technologies: Wireless Power, WoW 2016*, 2016, pp. 191–195, doi: 10.1109/WoW.2016.7772090.
[125] M. Kesler, "Highly Resonant Wireless Power Transfer: Safe, Efficient, and over Distance," *WiTricity Corp*, 2017. [Online]. Available: http://large.stanford.edu/courses/2016/ph240/surakitbovorn1/docs/kesler.pdf. [Accessed: 29-Sep-2020].
[126] WiTricity Corporation, "Leave the Filling Station Behind," *WiTricity Corp*, 2019. [Online]. Available: http://witricity.com/wp-content/uploads/2019/01/Tech-Paper_Leave-the-filling-station-behind_Jan-2019.pdf. [Accessed: 05-Mar-2021].
[127] WiTricity Corporation, "DRIVE 11 Evaluation System Wireless charging for EV & PHEV Platforms." [Online]. Available: https://witricity.com/wp-content/uploads/2019/11/DRIVE_11_20191104-1.pdf. [Accessed: 14-Apr-2021].
[128] P. P. Inc., "The 2nd Generation Plugless system - wireless EV charging for the future," 2021. [Online]. Available: https://www.pluglesspower.com/learn/2nd-generation-plugless/. [Accessed: 05-Mar-2021].
[129] EVATRAN Group, "PLUGLESS WIRELESS CHARGING FOR ELECTRIC VEHICLES," 2017. [Online]. Available: https://www.pluglesspower.com/wp-content/uploads/2017/03/Digital_Brochure_Generic.pdf. [Accessed: 05-Mar-2021].
[130] EVATRAN Group, "Plugless™ Level 2 EV Charging System (3.3kW) System Features," 2014. [Online]. Available: https://www.pluglesspower.com/wp-content/uploads/2014/02/Plugless_Tech_Specs.pdf. [Accessed: 05-Mar-2021].
[131] Plugless Power Inc., "Meet Plugless | The Wireless EV Charging Station," 2021. [Online]. Available: https://www.pluglesspower.com/. [Accessed: 05-Mar-2021].
[132] V. Cirimele, F. Freschi, and M. Mitolo, "Inductive power transfer for automotive applications: State-of-the-art and future trends," in *IEEE Industry Application Society, 52nd Annual Meeting: IAS 2016*, 2016, doi: 10.1109/IAS.2016.7731966.
[133] A. Brecher and D. Arthur, "Review and Evaluation of Wireless Power Transfer (WPT) for Electric Transit Applications," *FTA Res.*, no. FTA Report 0060, p. 61, 2014.
[134] P. Bansal, "Charging of electric vehicles: Technology and policy implications," *J. Sci. Policy Gov.*, 2015.
[135] WAVE official website, "Wireless Advanced Vehicle Electrification - Inductive Charging," 2019. [Online]. Available: https://waveipt.com/. [Accessed: 15-Mar-2021].
[136] F. Chen, N. Taylor, and N. Kringos, "Electrification of roads: Opportunities and challenges," *Applied Energy*, vol. 150. Elsevier Ltd, pp. 109–119, 05-Jul-2015, doi: 10.1016/j.apenergy.2015.03.067.
[137] M. Barth and S. Shaheen, "Policy and behavior research at the California partners for advanced highways and transit (PATH)," in *IEEE Conference on Intelligent Transportation Systems, Proceedings, ITSC*, 2006, pp. 17–22, doi: 10.1109/itsc.2006.1706712.

[138] M. Tomizuka, “Advanced vehicle control systems (AVCS) research for automated highway systems in California PATH,” 2002, pp. PLEN41–PLEN45, doi: 10.1109/vnis.1994.396876.
[139] S. E. Shladover, “Highway Electrification And Automation,” *UC Berkeley: California Partners for Advanced Transportation Technology*, 1992. [Online]. Available: https://escholarship.org/uc/item/8kk9d7f7. [Accessed: 15-Mar-2021].
[140] Systems Control Technology Inc., “Roadway Powered Electric Vehicle Project Track Construction And Testing Program Phase 3D,” *UC Berkeley: California Partners for Advanced Transportation Technology*, 1994. [Online]. Available: http://www.escholarship.org/uc/item/1jr98590. [Accessed: 14-Mar-2021].
[141] O. C. Onar, J. M. Miller, S. L. Campbell, C. Coomer, C. P. White, and L. E. Seiber, “A novel wireless power transfer for in-motion EV/PHEV charging,” in *Conference Proceedings - IEEE Applied Power Electronics Conference and Exposition - APEC*, 2013, pp. 3073–3080, doi: 10.1109/APEC.2013.6520738.
[142] O. C. Onar, J. M. Miller, S. L. Campbell, C. Coomer, C. P. White, and L. E. Seiber, “Oak ridge national laboratory wireless power transfer development for sustainable campus initiative,” in *2013 IEEE Transportation Electrification Conference and Expo: Components, Systems, and Power Electronics - From Technology to Business and Public Policy, ITEC 2013*, 2013, doi: 10.1109/ITEC.2013.6574506.
[143] J. M. Miller, P. T. Jones, J. M. Li, and O. C. Onar, “ORNL experience and challenges facing dynamic wireless power charging of EV’s,” *IEEE Circuits Syst. Mag.*, vol. 15, no. 2, pp. 40–53, Apr. 2015, doi: 10.1109/MCAS.2015.2419012.
[144] Oak Ridge National Laboratory, “ORNL demonstrates 120kW wireless charging for vehicles,” 2018. [Online]. Available: https://www.ornl.gov/news/ornl-demonstrates-120-kilowatt-wireless-charging-vehicles. [Accessed: 11-Mar-2021].
[145] M. Anderson, “Oak Ridge Inches Closer to 15-Minute Wireless EV Charging - IEEE Spectrum,” *IEEE Spectrum*, 2018. [Online]. Available: https://spectrum.ieee.org/energywise/energy/environment/oak-ridge-inches-closer-to-15minute-wireless-ev-charging. [Accessed: 11-Mar-2021].
[146] S. Y. Choi, B. W. Gu, S. Y. Jeong, and C. T. Rim, “Advances in wireless power transfer systems for roadway-powered electric vehicles,” *IEEE J. Emerg. Sel. Top. Power Electron.*, vol. 3, no. 1, pp. 18–36, Mar. 2015, doi: 10.1109/JESTPE.2014.2343674.
[147] S. Ahn, N. P. Suh, and D.-H. Cho, “The All-Electric Car You Never Plug In - IEEE Spectrum,” *IEEE Spectrum*, 2013. [Online]. Available: https://spectrum.ieee.org/transportation/advanced-cars/the-allelectric-car-you-never-plug-in. [Accessed: 15-Mar-2021].
[148] N. P. Suh and D. H. Cho, “Making the move: From internal combustion engines to wireless electric vehicles,” in *The On-line Electric Vehicle: Wireless Electric Ground Transportation Systems*, N. P. Suh and D. H. Cho, Eds. Springer, Cham, 2017, pp. 3–15.
[149] J. Kim *et al.*, “Coil design and shielding methods for a magnetic resonant wireless power transfer system,” *Proc. IEEE*, vol. 101, no. 6, pp. 1332–1342, 2013, doi: 10.1109/JPROC.2013.2247551.
[150] Y. J. Jang, Y. D. Ko, and S. Jeong, “Optimal design of the wireless charging electric vehicle,” in *2012 IEEE International Electric Vehicle Conference, IEVC 2012*, 2012, doi: 10.1109/IEVC.2012.6183294.
[151] Y. J. Jang, E. S. Suh, and J. W. Kim, “System architecture and mathematical models of electric transit bus system utilizing wireless power transfer technology,” *IEEE Syst. J.*, vol. 10, no. 2, pp. 495–506, Jun. 2016, doi: 10.1109/JSYST.2014.2369485.
[152] S. Jeong, Y. J. Jang, and D. Kum, “Economic Analysis of the Dynamic Charging Electric

Vehicle," *IEEE Trans. Power Electron.*, vol. 30, no. 11, pp. 6368–6377, Nov. 2015, doi: 10.1109/TPEL.2015.2424712.
[153] Y. J. Jang, S. Jeong, and Y. D. Ko, "System optimization of the On-Line Electric Vehicle operating in a closed environment," *Comput. Ind. Eng.*, vol. 80, pp. 222–235, Feb. 2015, doi: 10.1016/j.cie.2014.12.004.
[154] C. H. Lee, G. Jung, K. Al Hosani, B. Song, D. K. Seo, and D. Cho, "Wireless power transfer system for an autonomous electric vehicle," in *2020 IEEE Wireless Power Transfer Conference, WPTC 2020*, 2020, pp. 467–470, doi: 10.1109/WPTC48563.2020.9295631.
[155] K. Yeon-soo, "ICT minister nominee accused of wasting research money," *The Korea Times*, 2019. [Online]. Available: https://www.koreatimes.co.kr/www/tech/2019/04/325_265924.html. [Accessed: 11-Mar-2021].
[156] J. P. K. Sampath, D. M. Vilathgamuwa, and A. Alphones, "Efficiency Enhancement for Dynamic Wireless Power Transfer System with Segmented Transmitter Array," *IEEE Trans. Transp. Electrif.*, vol. 2, no. 1, pp. 76–85, Mar. 2016, doi: 10.1109/TTE.2015.2508721.
[157] J. Shin *et al.*, "Design and implementation of shaped magnetic-resonance-based wireless power transfer system for roadway-powered moving electric vehicles," *IEEE Trans. Ind. Electron.*, vol. 61, no. 3, pp. 1179–1192, 2014, doi: 10.1109/TIE.2013.2258294.
[158] J. Zhao, T. Cai, S. Duan, H. Feng, C. Chen, and X. Zhang, "A General Design Method of Primary Compensation Network for Dynamic WPT System Maintaining Stable Transmission Power," *IEEE Trans. Power Electron.*, vol. 31, no. 12, pp. 8343–8358, Dec. 2016, doi: 10.1109/TPEL.2016.2516023.
[159] J. Huh, S. W. Lee, W. Y. Lee, G. H. Cho, and C. T. Rim, "Narrow-width inductive power transfer system for online electrical vehicles," *IEEE Trans. Power Electron.*, vol. 26, no. 12, pp. 3666–3679, 2011, doi: 10.1109/TPEL.2011.2160972.
[160] S. Y. Choi, S. Y. Jeong, B. W. Gu, G. C. Lim, and C. T. Rim, "Ultraslim S-Type Power Supply Rails for Roadway-Powered Electric Vehicles Generalized Models on Self-Decoupled Dual Pick-Up Coils for a Large Lateral Tolerance," *IEEE Trans. Power Electron.*, vol. 30, no. 11, pp. 6456–6468, Nov. 2015, doi: 10.1109/TPEL.2015.2444894.
[161] C. Park, S. Lee, S. Y. Jeong, G. H. Cho, and C. T. Rim, "Uniform Power I-Type Inductive Power Transfer System with DQ-Power Supply Rails for On-Line Electric Vehicles," *IEEE Trans. Power Electron.*, vol. 30, no. 11, pp. 6446–6455, Nov. 2015, doi: 10.1109/TPEL.2015.2420372.
[162] F. Lu, H. Zhang, H. Hofmann, and C. C. Mi, "A Dynamic Charging System with Reduced Output Power Pulsation for Electric Vehicles," *IEEE Trans. Ind. Electron.*, vol. 63, no. 10, pp. 6580–6590, Oct. 2016, doi: 10.1109/TIE.2016.2563380.
[163] Y. Guo, L. Wang, Q. Zhu, C. Liao, and F. Li, "Switch-On Modeling and Analysis of Dynamic Wireless Charging System Used for Electric Vehicles," *IEEE Trans. Ind. Electron.*, vol. 63, no. 10, pp. 6568–6579, Oct. 2016, doi: 10.1109/TIE.2016.2557302.
[164] G. Buja, M. Bertoluzzo, and H. K. Dashora, "Lumped Track Layout Design for Dynamic Wireless Charging of Electric Vehicles," *IEEE Trans. Ind. Electron.*, vol. 63, no. 10, pp. 6631–6640, Oct. 2016, doi: 10.1109/TIE.2016.2538738.
[165] Q. Zhu, Y. Guo, L. Wang, S. Li, and C. Liao, "Neighboring Effects on the Deactivated Inverter in a Segmented Dynamic Wireless EV Charging System," in *2018 International Power Electronics Conference, IPEC-Niigata - ECCE Asia 2018*, 2018, pp. 3338–3343, doi: 10.23919/IPEC.2018.8507770.
[166] Wei Zhang, Siu-Chung Wong, C. K. Tse, and Qianhong Chen, "An Optimized Track

Length in Roadway Inductive Power Transfer Systems," *IEEE J. Emerg. Sel. Top. Power Electron.*, vol. 2, no. 3, pp. 598–608, Mar. 2014, doi: 10.1109/jestpe.2014.2301460.
[167] Q. Zhu, L. Wang, Y. Guo, C. Liao, and F. Li, "Applying LCC Compensation Network to Dynamic Wireless EV Charging System," *IEEE Trans. Ind. Electron.*, vol. 63, no. 10, pp. 6557–6567, Oct. 2016, doi: 10.1109/TIE.2016.2529561.
[168] S. Zhou and C. Chris Mi, "Multi-Paralleled LCC Reactive Power Compensation Networks and Their Tuning Method for Electric Vehicle Dynamic Wireless Charging," *IEEE Trans. Ind. Electron.*, vol. 63, no. 10, pp. 6546–6556, Oct. 2016, doi: 10.1109/TIE.2015.2512236.
[169] A. Kamineni, M. J. Neath, A. Zaheer, G. A. Covic, and J. T. Boys, "Interoperable EV detection for dynamic wireless charging with existing hardware and free resonance," *IEEE Trans. Transp. Electrif.*, vol. 3, no. 2, pp. 370–379, 2017, doi: 10.1109/TTE.2016.2631607.
[170] X. Liu, W. Han, C. Liu, and P. Pong, "Marker-free coil-misalignment detection approach using tmr sensor array for dynamic wireless charging system of electric vehicles," in *2018 IEEE International Magnetic Conference, INTERMAG 2018*, 2018, doi: 10.1109/INTMAG.2018.8508064.
[171] J. W. Jeong, S. H. Ryu, B. K. Lee, and H. J. Kim, "Tech tree study on foreign object detection technology in wireless charging system for electric vehicles," in *INTELEC, International Telecommunications Energy Conference (Proceedings)*, 2016, vol. 2016-September, doi: 10.1109/INTLEC.2015.7572294.
[172] T. Sonnenberg, A. Stevens, A. Dayerizadeh, and S. Lukic, "Combined foreign object detection and live object protection in wireless power transfer systems via real-time thermal camera analysis," in *Conference Proceedings - IEEE Applied Power Electronics Conference and Exposition - APEC*, 2019, vol. 2019-March, pp. 1547–1552, doi: 10.1109/APEC.2019.8721804.
[173] J. Lu, G. Zhu, and C. C. Mi, "Foreign object detection in wireless power transfer systems," *IEEE Trans. Ind. Appl.*, pp. 1–1, Feb. 2021, doi: 10.1109/tia.2021.3057603.
[174] G. C. Jang, S. Y. Jeong, H. G. Kwak, and C. T. Rim, "Metal object detection circuit with non-overlapped coils for wireless EV chargers," in *2016 IEEE 2nd Annual Southern Power Electronics Conference, SPEC 2016*, 2016, doi: 10.1109/SPEC.2016.7846132.
[175] G. R. Nagendra, L. Chen, G. A. Covic, and J. T. Boys, "Detection of EVs on IPT Highways," *IEEE J. Emerg. Sel. Top. Power Electron.*, vol. 2, no. 3, pp. 584–597, Feb. 2014, doi: 10.1109/jestpe.2014.2308307.
[176] Q. Deng *et al.*, "Edge position detection of on-line charged vehicles with segmental wireless power supply," *IEEE Transactions on Vehicular Technology*, vol. 66, no. 5. Institute of Electrical and Electronics Engineers Inc., pp. 3610–3621, 01-May-2017, doi: 10.1109/TVT.2016.2598183.
[177] L. A. L. Cardoso, J. L. Afonso, M. C. Martinez, and A. A. N. Melendez, "RFID-triggered power activation for smart dynamic inductive wireless power transfer," in *Proceedings IECON 2017 - 43rd Annual Conference of the IEEE Industrial Electronics Society*, 2017, vol. 2017-January, pp. 6967–6973, doi: 10.1109/IECON.2017.8217218.
[178] A. Azad, V. Kulyukin, and Z. Pantic, "Misalignment Tolerant DWPT Charger for EV Roadways with Integrated Foreign Object Detection and Driver Feedback System," in *ITEC 2019 - 2019 IEEE Transportation Electrification Conference and Expo*, 2019, doi: 10.1109/ITEC.2019.8790600.
[179] J. Sanz and L. G. Duarte, "UNPLUGGED-D2.4 Data Analysis and Conclusions APP v260515," 2015. [Online]. Available: http://unplugged.enide.eu/wordpress/wp-content/uploads/2015/12/D2.4-Data Analysis and Conclusions.pdf. [Accessed: 15-Mar-

2021].
[180] Z. Ai, Y. Liu, F. Song, and H. Zhang, “A Smart Collaborative Charging Algorithm for Mobile Power Distribution in 5G Networks,” *IEEE Access*, vol. 6, pp. 28668–28679, Apr. 2018, doi: 10.1109/ACCESS.2018.2818790.
[181] A. Echols, S. Mukherjee, M. Mickelsen, and Z. Pantic, “Communication infrastructure for dynamic wireless charging of electric vehicles,” in *IEEE Wireless Communications and Networking Conference, WCNC*, 2017, doi: 10.1109/WCNC.2017.7925821.
[182] M. A. Al-Absi, A. A. Al-Absi, and H. J. Lee, “Comparison between DSRC and other Short Range Wireless Communication Technologies,” in *International Conference on Advanced Communication Technology, ICACT*, 2020, vol. 2020, pp. 1–5, doi: 10.23919/ICACT48636.2020.9061543.
[183] A. G. Batres, A. Moghe, and J. Taiber, “A communication architecture for wireless power transfer services based on DSRC technology,” in *2016 IEEE Transportation Electrification Conference and Expo, ITEC 2016*, 2016, doi: 10.1109/ITEC.2016.7520269.
[184] Naseeruddin and V. C. Patil, “Issues faced in the experimental evaluation of ZigBee based battery status monitoring and wireless charge sharing system,” in *Proceedings of the 2017 2nd IEEE International Conference on Electrical, Computer and Communication Technologies, ICECCT 2017*, 2017, doi: 10.1109/ICECCT.2017.8117922.
[185] K. L. Lam, K. T. Ko, H. Y. Tung, H. C. Tung, K. F. Tsang, and L. L. Lai, “ZigBee electric vehicle charging system,” in *Digest of Technical Papers - IEEE International Conference on Consumer Electronics*, 2011, pp. 507–508, doi: 10.1109/ICCE.2011.5722709.
[186] “Multi V2X channels resource allocation algorithms for D2D 5G network performance enhancement,” *Veh. Commun.*, p. 100371, May 2021, doi: 10.1016/J.VEHCOM.2021.100371.
[187] A. Rana, A. Taneja, and N. Saluja, “Accelerating IoT applications new wave with 5G: A review,” *Mater. Today Proc.*, Apr. 2021, doi: 10.1016/j.matpr.2021.03.292.
[188] A. Sarker *et al.*, “An Efficient Wireless Power Transfer System to Balance the State of Charge of Electric Vehicles,” in *Proceedings of the International Conference on Parallel Processing*, 2016, vol. 2016-September, pp. 324–333, doi: 10.1109/ICPP.2016.44.
[189] R. Riemann, D. Z. W. Wang, and F. Busch, “Optimal location of wireless charging facilities for electric vehicles: Flow capturing location model with stochastic user equilibrium,” *Transp. Res. Part C Emerg. Technol.*, vol. 58, no. Part A, pp. 1–12, Sep. 2015, doi: 10.1016/j.trc.2015.06.022.
[190] Z. Bi *et al.*, “Life cycle assessment and tempo-spatial optimization of deploying dynamic wireless charging technology for electric cars,” *Transp. Res. Part C Emerg. Technol.*, vol. 100, pp. 53–67, Mar. 2019, doi: 10.1016/j.trc.2019.01.002.
[191] Z. Chen, F. He, and Y. Yin, “Optimal deployment of charging lanes for electric vehicles in transportation networks,” *Transp. Res. Part B Methodol.*, vol. 91, pp. 344–365, Sep. 2016, doi: 10.1016/j.trb.2016.05.018.
[192] H. Ushijima-Mwesigwa, M. Z. Khan, M. A. Chowdhury, and I. Safro, “Optimal Installation for Electric Vehicle Wireless Charging Lanes,” *J. Ind. Manag. Optim.*, vol. 17, no. 3, pp. 1315–1341, 2017, doi: 10.3934/jimo.2020023.
[193] T. D. Chen, K. M. Kockelman, and J. P. Hanna, “Operations of a shared, autonomous, electric vehicle fleet: Implications of vehicle & charging infrastructure decisions,” *Transp. Res. Part A Policy Pract.*, vol. 94, pp. 243–254, Dec. 2016, doi: 10.1016/j.tra.2016.08.020.

[194] M. Tajmohammadi, S. M. Mazinani, M. Nikooghadam, and Z. Al-Hamdawee, “LSPP: Lightweight and Secure Payment Protocol for Dynamic Wireless Charging of Electric Vehicles in Vehicular Cloud,” *IEEE Access*, vol. 7, pp. 148424–148438, 2019, doi: 10.1109/ACCESS.2019.2946241.
[195] M. Pazos-Revilla, A. Alsharif, S. Gunukula, T. N. Guo, M. Mahmoud, and X. Shen, “Secure and Privacy-Preserving Physical-Layer-Assisted Scheme for EV Dynamic Charging System,” *IEEE Trans. Veh. Technol.*, vol. 67, no. 4, pp. 3304–3318, Apr. 2018, doi: 10.1109/TVT.2017.2780179.
[196] X. Zhao, J. Lin, and H. Li, “Privacy-preserving billing scheme against free-riders for wireless charging electric vehicles,” *Mob. Inf. Syst.*, 2017, doi: 10.1155/2017/1325698.
[197] S. Arora, S. Goel, P. Chhikara, H. Singh, N. Kumar, and P. S. Rana, “An efficient scheme for wireless charging of electric vehicles using RFID with an optimal path planning,” in *2019 IEEE Globecom Workshops, GC Wkshps 2019 - Proceedings*, 2019, doi: 10.1109/GCWkshps45667.2019.9024537.
[198] K. Rabieh and M. Wei, “Efficient and privacy-aware authentication scheme for EVs pre-paid wireless charging services,” in *IEEE International Conference on Communications*, 2017, doi: 10.1109/ICC.2017.7996868.
[199] G. F. Savari, V. Krishnasamy, J. Sathik, Z. M. Ali, and S. H. E. Abdel Aleem, “Internet of Things based real-time electric vehicle load forecasting and charging station recommendation,” *ISA Trans.*, vol. 97, pp. 431–447, Feb. 2020, doi: 10.1016/j.isatra.2019.08.011.
[200] Z. Danping, L. Juan, C. Yuchun, L. Yuhang, and C. Zhongjian, “Research on electric energy metering and charging system for dynamic wireless charging of electric vehicle,” in *4th International Conference on Intelligent Transportation Engineering, ICITE 2019*, 2019, pp. 252–255, doi: 10.1109/ICITE.2019.8880214.
[201] A. Triviño-Cabrera, J. A. Aguado, and S. de la Torre, “Joint routing and scheduling for electric vehicles in smart grids with V2G,” *Energy*, vol. 175, pp. 113–122, May 2019, doi: 10.1016/j.energy.2019.02.184.
[202] R. Iacobucci, B. McLellan, and T. Tezuka, “Optimization of shared autonomous electric vehicles operations with charge scheduling and vehicle-to-grid,” *Transp. Res. Part C Emerg. Technol.*, vol. 100, pp. 34–52, Mar. 2019, doi: 10.1016/j.trc.2019.01.011.
[203] F. V. Cerna, M. Pourakbari-Kasmaei, R. A. Romero, and M. J. Rider, “Optimal delivery scheduling and charging of EVs in the navigation of a city map,” *IEEE Trans. Smart Grid*, vol. 9, no. 5, pp. 4815–4827, Sep. 2018, doi: 10.1109/TSG.2017.2672801.
[204] C. Liu, J. Wu, and C. Long, “Joint charging and routing optimization for electric vehicle navigation systems,” in *IFAC Proceedings Volumes (IFAC-PapersOnline)*, 2014, vol. 19, no. 3, pp. 2106–2111, doi: 10.3182/20140824-6-za-1003.01532.
[205] O. Simon and D. Shkadarevich, “Application of V2G communication for wireless interoperable power transfer,” in *2017 12th International Conference on Ecological Vehicles and Renewable Energies, EVER 2017*, 2017, doi: 10.1109/EVER.2017.7935929.
[206] Y. Benomar, M. El Baghdadi, O. Hegazy, Y. Yang, M. Messagie, and J. Van Mierlo, “Design and modeling of V2G inductive charging system for light-duty Electric Vehicles,” in *2017 12th International Conference on Ecological Vehicles and Renewable Energies, EVER 2017*, 2017, doi: 10.1109/EVER.2017.7935932.
[207] H. Ben Sassi, F. Errahimi, N. Essbai, and C. Alaoui, “V2G and wireless V2G concepts: State of the art and current challenges,” in *2019 International Conference on Wireless Technologies, Embedded and Intelligent Systems, WITS 2019*, 2019, doi: 10.1109/WITS.2019.8723851.
[208] Oak Ridge National Laboratory, “Successful delivery: ORNL demonstrates bi-

directional wireless charging on hybrid UPS truck | ORNL," 2020. [Online]. Available: https://www.ornl.gov/news/successful-delivery-ornl-demonstrates-bi-directional-wireless-charging-hybrid-ups-truck. [Accessed: 11-Mar-2021].
[209] Z. Fan, Z. Jie, and Q. Yujie, "A Survey on Wireless Power Transfer based Charging Scheduling Schemes in Wireless Rechargeable Sensor Networks," in *2018 IEEE 4th International Conference on Control Science and Systems Engineering, ICCSSE 2018*, 2018, pp. 194–198, doi: 10.1109/CCSSE.2018.8724809.
[210] G. Li, Q. Sun, L. Boukhatem, J. Wu, and J. Yang, "Intelligent vehicle-to-vehicle charging navigation for mobile electric vehicles via vanet-based communication," *IEEE Access*, vol. 7, pp. 170888–170906, 2019, doi: 10.1109/ACCESS.2019.2955927.
[211] D. Kosmanos *et al.*, "Route Optimization of Electric Vehicles Based on Dynamic Wireless Charging," *IEEE Access*, vol. 6, pp. 42551–42565, Jul. 2018, doi: 10.1109/ACCESS.2018.2847765.
[212] V. Chauhan and A. Gupta, "Scheduling Mobile Charging Stations for Electric Vehicle Charging," in *International Conference on Wireless and Mobile Computing, Networking and Communications*, 2018, vol. 2018-October, pp. 131–136, doi: 10.1109/WiMOB.2018.8589146.
[213] M. Sato, G. Yamamoto, T. Imura, and H. Fujimoto, "Experimental verification of wireless in-wheel motor using magnetic resonance coupling," in *9th International Conference on Power Electronics - ECCE Asia: "Green World with Power Electronics", ICPE 2015-ECCE Asia*, 2015, pp. 1667–1672, doi: 10.1109/ICPE.2015.7168001.
[214] T. Takeuchi, T. Imura, H. Fujimoto, and Y. Hori, "Power management of Wireless In-Wheel Motor by SOC control of wheel side Lithium-ion Capacitor," in *IECON Proceedings (Industrial Electronics Conference)*, 2016, pp. 4547–4552, doi: 10.1109/IECON.2016.7793109.
[215] H. Fujimoto, O. Shimizu, S. Nagai, T. Fujita, D. Gunji, and Y. Ohmori, "Development of wireless in-wheel motors for dynamic charging: From 2nd to 3rd generation," in *2020 IEEE PELS Workshop on Emerging Technologies: Wireless Power Transfer, WoW 2020*, 2020, pp. 56–61, doi: 10.1109/WoW47795.2020.9291287.
[216] Y. Guo *et al.*, "Thin, stretchable, universal wireless power transfer system for electric vehicle charging," 2020, doi: 10.1039/d0ra05379a.
[217] T. Dimsdale, "Rules of the Road: The Geopolitics of Electric Vehicles in Eurasia," *E3G*, 2019. [Online]. Available: https://www.jstor.org/stable/resrep21841.9?seq=1#metadata_info_tab_contents.
[218] T. Krisher, "AAA: Cold weather can cut electric car range over 40 percent," 2019. [Online]. Available: https://apnews.com/04029bd1e0a94cd59ff9540a398c12d1. [Accessed: 13-Mar-2021].
[219] Union of Concerned Scientists., "Electric Vehicle Survey Findings and Methodology," *Union of Concerned Scientists.*, 2019. [Online]. Available: http://www.jstor.org/stable/resrep24093.
[220] B. Usher, "THE RISE OF ELECTRIC VEHICLES," in *Renewable Energy: A Primer for the Twenty-First Century*, New York; Chichester, West Sussex: Columbia University Press, 2019, pp. 81–95.
[221] A. Trivedi, "The $6-trillion barrier holding back electric cars | Driving," 2018. [Online]. Available: https://driving.ca/auto-news/news/the-6-trillion-barrier-holding-back-electric-cars. [Accessed: 13-Mar-2021].
[222] D. Pinner, S. Knupfer, and R. Hensley, "Electric vehicles' resource implications on energy, raw materials, land | McKinsey," 2018. [Online]. Available: https://www.mckinsey.com/industries/automotive-and-assembly/our-insights/three-

surprising-resource-implications-from-the-rise-of-electric-vehicles#. [Accessed: 13-Mar-2021].
[223] A. Miles, "Standardization Of EV Charging In The EU | CleanTechnica," *Cleantechnica.com*, 2019. [Online]. Available: https://cleantechnica.com/2019/02/16/standardization-of-ev-charging-in-the-eu/. [Accessed: 13-Mar-2021].
[224] Canadian Automobile Association, "Electric Vehicle Government Incentives - CAA National," 2021. [Online]. Available: https://www.caa.ca/sustainability/electric-vehicles/government-incentives/. [Accessed: 11-May-2021].
[225] J. Neubauer and E. Wood, "The impact of range anxiety and home, workplace, and public charging infrastructure on simulated battery electric vehicle lifetime utility," *J. Power Sources*, vol. 257, pp. 12–20, Jul. 2014, doi: 10.1016/j.jpowsour.2014.01.075.
[226] A. Faisal, M. Kamruzzaman, T. Yigitcanlar, and G. Currie, "Understanding autonomous vehicles," *J. Transp. Land Use*, vol. 12, no. 1, pp. 45–72, 2019, doi: 10.2307/26911258.
[227] D. Milakis, B. Van Arem, and B. Van Wee, "Policy and society related implications of automated driving: A review of literature and directions for future research," *J. Intell. Transp. Syst. Technol. Planning, Oper.*, vol. 21, no. 4, pp. 324–348, Jul. 2017, doi: 10.1080/15472450.2017.1291351.
[228] S. A. Bagloee, M. Tavana, M. Asadi, and T. Oliver, "Autonomous vehicles: challenges, opportunities, and future implications for transportation policies," *J. Mod. Transp.*, vol. 24, no. 4, pp. 284–303, Dec. 2016, doi: 10.1007/s40534-016-0117-3.
[229] D. J. Fagnant, K. M. Kockelman, and P. Bansal, "Operations of shared autonomous vehicle fleet for Austin, Texas, market," *Transp. Res. Rec.*, vol. 2536, no. 1, pp. 98–106, Jan. 2015, doi: 10.3141/2536-12.
[230] M. W. Levin and S. D. Boyles, "Effects of autonomous vehicle ownership on trip, mode, and route choice," *Transp. Res. Rec.*, vol. 2493, pp. 29–38, 2015, doi: 10.3141/2493-04.
[231] S. Ma, Y. Zheng, and O. Wolfson, "Real-Time City-Scale Taxi Ridesharing," *IEEE Trans. Knowl. Data Eng.*, vol. 27, no. 7, pp. 1782–1795, Jul. 2015, doi: 10.1109/TKDE.2014.2334313.
[232] R. Snyder, "IMPLICATIONS OF AUTONOMOUS VEHICLES: A PLANNER'S PERSPECTIVE," *Inst. Transp. Eng. ITE J.*, vol. 86, no. 12, pp. 25–28, 2016.
[233] T. J. Crayton and B. M. Meier, "Autonomous vehicles: Developing a public health research agenda to frame the future of transportation policy," *J. Transp. Heal.*, vol. 6, pp. 245–252, 2017, doi: 10.1016/j.jth.2017.04.004.
[234] P. Godsmark, B. Kirk, V. Gill, and B. Flemming, "Automated Vehicles: The Coming of the Next Disruptive Technology," *Ottawa: the Conference Board of Canada*, 2015. [Online]. Available: https://www.conferenceboard.ca/e-library/abstract.aspx?did=6744. [Accessed: 14-Apr-2021].
[235] W. Zhang, S. Guhathakurta, J. Fang, and G. Zhang, "Exploring the impact of shared autonomous vehicles on urban parking demand: An agent-based simulation approach," *Sustain. Cities Soc.*, vol. 19, pp. 34–45, Dec. 2015, doi: 10.1016/j.scs.2015.07.006.
[236] T. Yigitcanlar, A. Mohamed, M. Kamruzzaman, and A. Piracha, "Understanding Transport-Related Social Exclusion: A Multidimensional Approach," *Urban Policy Res.*, vol. 37, no. 1, pp. 97–110, Jan. 2019, doi: 10.1080/08111146.2018.1533461.
[237] D. Heinrichs, "Autonomous driving and urban land use," in *Autonomous Driving: Technical, Legal and Social Aspects*, Springer Berlin Heidelberg, 2016, pp. 213–231.
[238] R. Zakharenko, "Self-driving cars will change cities," *Reg. Sci. Urban Econ.*, vol. 61, pp. 26–37, Nov. 2016, doi: 10.1016/j.regsciurbeco.2016.09.003.
[239] J. Meyer, H. Becker, P. M. Bösch, and K. W. Axhausen, "Autonomous vehicles: The next jump in accessibilities?," *Res. Transp. Econ.*, vol. 62, pp. 80–91, Jun. 2017, doi:

10.1016/j.retrec.2017.03.005.
[240] P. Fernandes and U. Nunes, “Platooning with IVC-enabled autonomous vehicles: Strategies to mitigate communication delays, improve safety and traffic flow,” *IEEE Trans. Intell. Transp. Syst.*, vol. 13, no. 1, pp. 91–106, Mar. 2012, doi: 10.1109/TITS.2011.2179936.
[241] Y. (2014). C. and A. V. 2040 V. Hendrickson, C., Biehler, A., & Mashayekh, “Connected and Autonomous Vehicles 2040 Vision,” *National Technical Information Service, Springfield, VA 22161*, 2014. [Online]. Available: https://traffic21.heinz.cmu.edu/wp-content/uploads/sites/23/2020/02/Joint-Statewide-Connected-and-Autonomous-Vehicles-2040-Vision-Final-Report-smaller.pdf. [Accessed: 14-Mar-2021].
[242] D. Farmer, “Autonomous Vehicles: the Implications on Urban Transportation and Traffic Flow Theory,” *ITE Journal*, vol. 86, no. 11, pp. 34–37, 2016.
[243] B. W. Smith, “Managing Autonomous Transportation Demand,” *Santa Clara Law Rev.*, vol. 52, no. 4, pp. 12–19, 2012.
[244] T. Litman, “Autonomous Vehicle Implementation Predictions: Implications for Transport Planning,” *Transp. Res. Board Annu. Meet.*, p. 22, 2015, doi: 10.1613/jair.301.
[245] L. M. Martinez and J. M. Viegas, “Assessing the impacts of deploying a shared self-driving urban mobility system: An agent-based model applied to the city of Lisbon, Portugal,” *Int. J. Transp. Sci. Technol.*, vol. 6, no. 1, pp. 13–27, Jun. 2017, doi: 10.1016/j.ijtst.2017.05.005.
[246] J. B. Greenblatt and S. Saxena, “Autonomous taxis could greatly reduce greenhouse-gas emissions of US light-duty vehicles,” *Nat. Clim. Chang.*, vol. 5, no. 9, pp. 860–863, Aug. 2015, doi: 10.1038/nclimate2685.
[247] Z. Wadud, D. MacKenzie, and P. Leiby, “Help or hindrance? The travel, energy and carbon impacts of highly automated vehicles,” *Transp. Res. Part A Policy Pract.*, vol. 86, pp. 1–18, Apr. 2016, doi: 10.1016/j.tra.2015.12.001.
[248] N. E. Vellinga, “From the testing to the deployment of self-driving cars: Legal challenges to policymakers on the road ahead,” *Comput. Law Secur. Rev.*, vol. 33, no. 6, pp. 847–863, Dec. 2017, doi: 10.1016/j.clsr.2017.05.006.
[249] W. Zeldin, “Netherlands: Legislation to Allow More Testing of Driverless Vehicles | Global Legal Monitor,” *LAW.gov*, 2017. [Online]. Available: https://www.loc.gov/law/foreign-news/article/netherlands-legislation-to-allow-more-testing-of-driverless-vehicles/. [Accessed: 14-Mar-2021].
[250] NHTSA, “Federal Automated Vehicles Policy: Accelerating the Next Revolution In Roadway Safety,” *U.S. Dep. Transp.*, no. September, p. 116, 2016, doi: 12507-091216-v9.
[251] UK Department for Transport, “The pathway to driverless cars: A code of practice for testing,” p. 14, 2015, doi: 10.1007/s13398-014-0173-7.2.
[252] T. Winkle, “Safety benefits of automated vehicles: Extended findings from accident research for development, validation and testing,” in *Autonomous Driving: Technical, Legal and Social Aspects*, Springer Berlin Heidelberg, 2016, pp. 335–364.
[253] D. Otte, M. Jänsch, and C. Haasper, “Injury protection and accident causation parameters for vulnerable road users based on German In-Depth Accident Study GIDAS,” *Accid. Anal. Prev.*, vol. 44, no. 1, pp. 149–153, Jan. 2012, doi: 10.1016/j.aap.2010.12.006.
[254] S. Singh, “Critical reasons for crashes investigated in the National Motor Vehicle Crash Causation Survey. (Traffic Safety Facts Crash•Stats. Report No. DOT HS 812 115),” *National Highway Traffic Safety Administration*, 2015. [Online]. Available:

https://crashstats.nhtsa.dot.gov/Api/Public/ViewPublication/812115. [Accessed: 14-Mar-2021].
[255] V. Dhar, "Equity, Safety, and Privacy in the Autonomous Vehicle Era," *Computer (Long. Beach. Calif).*, vol. 49, no. 11, pp. 80–83, Nov. 2016, doi: 10.1109/MC.2016.326.
[256] S. Gless, E. Silverman, and T. Weigend, "If robots cause harm, who is to blame? Self-driving cars and criminal liability," *New Crim. Law Rev.*, vol. 19, no. 3, pp. 412–436, Jun. 2016, doi: 10.1525/nclr.2016.19.3.412.
[257] "Vehicle Technology and Aviation Bill HC Bill 143," *Authority of the House of Commons*, 2017. [Online]. Available: https://publications.parliament.uk/pa/bills/cbill/2016-2017/0143/17143.pdf. [Accessed: 16-Mar-2021].
[258] R. de Bruin, "Autonomous Intelligent Cars on the European Intersection of Liability and Privacy.," *Eur. J. Risk Regul.*, vol. 7, no. 3, pp. 485–501, 2016, doi: 10.1017/S1867299X00006036.
[259] L. Collingwood, "Privacy implications and liability issues of autonomous vehicles," *Inf. Commun. Technol. Law*, 2017, doi: 10.1080/13600834.2017.1269871.
[260] C. Lee, "Grabbing the Wheel Early: Moving Forward on Cybersecurity and Privacy Protections for Driverless Cars," *Fed. Commun. Law J.*, vol. 69, no. 1, pp. 25–52, 2017.
[261] E. Yağdereli, C. Gemci, and A. Z. Aktaş, "A study on cyber-security of autonomous and unmanned vehicles," *J. Def. Model. Simul.*, 2015, doi: 10.1177/1548512915575803.
[262] California Institute of Technology, "EV Charging Transitioning to Paid | www.caltech.edu." [Online]. Available: https://www.caltech.edu/campus-life-events/campus-announcements/ev-charging-transitioning-to-paid. [Accessed: 12-Sep-2020].
[263] Ontario Energy Board, "Historical electricity rates | Ontario Energy Board," *2020*. [Online]. Available: https://www.oeb.ca/rates-and-your-bill/electricity-rates/historical-electricity-rates. [Accessed: 29-Dec-2020].
[264] EV Database, "Range of full electric vehicles cheatsheet - EV Database," 2020. [Online]. Available: https://ev-database.org/cheatsheet/range-electric-car. [Accessed: 29-Dec-2020].
[265] Caltech, "Models — ACN Research Portal 0.1 documentation." [Online]. Available: https://acnportal.readthedocs.io/en/latest/acnsim/models.html. [Accessed: 03-Jun-2021].
[266] M. Shute, "Dijkstra's Shortest Path Algorithm in Python | by Micah Shute | Cantor's Paradise," *Medium*, 2019. [Online]. Available: https://www.cantorsparadise.com/dijkstras-shortest-path-algorithm-in-python-d955744c7064. [Accessed: 03-Jun-2021].
[267] Z. J. Lee, S. Sharma, D. Johansson, and S. H. Low, "ACN-Sim: An open-source simulator for data-driven electric vehicle charging research," *arXiv*, 2020. .
[268] M. Farag, M. Fleckenstein, and S. Habibi, "Continuous piecewise-linear, reduced-order electrochemical model for lithium-ion batteries in real-time applications," *J. Power Sources*, vol. 342, pp. 351–362, Feb. 2017, doi: 10.1016/j.jpowsour.2016.12.044.
[269] J. Banks, J. I. S. Carson, B. L. Nelson, and D. M. Nicol, *Discrete Event System Simulation*, Fifth. New Jersey: Pearson, 2010.
[270] Ministry of Transportation Ontario, "Preliminary 2019 Ontario Road Safety Annual Report Selected Statistics," 2019.
[271] WiTricity Corporation, "Leave the Filling Station Behind," *WiTricity Corp*, 2019. [Online]. Available: http://witricity.com/wp-content/uploads/2019/01/Tech-Paper_Leave-the-filling-station-behind_Jan-2019.pdf. [Accessed: 29-Sep-2020].
[272] B. Vaidya and H. T. Mouftah, "Smart electric vehicle charging management for smart

cities," *IET Smart Cities*, vol. 2, no. 1, pp. 4–13, Mar. 2020, doi: 10.1049/iet-smc.2019.0076.
[273] Caltech, "ACN-Data -- A Public EV Charging Dataset," 2020. [Online]. Available: https://ev.caltech.edu/dataset. [Accessed: 15-Jun-2021].
[274] C. Develder, N. Sadeghianpourhamami, M. Strobbe, and N. Refa, "Quantifying flexibility in EV charging as DR potential: Analysis of two real-world data sets," in *2016 IEEE International Conference on Smart Grid Communications, SmartGridComm 2016*, 2016, pp. 600–605, doi: 10.1109/SmartGridComm.2016.7778827.
[275] Ministry of Transportation, "The Official Ministry of Transportation (MTO) Driver's Handbook," 2017. [Online]. Available: https://www.ontario.ca/document/official-mto-drivers-handbook/driving-along. [Accessed: 01-Jan-2021].
[276] Ministry of Transportation, "Consultation: speed limits on Ontario highways | Ontario.ca," 2020. [Online]. Available: https://www.ontario.ca/page/consultation-speed-limits-ontario-highways. [Accessed: 01-Jan-2021].

Appendix A Dynamic Wireless Charging Network Design Specification Tool Analysis

The novel DWCN design specification tool proposed enables implementers and analysts to choose the best parameters for construction of DWCNs. Since the DWCNs are not yet widely deployed and lack international standards, this tool gives the best possible recommendation for DWCN construction while considering compatibility with existing CNs and their standards.

The tool takes in parameters like number of EVSEs to be installed, length of track in meters, length and width of a WCP in meters, gap in meters that need to be maintained between each WCP installation, EVSE's charging rate in kW at which the battery of a CAEV is charged, the voltage at which an EVSE operates, and the vehicle speed tolerance that can be afforded to safely supply the promised charging to a CAEV in motion. The tool at minimum then calculates and suggests the total number of WCPs, required number of WCPs per EVSE, calculated length of track with WCPs installed, recommended average speed to receive charging from the track, time it will take to drive over the track in minutes and the exact locations at which each WCP should be installed on the road with gaps if any. Additional features that the design specification tool can calculate include the length of each EVSE with WCPs installed, the time to driver over a WCP and an EVSE in minutes, energy that can be delivered by an EVSE, WCP and the track in kWh, the total number of EVSEs and WCPs needed to deliver 1 kWh of energy to a vehicle in motion, total ampere needed for EVSE's operation, the recommended maximum energy threshold in kWh for the track and its EVSE and WCPs, and the recommended time slot in minutes to use for its reservations in the charge scheduling and trip planning system proposed.

The WCP_param_recomm() method of Simulation class in the simGen.py file employs equations (4.1) to (4.7). It can be used both independently in recommendations for real-world construction and with the designed simulator that may simulate the proposed charging infrastructure design to analyze and predict performance of the DWCN in a smart city.

This tool is used alone to conduct an analysis on the effect the parameters like length of a track, length of a WCP, gap between WCPs, charge rate of an EVSE and the number of EVSEs has on the overall performance of the DWCN that is to be constructed. For analysis the length of the WCPs is set at 10.0 m with 2.0 m width, gap between WCPs is set at 0.5 m, speed tolerance is set at 0.5 meters per second and the charge rate of an EVSE is set at 150 kW when

needed to be fixed. It should be noted that the tool following the guidelines of Ontario's government [275], [276] recommends using an average speed of 50 km/h for road lengths of 1 km to 5 km, 80 km/h for road lengths of 5 km to 10 km and 110 km/h for road lengths of 10 km and above.

First, the variable length of track is observed, and expectantly increasing the track length will increase the total number of WCPs needed to cover the track, as well as the time needed to driver over the track with the recommended average speed. Additionally, as the DWCN track length increases, the number of WCPs and EVSEs needed to deliver at least 1kWh of energy will also increase because there are more WCPs and EVSEs along the track to deliver the rest of the energy as can be seen in Figure A.1.

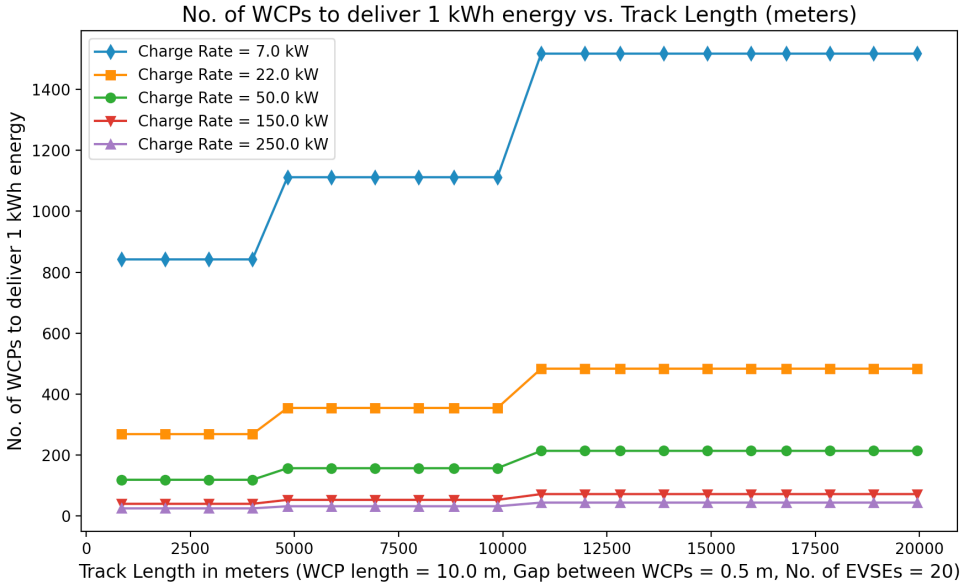

Figure A.1: Track length in meters vs. Number of WCPs to deliver 1 kWh energy.

Next, the charge rate is observed to have a profound effect on the energy delivered by an EVSE and a WCP, as increasing charge rate means that more energy can be delivered in a short time by fewer EVSEs and WCPs as can be seen in Figure A.2. It is observed that increasing the number of EVSEs will mean fewer WCPs for each EVSE to cover the track as can be seen in Figure A.3. However, depending on the cost per EVSE and per WCP, the implementer may decide whether having more EVSEs with fewer WCPs or more WCPs per EVSE is cost efficient for the DWCN.

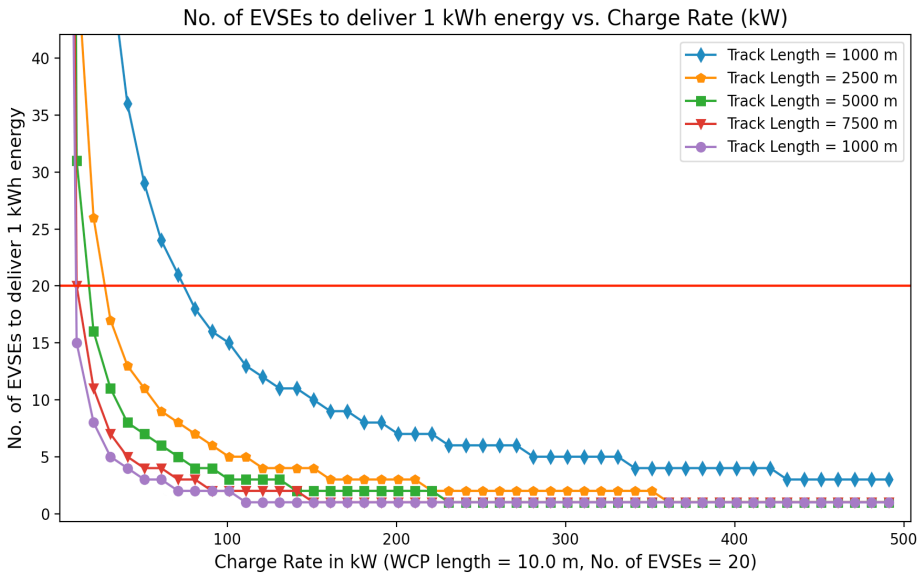

Figure A.2: Charge rate in kW vs. Number of EVSEs to deliver 1 kWh energy.

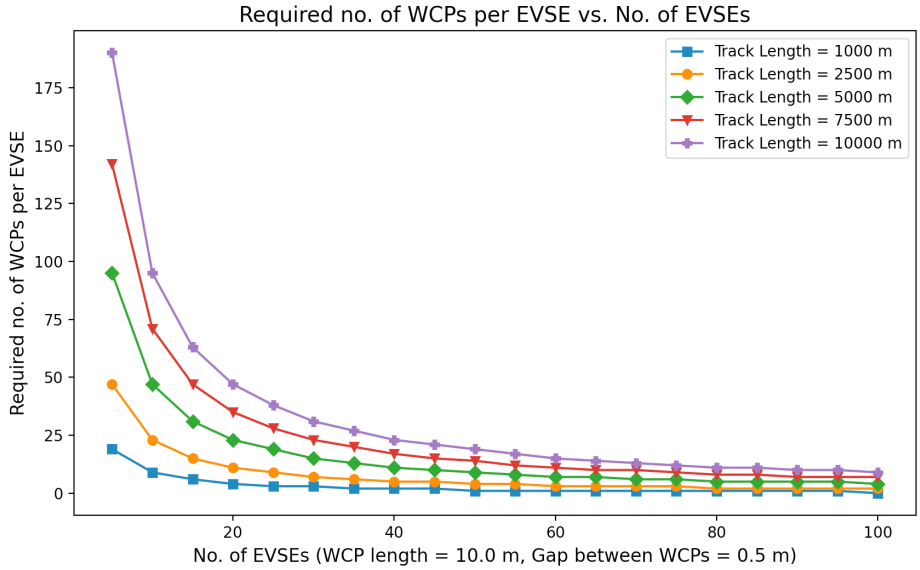

Figure A.3: Number of EVSEs vs. Required Number of WCPs per EVSE.

Now, increasing the length of the WCP is expected to decrease the number of WCPs required to cover the track as can be seen in Figure A.4 and will increase the amount of energy delivered by each WCP. Finally, increasing the gap between each WCP installation revealed that the track will be covered faster with fewer WCPs but at the cost of delivering less overall energy unless the charge rate is appropriately and safely increased to accommodate the decrease in overall charging deliverable by a track as depicted in Figure A.1 and Figure A.2 earlier. Further, it can be seen in Figure A.5 that the longer tracks can afford more gaps between WCP installations to deliver 1kWh energy with fewer number of EVSEs and WCPs.

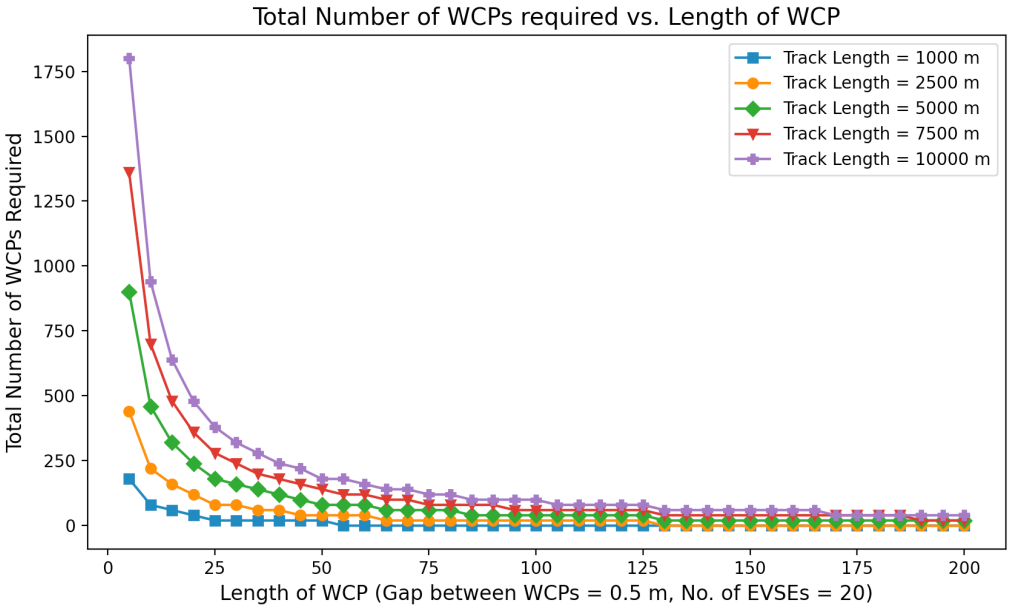

Figure A.4: Length of a WCP in meters vs. Total Number of WCPs.

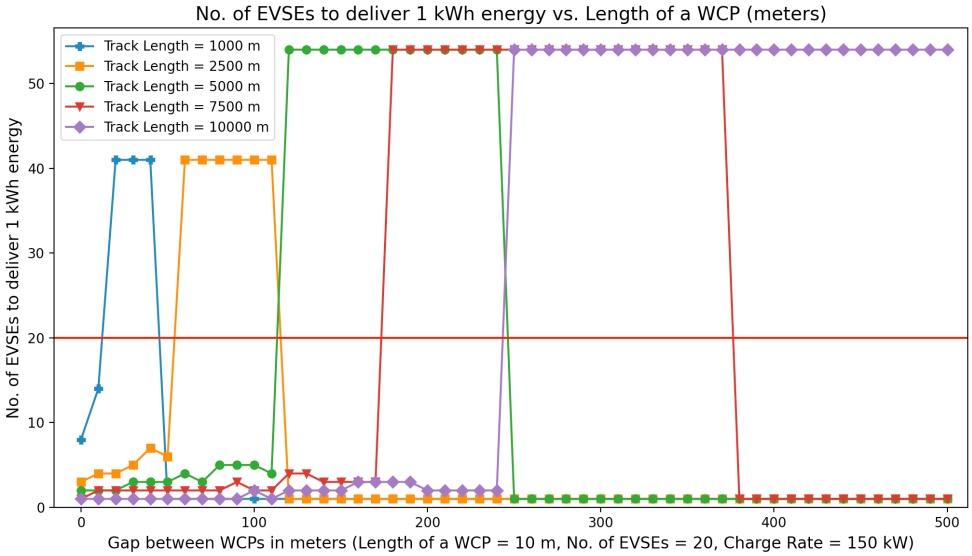

Figure A.5: Gap between WCPs in meters vs. Number of EVSEs to deliver 1 kWh energy.

Appendix B Analytical Verification and Simulation Run Analysis

B.1 Little's Law

Following the analytical approach, the conservative law or the Little's Law is used for verification of the existing system and other alternative systems designs in Chapter 5. The conservation equation (B.1) holds for almost all queueing systems or subsystems regardless of the number of servers, the queue discipline, or other special circumstances. It states that the L which is the average number of CAEVs in our system at any arbitrary time is equal to $\hat{\lambda}$, the long-run average arrival rate or throughput, multiplied by $\hat{w}$ that is the long-run average wait time. Especially, when the time T approaches infinity as well as the N, number of arrivals, approaches infinity, as can be seen in equation (B.2).

$$\hat{L} = \hat{\lambda}\hat{w} \tag{B.1}$$

$$L = \lambda w \text{ , allowing } T \to \infty \text{ and } N \to \infty \tag{B.2}$$

For computing the estimator L, the queueing system is considered over a period of time T, where L(t) denotes the number of CAEVs i in the system at time t. Also, let T_i be the total time from [0,T] which contained i CAEVs. Then the total area under the function L(t) can be computed by multiplying the rectangles of height i and length T_i as can be seen in Figure B.1. The estimator L is a time-weighted average as can be seen in equation (B.3) which is equivalent to the time-integrated average given by equation (B.4). The interest is in the long run behavior of the queuing system. As T approaches infinity, the observed time average number in the system $\hat{L}$ is expected to approach a limiting value, L, which is called the long-run time average number of CAEVs in the system with probability 1, as can be seen in equation (B.5). The limiting value L is of interest in this simulation, as it is independent from the initial conditions at time 0. Overall, the equations (B.3) to (B.5) easily apply to any queuing system or its sub-systems. Hence, the equation (B.3) was in particular used in the python simulation to compute the area over the total simulation time to get L.

To verify the long run statistics, the individual variables L, λ and w are collected from the simulation. Next, the λ and w are multiplied and compared with simulation predicted L to see if the Little's Law was proven correctly. If the L calculated analytically matches with the simulation predicted L for each server module and the overall simulation, then the system is considered successfully verified. Otherwise, the system needs to be debugged or the analytical calculations needs to be revisited.

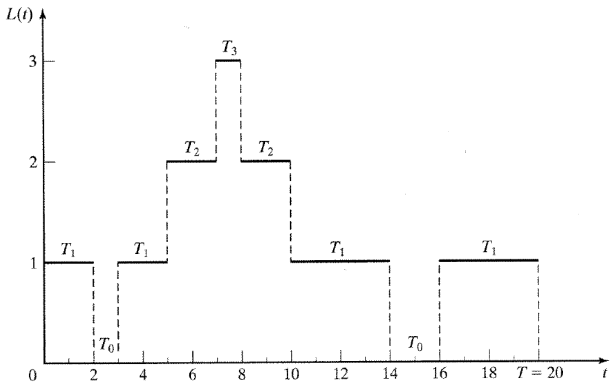

Figure B.1: Number of CAEVs in the system L(t) at time t over the time interval [0,T] [269].

$$\hat{\mathrm{L}} = \frac{1}{\mathrm{T}}\sum_{\mathrm{i}=0}^{\infty} \mathrm{iT_i} = \sum_{\mathrm{i}=0}^{\infty} \mathrm{i}\left(\frac{\mathrm{T_i}}{\mathrm{T}}\right) \tag{B.3}$$

$$\widehat{\mathrm{L}} = \frac{1}{\mathrm{T}}\int_0^{\mathrm{T}} \mathrm{L(t)dt} \tag{B.4}$$

$$\widehat{\mathrm{L}} = \frac{1}{\mathrm{T}}\int_0^{\mathrm{T}} \mathrm{L(t)dt} \to \mathrm{L\ as\ T} \to \infty \tag{B.5}$$

B.2 Estimation of Measures of Performance: Point Estimation, Confidence Intervals and Prediction Intervals

Let the performance of the simulated system measured be the parameter θ, and the set of simulation experimental results be the estimator $\hat{\theta}$. The performance parameter θ is usually used for ordinary mean and the ϕ is used for time-averaged mean for distinction. The point estimator of θ is given by equation (B.6) where $\hat{\theta}$ is a sample mean based on sample size n with simulation discrete-time data usually consists of many observations in the form $\{Y_1, Y_2 \ldots . Y_n\}$. It is desired to have an unbiased point estimator by satisfying the condition defined in (B.7). The point estimator of ϕ based on continuous-time data of the form $\{Y(t), 0 \leq t \leq T\}$ with T simulation run time is defined by equation (B.8). It is the time-weighted average of Y(t) over the interval [0, T]. This estimator is said to be biased for ϕ, as the expected value of the estimator is not equal to the performance parameter ϕ. The aim is to get unbiased estimators. So, θ or ϕ are mean measure of performance, and most performance parameters can fit into this proposed framework.

$$\hat{\theta} = \frac{1}{\mathrm{n}}\sum_{\mathrm{i}=1}^{\mathrm{n}} \mathrm{Y_i} \tag{B.6}$$

$$\mathrm{E}(\hat{\theta}) = \theta \tag{B.7}$$

$$\hat{\phi} = \frac{1}{\mathrm{T}}\int_0^{\mathrm{T}} \mathrm{Y(t)dt} \tag{B.8}$$

The point estimator of θ is the overall sample mean of some R independent replications or runs. Since $\hat{\theta}$ given by (B.6) is an estimation, it has some error associated with it that can be

measured by a CI. The sample variance across R replications is defined by (B.9), and the usual CI is given by (B.10) where Y_i are normally distributed and $\bar{Y}$ is the point estimator calculated using (B.6) and S is its standard deviation. The $\frac{S}{\sqrt{R}}$ is known as the standard error, and $t_{\frac{\alpha}{2},R-1}$ is the quantile of t-distribution with R-1 degrees of freedom that cuts off the area of each side of the t-distribution's tail by $\frac{\alpha}{2}$. The CI bounds the error with $100(1-\alpha)\%$ confidence of how far the $\bar{Y}$ is from the θ, but it can itself be wrong. The confidence level of 95% with α =0.05 significance level is chosen for all parameter estimations and it indicates the level of trust the error between the expected value of the estimator and the performance parameter can be bounded. One way to reduce the error is to increase the number of replications R.

$$S^2 = \frac{1}{n-1}\sum_{i=1}^{R}(Y_i - \bar{Y})^2 \tag{B.9}$$

$$\bar{Y} \pm t_{\frac{\alpha}{2},R-1}\left(\frac{S}{\sqrt{R}}\right) \tag{B.10}$$

The half-length H of a $100(1-\alpha)\%$ confidence interval for a mean θ is given by (B.11), which is simply the other half of equation (B.10). As an analyst, we can drive the simulation to a certain R number of replications so that the H is small enough for making accurate decisions with the simulation model. The acceptable size of H is usually set by the analyst.

$$H = t_{\frac{\alpha}{2},R-1}\left(\frac{S}{\sqrt{R}}\right) \tag{B.11}$$

PI measures the risk associated with the prediction being made. Unlike the CI the risk cannot be simulated away with more replications. The risk is an inherent part of the system, and with more replications the risk can only be evaluated better. The PIs are used to make promises about the estimation $\bar{Y}$ of a parameter θ on a particular day with high probability. The interval is defined in (B.12) where it is apparent that as R or number of replication increases, the length of the interval will never converge to 0.

$$\bar{Y} \pm t_{\frac{\alpha}{2},R-1}\, S\sqrt{1+\frac{1}{R}} \tag{B.12}$$